frontiers | Research Topics

Recent advances in agricultural waste recycling by microorganisms and their symbiosis

Edited by
Xiang Wang, Pengfei Cheng, Shuhao Huo, Zhigang Yu,
Qi Zhang and Cuixia Liu

Published in
Frontiers in Microbiology

ISSN 1664-8714
ISBN 978-2-8325-6491-2
DOI 10.3389/978-2-8325-6491-2

Generative AI statement
Any alternative text (Alt text) provided alongside figures in the articles in this ebook has been generated by Frontiers with the support of artificial intelligence and reasonable efforts have been made to ensure accuracy, including review by the authors wherever possible. If you identify any issues, please contact us.

About Frontiers

Frontiers is more than just an open access publisher of scholarly articles: it is a pioneering approach to the world of academia, radically improving the way scholarly research is managed. The grand vision of Frontiers is a world where all people have an equal opportunity to seek, share and generate knowledge. Frontiers provides immediate and permanent online open access to all its publications, but this alone is not enough to realize our grand goals.

Frontiers journal series

The Frontiers journal series is a multi-tier and interdisciplinary set of open-access, online journals, promising a paradigm shift from the current review, selection and dissemination processes in academic publishing. All Frontiers journals are driven by researchers for researchers; therefore, they constitute a service to the scholarly community. At the same time, the *Frontiers journal series* operates on a revolutionary invention, the tiered publishing system, initially addressing specific communities of scholars, and gradually climbing up to broader public understanding, thus serving the interests of the lay society, too.

Dedication to quality

Each Frontiers article is a landmark of the highest quality, thanks to genuinely collaborative interactions between authors and review editors, who include some of the world's best academicians. Research must be certified by peers before entering a stream of knowledge that may eventually reach the public - and shape society; therefore, Frontiers only applies the most rigorous and unbiased reviews. Frontiers revolutionizes research publishing by freely delivering the most outstanding research, evaluated with no bias from both the academic and social point of view. By applying the most advanced information technologies, Frontiers is catapulting scholarly publishing into a new generation.

What are Frontiers Research Topics?

Frontiers Research Topics are very popular trademarks of the *Frontiers journals series*: they are collections of at least ten articles, all centered on a particular subject. With their unique mix of varied contributions from Original Research to Review Articles, Frontiers Research Topics unify the most influential researchers, the latest key findings and historical advances in a hot research area.

Find out more on how to host your own Frontiers Research Topic or contribute to one as an author by contacting the Frontiers editorial office: frontiersin.org/about/contact

Recent advances in agricultural waste recycling by microorganisms and their symbiosis

Topic editors

Xiang Wang — Jinan University, China
Pengfei Cheng — Ningbo University, China
Shuhao Huo — Jiangsu University, China
Zhigang Yu — The University of Queensland, Australia
Qi Zhang — Nanchang University, China
Cuixia Liu — Zhongyuan University of Technology, China

Citation

Wang, X., Cheng, P., Huo, S., Yu, Z., Zhang, Q., Liu, C., eds. (2025). *Recent advances in agricultural waste recycling by microorganisms and their symbiosis*. Lausanne: Frontiers Media SA. doi: 10.3389/978-2-8325-6491-2

Table of contents

frontiers | Frontiers in Microbiology

TYPE Editorial
PUBLISHED 10 June 2025
DOI 10.3389/fmicb.2025.1631828

OPEN ACCESS

EDITED AND REVIEWED BY
William James Hickey,
University of Wisconsin-Madison,
United States

*CORRESPONDENCE
Qi Zhang
✉ zhangqi09300218@163.com
Shuhao Huo
✉ huo@ujs.edu.cn

RECEIVED 20 May 2025
ACCEPTED 26 May 2025
PUBLISHED 10 June 2025

CITATION
Zhang Q, Wang X, Cheng P, Huo S, Liu C and Yu Z (2025) Editorial: Recent advances in agricultural waste recycling by microorganisms and their symbiosis. *Front. Microbiol.* 16:1631828. doi: 10.3389/fmicb.2025.1631828

Editorial: Recent advances in agricultural waste recycling by microorganisms and their symbiosis

Qi Zhang[1]*, Xiang Wang[2], Pengfei Cheng[3], Shuhao Huo[4]*, Cuixia Liu[5] and Zhigang Yu[6]

[1]State Key Laboratory of Food Science and Resources, Engineering Research Center for Biomass Conversion, Ministry of Education, Nanchang University, Nanchang, Jiangxi, China, [2]Key Laboratory of Eutrophication and Red Tide Prevention of Guangdong Higher Education Institutes, College of Life Science and Technology, Jinan University, Guangzhou, China, [3]College of Food and Pharmaceutical Sciences, Ningbo University, Ningbo, Zhejiang, China, [4]School of Food and Biological Engineering, Jiangsu University, Zhenjiang, China, [5]School of Energy & Environment, Zhongyuan University of Technology, Zhengzhou, China, [6]Australian Centre for Water and Environmental Biotechnology (formerly AWMC), The University of Queensland, Brisbane, QLD, Australia

KEYWORDS

microalgae, wastewater treatment, resource utilization, microbial-algal symbiosis, metagenomics, transcriptomics, metabolomics, synthetic biology

Editorial on the Research Topic
Recent advances in agricultural waste recycling by microorganisms and their symbiosis

1 Introduction

The mounting environmental burden caused by agricultural waste has drawn increasing global concern. From crop residues and livestock manure to agro-industrial effluents, these waste streams are rich in organic matter and nutrients, yet often underutilized or improperly managed. Microorganisms-particularly microalgae, bacteria, and fungi-have emerged as powerful agents in transforming such waste into value-added products, offering sustainable alternatives to conventional waste treatment and resource recovery strategies. Within this context, our Research Topic was conceived to showcase emerging trends, collaborative approaches, and integrative biotechnologies driving the frontier of microbial waste recycling.

The published contributions in this Research Topic reflect a multifaceted research landscape that integrates applied microbiology, environmental engineering, and systems biology. Together, they illustrate how microbial consortia, metabolic regulation, and bioreactor optimization converge to unlock the potential of agricultural waste. Rather than presenting a mere listing of articles, this editorial highlights how these studies contribute to broader scientific and societal goals, including sustainable development, circular bioeconomy, and pollution control.

2 Overview of contributions

This Research Topic received and successfully published 11 peer-reviewed articles from authors across Asia, Europe, and Oceania. These studies exemplify recent scientific and technological advances in microbial-driven valorization of agricultural waste.

Several studies demonstrate the innovative use of microbial consortia to enhance composting efficiency and nutrient retention. For example, Wang et al. reported the use of thermotolerant strains to accelerate manure composting, providing insights into thermophilic microbial ecology under high-temperature conditions. Xie C. et al. expanded this by integrating tobacco waste into compost substrates, enhancing nitrogen preservation and seed germination-practical outcomes for soil fertility and sustainable agriculture.

Straw and lignocellulosic waste remain difficult substrates for bioconversion due to their recalcitrant structure. Ma et al. addressed this by employing *Rhodococcus wratislaviensis* YZ02 to achieve high cellulase activity and effective degradation under optimized fermentation conditions, pointing to the promise of actinobacteria in lignocellulose valorization. Complementary work by Yu et al. explored white-rot fungi and indigenous bacteria in a co-cultivation system, enhancing lignin degradation and producing protein-rich biomass suitable for ruminant feed. Chen et al. developed a multi-strain probiotic and enzyme synergistic fermentation system to convert distillers' grains into nutrient-rich animal feed, addressing both waste reduction and feed security. Xie Y. et al. performed solid-state fermentation of brewers' spent grain and tracked microbial succession and metabolite changes, offering insights for feed safety and compositional stability.

Symbiotic interactions among microalgae and bacteria are also gaining traction for their dual roles in pollutant removal and biomass production. Zheng, Liu, et al. designed an inverse fluidized bed bioreactor where algae-bacteria symbiosis achieved over 95% nitrogen removal without external aeration, indicating energy-efficient solutions for wastewater polishing. Zheng, Zhang, et al. also investigated microbial community evolution during para-nitrophenol (PNP) removal in an aerobic granular sludge system, enhancing our understanding of microbial pollutant degradation. Similarly, Mingcheng et al. leveraged microalgae for ammonia reduction, elucidating microbial functional pathways via metagenomic and transcriptomic profiling.

Advanced microbial detection and optimization techniques underpin several studies. Xie Y. et al. used high-throughput sequencing to monitor microbial succession during composting, offering predictive models for process control. Hao et al. studied the stress responses of diatoms under dehydration conditions, contributing to the theoretical foundation for applying microalgae in arid environment biotechnology. Zheng Y. et al. conducted a complete genome analysis of a *Bacillus velezensis* strain with broad-spectrum antagonistic activity, providing molecular evidence for its potential use in biocontrol and organic waste stabilization.

3 Conclusion

Taken together, the 11 articles featured in this Research Topic transcend traditional disciplinary boundaries. They collectively advocate for integrated microbiological approaches to agricultural waste management—highlighting not only innovations in laboratory settings, but also practical, scalable solutions for the field. These works underscore a shift toward ecosystem-inspired technologies, metabolic network engineering, and multi-functional microbial systems tailored to real-world complexity.

This Research Topic serves as both a benchmark and a catalyst for future research that integrates microbial ecology, biotechnology, and systems engineering in the pursuit of a more sustainable agricultural future. We thank all contributing authors, reviewers, and the Frontiers editorial team for their invaluable support and look forward to ongoing developments in this critical field.

Author contributions

QZ: Conceptualization, Data curation, Formal analysis, Funding acquisition, Investigation, Methodology, Project administration, Resources, Software, Supervision, Validation, Visualization, Writing – original draft, Writing – review & editing. XW: Writing – review & editing. PC: Writing – review & editing. SH: Writing – review & editing. CL: Writing – review & editing. ZY: Writing – review & editing.

Conflict of interest

The authors declare that the research was conducted in the absence of any commercial or financial relationships that could be construed as a potential conflict of interest.

The authors declared that they were an editorial board member of Frontiers, at the time of submission. This had no impact on the peer review process and the final decision.

Publisher's note

frontiers | Frontiers in Microbiology

TYPE Original Research
PUBLISHED 31 May 2024
DOI 10.3389/fmicb.2024.1405564

OPEN ACCESS

EDITED BY
Shuhao Huo,
Jiangsu University, China

REVIEWED BY
Surendra Sarsaiya,
Zunyi Medical University, China
Sami Abou Fayssal,
University of Forestry, Sofia, Bulgaria

*CORRESPONDENCE
Juanjuan Liu
✉ liu_juan825@ahu.edu.cn
Zemin Fang
✉ zemin_fang@ahu.edu.cn

†These authors share first authorship

RECEIVED 23 March 2024
ACCEPTED 16 May 2024
PUBLISHED 31 May 2024

CITATION
Yu L, An Z, Xie D, Yin D, Xie G, Gao X, Xiao Y, Liu J and Fang Z (2024) From waste to protein: a new strategy of converting composted distilled grain wastes into animal feed.
Front. Microbiol. 15:1405564.
doi: 10.3389/fmicb.2024.1405564

From waste to protein: a new strategy of converting composted distilled grain wastes into animal feed

Lei Yu[1,2,3†], Zichao An[1,2,3†], Dengdeng Xie[1,2,3], Diao Yin[1,2,3], Guopai Xie[4], Xuezhi Gao[4], Yazhong Xiao[1,2,3], Juanjuan Liu[1,2,3*] and Zemin Fang[1,2,3*]

[1]School of Life Sciences, Anhui University, Hefei, China, [2]Anhui Key Laboratory of Modern Biomanufacturing, Hefei, China, [3]Anhui Provincial Engineering Technology Research Center of Microorganisms and Biocatalysis, Hefei, China, [4]Anhui Golden Seed Winery Co., Ltd., Fuyang, China

Distilled grain waste (DGW) is rich in nutrients and can be a potential resource as animal feed. However, DGW contains as much as 14% lignin, dramatically reducing the feeding value. White-rot fungi such as *Pleurotus ostreatus* could preferentially degrade lignin with high efficiency. However, lignin derivatives generated during alcohol distillation inhibit *P. ostreatus* growth. Thus, finding a new strategy to adjust the DGW properties to facilitate *P. ostreatus* growth is critical for animal feed preparation and DGW recycling. In this study, three dominant indigenous bacteria, including *Sphingobacterium thermophilum* X1, *Pseudoxanthomonas byssovorax* X3, and *Bacillus velezensis* 15F were chosen to generate single and compound microbial inoculums for DGW composting to prepare substrates for *P. ostreatus* growth. Compared with non-inoculated control or single microbial inoculation, all composite inoculations, especially the three-microbial compound, led to faster organic metabolism, shorter composting process, and improved physicochemical properties of DGW. *P. ostreatus* growth assays showed the fastest mycelial colonization (20.43 $\mu g \cdot g^{-1}$ ergosterol) and extension (9 mm/d), the highest ligninolytic enzyme activities (Lac, 152.68 $U \cdot g^{-1}$; Lip, 15.56 $U \cdot g^{-1}$; MnP, 0.34 $U \cdot g^{-1}$; Xylanase, 10.98 $U \cdot g^{-1}$; FPase, 0.71 $U \cdot g^{-1}$), and the highest lignin degradation ratio (30.77%) in the DGW sample after 12 h of composting with the three-microbial compound inoculation when compared to other groups. This sample was relatively abundant in bacteria playing critical roles in amino acid, carbohydrate, energy metabolism, and xenobiotic biodegradation, as suggested by metagenomic analysis. The feed value analysis revealed that *P. ostreatus* mycelia full colonization in composted DGW led to high fiber content retention and decreased lignin content (final ratio of 5% lignin) but elevated protein concentrations (about 130 $g \cdot kg^{-1}$ DM). An additional daily weight gain of 0.4 kg/d was shown in cattle feeding experiments by replacing 60% of regular feed with it. These findings demonstrate that compound inoculant consisting of three indigenous microorganisms is efficient to compost DGW and facilitate *P. ostreatus* growth. *P. ostreatus* decreased the lignin content of composted DGW during its mycelial growth, improving the quality of DGW for feeding cattle.

KEYWORDS

distilled grain waste, composting, microbial inoculant, *Pleurotus ostreatus*, animal feed

1 Introduction

Ruminant feed is the basis of animal husbandry. With the improvement in people's living standards, the preference for meat products increases the demand for ruminant feed (Mizrahi et al., 2021). Conventional feed sources, such as corn, alfalfa grass, oat grass, and soybean meal, are insufficient in supply and quite expensive, limiting the development of livestock breeding, especially in underdeveloped areas. Thus, unconventional feed resources that do not compete with human nutrition, such as agro-industrial by-products of plant origin (e.g., distilled grains, oilseed waste, fruit and vegetable residues, sugar by-products, etc.) and agro-forestry waste (e.g., rice straw, coffee husks, cassava peels, cane trash, etc.) have attracted much attention from the feed industry and academia (Iram et al., 2020; Gupta et al., 2022).

Distilled grain waste (DGW), the primary by-product of the Chinese liquor industry, is composed of fermented grains, such as sorghum, wheat, corn, and rice husk (Tan et al., 2014). According to the National Bureau of Statistics, about 20 million tons of DGW are produced annually in China.[1] Due to the high nutrient content, high acidity, and high moisture content, DGW is very easy to decay (Wang et al., 2017). Currently, the common DGW disposal methods include incineration, landfills, stacking, or fertilizer, but these methods cannot fully utilize the DGW, even causing serious environmental risks, such as unpleasant odor generation, soil and groundwater pollution (Wang et al., 2018).

DGW is enriched in sugars, proteins, fats, vitamins, and minerals, along with cellulose and hemicellulose, which are good energy sources for ruminants (Zhang et al., 2013). However, DGW contains approximately 14% lignin, a recalcitrant aromatic polymer encapsulating cellulose and hemicellulose, causing a significant reduction in cellulose and hemicellulose utilization efficiency by rumen microbes (Vanholme et al., 2019), thus reducing the feeding value of DGW. Various methods are available to degrade lignin, including physical, chemical, and biological methods. Physical methods, including soaking and grinding, have limited ability to degrade lignin (Li et al., 2022; Reshmy et al., 2022). Chemical methods, including alkalinization and ammonification, can cause serious environmental pollution and safety hazards in spite of the strong lignin degradation ability (Kamimura et al., 2019). Currently, biological methods using microorganisms have attracted much attention for the advantages of environmental friendliness, low energy consumption, and high efficiency. In particular, white-rot fungi, a category of microorganisms in nature that are effective at lignin degradation, have drawn much more attention (Wang J. et al., 2022). It has been pronounced by the degradation of various agro-industrial wastes, e.g., olive pruning residues, tea wastes, and spent coffee grounds (Abou Fayssal et al., 2021; Werghemmi et al., 2022). This not only reduces lignin dispersion in the environment but also helps in the bioremediation of various pollutants of anthropogenic sources (Širić et al., 2022).

Pleurotus ostreatus, one of the widely cultivated edible white-rot fungi worldwide, harbors a powerful enzymatic machinery to degrade lignin for carbon source and energy, retaining cellulose for rumen microbe utilization (Fernández-Fueyo et al., 2016; Zhao et al., 2020; Okuda et al., 2021). These ligninolytic enzymes are composed of lignin peroxidase (LiP), manganese peroxidase (MnP), laccase (Lac), exoglucanase (FPase), and xylanase (Fernández-Fueyo et al., 2016; Dissasa, 2022). In addition, the mycelia of *P. ostreatus* are a source of additional protein that can be used as animal feed without isolation (Krupodorova et al., 2024). *P. ostreatus* can be used to convert lignin in DGW to prepare high-quality animal feed. However, high concentrations of toxic phenolics in DGW (about 3.5 mg/g phenolic compounds) limit the rapid colonization of fungal hypha (Wu et al., 2021).

As an environmentally friendly biotechnology, composting is widely used as a pretreatment to accelerate fungal mycelial colonization (Vieira and de Andrade, 2016). Microorganisms trigger composting. An insufficient number of native microorganisms and the elimination of some functional microorganisms during succession may lead to low composting efficiency (He et al., 2022). Accordingly, to accelerate the composting process, researchers add functional microbial inoculants to the composting materials. For example, Wan et al. (2020) inoculated a mixture of strains isolated from chicken manure compost into a new compost pile to improve the efficiency of composting. Similar findings were reported by Xu et al. (2022). They observed that inoculating thermotolerant ammonia-oxidizing bacteria extended the sanitation stage and enhanced composting efficiency in cattle manure composting.

Previously, a consortium-based microbial agent consisting of five dominant indigenous bacteria, including *Sphingobacterium* sp. X1, *Ureibacillus* sp. X2, *Pseudoxanthomonas* sp. X3, *Geobacillus* sp. X4, and *Aeribacillus* sp. X5 was developed. The compound microbial inoculum exhibited potential application in DGW composting, providing substrates for *P. ostreatus* cultivation (Wu et al., 2021). To simplify and optimize the composition of the compound inoculant, *Sphingobacterium* sp. X1 (namely *Sphingobacterium thermophilum* X1 in this research) and *Pseudoxanthomonas* sp. X3 (*Pseudoxanthomonas byssovorax* X3), as well as the newly screened *Bacillus velezensis* 15F and *Caldibacillus hisashii* 22S, were selected in this study to evaluate the effects of single and mixed microbial inoculation on *P. ostreatus* colonization in composted DGW. The ergosterol content representative for fungal growth, the DGW physicochemical properties, and the microbial community dynamics and functional metabolism were analyzed. The lignocellulosic enzyme activity secreted by *P. ostreatus* and the following effect on the lignocellulose degradation were finally used to evaluate the composting efficiency treated with various inoculations for 12 h. The feed value was also assessed for the DGW inoculated with the three-microbial compound agent and incubated with *P. ostreatus* for 15 d and 30 d.

2 Materials and methods

2.1 Screening, identification, and culture of bacteria

The raw DGW from the thermophilic phase (about 55–60°C) of DGW composting was diluted, spread on LB agar plates (LB, tryptone 10 g·L^{-1}, yeast extract 5 g·L^{-1}, NaCl 10 g·L^{-1}, Agar, 10 g·L^{-1}), and then incubated at 55°C for strain isolation as previously described (Wu et al., 2021). The 16S rRNA gene of each strain was amplified using the primers Bact-27F (5 -AGAGTTTGATCMTGGCTCAG-3) and Bact-1492R (5 -GGTTACCTTGTTACGACTT-3) and sequenced. The alignment of these sequences was analyzed with the National Center for Biotechnology Information Database (NCBI; https://www.ncbi.nlm.nih.gov/Blast.cgi) (Yoon et al., 2017). The phylogenetic tree of the four chosen bacteria was

1 https://data.stats.gov.cn

constructed using the MEGA 7 program based on the maximum likelihood method with 1,000 bootstrap replicates (Kumar et al., 2016).

The four bacteria inoculum were prepared under optimized conditions as follows. For *S. thermophilum* X1 (ON965531) and *P. byssovorax* X3 (ON966119), the culture medium was composed of 10 g·L^{-1} molasses and 15 g·L^{-1} peptone, with an inoculum size of 1% and a culture temperature of 30°C. For *B. velezensis* 15F (ON970380) and *C. hisashii* 22S (OQ554990), the culture medium was composed of 5 g·L^{-1} molasses and 10 g·L^{-1} peptone, with an inoculum size of 1% and a culture temperature of 37°C.

2.2 Composting materials and processing

The materials for composting were DGW, corncob, and lime. Raw DGW was kindly provided by Anhui Golden Seed Winery Co., Ltd. (Anhui, China). It was cooled to room temperature and stored at 4°C for less than 2 weeks before use. Corncob and lime were purchased from Dezhou Fubang Agricultural Development Co., Ltd. (Shandong, China). The physicochemical properties of composting materials were listed in Supplementary Table S1. Corncob was crushed to approximately 5 mm in length and mixed with DGW in the ratio of 3:7 to adjust the C/N ratio to 25–35. The pH was adjusted to 6–7 with an addition of 4% lime (based on raw DGW weight), and the moisture content was adjusted to 60–70% with tap water (Bari et al., 2020; Wu et al., 2021).

Composting was carried out in a ventilated room, following the method described by Wu et al. (2021). Each pile was made of 200 kg of a mixture composed of DGW and corncob. For single microbial inoculation composting, the bacteria were cultured to the logarithmic growth phase, individually harvested by centrifugation, resuspended in sterile water, and added into DGW with an addition of 2% (v/m) at a cell density of approximately 1×10^8 colony-forming units/mL. In compound microbial inoculation groups, the bacteria were mixed in equal proportions and diluted to the same volume as above. The Control Group CK was added with sterile water at 2% (v/m) final volume. Samples were collected at approximately 1 kg every 12 h or 24 h. Three samples were randomly taken from each pile at each time point. Piles were turned before each sampling to ensure aerobic conditions and the uniformity of the materials. Each sample was divided into three parts. One was stored at 4°C for analysis of pH, moisture content, electrical conductivity (EC), and germination index (GI), another was air-dried for *P. ostreatus*'s flask-cultivation and analysis of organic matter (OM) and total Kjeldahl nitrogen (TKN), and the last one was stored at −20°C for bacterial community and metabolism analysis.

2.3 *P. ostreatus* colonization and culture, and ergosterol content determination

P. ostreatus was maintained on PDA (potato dextrose agar, filtrate of boiled potato 200 g·L^{-1}, glucose 20 g·L^{-1}, agar 15 g·L^{-1}) slants at 4°C. Four mycelial blocks (5 mm diameter) of actively grown *P. ostreatus* were inoculated into liquid PDA medium and incubated at 25°C for 5 d with shaking at 150 rpm. Then, a homogenizer was used to mix the mycelium as the seed. The DGW materials sampled from different composting groups were adjusted to pH 7.0 and 65% humidity, followed by sterilization, and used as the substrates. The seed of *P. ostreatus* was inoculated at 5% (v/m) into DGW substrates and incubated at 25°C and 60% humidity in flasks. Ergosterol was extracted by saponification reaction after 7 d of *P. ostreatus* colonization using the method described by Wu et al. (2021). The ergosterol content was analyzed via high-performance liquid chromatography method with an XDB C18 column (250 mm × 4.6 mm, 5 μm; Agilent, Palo Alto, United Stated) and a UV detector (1,260 DAD) at 30°C. Methanol was used as the eluting buffer, and 1.0 mL/min was set as the flow rate.

The 12 h composted DGW of different groups was used as the substrates to prepare wrapped bags (about 1.5 kg). The *P. ostreatus* seed was inoculated into the bags and cultured in a humidity-, temperature-, and light-controlled production house. Bags from different groups were withdrawn every 5 d for the determination of lignocellulose contents and enzyme activity. For DGW inoculated with the three-microbial compound agent, bags were withdrawn when the substrates had half mycelia growth, full mycelia growth, and after a round of mushroom harvesting for feed value evaluation. The DGW without *P. ostreatus* seeding was used as the control.

2.4 Physicochemical parameters analysis

Temperature was measured at the center of piles every 12 h with an electronic thermometer. The moisture content was measured after drying fresh samples at 105°C. The EC and pH were determined by mixing fresh samples with deionized water at a ratio of 1:10 (m/v). After shaking for 0.5 h, the mixture was filtered to obtain the supernatant. The weight loss after ignition at 550°C for 4 h in a muffle furnace was used to determine the OM content (Lu et al., 2018). In accordance with the Chinese standard GB/T 6432–2018, TKN was measured. Following the method described by Qian et al., GI was detected (Qian et al., 2022).

2.5 Bacterial community and function analysis

Total genomic DNA was extracted from 12 h composted DGW samples of different groups using the DNeasy PowerSoil Kit (Qiagen, Germany), according to the manufacturer's instructions. Then, DNA was determined after Nanodrop checking. Universal primers (338F: 5 -ACTCCTACGGGAGGCAGCAG-3, 806R: 5 -GGACTACHVGG GTWTCTAAT-3) were performed to amplify V3-V4 region of the bacterial 16S rRNA gene. The amplicon libraries were constructed and sequenced on the MiSeq PE250 sequencer (Illumina, United States) at Shanghai Personal Biotechnology Co., Ltd. (Shanghai, China). Chao1, Shannon, and microbial community graphs were performed using the genescloud tools.[2] Bacterial composition and distributive abundance in the samples were conducted at the genus level using QIIME2 2019.4 and R packages (vision 3.2.0) based on the sequence data and visualized using MEGAN and GraPhlAn as previously described (Wu et al., 2021). Microbial functions were predicted using the software PICRUSt2 and drawn in a heatmap using the "pheatmap" package of the R software (version 3.6.3) (Kolde and Kolde, 2015). The correlation

2 https://www.genescloud.cn/

network diagram was drawn with Cytascape software (version 3.10.1) (Gong et al., 2023).

2.6 Determination of lignocellulose contents and enzyme activities during *P. ostreatus* cultivation

DGW substrates were sampled from the wrapped bags of *P. ostreatus* culture every 5 days during the first month for lignocellulose contents and enzyme activity determination. Three bags were withdrawn for each group at a time. The concentrations of cellulose, hemicellulose, and lignin were analyzed using the method described by Soest et al. (1991). Enzymes were extracted as described by Zeng et al. (2010). Lac activity was determined by 2, 2-azino-bis (3-ethylbenzothiazoline-6-sulfonic acid) (Couto et al., 2006). MnP activity was measured by the 2, 6-dimethylphenol (2, 6-DMP) method (Wariishi et al., 1992). The veratryl alcohol was used to determine Lip activity (Arora and Gill, 2001). Xylanase activity was determined by xylan solution and 3, 5-dinitrosalicylic acid (DNS) (Irfan et al., 2016). Whatman No. 1 filter paper strip (1 × 6 cm) and xylan solution were used as substrates for the determination of filter paperase (FPase) and xylanase activities, respectively (Zhao et al., 2021).

2.7 Determination of chemical composition in composted DGW samples

About 100 g samples were analyzed for dry matter (DM) content by drying them in a forced-air oven at 65°C for 48 h and then grinding to pass a 1.0 mm screen for chemical analysis. Crude protein (CP) was measured according to the methods of the Association of Official Analytical Chemists (AOAC, 1990) using a Kjeldahl nitrogen analyzer (SKD-100, Shanghai Peiou Analytical Instrument Co., LTD, China). Protein fractions, including true protein (TP), nonprotein-N (NpN), and free amino acid (FAA) were determined according to the method of Licitra et al. (1996). The neutral detergent fiber (NDF) and acid detergent fiber (ADF) contents were detected as described by Soest et al. (1991) without the use of heat-stable amylase and sodium sulphite by an XD-CXW-10 Fiber Analyzer (Shanghai Zida Instrument Co., LTD, China).

2.8 Cattle feeding

A cattle feeding experiment was conducted at the Livestock and Poultry Breeding Service Center of Fuyang City (Anhui, China). The protocol involving animals was approved and carried out strictly following the related regulations (Hefei, China).

The DGW substrates from Group C4 with full mycelia growth were collected together. For the safety and adaptation of cattle, DGW feed was mixed with regular feed. The total daily intake of each cattle was 18 kg, and feeding times were 4 am and 4 pm, respectively. Thirty cattle were divided into three groups. The feeding experiment lasted 4 weeks, and the weight of cattle was recorded. The feed of Group A was 100% regular feed, Group B was composed of 70% regular feed and 30% DGW feed, and Group C was composed of 40% regular feed and 60% DGW feed.

2.9 Statistical analysis

GraphPad Prism 9 was used for physicochemical, lignocellulose, enzymes, and chemical composition analyses. ChiPlot[3] was used for ergosterol analysis. The statistical significance was evaluated through one-way ANOVA, followed by Student's *t*-test with GraphPad Prism 9.0. The significance standard was p value <0.05. All experiments were conducted with three biological replications except for the cattle feeding experiment with 10 replications.

3 Results and discussion

3.1 Evaluation of the individual and combined inoculation effects of indigenous bacteria in DGW compost to accelerate *P. ostreatus* colonization

Sphingobacterium, *Pseudoxanthomonas*, *Bacillus*, and *Caldibacillus* are effective decomposers involved in the degradation of organic matter during various substrate composting (Neelkant et al., 2019; Wu et al., 2020; Chang et al., 2023; Li et al., 2023; Sun et al., 2023), occupying the four highest abundance for species richness during DGW composting (Wu et al., 2021). Each strain of these genera, including the strains *S. thermophilum* X1 and *P. byssovorax* X3 used previously (Wu et al., 2021), and the newly isolated ones *B. velezensis* 15F and *C. hisashii* 22S were selected for further single and compound microbial inoculated composting experiments (Supplementary Figure S1).

Firstly, DGW composting inoculated by individual strain was carried out. The samples were collected every 24 h and used as substrates for *P. ostreatus* colonization. Ergosterol content was chosen as a marker of fungal growth and colonization rate of *P. ostreatus* (Mansoldo et al., 2020; Wu et al., 2021; Wang Q. et al., 2022). *P. ostreatus* could not grow when directly using the mixed raw DGW as substrates (Supplementary Figure S2). However, the ergosterol contents gradually increased in DGW samples composted for 0–48 h, suggesting decreased toxic substances and increased soluble nutrients (Yadav et al., 2020; Wu et al., 2021). DGW substrates treated by *S. thermophilum* X1 (named T1), *P. byssovorax* X3 (T2), and *B. velezensis* 15F (T3) were more suitable for *P. ostreatus* growth. Furthermore, T1 and T3 inoculation also accelerated the mycelial colonization since their ergosterol contents (20.51 and 18. 58 $\mu g \cdot g^{-1}$ in DGW composted for 48 h) peaked 24 h earlier than CK group (17. 48 $\mu g \cdot g^{-1}$ in DGW composted for 72 h). Conversely, *C. hisashii* 22S (T4) inoculation did not affect *P. ostreatus* growth. The ergosterol contents between Groups T4 and CK were almost similar during the whole composting process (Supplementary Figure S2).

Thus, T1, T2, and T3 were further selected and combined to generate four composite microbial inoculants, including C1 (T1 and T2), C2 (T1 and T3), C3 (T2 and T3), and C4 (T1, T2, and T3). Another composting experiment was performed, and composting settings were named Groups T1-T3 and C1-C4 according to inoculated microbial agents, respectively. Samples were taken every

3 https://www.chiplot.online/

12 h to compare the effects of single and compound microbial inoculated DGW compost on *P. ostreatus* growth. In comparison with no detected ergosterol content in DGW treated with single microbial inoculants and composted for 12 h, *P. ostreatus* could grow well in DGW inoculated with composite microbial inoculants (Figure 1). Among them, the highest ergosterol content was detected in Group C4 (20.43 $\mu g \cdot g^{-1}$), about twice that of the Groups C1 to C3 (10.01 $\mu g \cdot g^{-1}$, 11.48 $\mu g \cdot g^{-1}$, and 10.53 $\mu g \cdot g^{-1}$, respectively). The mycelial colonization was accelerated in composite inoculum treated groups by 12 h as compared with the single microbial treated groups, with the peaked ergosterol contents in DGW composted for 24 h at 20.58, 23.14, 21.05, and 24.89 $\mu g \cdot g^{-1}$, respectively, in Groups C1 to C4 (Figure 1B). More importantly, the ergosterol content in Group C4 which used DGW composted for 12 h as the substrate was comparable to the peaked ones in other groups.

3.2 The three-microbial compound inoculum harbors the best effect on the improvement of physicochemical properties of DGW compost

The physicochemical properties of DGW compost were analyzed for each efficient group every 12 h to explore the mechanism promoting *P. ostreatus* colonization. The DGW composting process could be divided into mesophilic, thermophilic (> 50°C), and cooling phases (Wu et al., 2021). As shown in Figure 2A, all microbial inoculations accelerated the composting process, suggesting more active microbial metabolism and faster degradation of organic matter (Yang and Zhang, 2022). The groups entered the thermophilic phase following the order of C4 > C2 > C3 > C1 > T1 > T3 > T2 > CK (at 12 h of composting). Compared to Group CK, inoculated groups had higher temperatures in mesophilic and thermophilic phases at the same composting time. The temperature of DGW treated with C4 reached the peak of 68.3°C at 24 h of composting, whereas the other groups had the highest temperatures with a range from 67.0°C to 68.0°C at 36 h of composting. The acceleration of composting temperature is essential for the rapid killing of potential pathogens, such as *Enterobacter* and *Acinetobacter*, in the raw DGW, as well as for the compost hastening maturity (Joseph et al., 2018). Following this fact, the temperatures in microbial inoculated groups decreased faster than Group CK after 36 h of composting, with Group C4 entering the cooling phase most quickly (Figure 2A), perhaps due to the fastest consumption of soluble and readily assimilable compounds (Chan et al., 2016; Zhao et al., 2016; Sánchez et al., 2017).

The active metabolism during DGW composting was also reflected by the continuously decreased moisture content in all groups (Figure 2B). Consistent with the order of temperature rising rate that was responsible for moisture evaporation, the degree of moisture content reduction was in the order of C4 > C2 > C3 > C1 > T1 > T3 > T2 > CK. Similar results were also found in other compostings, such as organic–inorganic aerobic composting and chicken manure composting with maize straw (Yu et al., 2019; Wan et al., 2020). Group C4 showed the fastest drop in moisture content (Figure 2B), suggesting the maximum moisture dissipation caused by most active microbial metabolism. At the initial stage, the high moisture content (68.03%) might let microorganisms utilize the organic matter to produce certain organic acids, such as lactic acid and butyric acid, in the anaerobic fermentation piles (Zhang et al., 2019), resulting in a temporary drop in pH to 5.6–6.2 after 12 h of composting in each group (Figure 2C). After this period, all groups maintained a steady increasing pH in the thermophilic phase and stabilized at a pH of about 8.5 in the cooling phase. The pH values of microbial inoculated groups, especially Group C4, not only decreased faster

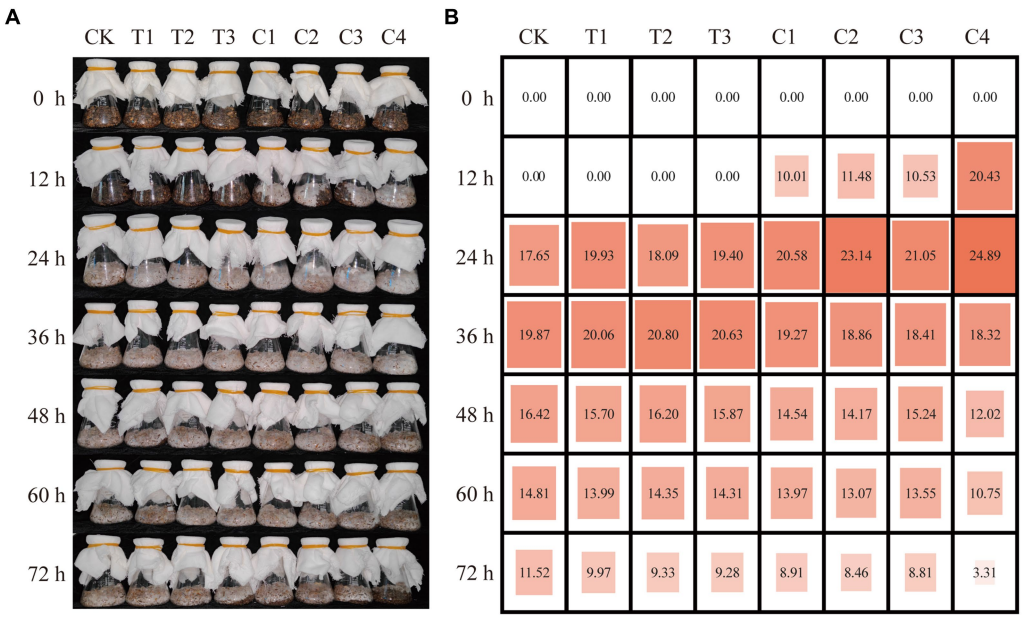

FIGURE 1
The effects of individual and combined inoculants on DGW compost to accelerate *P. ostreatus* colonization. Growth **(A)** and the ergosterol content ($\mu g \cdot g^{-1}$) **(B)** of *P. ostreatus* colonized in DGW inoculated with individual or combined inoculums every 12 h of composting.

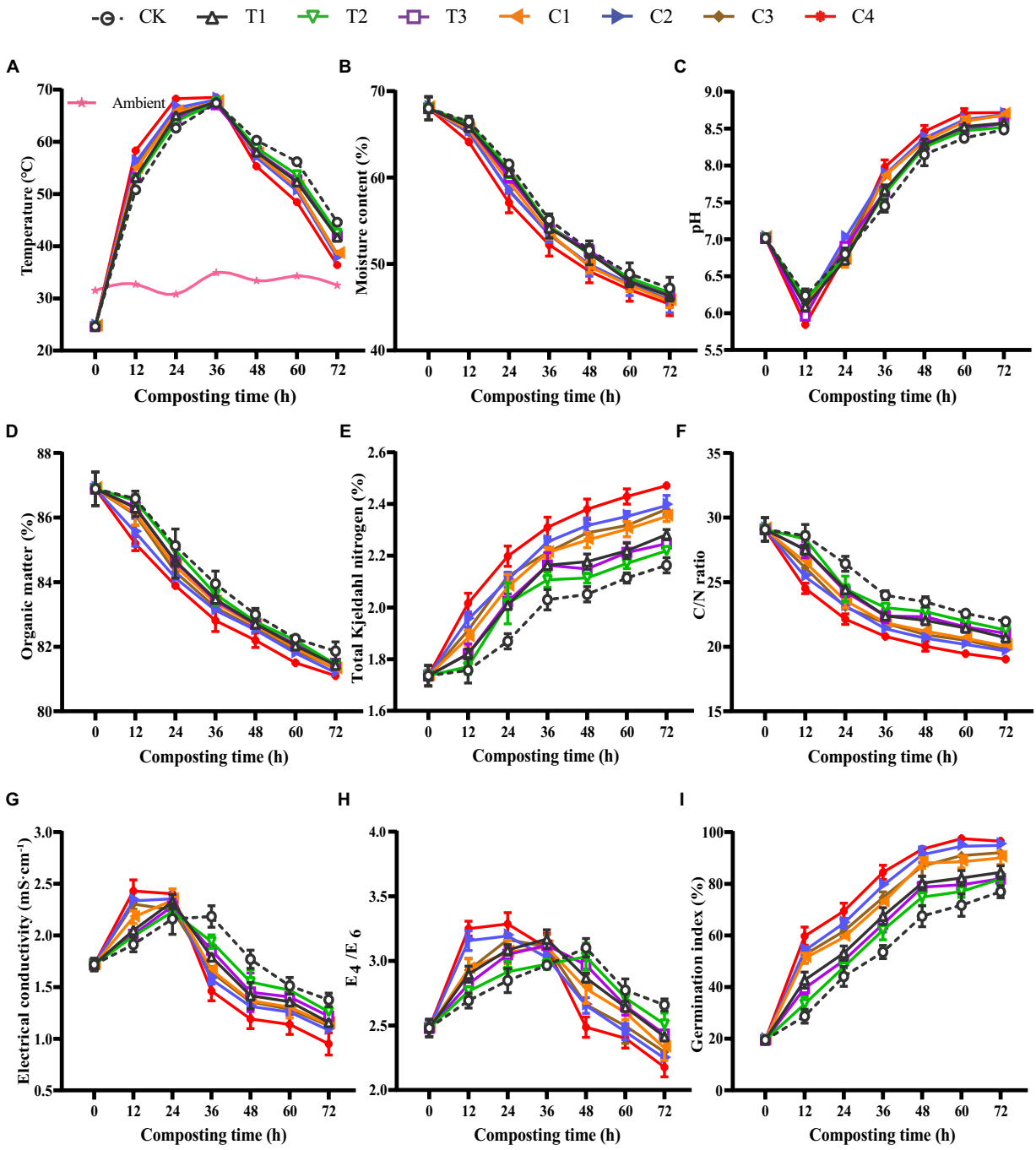

FIGURE 2
The physicochemical properties of DGW composting with individual or combined inoculations. **(A)** Temperature. **(B)** Moisture content. **(C)** pH. **(D)** Organic matter. **(E)** Total Kjeldahl nitrogen. **(F)** C/N ratio. **(G)** Electrical conductivity. **(H)** E_4/E_6. **(I)** Germination index.

during the first 12 h of composting but also rose faster later than that of the CK group (Figure 2C).

The increased pH was attributed to the degradation of organic acids and the utilization of nitrogenous organic matter and ammonification by microorganisms (Yang et al., 2020). Compared with Group CK, the OM decreased faster in microbial-inoculated groups during the DGW composting process (Figure 2D), suggesting a stronger depletion of OM (Zhang et al., 2019; Duan et al., 2020). The degradation of OM followed the order of C4 > C2 > C3 > C1 > T1 > T3 > T2 > CK. Correspondingly, the change of the TKN concentration was opposite among the eight groups because of the reduction of the compost mass caused by OM degradation (Figure 2E). The metabolism of carbon is often faster than nitrogen in composting studies using various substrates including DGW (Wu et al., 2020, 2021; Wang L. et al., 2022). Thus, the C/N ratio in Group C4 was the lowest among the eight groups, followed by two microbial inoculated groups (Figure 2F).

The rapid decomposition of various OM into small soluble molecular components such as organic acids and NH_4^+ by microorganisms and the reduced compost mass is assumed to lead to

increased EC (Chen et al., 2020; Sun et al., 2023). In the mesophilic phase and early stage of the thermophilic phase, the EC values increased in all groups, with microbial inoculated groups higher than Group CK (Figure 2G). However, in the late stage of the thermophilic phase and the cooling phase, the volatilization of organic acids or NH_3 and humification conversion resulted in decreased EC values (Bernal et al., 2009; Xu et al., 2021; Sun et al., 2023). This was also confirmed by the changes in E_4/E_6 value, which represented the condensation degree of the aromatic substances and indicated inverse proportion to the humification levels (Wan et al., 2020). The EC and E_4/E_6 in microbial inoculated groups not only decreased earlier but also harbored lower values than Group CK (Figures 2G,H). Therefore, the inoculation of microorganisms reinforced both the microbial metabolism and humic substance formation in DGW compost. Among the composite inoculants, C4 worked the most efficiently.

The GI value can be used as an indicator of the toxicity of a sample (Kong et al., 2022). With the degradation of toxic substances such as organic acids, alcohols, and aldehydes, and increased humification, the GI value showed an increasing trend (Figure 2I). Group C4 had a GI value of 69.2% after 24 h of composting, in comparison with 44.1% in Group CK. Whereas after 48 h of composting, the GI value rose to about 95% in Group C4, indicating the almost total degradation of toxic substances and the maturation of compost (Xu et al., 2021; Sun et al., 2023). Meanwhile, the GI values in Group CK and three single-microbial inoculated groups were lower than 80%. These results in total suggested that the physicochemical properties of DGW compost were improved by microbial inoculation, and the microbial inoculant C4 consisting of T1, T2, and T3 was an effective compound agent for DGW composting.

3.3 The three-microbial compound inoculum changes the bacterial community dynamics and functional metabolism in DGW compost

Bacterial community succession is an intrinsic factor in changing the physicochemical properties of DGW (Chen X. et al., 2022; Qv et al., 2023). The DGW samples composted for 12 h, in which the growth rates of *P. ostreatus* dramatically differed among groups inoculated with different types of bacteria (Figure 1), were chosen for 16S rDNA sequencing. Compared to CK, the Chao1 index and Shannon index suggested that the richness and diversity of the microbial community decreased in almost all microbial inoculated groups (Figure 3A). The lowest Chao1 and Shannon indexes were both observed in Group C4 (Figure 3A). Therefore, microbial inoculation addition led to the enrichment of superior microorganisms in DGW compost. These alterations were consistent with swine manure and rice straw co-composting with *Streptomyces griseorubens* inoculation (Chi et al., 2020) but inconsistent with sewage sludge composting inoculated with a compound bacteria agent (Chen X. et al., 2022). According to Figure 2A, microbial inoculations have driven the composting process to the thermophilic phase at 12 h of composting. The heat might be responsible for decreased microbial richness and diversity. Furthermore, the non-metric multidimensional scaling (NMDS) analysis suggested that the microbial communities were distant from each other among groups (Supplementary Figure S3), in line with the altered DGW properties.

After composting for 12 h, *Weissella, Acinetobacter, Acetobacter, Klebsiella,* and *Bacillus* were the top 5 dominant genera. *Weissella*, a genus of lactic acid bacteria, plays a key role in promoting nitrogen cycling and accelerating composting (He et al., 2022; Jin et al., 2022; Lu et al., 2023). Microbial inoculants for each group stimulated the growth of *Weissella*. Among, the highly significant difference in the relative abundance of *Weissella* between Group CK (17.02%) and C4 (30.73%) may account for the fastest fermentation in Group C4 (Figure 3B; Supplementary Figure S4; $p < 0.001$). Similarly, the highest relative abundance of *Acetobacter* was found in Group C4, probably related to the fact that it degraded the most alcohol in DGW samples (El-Askri et al., 2022; Matsumoto et al., 2023). On the contrary, the relative abundance of *Klebsiella*, a genus of pathogenic bacteria, was lower in microbial inoculated groups compared to CK, especially in Groups C2-C4 (Figure 3B; Supplementary Figure S4), probably because of their higher temperature at 12 h of composting than CK to kill more pathogens. Another genus, *Acinetobacter*, is essential for organic matter degradation during composting (Wu et al., 2022), but no significant difference was observed among groups. The abundance of *Bacillus*, which is widely found in the composting process and plays a vital role in the degradation of organic matter (Zhang et al., 2021), was balanced in the remaining groups, except for Group T3 which was inoculated with a relatively high number of *B. velezensis* 15F. Furthermore, the relative abundance of *Sphingobacterium* in C1, C2, and C4 groups treated with *S. thermophilum* X1 was higher than that of other groups (Supplementary Figure S4). A similar phenomenon was observed for the genus *Pseudoxanthomonas*. These results indicated that inoculated microorganisms survived during DGW composting and correlated with bacterial community dynamics, temperature changes, and organic matter degradation in composting since *Pseudoxanthomonas* has been demonstrated to degrade environmental hydrocarbons and *Sphingobacterium* is a biomarker for organic biodegradation strengthening toward humification (Mohapatra and Phale, 2021; Qi et al., 2022).

Next, the correlation network diagram between bacterial communities and physicochemical properties of DGW was further performed with Cytascape software. Thirty-three paired correlations were obtained [$|r| > 0.6$, $p < 0.05$], among which *Weissella* and *Rummeliibacillus* having a large number of connections with DGW physicochemical properties. As shown in Figure 3C, *Weissella* and *Sphingobacterium* abundance was positively correlated with temperature, TN, EC, E4/E6, and GI, but negatively correlated with C/N. Conversely, the abundance of *Klebsiella*, *Rummeliibacillus* and *Lactobacillus* was positively correlated with C/N, but negatively correlated with temperature, TN, EC, E4/E6, and GI (Figure 3C). The temperature was also positively associated with other genera including *Acinetobacter* that are thermophilic bacteria and harbor strong degradation abilities of carbohydrates and cellulose (Karthika et al., 2020; Gao et al., 2021; Cazaudehore et al., 2022).

High levels of microbial activity are always associated with increased microbial metabolism (Zhou et al., 2019; Zhong et al., 2020). After inoculation, the levels of amino acid, carbohydrate, energy, cofactors, and vitamins metabolisms in Groups T1 and C1-C4 were higher than in the CK group (Figure 3D). The xenobiotic biodegradation and metabolism, as well as terpenoid and polyketide metabolism, was accelerated in inoculated groups except for Group T2. Among, Group C4 showed the highest metabolism levels of the six metabolic functions, which may be related to the strongest

10.3389/fmicb.2024.1405564

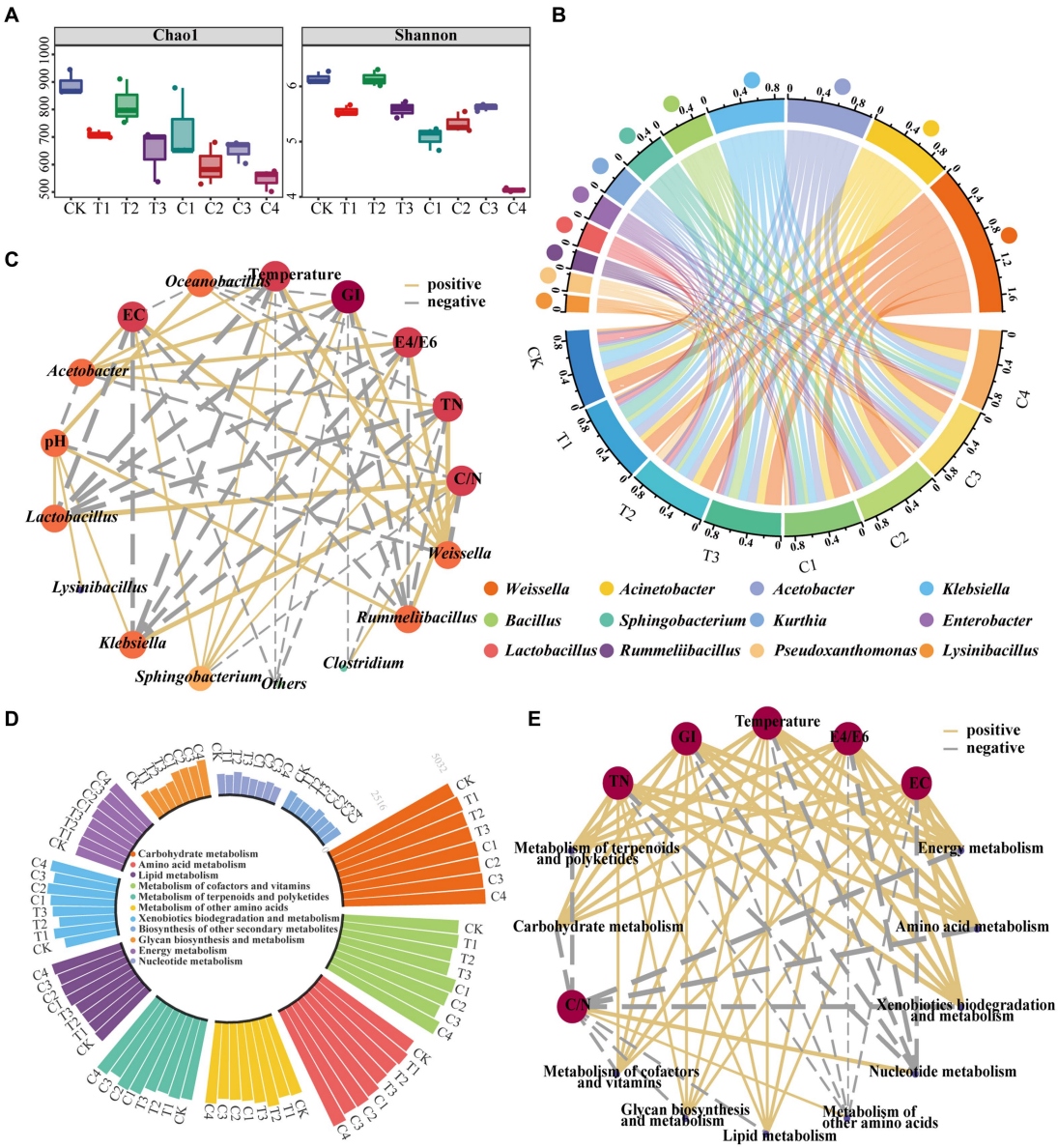

FIGURE 3
Changes in bacterial community composition and potential functions in composted DGW samples. DGW samples were treated with individual and combined inoculations and composted for 12 h. **(A)** Changes in the Chao1 index and Shannon index. **(B)** Variations of the microbial community at the genus level. **(C)** The correlation network diagram between bacterial communities and physicochemical properties of DGW. **(D)** Variations of microbial metabolic functions. **(E)** The correlation network diagram between bacterial functions and physicochemical properties of DGW.

depletion of complex organic matter in DGW, including carbohydrates, alcohols, phenols, and aldehydes, and the fastest increase in temperature (Figure 3D). In addition, the glycan biosynthesis and metabolism was much higher in Group C4 than other groups, in consistency with the higher ergosterol content of Group C4. Relatively, Group T2 had the highest metabolism of other amino acids and nucleotide metabolism. The correlation network diagram between metabolic functions and physicochemical properties of DGW showed 60 paired correlations [$|r|>0.6$, $p<0.05$]. The correlation between GI and temperature tended to be consistent. Both of them were positively associated not only with the metabolism of amino acids, carbohydrates, lipids, energy, cofactors and vitamins, and terpenoids and polyketides but also with glycan biosynthesis and metabolism and xenobiotics biodegradation and metabolism (Figure 3E). Therefore, the three microbial compound inoculum could drive the bacterial community dynamics and metabolism change, upregulate the composting temperature, and improve DGW physicochemical properties, ultimately facilitating *P. ostreatus* growth.

3.4 *P. ostreatus* decreases the lignin content and improves the feed value of composted DGW

DGW materials treated with microbial inoculums and composted for 12 h were withdrawn and wrapped into substrate bags (about

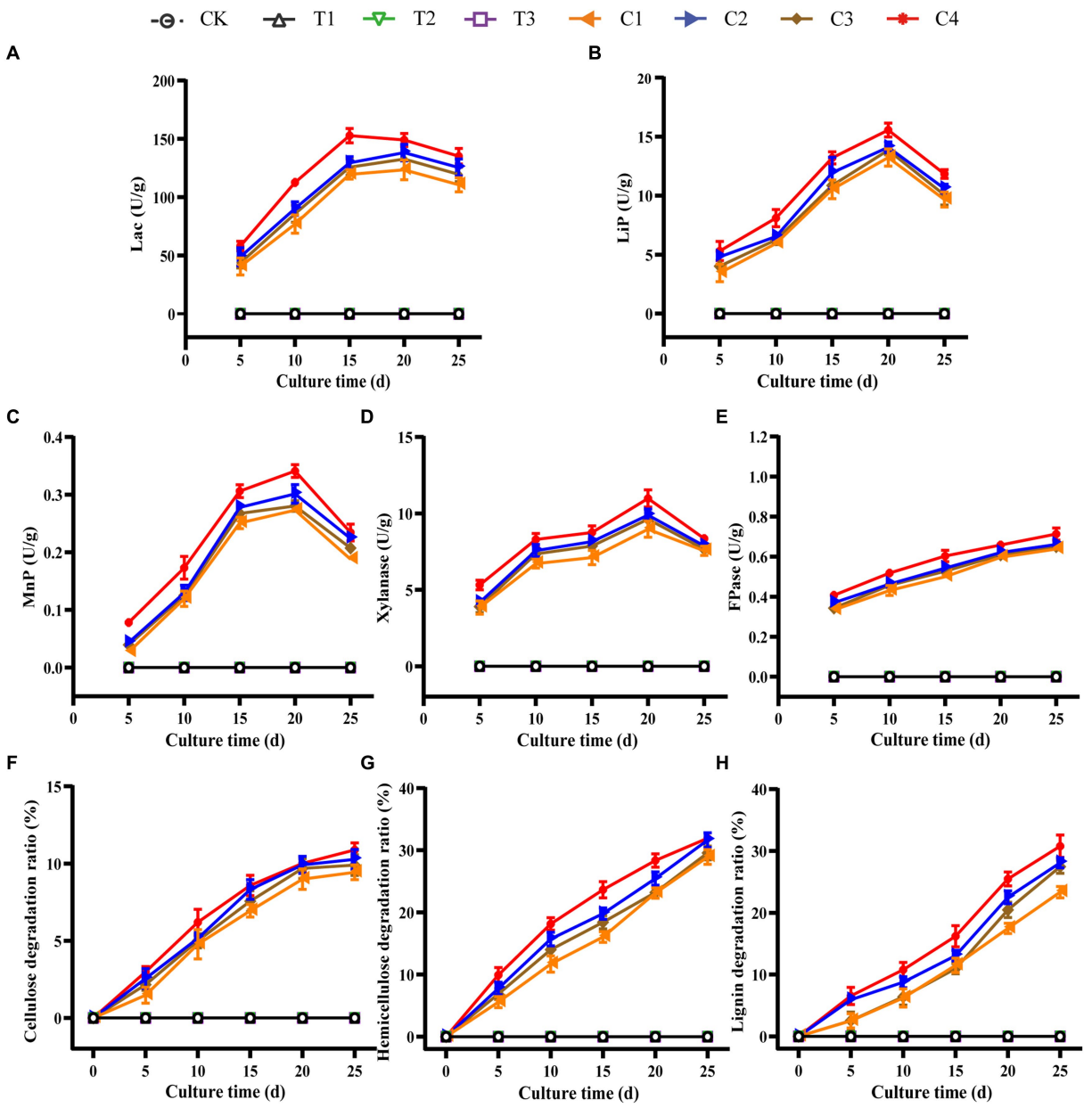

FIGURE 4
Dynamic changes of the lignocellulose degradation and relative enzymatic activities in substrate bags. DGW materials treated by microbial inoculums and composted for 12 h were used as substrates to wrap into bags. *P. ostreatus* mycelia were inoculated to culture mushrooms. The substrates were withdrawn every 5 d to detect activities of Lac **(A)**, LiP **(B)**, MnP **(C)**, xylanase **(D)**, FPase **(E)**, and the degradation ratios of cellulose **(F)**, hemicellulose **(G)**, and lignin **(H)**.

1.5 kg) to cultivate *P. ostreatus*. The lignocellulose degradation and relative enzymatic activities in DGW were measured every 5 d to compare the mycelial growth status. There was no lignocellulosic enzyme activity and lignocellulose degradation in Groups CK and T1 to T3 (Figures 4A–H), in line with the absence of ergosterol in these groups (Figure 2B). However, the corresponding enzyme activities and degradation ratios of cellulose, hemicellulose, and lignin in all compound microbial inoculated groups were substantially enhanced. Group C4 had the highest LiP, MnP, Lac, FPase, and Xylanase activities (Figures 4A–E) in association with the highest degradation of lignocellulose (Figures 4F–H). Specifically, Lac activity in Group C4 peaked at 15 d with 152.68 $U \cdot g^{-1}$, LiP activity peaked at 20 d with 15.56 $U \cdot g^{-1}$, MnP activity was the highest at 20 d with 0.34 $U \cdot g^{-1}$, Xylanase activity was the highest at 20 d with 10.98 $U \cdot g^{-1}$, and FPase activity continued to increase to 0.71 $U \cdot g^{-1}$ at 25 d. The degradation ratios of cellulose and hemicellulose were similar between microbial inoculated groups; for example, Group C4 harbored 10.88% cellulose degradation (Figure 4F) and 31.93% hemicellulose degradation (Figure 4G). The highest level of degradation in lignin at 25 d was observed in Group C4, with a 30.77% degradation ratio and higher than other compound microbial inoculated groups (Figure 4H). In addition, the mycelial extension speed in the bag in Group C4 was

10.3389/fmicb.2024.1405564

TABLE 1 Chemical compositions of the Group 4 DGW substrates with different states of mycelial growth.

	Trial 1				Trial 2			
	Before	Half	Full	After	Before	Half	Full	After
DM (g·kg^{-1})	463.0	356.9	343.4	372.0	464.0	366.5	348.5	374.0
CP (g·kg^{-1} DM)	91.0	101.5	129.5	87.5	87.5	103.3	131.3	99.3
TP (g·kg^{-1} DM)	71.8	98.0	110.3	73.5	70.0	98.0	105.0	77.0
NpN (g·kg^{-1} DM)	3.1	0.6	3.1	2.2	2.8	0.8	4.2	3.6
NDF (g·kg^{-1} DM)	736.3	730.0	725.9	739.0	735.3	731.4	706.1	688.6
ADF (g·kg^{-1} DM)	441.9	449.3	442.8	463.2	447.4	470.0	491.8	438.0
WSC (g·kg^{-1} DM)	41.6	37.4	36.4	48.3	38.6	43.7	28.7	44.7
FAA (mg·100 g^{-1} DM)	33.4	70.7	41.7	25.3	33.0	69.0	44.5	26.4

Before, DGW without mycelial colonization; Half, DGW with half mycelia growth; Full, DGW with full mycelia growth; After, DGW after a round of mushroom harvesting. DM, dry matter; CP, crude protein; TP, true protein; NpN, nonprotein nitrogen; NDF, neutral detergent fiber; ADF, acid detergent fiber; WSC, water soluble carbohydrate; FAA, free amino acid.

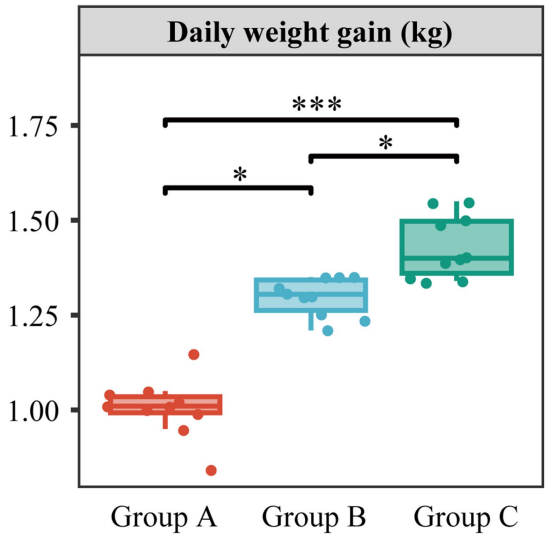

FIGURE 5
Daily weight gain of cattle using DGW feed. Cattle in groups A, B, and C were given feed including 0, 30, and 60% DGW, respectively. (significant statistical differences: * $p < 0.05$, *** $p < 0.001$). Data present means ± SD, $n = 10$.

substantially accelerated, reaching 9 mm/d, as compared to about 6 mm/d in Groups C1–C3.

The DGW substrates from Group C4 with half mycelia growth, full mycelia growth, and after a round of mushroom harvesting were evaluated for their feed value. In accordance with the conclusion that *P. ostreatus* had effective and widespread applications in lignin removal from various by-products for animal feed, such as cornstalk (Chen et al., 2017) and purple field corn stover (Khonkhaeng and Cherdthong, 2019), the final lignin ratio decreased from 14% in raw DGW to about 12%, 5%, and 5%, respectively. As shown in Table 1, the content of DM in the substrate decreased gradually following mycelial growth. In contrast, the contents of CP and TP increased, with an 11.5% and a 36.5% increment in the substrate with half mycelia growth and a 42.3% and a 53.6% increase in the substrate with full mycelia growth as compared with DGW without mycelial colonization, respectively. After a round of harvesting, the total protein concentrations in the substrate decreased to levels comparable to the DGW without mycelial colonization. Furthermore, all substrates tested were high in fiber content (736.3 and 441.9 g/kg DM for NDF and ADF in DGW without mycelia colonization, 730.0 and 449.3 g·kg^{-1} DM for NDF and ADF in the DGW with half mycelia growth, and 725.9 and 442.8 g·kg^{-1} DM for NDF and ADF in the DGW with full mycelia growth, respectively, in Trail 1). Hence, *P. ostreatus* mycelia colonized DGW substrate, particularly when fully grown, maintained a high fiber content while increasing protein levels and reducing lignin content. This value indicates its potential use in preparing ruminant feed (Zebeli et al., 2012; Erickson et al., 2020; Chen L. et al., 2022). In addition, compared with the DGW without *P. ostreatus* culture, the water soluble carbohydrate in the DGW with full mycelia growth was slightly higher whereas the free amino acid content was slightly lower.

3.5 The composted DGW with full mycelial growth is a favorable ruminant feed

DGW from Group C4 with full mycelial growth was further collected for animal feeding studies. Three batches of cattle feeding experiments were performed to compare the effect of different amounts of DGW addition on weight gain (Figure 5). Cattle in group C (60% DGW feed and 40% regular feed) had a daily weight gain of 1.4 kg, followed by 1.3 kg in group B (30% DGW feed and 70% regular feed) and 1.0 kg in group A (100% regular feed). This result indicated that DGW, after fermentation with the compound microbial inoculum C4 followed by *P. ostreatus* culture, is a favorable ruminant feed. This feed is composed of the physical and chemical properties-optimized DGW, fungal mycelia, and the extracellular enzymes and bioactive compounds secreted from mycelia (Antunes et al., 2020). These substances provide high nutritional value for ruminants.

4 Conclusion

Three strains were employed and inoculated in DGW in different combinations to explore a new recycling strategy of DGW. After pretreatment of DGW with the compound microbial inoculant consisting of three effective strains, the physicochemical properties of

DGW were mostly improved through driving by the changes of microbial community structures and functions. The *P. ostreatus* colonization and mycelial growth were substantially faster, resulting in decreased lignin content and increased protein concentrations in the substrate. Cattle feeding using the composted DGW with full mycelial growth leading to more weight gain further reveals its potential application in ruminant feed. Therefore, a new approach comprised of microbial inoculated composting, *P. ostreatus* culture, and followed by animal feeding is suitable and highly valued for DGW cycling. Subsequent studies can be proposed based on this study to combine *P. ostreatus* culture and other strategies to elevate the protein content further, optimize the feed value, and prolong the storage period.

Data availability statement

The raw sequencing data were uploaded to the National Center for Biotechnology Information (NCBI) Sequence Read Archive (SRA) database with the accession number PRJNA917117.

Ethics statement

The animal study was approved by the ethical and humane committee of Anhui University. The study was conducted in accordance with the local legislation and institutional requirements.

Author contributions

LY: Data curation, Investigation, Writing – original draft, Conceptualization. ZA: Data curation, Investigation, Writing – original draft, Methodology. DX: Investigation, Writing – original draft. DY: Investigation, Writing – original draft. GX: Methodology, Resources, Writing – review & editing. XG: Methodology, Resources, Writing – review & editing. YX: Writing – review & editing. JL: Writing – review & editing, Conceptualization, Data curation, Supervision, Writing – original draft. ZF: Conceptualization, Supervision, Writing – review & editing, Funding acquisition.

Funding

The author(s) declare financial support was received for the research, authorship, and/or publication of this article. This work was supported by the Science and Technology Major Project of Anhui Province (No. 202103a06020006, 17030701059), the Science Fund for Distinguished Young Scholars of Anhui Province (No. 2008085J12), and the Key Research Program of the Department of Education of Anhui Province (KJ2021A0056).

Conflict of interest

GX and XG were employed by Anhui Golden Seed Winery Co., Ltd.

The remaining authors declare that the research was conducted in the absence of any commercial or financial relationships that could be construed as a potential conflict of interest.

Publisher's note

Supplementary material

The Supplementary material for this article can be found online at: https://www.frontiersin.org/articles/10.3389/fmicb.2024.1405564/full#supplementary-material

References

Abou Fayssal, S., Alsanad, M. A., Yordanova, M., el Sebaaly, Z., Najjar, R., and Sassine, Y. (2021). Effect of olive pruning residues on substrate temperature and production of oyster mushroom (*Pleurotus ostreatus*). *Acta Hortic.* 1327, 245–252. doi: 10.17660/ActaHortic.2021.1327.32

Antunes, F., Marçal, S., Taofiq, O., Morais, A. B., Freitas, A. C., Ferreira, I. R., et al. (2020). Valorization of mushroom by-products as a source of value-added compounds and potential applications. *Molecules* 25:2672. doi: 10.3390/molecules25112672

AOAC (1990). *Official methods of analysis. 15th* Edn. Artington, Virginia: Association of official analytical chemists.

Arora, D. S., and Gill, P. K. (2001). Comparison of two assay procedures for lignin peroxidase. *Enzyme Microb. Technol.* 28, 602–605. doi: 10.1016/s0141-0229(01)00302-7

Bari, E., Daniel, G., Yilgor, N., Kim, J. S., Singh, A. P., Ribera, J., et al. (2020). Comparison of the decay behavior of two white-rot fungi in relation to wood type and exposure conditions. *Microorganisms* 8:1931. doi: 10.3390/microorganisms8121931

Bernal, M. P., Alburquerque, J. A., and Moral, R. (2009). Composting of animal manures and chemical criteria for compost maturity assessment. *Bioresour. Technol.* 100, 5444–5453. doi: 10.1016/j.biortech.2008.11.027

Cazaudehore, G., Monlau, F., Gassie, C., Lallement, A., and Guyoneaud, R. (2022). Active microbial communities during biodegradation of biodegradable plastics by mesophilic and thermophilic anaerobic digestion. *J. Hazard. Mater.* 443:130208. doi: 10.1016/j.jhazmat.2022.130208

Chan, M. T., Selvam, A., and Wong, J. C. (2016). Reducing nitrogen loss and salinity during 'struvite' food waste composting by zeolite amendment. *Bioresour. Technol.* 200, 838–844. doi: 10.1016/j.biortech.2015.10.093

Chang, Y., Zhou, K., Yang, T., Zhao, X., Li, R., Li, J., et al. (2023). *Bacillus licheniformis* inoculation promoted humification process for kitchen waste composting: organic components transformation and bacterial metabolic mechanism. *Environ. Res.* 237:117016. doi: 10.1016/j.envres.2023.117016

Chen, H., Awasthi, S. K., Liu, T., Duan, Y., Ren, X., Zhang, Z., et al. (2020). Effects of microbial culture and chicken manure biochar on compost maturity and greenhouse gas emissions during chicken manure composting. *J. Hazard. Mater.* 389:121908. doi: 10.1016/j.jhazmat.2019.121908

Chen, Y., Fan, H., and Meng, F. (2017). *Pleurotus ostreatus* decreases cornstalk lignin content, potentially improving its suitability for animal feed. *J. Sci. Food Agr.* 97, 1592–1598. doi: 10.1002/jsfa.7907

Chen, L., Li, W., Zhao, Y., Zhang, S., and Meng, L. (2022). Evaluation of bacterial agent/nitrate coupling on enhancing sulfur conversion and bacterial community succession during aerobic composting. *Bioresour. Technol.* 362:127848. doi: 10.1016/j.biortech.2022.127848

Chen, X., Yan, F., Liu, T., Zhang, Y., Li, X., Wang, M., et al. (2022). Ruminal microbiota determines the high-fiber utilization of ruminants: evidence from the ruminal microbiota transplant. *Microbiol. Spectr.* 30:10. doi: 10.1002/adfm.202003619

Chi, C. P., Chu, S., Wang, B., Zhang, D., Zhi, Y., Yang, X., et al. (2020). Dynamic bacterial assembly driven by *Streptomyces griseorubens* JSD-1 inoculants correspond to composting performance in swine manure and rice straw co-composting. *Bioresour. Technol.* 313:123692. doi: 10.1016/j.biortech.2020.123692

Couto, S. R., Couto, S. R., Rodríguez, A. G., Paterson, R. M., Lima, N., and Teixeira, J. A. (2006). Laccase activity from the fungus *Trametes hirsuta* using an air-lift bioreactor. *Lett. Appl. Microbiol.* 060316073800005–060316073800616. doi: 10.1111/j.1472-765X.2006.01879.x

Dissasa, G. (2022). Cultivation of different oyster mushroom (*Pleurotus* species) on coffee waste and determination of their relative biological efficiency and pectinase enzyme production. *Ethiopia. Int. J. Microbiol.* 2022:5219939. doi: 10.1155/2022/5219939

Duan, M., Zhang, Y., Zhou, B., Qin, Z., Wu, J., Wang, Q., et al. (2020). Effects of *Bacillus subtilis* on carbon components and microbial functional metabolism during cow manure–straw composting. *Bioresour. Technol.* 303:122868. doi: 10.1016/j.biortech.2020.122868

El-Askri, T., Yatim, M., Sehli, Y., Rahou, A., Belhaj, A., Castro, R., et al. (2022). Screening and characterization of new *Acetobacter fabarum* and *Acetobacter pasteurianus* strains with high ethanol-thermo tolerance and the optimization of acetic acid production. *Microorganisms* 10:1741. doi: 10.3390/microorganisms10091741

Erickson, P. S., Anderson, J. L., Kalscheur, K. F., Lascano, G. J., Akins, M. S., and Heinrichs, A. J. (2020). Symposium review: strategies to improve the efficiency and profitability of heifer raising. *J. Dairy Sci.* 103, 5700–5708. doi: 10.3168/jds.2019-17419

Fernández-Fueyo, E., Ruiz-Dueñas, F. J., López-Lucendo, M. F., Pérez-Boada, M., Rencoret, J., Gutiérrez, A., et al. (2016). A secretomic view of woody and nonwoody lignocellulose degradation by *Pleurotus ostreatus*. *Biotechnol. Biofuels* 9:49. doi: 10.1186/s13068-016-0462-9

Gao, G., Liao, Z., Cao, Y., Zhang, Y., Zhang, Y., Wu, M., et al. (2021). Highly efficient production of bacterial cellulose from corn Stover total hydrolysate by *Enterobacter* sp. FY-07. *Bioresource. Technol.* 341:125781. doi: 10.1016/j.biortech.2021.125781

Gong, Y.-X., Li, J., Deng, X., Chen, Y., Chen, S., Huang, H., et al. (2023). Application of starch degrading bacteria from tobacco leaves in improving the flavor of flue-cured tobacco. *Front. Microbiol.* 14:14. doi: 10.3389/fmicb.2023.1211936

Gupta, J., Kumari, M., Mishra, A., Swati, A. M., and Thakur, I. S. (2022). Agro-forestry *waste manage*. *Chemosphere* 287:132321. doi: 10.1016/j.chemosphere.2021.132321

He, Y., Zhang, Y., Huang, X., Xu, J., Zhang, H., Dai, X., et al. (2022). Deciphering the internal driving mechanism of microbial community for carbon conversion and nitrogen fixation during food waste composting with multifunctional microbial inoculation. *Bioresour. Technol.* 360:127623. doi: 10.1016/j.biortech.2022.127623

Iram, A., Cekmecelioglu, D., and Demirci, A. (2020). Distillers' dried grains with solubles (DDGS) and its potential as fermentation feedstock. *Appl. Microbiol. Biot.* 104, 6115–6128. doi: 10.1007/s00253-020-10682-0

Irfan, M., Asghar, U., Nadeem, M., Nelofer, R., and Syed, Q. (2016). Optimization of process parameters for xylanase production by *Bacillus* sp. in submerged fermentation. *J. Radiat. Res. Appl. Sc.* 9, 139–147. doi: 10.1016/j.jrras.2015.10.008

Jin, Z., Lu, T., Feng, W., Jin, Q., Wu, Z., and Yang, Y. (2022). Development of the degradation bacteria in household food waste and analysis of the microbial community in aerobic composting. *Biotechnol. Appl. Bioc.* 70, 622–633. doi: 10.1002/bab.2385

Joseph, S., Kammann, C., Shepherd, J. G., Conte, P., Schmidt, H. P., Hagemann, N., et al. (2018). Microstructural and associated chemical changes during the composting of a high temperature biochar: mechanisms for nitrate, phosphate and other nutrient retention and release. *Sci. Total Environ.* 618, 1210–1223. doi: 10.1016/j.scitotenv.2017.09.200

Kamimura, N., Sakamoto, S., Mitsuda, N., Masai, E., and Kajita, S. (2019). Advances in microbial lignin degradation and its applications. *Curr. Opin. Biotech.* 56, 179–186. doi: 10.1016/j.copbio.2018.11.011

Karthika, A. S., Seenivasagan, R., Kasimani, R., Babalola, O., and Vasanthy, M. (2020). Cellulolytic bacteria isolation, screening and optimization of enzyme production from vermicompost of paper cup waste. *Waste Manag.* 116, 58–65. doi: 10.1016/j.wasman.2020.06.036

Khonkhaeng, B., and Cherdthong, A. (2019). *Pleurotus ostreatus* and Volvariella volvacea can enhance the quality of purple field corn Stover and modulate ruminal fermentation and feed utilization in tropical beef cattle. *Animals* 9:1084. doi: 10.3390/ani9121084

Kolde, R., and Kolde, M. R. (2015). Package 'pheatmap'. R package 1.

Kong, Y., Wang, G., Chen, W., Yang, Y., Ma, R., Li, D., et al. (2022). Phytotoxicity of farm livestock manures in facultative heap composting using the seed germination index as indicator. *Ecotoxicol. Environ. Saf.* 247:114251. doi: 10.1016/j.ecoenv.2022.114251

Krupodorova, T., Barshteyn, V., Tsygankova, V., Sevindik, M., and Blume, Y. (2024). Strain-specific features of *Pleurotus ostreatus* growth in vitro and some of its biological activities. *BMC Biotechnol.* 24:9. doi: 10.1186/s12896-024-00834-9

Kumar, S., Stecher, G., and Tamura, K. (2016). MEGA7: molecular evolutionary genetics analysis version 7.0 for bigger datasets. *Mol. Biol. Evol.* 33, 1870–1874. doi: 10.1093/molbev/msw054

Li, H., He, Y., Yan, Z., Yang, Z., Tian, F., Liu, X., et al. (2023). Insight into the microbial mechanisms for the improvement of spent mushroom substrate composting efficiency driven by phosphate-solubilizing *Bacillus subtilis*. *J. Environ. Manag.* 336:117561. doi: 10.1016/j.jenvman.2023.117561

Li, F., Zhao, Y., Xue, L., Ma, F., Dai, S. Y., and Xie, S. (2022). Microbial lignin valorization through depolymerization to aromatics conversion. *Trends Biotechnol.* 40, 1469–1487. doi: 10.1016/j.tibtech.2022.09.009

Licitra, G., Hernández, T., and Soest, P. (1996). Standardization of procedures for nitrogen fractionation of ruminant feeds. *Anim. Feed. Sci. Tech.* 57, 347–358. doi: 10.1016/0377-8401(95)00837-3

Lu, J., Qiu, Y., Muhmood, A., Zhang, L., Wang, P., and Ren, L. (2023). Appraising co-composting efficiency of biodegradable plastic bags and food wastes: assessment microplastics morphology, greenhouse gas emissions, and changes in microbial community. *Sci. Total Environ.* 875:162356. doi: 10.1016/j.scitotenv.2023.162356

Lu, Q., Zhao, Y., Gao, X., Wu, J., Zhou, H., Tang, P., et al. (2018). Effect of tricarboxylic acid cycle regulator on carbon retention and organic component transformation during food waste composting. *Bioresour. Technol.* 256, 128–136. doi: 10.1016/j.biortech.2018.01.142

Mansoldo, F. P., Firpo, R., Cardoso, V. S., Queiroz, G. N., Cedrola, S. L., Godoy, M. G., et al. (2020). New method for rapid identification and quantification of fungal biomass using ergosterol autofluorescence. *Talanta* 219:121238. doi: 10.1016/j.talanta.2020.121238

Matsumoto, N., Matsutani, M., Tanimoto, Y., Nakanishi, R., Tanaka, S., Kanesaki, Y., et al. (2023). Implication of amino acid metabolism and cell surface integrity for the thermotolerance mechanism in the thermally adapted acetic acid bacterium *Acetobacter pasteurianus* TH-3. *J. Bacteriol.* 205:e0010123. doi: 10.1128/jb.00101-23

Mizrahi, I., Wallace, R. J., and Moraïs, S. (2021). The rumen microbiome: balancing food security and environmental impacts. *Nat. Rev. Microbiol.* 19, 553–566. doi: 10.1038/s41579-021-00543-6

Mohapatra, B., and Phale, P. S. (2021). Microbial degradation of naphthalene and substituted naphthalenes: metabolic diversity and genomic insight for bioremediation. *Front. Bioeng. Biotechnol.* 9:602445. doi: 10.3389/fbioe.2021.602445

Neelkant, K. S., Shankar, K., Jayalakshmi, S. K., and Sreeramulu, K. (2019). Optimization of conditions for the production of lignocellulolytic enzymes by *Sphingobacterium* sp. ksn-11 utilizing agro-wastes under submerged condition. *Prep. Biochem. Biotech.* 49, 927–934. doi: 10.1080/10826068.2019.1643735

Okuda, N., Nakazawa, T., Horii, M., Wu, H., Kawauchi, M., Sakamoto, M., et al. (2021). Overexpressing *Pleurotus ostreatus rho1b* results in transcriptional upregulation of the putative cellulolytic enzyme-encoding genes observed in *ccl1* disruptants. *Environ. Microbiol.* 23, 7009–7027. doi: 10.1111/1462-2920.15786

Qi, C., Yin, R., Cheng, J., Xu, Z., Chen, J., Gao, X., et al. (2022). Bacterial dynamics for gaseous emission and humification during bio-augmented composting of kitchen waste with lime addition for acidity regulation. *Sci. Total Environ.* 848:157653. doi: 10.1016/j.scitotenv.2022.157653

Qian, X., Bi, X., Xu, Y., Yang, Z., Wei, T., Xi, M., et al. (2022). Variation in community structure and network characteristics of spent mushroom substrate (SMS) compost microbiota driven by time and environmental conditions. *Bioresour. Technol.* 364:127915. doi: 10.1016/j.biortech.2022.127915

Qv, M., Bao, J., Wang, W., Dai, D., Wu, Q., Li, S., et al. (2023). Bentonite addition enhances the biodegradation of petroleum pollutants and bacterial community succession during the aerobic co-composting of waste heavy oil with agricultural wastes. *J. Hazard. Mater.* 462:132655. doi: 10.1016/j.jhazmat.2023.132655

Reshmy, R., Athiyaman Balakumaran, P., Divakar, K., Philip, E., Madhavan, A., Pugazhendhi, A., et al. (2022). Microbial valorization of lignin: prospects and challenges. *Bioresour. Technol.* 344:126240. doi: 10.1016/j.biortech.2021.126240

Sánchez, Ó. J., Ospina, D. A., and Montoya, S. (2017). Compost supplementation with nutrients and microorganisms in composting process. *Waste Manag.* 69, 136–153. doi: 10.1016/j.wasman.2017.08.012

Širić, I., Kumar, P., Adelodun, B., Abou Fayssal, S., Bachheti, R. K., Bachheti, A., et al. (2022). Risk assessment of heavy metals occurrence in two wild edible oyster mushrooms (*Pleurotus* spp.) collected from Rajaji national park. *J. Fungi.* 8:1007. doi: 10.3390/jof8101007

Soest, P. J. V., Robertson, J. B., and Lewis, B. A. (1991). Methods for dietary fiber, neutral detergent fiber, and nonstarch polysaccharides in relation to animal nutrition. *J. Dairy Sci.* 74, 3583–3597. doi: 10.3168/JDS.S0022-0302(91)78551-2

Sun, X., Li, Z., Li, J., Li, Z., Ma, Y., Zhou, Z., et al. (2023). Dynamic composting actuated by a *Caldibacillus thermoamylovorans* isolate enables biodecomposability and reusability of *Cinnamomum camphora* garden wastes. *Bioresour. Technol.* 376:128852. doi: 10.1016/j.biortech.2023.128852

Tan, L., Sun, Z., Zhang, W., Tang, Y., Morimura, S., and Kida, K. (2014). Production of bio-fuel ethanol from distilled grain waste eluted from Chinese spirit making process. *Bioprocess Biosyst. Eng.* 37, 2031–2038. doi: 10.1007/s00449-014-1178-5

Vanholme, R., De Meester, B., Ralph, J., and Boerjan, W. (2019). Lignin biosynthesis and its integration into metabolism. *Curr. Opin. Biotech.* 56, 230–239. doi: 10.1016/j.copbio.2019.02.018

Vieira, F. R., and de Andrade, M. C. N. (2016). Optimization of substrate preparation for oyster mushroom (*Pleurotus ostreatus*) cultivation by studying different raw materials

and substrate preparation conditions (composting: phases I and II). *World. J. Microb. Biot.* 32:190. doi: 10.1007/s11274-016-2152-y

Wan, L., Wang, X., Cong, C., Li, J., Xu, Y., Li, X., et al. (2020). Effect of inoculating microorganisms in chicken manure composting with maize straw. *Bioresour. Technol.* 301:122730. doi: 10.1016/j.biortech.2019.122730

Wang, J., Li, L., Xu, H., Zhang, Y., Liu, Y., Zhang, F., et al. (2022). Construction of a fungal consortium for effective degradation of rice straw lignin and potential application in bio-pulping. *Bioresour. Technol.* 344:126168. doi: 10.1016/j.biortech.2021.126168

Wang, Q., Meng, L., Wang, X., Zhao, W., Shi, X., Wang, W., et al. (2022). The yield, nutritional value, umami components and mineral contents of the first-flush and second-flush *Pleurotus pulmonarius* mushrooms grown on three forestry wastes. *Food Chem.* 397:133714. doi: 10.1016/j.foodchem.2022.133714

Wang, L., Qu, F., Zhu, Z., Zhao, Y., Chen, X., Shi, M., et al. (2022). The important role of tricarboxylic acid cycle metabolism pathways and core bacterial communities in carbon sequestration during chicken manure composting. *Waste Manag.* 150, 20–29. doi: 10.1016/j.wasman.2022.06.034

Wang, T. T., Sun, Z. Y., Huang, Y. L., Tan, L., Tang, Y. Q., and Kida, K. (2018). Biogas production from distilled grain waste by thermophilic dry anaerobic digestion: pretreatment of feedstock and dynamics of microbial community. *Appl. Biochem. Biotech.* 184, 685–702. doi: 10.1007/s12010-017-2557-6

Wang, S. P., Zhong, X. Z., Wang, T. T., Sun, Z. Y., Tang, Y. Q., and Kida, K. (2017). Aerobic composting of distilled grain waste eluted from a Chinese spirit-making process: the effects of initial pH adjustment. *Bioresour. Technol.* 245, 778–785. doi: 10.1016/j.biortech.2017.09.051

Wariishi, H., Vallis, K., and Gold, M. H. (1992). Manganese(II) oxidation by manganese peroxidase from the basidiomycete *Phanerochaete chrysosporium*. Kinetic mechanism and role of chelators. *J. Biol. Chem.* 267, 23688–23695. doi: 10.1016/s0021-9258(18)35893-9

Werghemmi, W., Abou Fayssal, S., Mazouz, H., Hajjaj, H., and Hajji, L. (2022). Olive and green tea leaves extract in *Pleurotus ostreatus* var. florida culture media: effect on mycelial linear growth rate, diameter and growth induction index. *Earth Env Sci T R So.* 1090:012020. doi: 10.1088/1755-1315/1090/1/012020

Wu, X., Sun, Y., Deng, L., Meng, Q., Jiang, X., Bello, A., et al. (2020). Insight to key diazotrophic community during composting of dairy manure with biochar and its role in nitrogen transformation. *Waste Manag.* 105, 190–197. doi: 10.1016/j.wasman.2020.02.010

Wu, S., Zhou, R., Ma, Y., Fang, Y., Xie, G., Gao, X., et al. (2021). Development of a consortium-based microbial agent beneficial to composting of distilled grain waste for *Pleurotus ostreatus* cultivation. *Biotechnol. Biofuels* 14:242. doi: 10.1186/s13068-021-02089-4

Wu, X., Wang, J., Yu, Z., Amanze, C., Shen, L., Wu, X., et al. (2022). Impact of bamboo sphere amendment on composting performance and microbial community succession in food waste composting. *J Environ Manage* 303:114144. doi: 10.1016/j.jenvman.2021.114144

Xu, Z., Li, R., Liu, T., Zhang, G., Wu, S., Xu, K., et al. (2022). Effect of inoculation with newly isolated thermotolerant ammonia-oxidizing bacteria on nitrogen conversion and microbial community during cattle manure composting. *J. Environ. Manag.* 317:115474. doi: 10.1016/j.jenvman.2022.115474

Xu, Z., Ma, Y., Zhang, L., Han, Y., Yuan, J., Li, G., et al. (2021). Relating bacterial dynamics and functions to gaseous emissions during composting of kitchen and garden wastes. *Sci. Total Environ.* 767:144210. doi: 10.1016/j.scitotenv.2020.144210

Yadav, A., Kujur, A., Kumar, A., Singh, P. P., Gupta, V., and Prakash, B. (2020). Encapsulation of *Bunium persicum* essential oil using chitosan nanopolymer: preparation, characterization, antifungal assessment, and thermal stability. *Int. J. Biol. Macromol.* 142, 172–180. doi: 10.1016/j.ijbiomac.2019.09.089

Yang, Y., Awasthi, M. K., Bao, H., Bie, J., Lei, S., and Lv, J. (2020). Exploring the microbial mechanisms of organic matter transformation during pig manure composting amended with bean dregs and biochar. *Bioresour. Technol.* 313:123647. doi: 10.1016/j.biortech.2020.123647

Yang, W., and Zhang, L. (2022). Addition of mature compost improves the composting of green waste. *Bioresour. Technol.* 350:126927. doi: 10.1016/j.biortech.2022.126927

Yoon, S. H., Ha, S. M., Kwon, S., Lim, J., and Chun, J. (2017). Introducing EzBioCloud: a taxonomically united database of 16S rRNA gene sequences and whole-genome assemblies. *Int. J. Syst. Evol. Microbiol.* 67, 1613–1617. doi: 10.1099/ijsem.0.001755

Yu, H., Xie, B., Khan, R., and Shen, G. M. (2019). The changes in carbon, nitrogen components and humic substances during organic-inorganic aerobic co-composting. *Bioresour. Technol.* 271, 228–235. doi: 10.1016/j.biortech.2018.09.088

Zebeli, Q., Aschenbach, J. R., Tafaj, M., Boguhn, J., Ametaj, B. N., and Drochner, W. (2012). Invited review: role of physically effective fiber and estimation of dietary fiber adequacy in high-producing dairy cattle. *J. Dairy Sci.* 95, 1041–1056. doi: 10.3168/jds.2011-4421

Zeng, G., Yu, M., Chen, Y., Huang, D., Zhang, J., Huang, H., et al. (2010). Effects of inoculation with *Phanerochaete chrysosporium* at various time points on enzyme activities during agricultural waste composting. *Bioresour. Technol.* 101, 222–227. doi: 10.1016/j.biortech.2009.08.013

Zhang, S., Xia, T., Wang, J., Zhao, Y., Xie, X., Wei, Z., et al. (2021). Role of *Bacillus* inoculation in rice straw composting and bacterial community stability after inoculation: unite resistance or individual collapse. *Bioresour. Technol.* 337:125464. doi: 10.1016/j.biortech.2021.125464

Zhang, J., Ying, Y., and Yao, X. (2019). Effects of turning frequency on the nutrients of *Camellia oleifera* shell co-compost with goat dung and evaluation of co-compost maturity. *PLoS One* 14:2841. doi: 10.1371/journal.pone.0222841

Zhang, J., Zhang, W. X., Li, S. Z., You, L., Zhang, C., Sun, C. Z., et al. (2013). A two-step fermentation of distillers' grains using *Trichoderma viride* and *Rhodopseudomonas palustris* for fish feed. *Bioprocess Biosyst. Eng.* 36, 1435–1443. doi: 10.1007/s00449-013-0887-5

Zhao, B., Al Rasheed, H., Ali, I., and Hu, S. (2021). Efficient enzymatic saccharification of alkaline and ionic liquid-pretreated bamboo by highly active extremozymes produced by the co-culture of two halophilic fungi. *Bioresour. Technol.* 319:124115. doi: 10.1016/j.biortech.2020.124115

Zhao, Y., Lu, Q., Wei, Y., Cui, H., Zhang, X., Wang, X., et al. (2016). Effect of actinobacteria agent inoculation methods on cellulose degradation during composting based on redundancy analysis. *Bioresour. Technol.* 219, 196–203. doi: 10.1016/j.biortech.2016.07.117

Zhao, X., Wang, F., Fang, Y., Zhou, D., Wang, S., Wu, D., et al. (2020). High-potency white-rot fungal strains and duration of fermentation to optimize corn straw as ruminant feed. *Bioresour. Technol.* 312:123512. doi: 10.1016/j.biortech.2020.123512

Zhong, X. Z., Li, X. X., Zeng, Y., Wang, S. P., Sun, Z. Y., and Tang, Y. Q. (2020). Dynamic change of bacterial community during dairy manure composting process revealed by high-throughput sequencing and advanced bioinformatics tools. *Bioresour. Technol.* 306:123091. doi: 10.1016/j.biortech.2020.123091

Zhou, G., Xu, X., Qiu, X., and Zhang, J. (2019). Biochar influences the succession of microbial communities and the metabolic functions during rice straw composting with pig manure. *Bioresour. Technol.* 272, 10–18. doi: 10.1016/j.biortech.2018.09.135

frontiers | Frontiers in Microbiology

TYPE Original Research
PUBLISHED 04 July 2024
DOI 10.3389/fmicb.2024.1403011

OPEN ACCESS

EDITED BY
Shuhao Huo,
Jiangsu University, China

REVIEWED BY
Hossam H. Azzaz,
National Research Centre, Egypt
Hussein Murad,
National Research Centre, Egypt
Digvijay Verma,
Babasaheb Bhimrao Ambedkar University, India

*CORRESPONDENCE
Liming Lu
✉ lulm@hqu.edu.cn

RECEIVED 18 March 2024
ACCEPTED 25 June 2024
PUBLISHED 04 July 2024

CITATION
Chen K, Deng X, Jiang D, Qin L, Lu M, Jiang W, Yang M, Zhang L, Jiang J and Lu L (2024) Efficient conversion of distillers grains as feed ingredient by synergy of probiotics and enzymes.
Front. Microbiol. 15:1403011.
doi: 10.3389/fmicb.2024.1403011

Efficient conversion of distillers grains as feed ingredient by synergy of probiotics and enzymes

Kai Chen[1,2,3], Xiangrong Deng[1], Dahai Jiang[1,2,3], Lanxian Qin[1], Mengqi Lu[1], Wenxuan Jiang[1,2,3], Manqi Yang[1,2,3], Liangliang Zhang[1,2,3], Jianchun Jiang[1,2,3,4] and Liming Lu[1,2,3]*

[1]Academy of Advanced Carbon Conversion Technology, Huaqiao University, Xiamen, China, [2]Fujian Provincial Key Laboratory of Biomass Low-Carbon Conversion, Huaqiao University, Xiamen, China, [3]College of Chemical Engineering, Huaqiao University, Xiamen, China, [4]Institute of Chemical Industry of Forest Products, Nanjing, China

The direct feeding value of distillers grains is low due to the presence of higher cellulose, lignin and anti-nutritional factors such as mannan and xylan. In this study, complex enzymes and probiotic flora based on "probiotic enzyme synergy" technology were used to produce fermented distillers grains. The optimal substrate ratio, moisture content, fermentation time and temperature were determined. Subsequently, scale-up experiments were conducted to determine the performance of fermented feed. The results showed that multi-probiotic (*Lactobacillus casei*, *Bacillus subtilis*, *Saccharomyces cerevisiae*, and *Aspergillus oryzae*) cooperated with complex enzymes (glucanase, mannanase, xylanase) showed excellent fermentation effect, crude protein, trichloroacetic acid soluble protein and fat increased by 31.25, 36.68, and 49.11% respectively, while crude fiber, acidic fiber and neutral fiber decreased by 34.24, 26.91, and 33.20%, respectively. The anti-nutritional factors mannan and arabinoxylan were reduced by 26.96 and 40.87%, respectively. Lactic acid, acetic acid, and propionic acid in the fermented organic acids increased by 240.93, 76.77, and 89.47%, respectively. Butyric acid increased significantly from scratch, and the mycotoxin degradation effect was not significant. This study provides a potential approach for high-value utilization of distillers grains.

KEYWORDS

distillers grains, fermented feed, probiotics, enzyme, anti-nutritional factors

1 Introduction

The shortage of feed raw materials, especially protein feed, is a huge problem facing the Chinese feed industry (Xiong and Yang, 2021). Liquor grains refer to the by-product produced by microbial fermentation in the industrial production of liquor. Its composition varied according to the crop raw materials such as corn, wheat and sorghum used in brewing and the process conditions used in the brewing process. But in general, distillers grains usually contain a lot of organic matter and have a high nutritional level. It is rich in crude protein and crude fiber, accounting for about 13–27% and 16–28%, respectively. Followed by less ash and fat, accounting for 9–13% and 3–10%, respectively, (Liu, 2011). In 2022, the amount of liquor grain production in China had reached more than 20 million tons. The huge production of distillers

grains has laid a good foundation for the development of the distillers grain resource utilization industry. Although distillers grains have high nutritional value, its high dietary fiber content limits its application in pig breeding. Directly applying distillers grains to pig feed will lead to low digestion efficiency and even cause stress in animals due to anti-nutritional factors in the raw materials, such as mannan, arabinoxylan, and glucan (Kim and Duarte, 2021). Therefore, we need to find an effective method to improve the performance of distillers grains efficiently and enhance its application value in the feed industry.

Many studies have shown that multi-enzymes can have effective effects on feed utilization of non-starch polysaccharides (NSPs), including improving growth and animal health, due to synergistic effects by enzymes. For instance, adding complex multi-enzymes (protease, α-amylase, β-glucanase and xylanase) to the feed of weaned piglets improves the utilization rate and the diversity of hindgut fecal microorganisms (Park et al., 2020). There are also many studies showing that the use of microorganisms for solid-state fermentation can transform miscellaneous meal, optimize its nutritional composition, and improve its feeding value in pig production efficiently. Czech added 8% fermented rapeseed meal to piglet diets, which had a beneficial effect on the immune status of piglets (Czech et al., 2021); *Bacillus subtilis* and *Enterococcus faecalis* were used to conduct two-stage fermentation to improve the digestibility of dry matter and crude protein of corn-soybean meal mixed feed (Shi et al., 2017). The research found that fermented cotton meal feed could improve the feed conversion rate and intestinal barrier function of weaned piglets by regulating intestinal flora (Gu et al., 2021).

Adding probiotics to the diet, in addition to anti-toxin and reduce diarrhea, can also improve the intestinal health and nutrient digestibility of pigs, thereby benefiting the pigs' nutrient utilization and growth performance (Liu et al., 2018). *Aspergillus oryzae*, *Saccharomyces cerevisiae*, *Lactobacillus casei*, and *Bacillus subtilis* are probiotic strains that are allowed to be added to feed according to the "Feed Additive Species Catalog" promulgated by the Ministry of Agriculture and Rural Affairs of China, and can be used to develop a variety of unconventional feed ingredients (Nunes et al., 2018). *Aspergillus oryzae* and *Bacillus subtilis* are aerobic microorganisms, *Saccharomyces cerevisiae* is a facultative anaerobic microorganism, and *Lactobacillus casei* is an anaerobic probiotic. The composite flora could ensure that probiotics were growing and metabolizing vigorously at all stages of fermentation, which improved the performance of feed ingredient fermentation (Ilango and Antony, 2021). However, there are currently few studies on the use of multiple probiotics to ferment white distillers grains with complex enzymes, and the research on the nutritional value of distillers grains co-fermented by probiotics and enzymes is still unclear. Therefore, this article aims to study the effects of nutrients, anti-nutritional factors, mycotoxins using *Aspergillus oryzae*, *Saccharomyces cerevisiae*, *Lactobacillus casei*, *Bacillus subtilis* and complex enzyme reagents to ferment distillers grains, then establish optimal fermentation conditions, in order to open up new areas for developing the pioneering exploration of new stable and functional fermented biological feeds.

2 Materials and methods

2.1 Instruments and reagents

2.1.1 Substrate for fermentation

The fermentation substrates: distillers grains, bran, soybean meal, corn and molasses used in this study were all sourced from the local market and stored at room temperature (about 25°C) in a cool and dark cabinet. The nutritional composition of the fermentation substrate is shown in Table 1.

2.1.2 Probiotics

The probiotics used in this study were *Aspergillus oryzae* (CGMCC No. 18109), *S. cerevisiae* (CGMCC No. 28099), *Lactobacillus casei* (CGMCC No. 8149) and *Bacillus subtilis* (CGMCC No. 8148) were from the laboratory's original collection and stored in China General Microbiological Culture Collection Center (CGMCC). *Aspergillus oryzae* was cultured in modified Marsden medium at 30°C and 200 rpm for 48 h, *Saccharomyces cerevisiae* was cultured in YPD medium at 30°C and 200 rpm for 24 h, *Lactobacillus casei* was cultured in MRS medium at 37°C and 200 rpm for 12 h, and *Bacillus subtilis* was cultured in LB medium at 37°C and 200 rpm for 12 h.

2.1.3 Complex enzyme

The enzyme preparation used in this study is composed of multiple enzymes, including xylanase activity ≥20,000 U/g; β-glucanase activity ≥2,500 U/g; β-mannanase activity ≥600 U/g; fiber enzyme activity ≥800 U/g; amylase activity ≥3,000 U/g.

2.1.4 Instruments and equipment

Kjeldahl nitrogen determination instrument K1100F (Haineng, Shandong, China).

Fiber Digestion Apparatus F2000 (Haineng, Shandong, China).

Fat analyzer SOX606 (Haineng, Shandong, China).

High Performance Liquid Chromatograph 1,260 Infinity II (Agilent, United States).

TABLE 1 Nutrient composition of fermentation substrates.

Sample	Crude protein (CP), %	Crude fiber (CF), %	Fat, %
Distillers grains	19.70	3.42	6.10
Corn	12.10	7.36	7.30
Wheat bran	18.50	3.81	8.20
Soybean meal	37.60	0.94	12.90
Molasses	9.70	0.25	0.80

2.2 Optimization of fermentation substrate ratio

In order to obtain excellent fermentation results, the following experiments were designed to explore the optimal fermentation moisture content and appropriate ratio of the fermentation substrate. The fermentation effect was evaluated based on the crude protein content and acid-soluble protein content after fermentation. The probiotic liquid of *Aspergillus oryzae*: *Saccharomyces cerevisiae*: *Lactobacillus casei*: *Bacillus subtilis* is added in a ratio of 1:1:1:1. The total amount added is 10% of the substrate. The amount of compound enzyme preparation is 1‰ of the substrate. The mixture was stirred evenly, put into one-way valve fermentation bags, and fermented at room temperature (28–33°C) for 5 days.

2.2.1 Suitable moisture content for fermentation

Traditional fermented feed was used 20% corn, 20% soybean meal and 60% wheat bran as substrates, the fermentation effects of the substrates at moisture contents of 10, 30, and 50% were explored.

2.2.2 Fermentation substrate

The 90% bran group was took as a control, the fermentation effect of the substrate under different distillers grains-bran ratios was studied. The fermentation substrate ratio was showed in Table 2.

2.2.3 Optimization of fermentation conditions

In order to determine the material-to-liquid ratio, temperature and time, which were the most important elements in the fermentation, an orthogonal experiment with three factors and three levels was designed using Design-Expert8.0.6 software. Box–Behnken response surface optimization design was used, and the crude protein content after fermentation was used as response, response surface data fitting analysis was conducted to establish optimal fermentation conditions. The orthogonal test factor level table was showed in Table 3. The Box–Behnken response surface optimization design was showed in Table 4.

2.2.4 Distillers grains fermentation experiment under optimized conditions

After a series of previous experiments, the optimal substrate ratio for probiotic-enzyme collaborative fermentation of distillers grains, as well as the fermentation material-to-liquid ratio, temperature and time with the best conversion effect was obtained. Fermentation was carried out again under the optimal fermentation conditions optimized above, and the crude protein, trichloroacetic acid soluble protein, crude fiber, acid detergent fiber, neutral detergent fiber, acid detergent lignin, fat and pH value of the system before and after fermentation were measured to evaluate the transforming effect of probiotic enzyme synergy on the nutrient composition of the system before and after fermentation. Contents of organic acids before and after fermentation, including lactic acid, acetic acid, propionic acid and butyric acid were determined. The anti-nutritional factors of mannan and xylan in the feed before and after fermentation were also determined. In addition, mycotoxins including aflatoxin B1, deoxynivalenol (DON) and zearalenone were measured before and after fermentation.

2.2.5 Determination of nutrients

2.2.5.1 Determination of crude protein and trichloroacetic acid soluble protein

According to GB/T 6432–2018, the Kjeldahl nitrogen determination method is used to determine crude protein and acid-soluble protein. First, the sample is digested at 400°C for 4 h in a digestion instrument. After cooling, it is placed in a KF1100 Kjeldahl nitrogen determination instrument for titration to obtain the nitrogen content. The protein content can be obtained by multiplying the nitrogen content by the conversion factor of 6.25. The crude protein sample is directly digested. Before measuring the acid-soluble protein, 5 g of the sample should be dissolved in 100 mL of 15% trichloroacetic acid solution, shaken at 150 rpm for 30 min, and left to stand for 5 min. The upper solution was centrifuged at 4,000 rpm for 5 min to obtain a supernatant sample and digest it.

2.2.5.2 Determination of fiber content

The filter bag method was used to determine crude fiber, neutral detergent fiber (NAF), acid detergent fiber (NDF) and acid detergent lignin (ADL) according to GB/T 6434–2022. Place the sample in the F2000 fiber digestion instrument and add the corresponding digestion solution according to the different measurement indicators for digestion. Weigh the mass before and

TABLE 2 Fermentation substrate ratio.

Group	Distillers grains, %	Wheat bran, %	Corn, %	Soybean meal, %	Molasses, %
1	35	55	5	3	2
2	45	45	5	3	2
3	55	35	5	3	2
4	65	25	5	3	2
Control	0	90	5	3	2

TABLE 3 Orthogonal test factor level table.

Level	(A) Moisture content, %	(B) Temperature, °C	(C) Time, day
1	1:1.1	28	5
2	1:1	32.5	7
3	1:0.9	37	9

TABLE 4 Box–Behnken response surface optimization design experiment.

Run	(A) Moisture content, %	(B) Temperature, °C	(C) Time, day
7	1:1.1	32.5	9
10	1:1.1	37.0	7
13	1:1	32.5	7
14	1:1.1	32.5	5
15	1:1	37.0	9
11	1:0.9	28.0	7
9	1:1	37.0	5
8	1:1	32.5	7
3	1:1	28.0	5
16	1:1.1	28.0	7
12	1:1	32.5	7
5	1:1	28.0	9
2	1:1	32.5	7
1	1:0.9	32.5	5
4	1:1	32.5	7
17	1:0.9	37.0	7
6	1:0.9	32.5	9

after digestion, and obtain the result based on the difference. According to the formula provided by National Renewable Energy Laboratory (NREL), the hemicellulose content and cellulose content of the sample is obtained: hemicellulose content = acid fiber content − neutral fiber content; cellulose content = acid fiber content − acid lignin content.

2.2.5.3 Determination of fat content

The fat of the sample was determined to use Soxhlet extraction method according to GB/T 6433–2006. Place the sample in the SOX606 fat analyzer, use petroleum ether with a boiling range of 60–80°C for extraction, and extract at 90°C for 6 h. Dry the receiving cup to constant weight, and the fat content of the sample can be obtained from the mass difference before and after measurement.

2.2.6 Determination of anti-nutritional factors

2.2.6.1 Determination of mannan content

The phenol method was used to determine the mannan content. Dissolve the sample in 0.6% sodium hydroxide solution, place in a 75°C water bath for 30 min, cool and filter, and dilute to volume to obtain a sample solution. Take 1 mL of the sample solution and add 1.0 mL of 5% phenol solution. After mixing, add 5.0 mL of concentrated sulfuric acid, shake and mix, place in a boiling water bath for hydrolysis for 20 min, take out and cool, and measure the absorbance value at a wavelength of 490 nm. The standard curve operation is the same. Calculate the mannan content of the sample according to the linear regression equation of the standard curve.

$$\text{Mannan content}\,(\%) = \frac{C \times 10^{-3} \times 0.9 \times 100}{M}$$

In the formula, C is the mannose content (μg/ml) of the sample calculated from the standard curve; M is the sample mass (g); 0.9 is the coefficient for converting mannose into mannan.

2.2.6.2 Determination of arabinoxylan content

The arabinoxylan content was determined by the lichenol-hydrochloric acid method. Weigh about 100 mg of the sample into a 25 mL stoppered test tube, add 2 mL of 2 mol/L HCl, hydrolyze in a boiling water bath (100°C) for 2 h, filter into a 100 mL volumetric flask, and wash the residue with a small amount of distilled water several times (the washing liquid is also added volumetric flask) and dilute to volume (filter to volume). Take 1 mL of hydrolyzate and add 2.0 mL of distilled water, then add 3 mL of 0.1% $FeC1_3$ and 0.3 mL of 1% lichenol, and react in a boiling water bath for 40 min. Take out tap water and cool for 10 min. Use a 1.0 cm cuvette to perform the test at 580 nm and 670 nm wavelengths. Measure the absorbance. For samples whose absorbance exceeds the standard curve, dilute the hydrolyzate to within the range of the standard curve.

$$\text{Xylan content}\,(\%) = \frac{\left[(A - b)/a\right] \times n \times 0.88 \times 100}{m}$$

In the formula, a and b constants (obtained from the regression equation of the standard curve); A is the absorbance difference of the sample at 670 and 580 nm; 0.88 is the polymerization coefficient; n is the dilution factor; m represents the mass.

2.2.7 Determination of organic acids

The determination of organic acids was based on the method of Scherer with slight modifications (Scherer et al., 2012). Weigh 5 g of the sample and add 35 mL of distilled water, shake in a constant

TABLE 5 The influence of different moisture content on fermented traditional feed.

Group (moisture)	CP, %			TCA-SP, %		
	Raw feed	Fermented feed	Change rate	Raw feed	fermented feed	Change rate
1 (10%)	23.78	23.70	−0.3%	2.03	1.74	−14.3%
2 (30%)	23.78	29.88	25.6%	2.03	6.76	233%
3 (50%)	23.78	30.62	28.7%	2.03	12.27	504%

TABLE 6 The influence of different distillers grains-bran ratios on fermented traditional feed.

Group	CP, %			TCA-SP, %		
	Raw feed	fermented feed	Change rate	Raw feed	fermented feed	Change rate
1	21.37	22.77	6.6%	3.11	5.47	75.9%
2	21.44	24.82	15.8%	3.29	5.54	68.3%
3	21.51	22.35	3.9%	3.47	5.70	64.3%
4	21.57	24.50	13.6%	3.65	5.35	46.6%
Control	21.14	22.28	5.4%	2.46	5.53	124.8%

temperature shaking incubator (200 rpm, 4°C), and centrifuge for 15 min (4°C, 10,000 g) after 24 h. The collected supernatant was filtered using a 0.22 micron filter membrane and determined by HPLC (Agilent). The chromatographic column is an Agilent C_{18} column (250 mm × 4.6 mm, 5 μm), the mobile phase A is methanol, and the mobile phase B is 0.02 mol/L NaH_2PO_4 (phosphoric acid adjusts the pH to 2.70). Isogradient elution, the mobile phase is 14% A, 86% B, the running time of a single sample is 25 min, the flow rate is 1 mL/min, the column temperature is 30°C, the detection wavelength is 210 nm, and the injection volume is 20 μL. Standard lactic acid, acetic acid, propionic acid, and butyric acid are all chromatographically pure (sigma).

2.2.8 Determination of mycotoxins

The mycotoxins detected in this experiment: aflatoxin B1, zearalenone, and DON were all measured using PriboFast® ELISA detection kits, which were purchased from Qingdao Pribolab Company.

2.2.9 Data analysis

The data were analyzed by a one-way analysis of variance using the General Linear Models in SPSS20.0 software. Design-Expert8.0.6 software was used to design the response surface optimization experiment and analysis data fitting out the best fermentation conditions. *p*-value of 0.05 was used to indicate of a significant difference. The results are expressed as the means and standard d eviations.

3 Results

3.1 Optimization of fermentation substrate ratio

As shown in Table 5, the effect of water content on fermentation results was explored. When the moisture content was 50% (group 3), the crude protein content increased by 28.7% and the acid-soluble protein content increased by 504%. At this time, the crude protein and acid-soluble protein of the fermented sample increased most significantly.

As shown in Table 6, the impact of different distillers grains-bran ratios on the fermentation effect was explored. The results showed that the crude protein of group 2 increased by 15.8% after fermentation, and the crude protein improvement effect was the best. The acid-soluble protein in group 1 increased by 75.9% compared with that before fermentation, and the acid-soluble protein in experimental group 2 increased by 68.3% compared with that before fermentation. Group 1 and 2 performed excellently. The ratio of experimental group 2 (45% distillers grains, 45% wheat bran, 5% corn, 3% soybean meal, and 2% molasses) was selected as the substrate ratio for subsequent experiments.

3.2 Fermentation condition response surface optimization results

CP content of 17 fermented groups designed by Box–Behnken response surface optimization were showed in Table 7. The CP content of Run 13 is the highest in the 17 fermented groups, 17.06%.

Figure 1 showed the interaction between different variables, and Design-Expert software gave the fitting formula $Y = -298.17703 + 10.91006 \times A + 0.40698 \times B - 1.18813 \times C + 0.00444444 \times AB + 0.016875 \times AC + 0.017500 \times BC - 0.097375 \times A^2 - 0.012321 \times B^2 - 0.024250 \times C^2$, A is the moisture content, B is the temperature, and C is the fermentation time. Among them, the relationship between temperature and material-liquid ratio, time and material-liquid ratio is significant, but the relationship between temperature and time is not obvious. According to the Design-Expert software prediction, the fermentation effect is best when the moisture content of the fermentation system is 57.35%, the temperature is 31.81°C, and the time is 6.98 days. The predicted value of crude protein content at this time is 17.01%, and the credibility is 95%.

TABLE 7 Response surface optimization design experimental results.

Run	(A) Moisture content, %	(B) Temperature, °C	(C) Time, day	CP, %
7	1:1.1	32.5	9	16.78
10	1:1.1	37.0	7	16.37
13	1:1	32.5	7	17.06
14	1:1.1	32.5	5	16.99
15	1:1	37.0	9	16.38
11	1:0.9	28.0	7	16.95
9	1:1	37.0	5	16.41
8	1:1	32.5	7	16.95
3	1:1	28.0	5	16.51
16	1:1.1	28.0	7	17.02
12	1:1	32.5	7	16.12
5	1:1	28.0	9	16.21
2	1:1	32.5	7	16.42
1	1:0.9	32.5	5	16.61
4	1:1	32.5	7	16.73
17	1:0.9	37.0	7	16.66
6	1:0.9	32.5	9	16.81

3.3 Amplify experimental results

Based on the optimal fermentation results obtained from response surface analysis, some modifications were made to comply with actual production conditions. It was finally determined that the water content was 57% (the material-to-liquid ratio was 1:1), 31.8°C, and 7 days as the conditions for scale-up production. And a series of indicators of the distillers grains after the amplification experiment were tested to determine whether the feeding value of the fermented distillers grains has been improved.

3.4 Nutrient analysis

As shown in Table 8, the crude protein content of distillers grains after fermentation significantly increased from 15.55 to 20.41%, an increase of 31.25%, and the acid-soluble protein content increased from 1.99 to 2.72%, an increase of 36.68%. The fat content of distillers grains after fermentation is 4.19%, which is 49% higher than 2.81% before fermentation. The difference is extremely significant. In this study, the *CF*, NAF, NDF, and ADL contents before fermentation were 24.65, 59.82, 34.10, and 12.46%, respectively. The cellulose content and hemicellulose content before fermentation were 21.64 and 25.72%, respectively. These complex polysaccharides can be degraded into simple sugars by enzymes and microorganisms. After fermentation, the crude fiber content of distillers grains was 43.72%, a significant decrease of 34%. After fermentation, the NAF, NDF, and ADL contents were 43.72, 22.78, and 8.68% respectively, all of which showed significant decreases, with respective decreases of 26.91, 33.20, and 30.34%. The converted cellulose content was 14.1%, a decrease of 34.84%; the hemicellulose content after fermentation was 20.98%, a decrease of 16.41%. The pH of the lees dropped from 6.16 before fermentation to 4.23, and the difference was extremely significant.

3.5 Analysis of anti-nutritional factors

The analysis of anti-nutritional factors was showed in Table 9, the mannan content decreased from 12.09 to 8.83% after fermentation, a decrease of 26.96% that indicated the difference was extremely significant, and the arabinoxylan content decreased from 4.82 to 2.85% after fermentation, a decrease of 40.87% that indicated the difference is significant.

3.6 Analysis of organic acids

As shown in Figure 2, The retention time of lactic acid is 3.886 min, that of acetic acid is 4.197 min, that of propionic acid is 7.665 min, and that of butyric acid is 18.391 min. Due to the complex composition of the sample, it is difficult to separate each peak shape and determine the retention time of the organic acid in feed samples completely. The organic acid peak elution time of samples before and after fermentation can be determined by adding a standard mixture of known concentration to the sample as an internal standard.

As shown in Table 10, the organic acid (lactic acid, acetic acid, propionic acid and butyric acid) contents of the samples after fermentation increased significantly. The lactic acid content increased from 2.59 mg/g before fermentation to 8.83 mg/g, an increase of 240.93%. The acetic acid content increased from 3.10 mg/g before fermentation to 5.48 mg/g, an increase of 76.77%. The content of propionic acid after fermentation was 1.80 mg/g, which was 89.47% higher than the 0.95 mg/g before fermentation. Butyric acid was not detected before fermentation, and the butyric acid content after fermentation was 0.51 mg/g.

3.7 Mycotoxin analysis

As shown in Table 11, the contents of DON and Aflatoxin B1 in distillers grains before and after fermentation have almost no change, but

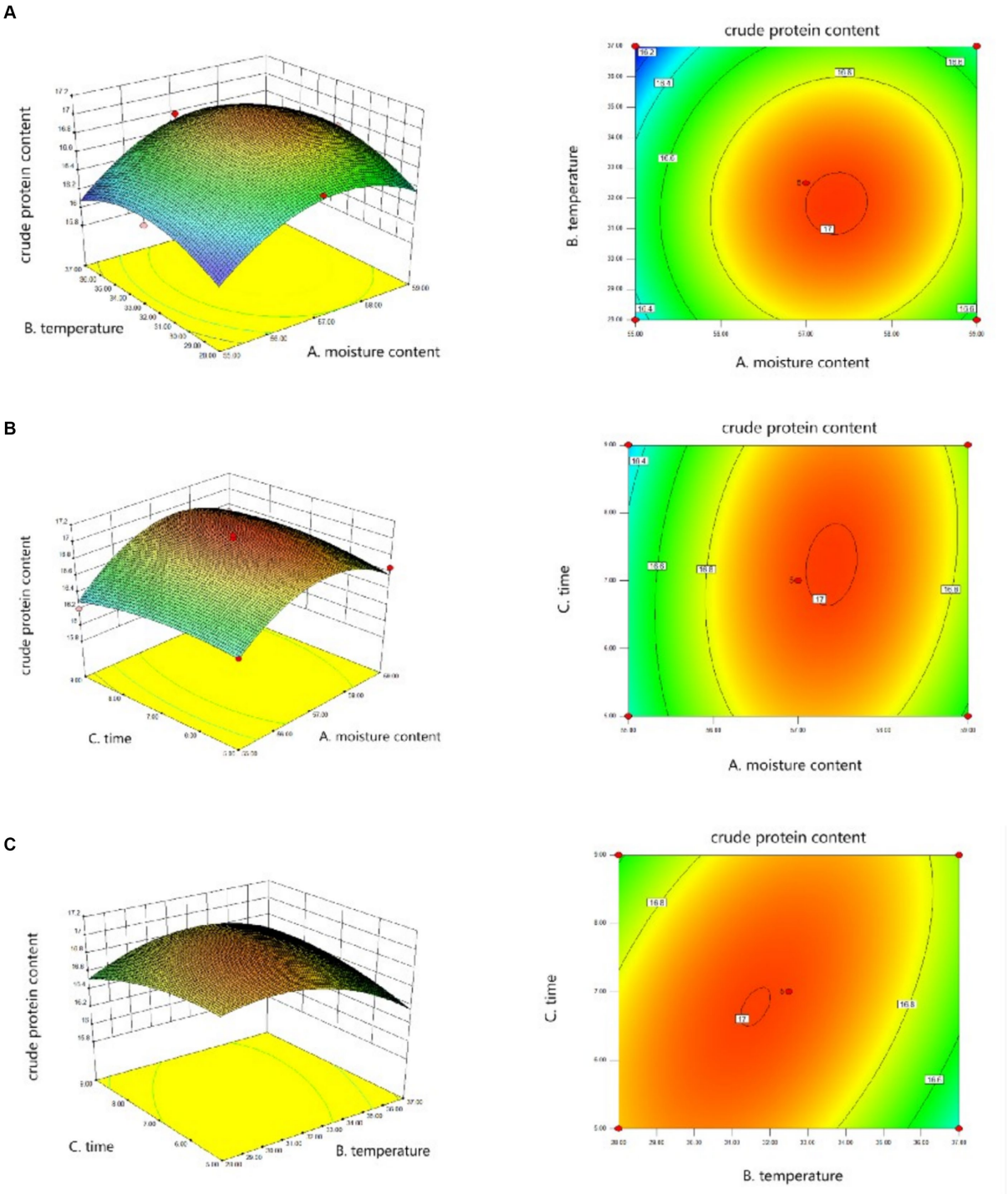

FIGURE 1
Response surface data fitting diagram. **(A)** Surface and contour plots of the interaction effect of moisture content and temperature on crude protein content. **(B)** Surface and contour plots of the interaction effect of moisture content and time on crude protein content. **(C)** Surface and contour plots of the interaction effect of temperature and time on crude protein content.

the DON and Aflatoxin B1 in feed after fermentation are both within the scope of the national feed safety standards, and the national standards are 5,000 and 30 μg/kg, respectively. The zearalenone content after fermentation decreased from 8.70 to 6.80 μg/kg compared with before fermentation. Although the difference was not significant, it showed a decreasing trend, the content of mycotoxin before and after fermentation was within the national safety standard of 1,000 μg/kg (Gong et al., 2017).

4 Discussion

During the fermentation process, microorganisms are very sensitive to temperature and moisture. Normally, *Aspergillus oryzae* and *Saccharomyces cerevisiae* maintain vigorous vitality at 28–30°C, while the optimal growth temperature of *Lactobacillus casei* and *Bacillus subtilis* is generally 37°C (Alonso, 2016). The

TABLE 8 Effect of fermentation on the concentration of nutrients.

Item, %	Group			*P*-value
	Raw mixed feed	Fermented feed	Change rate	
CP	15.55 ± 0.11	20.41 ± 0.16	31.25%	<0.001
TCA-SP	1.99 ± 0.13	2.72 ± 0.27	36.68%	0.039
Fat	2.81 ± 0.27	4.19 ± 0.38	49.11%	<0.001
CF	24.65 ± 0.15	16.21 ± 0.26	−34.24%	0.007
NAF	59.82 ± 0.79	43.72 ± 2.08	−26.91%	0.003
NDF	34.10 ± 2.55	22.78 ± 0.15	−33.20%	<0.001
ADL	12.46 ± 1.01	8.68 ± 0.74	−30.34%	<0.001
pH	6.16 ± 0.17	4.23 ± 0.05	−31.33%	<0.001

TABLE 9 Effect of fermentation on the concentration of anti-nutritional factors.

Antinutritional factors, μg/mL	Group			*P*-value
	Raw mixed feed	Fermented feed	Change rate	
Mannan	12.09 ± 0.89	8.83 ± 0.55	−26.96%	<0.001
Arabinoxylan	4.82 ± 1.34	2.85 ± 1.03	−40.87%	0.025

four probiotic strains used in this study have different suitable growth environments. When the temperature is 28 and 37°C, the response of fermentation is not as good as that at 32.5°C. At 32.5°C, all the four strains grew under relatively mild conditions. Although this strains were not grown under their respective optimal growth temperatures, they showed the ability to degrade polysaccharides such as cellulose and convert them into proteins through metabolism. The material-to-liquid ratio, that is, the moisture content, affects the fermentation significantly. High moisture reduces the porosity of the matrix, promotes particle aggregation and inhibits gas exchange. Conversely, low moisture can negatively impact microbial metabolism by reducing the stability of extracellular enzymes and limiting nutrient solubility (Ezeilo et al., 2019). Although the correlation between fermentation time and temperature is not significant, it is also an important factor affecting the fermentation results. The fermentation time of 7 days is better than that of 5 and 9 days. This maybe because the growth rate of the mold was slow resulting the growth of *Aspergillus oryzae* had not reached its optimal state at 5 days (Zuo et al., 2023). The insufficient biomass leads to insufficient protein conversion ability. At 9 days, it may be because the fermentation time is too long, resulting in too much biomass, which competes for substrates to maintain the growth and development of the probiotic, and part of the transformed nutrients are consumed and wasted by the probiotic. Liu optimized a better distiller's grain fermentation process through single factor and orthogonal experiments, and found that the fermented distiller's grain produced under these conditions has better feeding value (Liu et al., 2023). Therefore, the above-mentioned suitable fermentation conditions are conducive to the production of high-quality and stable fermented feed.

Ibarruri reported that the natural protein in distillers grains increased by 18–24% through SSF in 7 days (Ibarruri et al., 2019), lower than in this research, indicating that the probiotic-enzyme collaborative fermentation technology used in this study had good ability to improve the nutritional value of distillers grains. During the fermentation process, microorganisms may degrade polysaccharides in distillers grains into monosaccharides or oligosaccharides, Therefore, DDGS often contain higher concentrations of non-fermentable components such as fats and proteins, which is consistent with the previous report of Rho et al. (2020). Liu et al. (2023) reported a study on the use of microbial flora to degrade crude fiber of distillers grains. The results showed that the conversion rates of cellulose and hemicellulose were 19.64 and 10.88%, respectively. Astudillo-Neira et al. (2022) reported that carbohydrates from lignocellulosic feed can be released by fungi for fermentation. Datsomor et al. (2022) reported that the *P. ostreatus* treated straw had a lower lignin content (3.3%) compared to the *P. chrysosporium* (6.2%) with the raw straw recording the 8.2% lignin fraction. Wei et al. (2023) reported that under the optimal parameters for fungal fermentation of *Codonopsis pilosula* straw, the cellulose degradation rate and lignin degradation rate reached 13.65 and 10.73%, respectively. These reports are consistent with our research results, proving that cellulose, hemicellulose and lignin in distillers grains can be degraded by microorganisms into simple sugars such as glucose and xylose. The pH after fermentation is significantly lower than before fermentation. A lower pH value can inhibit the growth of miscellaneous probiotic and reduce the adverse effects on the fermentation effect. At the same time, a lower pH value can improve the palatability of the feed (Nguyen et al., 2020). This may be due to the fact that *Lactobacillus casei* fermentation produces a large amount of lactic acid during the fermentation process, which plays a crucial role in quickly lowering the pH, and acetic acid, propionic acid and butyric acid are also produced after fermentation, which can all lower the pH.

The reason why the anti-nutritional factors showed a significant decrease was the addition of 0.1% complex enzyme, which included mannanase and arabinoxylanase, which had a directional degradation effect on these two anti-nutritional factors (Zangaro et al., 2019).

10.3389/fmicb.2024.1403011

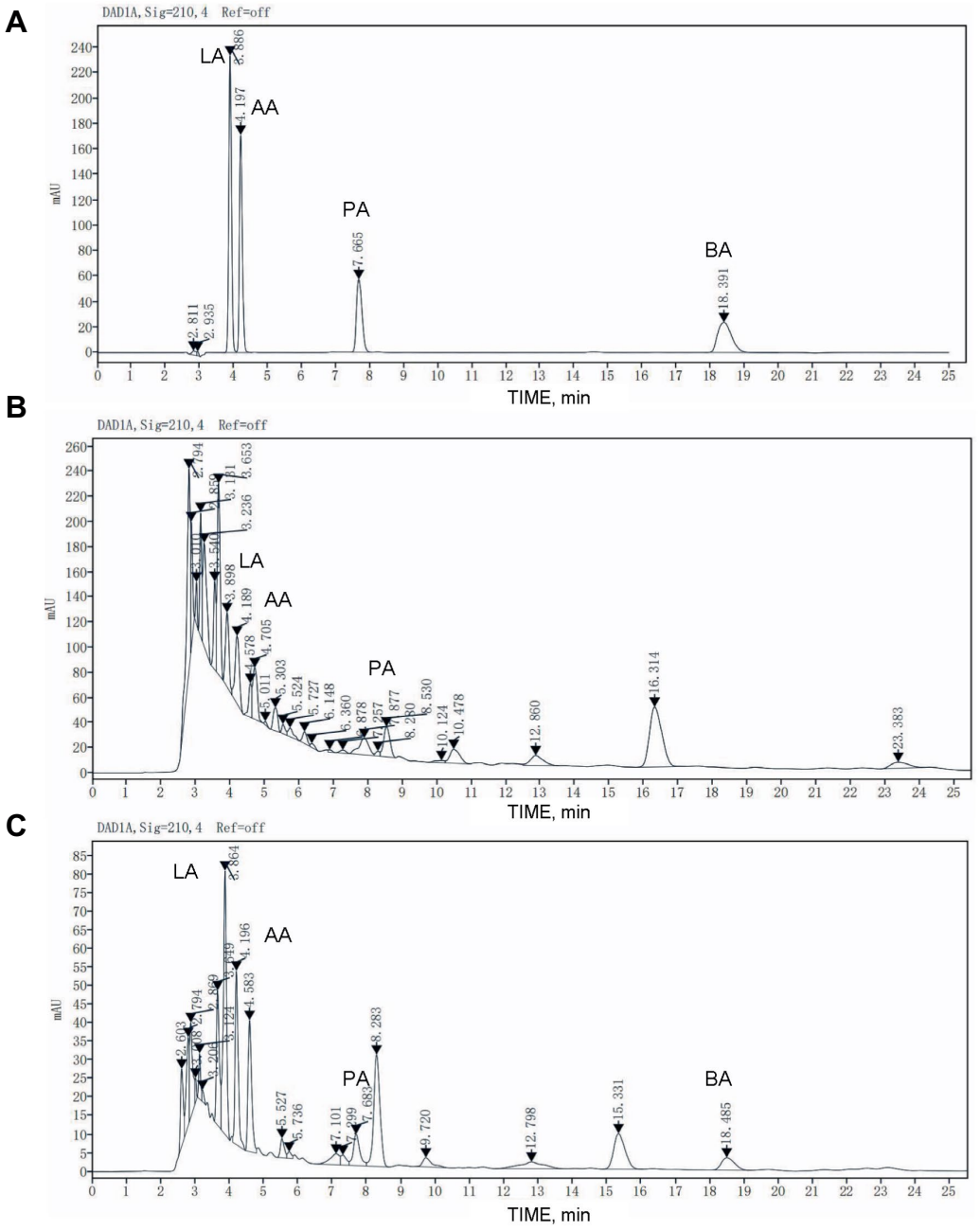

FIGURE 2
HPLC chromatogram of organic acid in the raw feed and fermented feed. **(A)** The chromatogram of organic acid standard substance. **(B)** The raw feed. **(C)** The fermented feed. LA, lactic acid; AA, acetic acid; PA, propionic acid; BA, butyric acid.

TABLE 10 **Effect of fermentation on the concentration of organic acids.**

Organic acid, mg/g	Group			*P*-value
	Raw mixed feed	Fermented feed	Change rate	
Lactic	2.59 ± 0.01	8.83 ± 0.03	240.93%	<0.001
Acetic	3.10 ± 0.03	5.48 ± 0.01	76.77%	<0.001
Propionic	0.95 ± 0.01	1.80 ± 0.01	89.47%	<0.001
Butyric	ND	0.51 ± 0.01		<0.001

TABLE 11 Effect of fermentation on the concentration of mycotoxins.

Mycotoxin, μg/kg	Group			*P*-value
	Raw mixed feed	Fermented feed	The limit standard	
DON	998.27 ± 18.69	1007.87 ± 14.20	<5,000	0.34
Aflatoxin B1	10.53 ± 2.69	10.63 ± 0.97	<30	0.944
Zearalenone	8.70 ± 2.15	6.80 ± 2.77	<1,000	0.405

However, the effect of adding complex enzymes exclusively was not significant generally due to the solid-state fermentation. According to the research of Kapoor et al. (2019), the efficiency of enzymatic hydrolysis increases with the increase of enzyme loading and decreases with the increase of solid loading. It is speculated that among the four strains of probiotics added in this experiment, some strains had the ability to degrade polysaccharides such as mannan and arabinoxylan. This also shows that the synergistic effect of probiotic and enzymes on improving the properties of distillers grains is better than that of adding enzyme preparations only.

The lactic to acetic ratio (the ratio of lactic acid content to acetic acid content) is an important indicator for evaluating the fermentation effect of feed. It is generally believed that the fermentation is abnormal when the ratio is less than 1 (Canibe et al., 2010). The ratio of lactic to acetic in this experiment increased from 0.83 to 1.61 after fermentation. *Lactobacillus casei* fermentation produces a large amount of lactic acid, which plays a vital role in lowering pH rapidly, thereby inhibiting the growth of aerobic harmful probiotic and mold and reducing nutrient loss. The increase in acetic acid content during the fermentation process is beneficial to improving the aerobic stability of the fermentation process and inhibiting the reproduction of some undesirable probiotic (Kim and Lee, 2021). We believed that the fermented distillers grains at this time have a lower pH value, which can inhibit the contamination of miscellaneous probiotic, and the lactic acid has a special fragrance and acidic taste, which is beneficial to enhancing the feed's palatability and animals' willingness to ingestion (Yang et al., 2006). Propionic acid is one of the metabolites of pig intestinal microorganisms. It plays an important role in regulating body health and metabolism, such as anti-inflammatory factors. It can enhance intestinal health and function, growth performance and overall health in many aspects, and is often used in the mildew-proof (Longpré et al., 2016). Butyric acid plays an energy supply role in the hind intestine of pigs, and can also significantly reduce the pH value of the intestine, significantly reduce the number of harmful probiotic such as *Escherichia coli* and *Salmonella*, and improve the diarrhea problem of weaned piglets. However, butyric acid is easily oxidized and denatured, producing a pungent odor. A trace amount of butyric acid was produced after fermentation in this experiment, which had no significant impact on the aromatic smell of the fermented feed (Słupecka-Ziemilska et al., 2022; Uddin et al., 2023). Biagi et al. (2007) reported that adding a small amount of butyric acid as a feed additive to the feed can improve the microbial intestinal flora of piglets and immune system.

There was almost no change in the contents of DON and Aflatoxin B1 in the distillers grains before and after fermentation, indicating that the strain may lack the ability to degrade the above two toxins or the toxin content is too low, resulting in insignificant fermentation degradation effect. The content of zearalenone showed a decreasing trend after fermentation. In short, although fermentation has no significant effect on reducing mycotoxins, the mycotoxin indicators after fermentation are within the range of national standards (DON<5,000 μg/kg, Aflatoxin B1 < 30 μg/kg, zearalenone<1,000 μg/kg), so fermented distillers grains can be considered safe and harmless as feed (Binder et al., 2007).

5 Conclusion

Distillers grains are an agricultural and sideline product with high feeding potential. The synergistic solid-state fermentation technology of probiotic enzymes can effectively improve the feeding performance of distillers grains. Under the fermentation conditions of 57% moisture content, 31.8°C, and 7 days, the fermented mixed feed showed the highest crude protein content, the anti-nutritional factors were reduced significantly, the organic acid content was increased significantly, and the performance as a feed material was greatly improved. This study provides a potential way for the high-value development of distillers grains.

Data availability statement

The raw data supporting the conclusions of this article will be made available by the authors, without undue reservation.

Author contributions

KC: Data curation, Investigation, Writing – original draft. XD: Writing – review & editing, Investigation, Methodology. DJ: Writing – review & editing, Validation. LQ: Writing – review & editing, Investigation. ML: Writing – review & editing, Investigation. MY: Writing – review & editing, Software. WJ: Writing – review & editing, Software. LZ: Writing – review & editing, Project administration. JJ: Conceptualization, Writing – review & editing, Supervision. LL: Supervision, Writing – review & editing, Project administration.

Funding

The author(s) declare that financial support was received for the research, authorship, and/or publication of this article. This work was supported by the FuXiaQuan Self-created Zone Collaborative Project (3502ZCQXT2023001), Nanping Science and Technology

Plan Project (N2022B001), Central Government Guides Local Scientific and Technological Development Project (2023 L3058), Xiamen Science and Technology Commissioner Project (2023KTP08), Xiamen Science and Technology Plan Project (3502Z20226033), and Scientific Research Funds of Huaqiao University (22BS134).

Acknowledgments

We would like to thank the editor and reviewers for their valuable contributions to this special topic. We would like to thank Instrumental Analysis Center of Huaqiao University for providing the instrument of HPLC (Agilent 1260 Infinity II).

Conflict of interest

The authors declare that the research was conducted in the absence of any commercial or financial relationships that could be construed as a potential conflict of interest.

Publisher's note

All claims expressed in this article are solely those of the authors and do not necessarily represent those of their affiliated organizations, or those of the publisher, the editors and the reviewers. Any product that may be evaluated in this article, or claim that may be made by its manufacturer, is not guaranteed or endorsed by the publisher.

References

Alonso, S. (2016). Novel preservation techniques for microbial cultures. *Novel Ferment. Technol.*, 7–33. doi: 10.1007/978-3-319-42457-6_2

Astudillo-Neira, R., Muñoz-Nuñez, E., Quiroz-Carreno, S., Avila-Stagno, J., and Alarcon-Enos, J. (2022). Bioconversion in ryegrass-fescue hay by pleurotus ostreatus to increase their nutritional value for ruminant. *Agriculture* 12:534. doi: 10.3390/agriculture12040534

Biagi, G., Piva, A., Moschini, M., Vezzali, E., and Roth, F. X. (2007). Performance, intestinal microflora, and wall morphology of weanling pigs fed sodium butyrate. *J. Anim. Sci.* 85, 1184–1191. doi: 10.2527/jas.2006-378

Binder, E. M., Tan, L. M., Chin, L. J., Handl, J., and Richard, J. (2007). Worldwide occurrence of mycotoxins in commodities, feeds and feed ingredients. *Anim. Feed Sci. Tech.* 137, 265–282. doi: 10.1016/j.anifeedsci.2007.06.005

Canibe, N., Pedersen, A. Ø., and Jensen, B. B. (2010). Impact of acetic acid concentration of fermented liquid feed on growth performance of piglets. *Livest. Sci.* 133, 117–119. doi: 10.1016/j.livsci.2010.06.040

Czech, A., Grela, E. R., and Kiesz, M. (2021). Dietary fermented rapeseed or/and soybean meal additives on performance and intestinal health of piglets. *Sci. Rep.* 11:16952. doi: 10.1038/s41598-021-96117-w

Datsomor, O., Gou-Qi, Z., and Miao, L. (2022). Effect of ligninolytic axenic and coculture white-rot fungi on rice straw chemical composition and in vitro fermentation characteristics. *Sci. Rep.* 12:1129. doi: 10.1038/s41598-022-05107-z

Ezeilo, U. R., Lee, C. T., Huyop, F., Zakaria, I. I., and Wahab, R. A. (2019). Raw oil palm frond leaves as cost-effective substrate for cellulase and xylanase productions by Trichoderma asperellum UC1 under solid-state fermentation. *J. Environ. Manag.* 243, 206–217. doi: 10.1016/j.jenvman.2019.04.113

Gong, Y., Li, F., and Routledge, M. N. (2017). Mycotoxins in China: occurrence and exposure. *Food Saf. China*, 83–101. doi: 10.1002/9781119238102.ch7

Gu, X., Li, Z., Li, H., and Ma, X. (2021). Fermented cottonseed meal as a partial replacement for soybean meal could improve the growth performance, immunity and antioxidant properties, and nutrient digestibility by altering the gut microbiota profile of weaned piglets. *Front. Microbiol.* 12:734389. doi: 10.3389/fmicb.2021.734389

Ibarruri, J., Cebrián, M., and Hernández, I. (2019). Solid state fermentation of brewer's spent grain using Rhizopus sp. to enhance nutritional value. *Waste Biomass Valori.* 10, 3687–3700. doi: 10.1007/s12649-019-00654-5

Ilango, S., and Antony, U. (2021). Probiotic microorganisms from non-dairy traditional fermented foods. *Trends Food Sci. Tech.* 118, 617–638. doi: 10.1016/j.tifs.2021.05.034

Kapoor, M., Semwal, S., Satlewal, A., Christopher, J., Gupta, R. P., Kumar, R., et al. (2019). The impact of particle size of cellulosic residue and solid loadings on enzymatic hydrolysis with a mass balance. *Fuel* 245, 514–520. doi: 10.1016/j.fuel.2019.02.094

Kim, S. W., and Duarte, M. E. (2021). Understanding intestinal health in nursery pigs and the relevant nutritional strategies. *Anim. Biosci.* 34, 338–344. doi: 10.5713/ab.21.0010

Kim, J. H., and Lee, S. Y. (2021). Effect of NaCl addition on the antibacterial effectiveness of acetic acid and its salts against pathogenic bacteria. *Food Control* 123:107704. doi: 10.1016/j.foodcont.2020.107704

Liu, K. (2011). Chemical composition of distillers grains, a review. *J. Agric. Food. Chem.* 59, 1508–1526. doi: 10.1021/jf103512z

Liu, J., Wang, S., Wang, Z., Shen, C., Liu, D., Shen, X., et al. (2023). Pretreatment of Luzhou distiller's grains for feed protein production using crude enzymes produced by a synthetic microbial consortium. *Bioresour. Technol.* 390:129852. doi: 10.1016/j.biortech.2023.129852

Liu, W. C., Ye, M., Liao, J. H., Zhao, Z. H., Kim, I. H., and An, L. L. (2018). Application of complex probiotics in swine nutrition–a review. *Ann. Anim. Sci.* 18, 335–350. doi: 10.2478/aoas-2018-0005

Longpré, J., Fairbrother, J. M., Fravalo, P., Arsenault, J., LeBel, P., Laplante, B., et al. (2016). Impact of mash feeding versus pellets on propionic/butyric acid levels and on total Escherichia coli load in the gastrointestinal tract of growing pigs. *J. Anim. Sci.* 94, 1053–1063. doi: 10.2527/jas.2015-9617

Nguyen, D. H., Seok, W. J., and Kim, I. H. (2020). Organic acids mixture as a dietary additive for pigs—a review. *Animals* 10:952. doi: 10.3390/ani10060952

Nunes, C. S., Kunamneni, A., Kumar, V., and Habte-Tsion, H. M. (2018). Registration of food and feed additives (enzymes) in the United States, Canada, and China. *Enzym. Hum. Anim. Nutr.*, 457–480. doi: 10.1016/B978-0-12-805419-2.00024-1

Park, S., Li, W., St-Pierre, B., Wang, Q., and Woyengo, T. A. (2020). Growth performance, nutrient digestibility, and fecal microbial composition of weaned pigs fed multi-enzyme supplemented diets. *J. Anim. Sci.* 98:skaa306. doi: 10.1093/jas/skaa306

Rho, Y., Patterson, R., Joye, I., Martinez, M., Squires, E. J., and Kiarie, E. G. (2020). Fiber degrading enzymes increased monosaccharides release and fermentation in corn distillers dried grains with solubles and wheat middlings steeped without or with protease. *Transl. Anim. Sci.* 4:txaa153. doi: 10.1093/tas/txaa153

Scherer, R., Rybka, A. C. P., Ballus, C. A., Meinhart, A. D., Teixeira Filho, J., and Godoy, H. T. (2012). Validation of a HPLC method for simultaneous determination of main organic acids in fruits and juices. *Food Chem.* 135, 150–154. doi: 10.1016/j.foodchem.2012.03.111

Shi, C., Zhang, Y., Lu, Z., and Wang, Y. (2017). Solid-state fermentation of corn-soybean meal mixed feed with *Bacillus subtilis* and *Enterococcus faecium* for degrading antinutritional factors and enhancing nutritional value. *J. Anim. Sci. Biotechnol.* 8, 50–59. doi: 10.1186/s40104-017-0184-2

Słupecka-Ziemilska, M., Pierzynowski, S. G., Szczurek, P., Pierzynowska, K., Wychowański, P., Seklecka, B., et al. (2022). Milk formula enriched with sodium butyrate influences small intestine contractility in neonatal pigs. *Nutrients* 14:4301. doi: 10.3390/nu14204301

Uddin, M. K., Mahmud, M. R., Hasan, S., Peltoniemi, O., and Oliviero, C. (2023). Dietary micro-fibrillated cellulose improves growth, reduces diarrhea, modulates gut microbiota, and increases butyrate production in post-weaning piglets. *Sci. Rep.* 13:6194. doi: 10.1038/s41598-023-33291-z

Wei, T., Chen, H., Wu, D., Gao, D., Cai, Y., Cao, X., et al. (2023). Response surface methodology for the mixed fungal fermentation of *Codonopsis pilosula* straw using Trichoderma reesei and Coprinus comatus. *PeerJ.* 11:e15757. doi: 10.7717/peerj.15757

Xiong, X. Z., and Yang, C. (2021). Re-recognition of China's food security: supply and demand status,self-sufficiencylevel and guarantee strategy of feed grain. *World Agric.* 2021:4-12+32+119. doi: 10.13856/j.cn11-1097/s.2021.08.001

Yang, S. Y., Ji, K. S., Baik, Y. H., Kwak, W. S., and McCaskey, T. A. (2006). Lactic acid fermentation of food waste for swine feed. *Bioresour. Technol.* 97, 1858–1864. doi: 10.1016/j.biortech.2005.08.020

Zangaro, C. A., Patterson, R., and Woyengo, T. A. (2019). Porcine in vitro digestion and fermentation characteristics of corn wet distillers' grains and dried distillers grains with solubles without or with multi-enzyme. *Anim. Feed Sci. Tech.* 254:114205. doi: 10.1016/j.anifeedsci.2019.114205

Zuo, H., Ji, L., Pan, J., Chen, X., Gao, C., Liu, J., et al. (2023). Engineering growth phenotypes of aspergillus oryzae for L-malate production. *Bioresour. Bioprocess.* 10:25. doi: 10.1186/s40643-023-00642-7

frontiers | Frontiers in Microbiology

TYPE Original Research
PUBLISHED 10 July 2024
DOI 10.3389/fmicb.2024.1409697

OPEN ACCESS

EDITED BY
Qi Zhang,
Nanchang University, China

REVIEWED BY
Eliane Ferreira Noronha,
University of Brasilia, Brazil
Tao Peng,
Shantou University, China

*CORRESPONDENCE
Kun Zhang
zk@yzu.edu.cn
Hua Li
lihua@njau.edu.cn

†These authors have contributed equally to this work

RECEIVED 30 March 2024
ACCEPTED 27 June 2024
PUBLISHED 10 July 2024

CITATION
Ma D, Chen H, Liu D, Feng C, Hua Y, Gu T, Guo X, Zhou Y, Wang H, Tong G, Li H and Zhang K (2024) Soil-derived cellulose-degrading bacteria: screening, identification, the optimization of fermentation conditions, and their whole genome sequencing.
Front. Microbiol. 15:1409697.
doi: 10.3389/fmicb.2024.1409697

Soil-derived cellulose-degrading bacteria: screening, identification, the optimization of fermentation conditions, and their whole genome sequencing

Degao Ma[1†], Haoyu Chen[2†], Duxuan Liu[2], Chenwei Feng[2], Yanhong Hua[2], Tianxiao Gu[2], Xiao Guo[2], Yuchen Zhou[3], Houjun Wang[1], Guifeng Tong[1], Hua Li[4]* and Kun Zhang[2,5]*

[1]Yangzhou Environmental Monitoring Center of Jiangsu Province, Yangzhou, China, [2]College of Plant Protection, Yangzhou University, Yangzhou, China, [3]Department of Pharmacy, Medical School of Yangzhou University, Yangzhou University, Yangzhou, China, [4]College of Engineering, Nanjing Agricultural University, Nanjing, China, [5]Joint International Research Laboratory of Agriculture and Agri-Product Safety of Ministry of Education of China, Yangzhou University, Yangzhou, China

Straw cellulose is an abundant renewable resource in nature. In recent years, the conversion of cellulose from waste straw into biofuel by specific microorganisms' fragmentation has attracted extensive attention. Although many bacteria with the ability to degrade cellulose have been identified, comprehensive bioinformatics analyses of these bacteria remain limited, and research exploring optimal fragmentation conditions is scarce. Our study involved the isolation and screening of bacteria from various locations in Yangzhou using carboxymethyl cellulose (CMC) media. Then, the cellulose-degrading bacteria were identified using 16S rRNA and seven candidate bacterial strains with cellulose degrading ability were identified in Yangzhou city for the first time. The cellulase activity was determined by the 3,5-dinitrosalicylic acid (DNS) method in different fragmentation conditions, and finally two bacteria strains with the strongest cellulose degradation ability were selected for whole genome sequencing analysis. Sequencing results revealed that the genome sizes of *Rhodococcus wratislaviensis* YZ02 and *Pseudomonas Xanthosomatis* YZ03 were 8.51 Mb and 6.66 Mb, containing 8,466 and 5,745 genes, respectively. A large number of cellulose degradation-related genes were identified and annotated using KEGG, GO and COG analyses. In addition, genomic CAZyme analysis indicated that both *R. wratislaviensis* YZ02 and *P. Xanthosomatis* YZ03 harbor a series of glycoside hydrolase family (GH) genes and other genes related to cellulose degradation. Our finding provides new options for the development of cellulose-degrading bacteria and a theoretical basis for improving the cellulose utilization of straw.

KEYWORDS

cellulose degrading, soil bacterial, Cellulase activity assays, whole genome sequencing, glycoside hydrolase family genes

Introduction

Straw, a renewable resource rich in organic matter and possessing high recycling value, plays a crucial role in sustainable agricultural practices (Li, 2010). Integrating straw back into the fields has proven to be an effective environmental strategy, particularly for farmers in the Yangtze River basin. This approach enhances the soil's physical and chemical properties, increases organic matter content, and ultimately boosts crop yields (Hui-juan and Xia-li, 2018). However, soils enriched with organic matter can exacerbate airborne vegetable diseases, indirectly diminishing the quality of agricultural products through toxic metabolites (Xie et al., 2022). As the grain production increases yearly in China (Wang et al., 2018), so does the straw production. Large amount of the straw was left after harvesting of the crops in the field, and only a small portion of crop straw was further processed for animal feed, household fuel, soil amendment, industrial material (Shi et al., 2023). Most crop straw was wasted in the field, which named for returning the straw back to the field for degradation and production for organic matter. Straw does not decompose easily under natural conditions for their dense cross-linking of chemical bond between the cellulose, hemicellulose, and lignin (Yang et al., 2022). Direct burning of straw is the simplest and most common method, but the smoke and dust produced by burning seriously increase greenhouse gas emissions (Han et al., 2023), and damage the atmospheric environment where people lives (Xin-Yu et al., 2020). Consequently, the development of efficient straw degradation strategies becomes imperative for both high-quality agricultural advancement and environmental preservation (Liu and Han, 2021).

Straw is composed of lignin, cellulose and hemicellulose, making it resistant to degradation under natural conditions (Jin and Chen, 2007). Cellulose is a chain-like organic polymers that linking glucose unit by β-1,4 glycosidic linkages, and is the most abundant polysaccharide on the Earth (McDonald et al., 2012). Cellulose molecules exist in the form of molecular beams, aggregated in the order of microfibrils, forming a fine crystal structure, which is difficult to degrade by chemical reagents (Chen, 2011). However, the microbial decomposition of cellulose offers benefits such as cost-effectiveness, minimal harmful by-products, and relatively simple processing conditions (Asgher et al., 2017).

Microorganisms convert cellulose of straw into soluble sugars and glucose by producing cellulase (Wood and Garcia-Campayo, 1990), which is the typical example that turning the waste into treasure and largely increase the added value of the target agricultural product. Cellulase is an enzyme system consisting of a mixture of several enzymes, which are primarily classified into into three main types: β-glucosidase, exo-β-1,4-glucanases, and endo-β-1,4-glucosidases (Uzuner and Cekmecelioglu, 2019). All three types of enzymes belong to the glycoside hydrolases (GH) family as described in the Carbohydrate Activity Enzyme Database (CAZY), and these enzymes hydrolyze cellulose thoroughly in a manner of activity complementarity and coordination (Pollegioni et al., 2015). Cellulases are usually produced by microorganisms growing on humus-rich soils, and many plant pathogens can also express cellulases for their effective invade of plant cell wall (Lakshmi and Narasimha, 2012). Therefore, cellulase-producing microorganisms can be easily isolated from soil samples in forests and nature reserves (Lakshmi and Narasimha, 2012).

Bacteria and fungi in soil are the primary organisms responsible for degradation of cellulose which is the predominant polymeric component of plant cell walls (Baldrian and Valášková, 2008). Fungi have a relative higher capacity to produce cellulases than bacteria (Mondal et al., 2021), of which *Penicillium* sp. (Du et al., 2018), *Trichoderma* sp. (Dashtban et al., 2009), and *Aspergillus* sp.(Zhang et al., 2014) have been extensively studied in cellulases production. However, fungi pose challenges for transgenic manipulation, which hinders their practical application in cellulose degradation (Wang et al., 2013). Conversely, bacteria are often considered to be perfect tools for genome manipulation and functional modification due to their relative small genome size and with the ability to clone individual cellulases or express recombinant cellulases (Ma et al., 2020), as well as a shorter and more stable production cycle of bacterial cellulases. Hence, there is great potential for bacteria to develop stable cellulases in cellulose degradation (Ladeira et al., 2015). In recent years, numerous studies have been carried out to screen and identify bacteria with the ability to degrade cellulose from a variety of sources. For example, *Bacillus subtilis* BY4 (Kazeem et al., 2017) was isolated from oil palm empty fruits-chicken dung compost, *Bacillus sphaericus* BS-5 (Xu et al., 2017) was isolated from soil, and *Bacillus subtilis* BY-16 (Ma et al., 2015) was isolated from the gastrointestinal tract of Tibetan pig. However, the cellulose-degrading ability of *Rhodococcus* and *Pseudomonas* have not been reported so far, while the current library of bacteria with cellulose-degrading ability is not sufficient (Ma et al., 2020). Therefore, screening different bacterial species with cellulase degrading ability is crucial for the research and application of cellulose-degrading in straw's further development and utilization on agriculture.

However, the low cellulase yield of bacteria has significantly limited the wide usage in practical applications, especially within industry settings. Enhancing the cellulase production yield of targeted bacterial strains through the optimization of fermentation conditions and genetic manipulation of crucial cellulase-encoding genes is essential for overcoming application barriers (Campano et al., 2015). To adjust the bacterial culture conditions, which mainly include temperature, pH, carbon source, and nitrogen source, the target bacteria could efficiently increase the yield and activity of the cellulase (Aswini et al., 2020). Recent advances in whole-genome sequencing and bioinformatics prediction technologies have identified series of gene candidates for cellulase (Yadav and Dubey, 2018; Yadav et al., 2019; Lu et al., 2020; Paudel et al., 2022; He et al., 2023), thereby providing a cellulase gene library for potential use in future application. According to the coding information, it's possible to genetically improve the cellulase yield and single enzymatic activity of the target bacteria, which will be one of the most effective ways to lift the industrial application restrictions of the target bacteria in future. For instance, the cellulase gene from *Bacillus* was cloned and expressed efficiently in *E. coli*, and the corresponding cellulase has exhibited high catalytic activity *in vitro* (Kim and Ku, 2018). However, the entire set of cellulase systems in different microbial is not yet fully explored, and a deep understanding of the genomic information of different cellulase-producing strains is of great urgent and important for development of high yield and enzymatic activity cellulase-producing genetic engineered bacteria.

Our investigation provided the candidate strategy and the target bacterial strain from theoretical basis for the full utilization of straw resources on industry in the future.

Materials and methods

Isolation and screening of strains

After removing plant debris on ground surface, the soils (20 cm deep) were collected and placed in sterile sealed bags. Approximately 10 g of soil sample was added to 40 mL sterile distilled water in a 50 tube (Cat. No. CLS430304, Corning, Millipore, Sigma-Aldrich, Shanghai), followed by shaking 10 min for fully dissolving of the soil microorganisms. After allowing the tube to stand for 5 min, 1 mL of the supernatant was carefully extracted and spread onto plates containing enrichment CMC medium (CMC -Na 10 g/mL, KH_2PO_4 1 g/mL, NaCl 0,1 g/mL, $FeCl_3$ 0,01 g/L, $NaNO_3$ 2,5 g/L, $CaCl_2.6H_2O$ 0,1 g/L). These plates were then incubated in a constant temperature incubator (Cat. No. HD201801773, Boxun, Shanghai, China) at 28°C for 3 days. The bacteria obtained from the enrichment medium were diluted 10^{-2}, 10^{-3}, and 10^{-4} and coated evenly on above medium. The bacteria were then cultured at 28°C for a further 72 h to facilitate the development of pure colonies. Subsequently, the purified strains were inoculated in the Congo Red carboxymethyl cellulose medium and cultured at 28°C for 72 h, followed by preliminary screening based on the ratio of the diameter of the hydrolysis circle to the diameter of the colony.

Molecular identification of bacteria

Single colonies were inoculated into LB liquid medium (NaCl 10 g/L, Yeast extract 5 g/L, Tryptone 10 g/L) and incubated at 28°C, 200 g on a shaker (Cat.No.MQ2023100755YA, Minquan, Shanghai, China) for 24 h. The bacterial culture medium was centrifuged at 10,000 g, and the supernatant was aspirated. The genomic DNA of the bacteria was extracted employing the Solarbio Bacterial Genomic DNA Extraction Kit (Cat. No. D1600-50, Solarbio, Beijing, China). This extracted genomic DNA served as a template for the polymerase chain reaction (PCR) amplification of the 16S rDNA fragments, using 27F (5'-AGAGTTTGATCCTGGCTCAG-3′) and 1492R (5'-GGCTACCTTGTTACGACTT-3′) as the forward and reverse primers, respectively. The PCR products were detected via 1% agarose gel electrophoresis and analyzed using a gel imaging system (JS-780D, Peiqing Technology, Shanghai, China) to identify the presence of target bands and then purified using agarose gel DNA purification Kit (Takara, Dalian, China). These bands were cut, recovered, and inserted into the pMD19-T vector. The ligated vector was transformed into *Escherichia coli* DH5α cells. A single colony was selected and sent to Shanghai Sangon Biologicals Inc. for sequencing analysis. The sequencing results were blasted in National Center for Biotechnology Information (NCBI). These sequences were then aligned using the MUSCLE function in MEGA 11 software, and a phylogenetic tree was constructed utilizing the Neighbor-Joining method with a bootstrap value of 1000. Finally, the phylogenetic tree was visually enhanced using ITOL for further analysis.

To accurately characterize strains YZ02 and YZ03, we constructed phylogenetic trees based on the common core genes of bacterial genomes of the same genus in the NCBI database. This process was facilitated by the EasyCGTree software platform, developed by Zhang et al., which operates on the Perl programming language (Zhang et al., 2023). Utilizing whole-genome sequencing data, we acquired the amino acid sequences for the majority of bacteria in the corresponding genus from the NCBI genomic database. A profile HMM (hidden Markov model) database was established using 120 ubiquitous genes (equating to 120 protein domains) present across the domain Bacteria (Parks et al., 2017). We then used HMMER[1] to search for homologous genes, MUSCLE (Manuel, 2013) for sequence comparisons, trimAI (Capella-Gutiérrez et al., 2009) to screen conserved regions, and FasTree to construct a super tree (ST) based on the 120 core genes, the bacteria were identified to the species level.

Scanning electron microscopy (SEM)

Bacteria were cultured in liquid LB medium for 24 h, followed by centrifugation at 8000 g for 1 min. The cells were then washed with 0.1 M PBS buffer solution (pH 7.4) and fixed in 2.5% glutaraldehyde at 4 degrees Celsius overnight. Subsequently, the bacteria underwent thorough washing with distilled water and PBS buffer. Dehydration was carried out using a series of alcohol solutions with increasing concentrations: 30, 50, 70, 80, 90, 95, and 100%. Each alcohol concentration was used twice, with each exposure lasting for 15 min. The samples were then dried in a critical point drier using CO_2. For electron microscopy preparation, the dried specimens were coated with approximately 35 nm of gold–palladium (Jesus et al., 2015). The sample was observed and photographed under condition of a voltage of 5.00 kV and a magnification of 15,000-fold using a field emission scanning electron microscope (GeminiSEM 300, Carl Zeiss, Oberkochen, Germany).

Cellulose activity assay

The enzymatic activities of various cellulase enzymes were determined by employing the 3,5-dinitrosalicylic acid (DNS) method, a colorimetric assay technique that is widely used to quantify reducing sugars, such as glucose, that result from enzymatic reactions involving carbohydrate substrates (Miller, 2002). This method was originally described by and involves the addition of DNS reagent to the reaction mixture containing the enzyme and its substrate. Upon heating, the reducing sugars react with the DNS reagent, resulting in a color change that can be measured spectrophotometrically. The absorbance correlates with the concentration of reducing sugars and, hence, the activity of the enzyme. Carboxymethylcellulose (CMC) was the substrate to assess the activity of endo-1,4-β-glucanase (CMCase), which breaks down the internal bonds of the cellulose molecule, resulting in shorter polysaccharide chains. Absorbent cotton, which is composed of long-chain cellulose fibers, was used to measure the activity of exo-1,4-β-glucanase (C1 enzyme), which cleaves cellulose from the ends of the chains to release cellobiose or glucose. Salicin, a glucoside derived from willow bark, served as the substrate for β-glucosidase (BG) (Somogyi, 1952), which hydrolyzes cellobiose and other β-d-glucosides to glucose. The enzyme activity unit is defined according to international regulations: the amount of enzyme

1 http://hmmer.org/

required to catalyze the hydrolysis of cellulose to 1 μmol of glucose in 1 min is defined as one enzyme activity unit (IU/mL) (Eveleigh et al., 2009). To investigate the temporal dynamics of enzyme activity, samples were collected at 12-h intervals, centrifuged, and the supernatants were preserved at −20 Celsius. This systematic method facilitated the preservation of enzymatic activity and the exploration of the relationship between enzyme production and time elapsed. Fermentation cultures of the isolates were performed using straw powder as the sole carbon source. Each 10 mL test tube contained 0,2 g (W_0) of straw powder. After 15 days of fermentation, the remaining straw powder in the test tubes was dried and weighed (W_{15}). The straw degradation rate was calculated as (W_0 - W_{15}) / W_0.

Gene prediction and functional annotation

The genomic DNA extraction from bacterial tissue utilized an optimized SDS (Sodium Dodecyl Sulfate) method, which is effective in lysing cells and denaturing proteins, making it a popular choice for extracting high-quality DNA. Specifically, 1,0 g of bacterial tissue was processed to extract DNA. Samples were then tested and purified using Ligation Sequencing Kit (SQK-LSK110, Oxford Nanopore Technologies, Oxford, UK). Libraries were created according to the instructions. For the preparation of small fragment libraries, the VAHTS Universal Plus DNA Library Prep Kit (ND617-01, Vazyme, Nanjing, China) and MGI V2/for Illumina V2 Kit (NDM627-01, Vazyme, Nanjing, China) were employed. After passing quality control, the libraries were sequenced using the Nanopore PromethION and Illumina NovaSeq 6,000 platforms. After sequencing, data processing involved filtering splices, short fragments, and low-quality reads to retain high-quality data for further analysis. The bacterial genome assembly was initiated with Nanopore long-read data using Flye software, an assembler designed for long reads that can efficiently manage the complexities and errors associated with them. The initial assembly was then refined using Pilon software (1.24) with Illumina short-read data for error correction, ensuring a high-quality genome assembly (Wang et al., 2014). Gene sequences extracted from the assembled genome were annotated against functional databases such as COG, KEGG, Uniprot, and Refseq using BLAST+ (version 2.11.0+), a widely used tool for comparing nucleotide or protein sequences to sequence databases and identifying functional information. Additionally, to specifically identify carbohydrate-related enzyme genes, protein sequences were annotated using HMMER against the CAZy database, a specialized resource for carbohydrate-active enzymes.

Result

Isolation and morphology observation of these cellulose-degrading bacteria

Soil samples were collected from various humus-rich and undisturbed soil environment including parks, protected areas, farmlands, and wastelands in Yangzhou City (Figures 1A,B). Single colonies obtained via the dilution plating method were subsequently examined for colony morphology, size, and the color of metabolites on the plate. Scanning electron microscopy (SEM) analysis was employed to examine each bacterial strain's morphology. It was found that all of the strains are rigid rod-shaped particle (Figure 1C), which implied the species of these bacterial.

After 48 h of culture, the YZ02 strain's colony exhibited a slightly red color with a lightened and opaque surface. SEM observation revealed that YZ02's cells were rod-shaped (Figure 1C). The YZ03 strain's colony was round with a smooth surface and white color; its cells also displayed a rigid rod shape under SEM (Figure 1C). The HJ01 strain's colony was yellow, emitting yellow fluorescence around the colony, with rod-shaped cells under SEM (Figure 1C). The colony of HJ02 strain were round, white, and opaque, and their cells were also rod-shaped (Figure 1C). The colony of BY03 strain were 3–5 mm in diameter and showed yellowish color, and their cells were also rod-shaped (Figure 1C). The colony of GY03 strain showed milky white color and was opaque, and the cells are also rod-shaped. The colonies of strain BY02 appeared as round, beige, opaque structures with a raised center, regular, smooth, and moist edges, and contained rod-shaped cells. All the described strains were categorized as rod-shaped bacteria, yet precise molecular identification is necessary to determine their taxonomic classifications and species identities conclusively.

Molecular identification of the obtained bacteria's strain

For further identification of the isolated bacterial strains, 16S rRNA gene sequencing was conducted with specific primer pairs. The PCR amplification yielded fragments of 1,500 bp, indicative of the 16S rRNA gene presence in the strains. Sequences were submitted to NCBI for BLAST analysis, and a phylogenetic tree was constructed based on the 16S rRNA gene sequences (Figure 2A). Phylogenetic analysis revealed that the seven strains belong to three genera: *Rhodococcus, Pseudomonas*, and *Priestia*. *R. wratislaviensis* YZ02 shared a close phylogenetic relationship with *Rhodococcus wratislaviensis* (NR 026524.1) (Figure 2A), while strain HJ02 aligned closely with *Priestia qingshengii* strain G19 (NR 133978.1) (Figure 2A). The remaining strains BY02, YZ03, GY03, HJ01 and BY03 were classified as *Pseudomonas*, exhibiting close relationships with *Pseudomonas mosselii* strain CFML 90–83 (NR 024924.1), *Pseudomonas xantholysini*, *Pseudomonas putida* strain Sas-14 (JQ782896.1), *Pseudomonas straminea* strain CB-7 (NR 036908.1), and *Pseudomonas glycinae* MS586 (NR 179889.1), respectively (Figure 2A). Supplementary Table S1 provides the detailed information of each isolate.

In conjunction with prior morphological and SEM observations (Figure 1C), we confirmed that strain HJ02 is *Priestia qingshengii*, aligning with characteristics of *Priestia qingshengii* previously isolated from a rock surface (Xi et al., 2014). Similarly, strain BY03 was identified as *Pseudomonas glycinae,* consistent with previous isolations from soybean roots (Jia et al., 2020). The morphological characteristics of strain HJ01 were consistent with those described by Iizuka and Komagata (1963). Nevertheless, due to the inherent limitations of 16S rRNA gene resolution at the species level, *R. wratislaviensis* YZ02 and *P. xanthosomatis* YZ03 were selected for whole-genome sequencing to provide more definitive identifications.

Upon obtaining the whole-genome maps for these strains, a comparative genomic analysis with other strains within the same

A

B

Number	Location	Vegetation cover	Latitude(°N)	Longitude (°E)
1	Baoying	Tree	33.140723	119.31032
2	Baoying	Weed	32.889283	119.457785
3	Baoying	Tree	32.87082	119.477024
4	Gaoyou	Wheat	32.42717	119.238112
5	Gaoyou	Tree	32.426908	119.209512
6	Gaoyou	Wheat	32.285179	119.08079
7	Yizhen	Tree	32.270017	119.065044
8	Yizhen	Weed	32.234418	119.361572
9	Yizhen	Shrub	33.307575	119.611194
10	Yizhen	Shrub	33.209038	119.330675
11	Yizhen	Tree	32.709362	119.437469
12	Yizhen	Weed	32.662659	119.519985
13	Hanjiang	Tree	32.772589	119.738603
14	Hanjiang	Weed	32.546924	119.666849
15	Hanjiang	Weed	32.354461	119.684236
16	Baoying	Tree	32.491011	119.435437
17	Baoying	Weed	32.432841	119.570414
18	Gaoyou	Weed	32.325289	119.444357

C

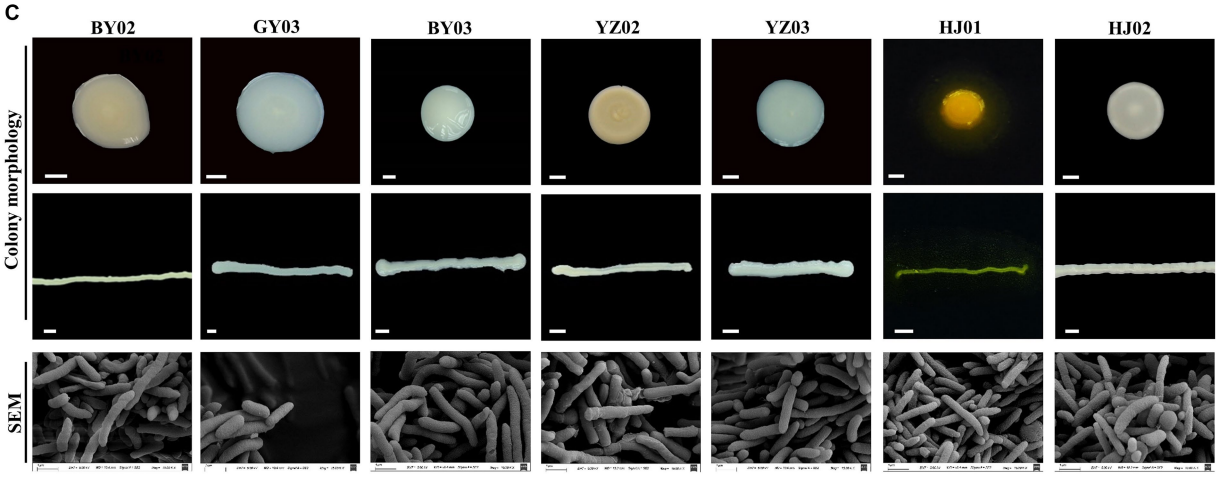

FIGURE 1
Isolation and Screening of Cellulose-Degrading strains from soil. **(A)** Sampling sites of the collected soil samples. **(B)** Detailed information on each sampling location. **(C)** Representative images of isolated colonies on selective media plates and under scanning electron microscopy (SEM) images of the same isolates. Baoying-02, the number 2# isolated from Baoying city, so named it BY02, it is *Pseudomonas mosselii*; the number 3# Gaoyou-03 isolated from Gaoyou city, so named it GY03, it is *Pseudomonas putia*; Baoying-03, the number 3# isolated from Baoying city so name it BY03, it is *Pseudomonas glycinae*; Yizheng-02, the number 3# isolated from Yizheng city so name it YZ02, it is *Rhodococcus wratislaviensis*; Yizheng-03, the number 3# isolated from Yizheng city so name it YZ03, it is *Pseudomonas xanthosomatis*; Hanjiang-01, the number 1# isolated from Hanjiang district so named it HJ01, it is *Pseudomonas straminea*; Hanjiang-02, the number 2# isolated from Hanjiang so named it HJ02, it is *Prestia qingshengii*; Scale bar: 0.3 mm.

genus was conducted to construct a phylogenetic tree based on 120 core genes (Figures 2B,C). The analysis confirmed that *R. wratislaviensis* YZ02 and *P. xanthosomatis* YZ03 exhibit the closest genetic affiliations to *Rhodococcus wratislaviensis* and *Pseudomonas xanthosomatis*, respectively. Therefore, we definitively categorized strain YZ02 and strain YZ03 as *Rhodococcus wratislaviensis* YZ02 and *Pseudomonas xanthosomatis* YZ03, respectively.

Cellulase enzyme activities assay

To investigate the cellulase activities of the isolated strains and identify the one with the highest activity, we employed the DNS (3,5-dinitrosalicylic acid) assay to measure the concentration of reducing sugars. This approach facilitated the precise and accurate assessment of the strains' cellulase activities. As shown in Figure 3A, after 72 h of fermentation, all seven strains exhibited satisfactory enzyme activities. However, *R. wratislaviensis* YZ02 and *P. xanthosomatis* YZ03 stood out, exhibiting the most robust CMCase, endoglucanase (C1), and β-glucosidase (BG) activities compared to the others. Consequently, *R. wratislaviensis* YZ02 and *P. xanthosomatis* YZ03 were chosen for subsequent investigations to explore their enzyme production peaks. For *R. wratislaviensis* YZ02, the activities of CMCase and C1 peaked at 72 h of fermentation, while the activity of BG reached its maximum at 60 h. Following this peak, the activities of all cellulases gradually declined. To explore the relationship between cellulase activity and bacterial growth, we quantity the cells at OD600 at various time points to indicate the bacterial number. The results

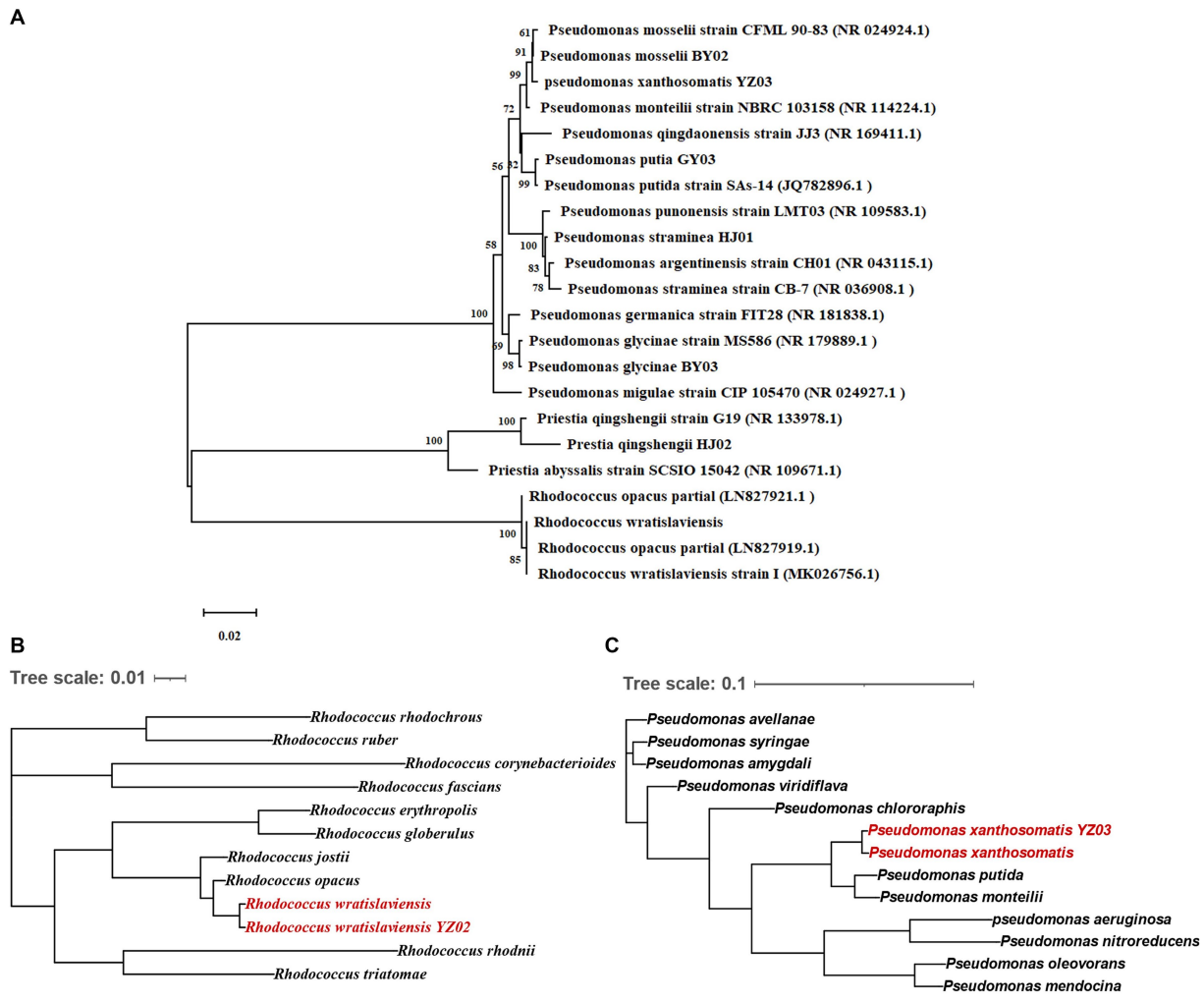

FIGURE 2
Neighbor-joining tree showing the phylogenetic position of cellulose-degrading bacteria. **(A)** Neighbor-joining tree constructed based on 16S rRNA gene sequences depicting the genetic relatedness of strains YZ02, GY03, BY03, YZ02, YZ03, HJ01 and HJ02. The evolutionary history was inferred using the Neighbor-Joining method. The optimal tree is shown. The percentage of replicate trees in which the associated taxa clustered together in the bootstrap test (1,000 replicates) are shown next to the branches The evolutionary distances were computed using the Maximum Composite Likelihood method. **(B)** This tree illustrates the evolutionary relationships of strain YZ02 based on the sequence alignment of a panel of 120 conserved genes. Each node represents a distinct bacterial taxon, and the branches reflect the inferred evolutionary pathways and genetic distances between species. **(C)** This tree illustrates the evolutionary relationships of strain YZ03 based on the sequence alignment of a panel of 120 conserved genes. Each node represents a distinct bacterial taxon, and the branches reflect the inferred evolutionary pathways and genetic distances between species.

indicated that the bacterial count exhibited a similar trend to that of cellulase activities (Figure 3B). Similarly, for *P. xanthosomatis*, the activities of all three cellulases peaked at 72 h of fermentation, and the OD600 values mirrored the trend of cellulase activities (Figure 3C). After standardizing the data, we observed that the relative maximum enzyme activity of YZ03 (12.95 IU/mL) exceeded that of YZ02 (12.66 IU/mL) (Figure 3D). Subsequently, response surface methodology (RSM) experiments were conducted to investigate the optimal fermentation conditions for YZ02. The results indicated that under the conditions of a fermentation time of 72 h, pH of 6, and temperature of 45°C, *R. wratislaviensis YZ02* achieved the highest cellulase activity (Figures 3D–F). Figures 3G,H demonstrate that after 15 days of fermentation, 55% of the straw powder in the medium was degraded and *R. wratislaviensis* YZ02 had a strong ability to degrade straw powder. Figure 3G demonstrates that *R. wratislaviensis* YZ02 exhibits strong degradation capability towards sieved straw powder. After 15 days of fermentation, the treatment group with the addition of *R. wratislaviensis* YZ02 had only half of the straw powder remaining (Figure 3G). The degradation capability of *R. wratislaviensis* YZ02 was significantly higher compared to strain HJ01. Figure 3I quantitatively analyzed the residual straw powder in each treatment group by weighing, revealing that *R. wratislaviensis* YZ02 degraded 55% of the straw powder in the system after 15 days of fermentation.

Whole genome sequencing genome sequencing and annotation

Combined with the results of previous enzyme activity analyses, we selected two strains YZ02 and YZ03, with the highest cellulase activity from the isolates for Whole genome sequencing and annotation. Whole genome sequencing of *R. wratislaviensis YZ02*

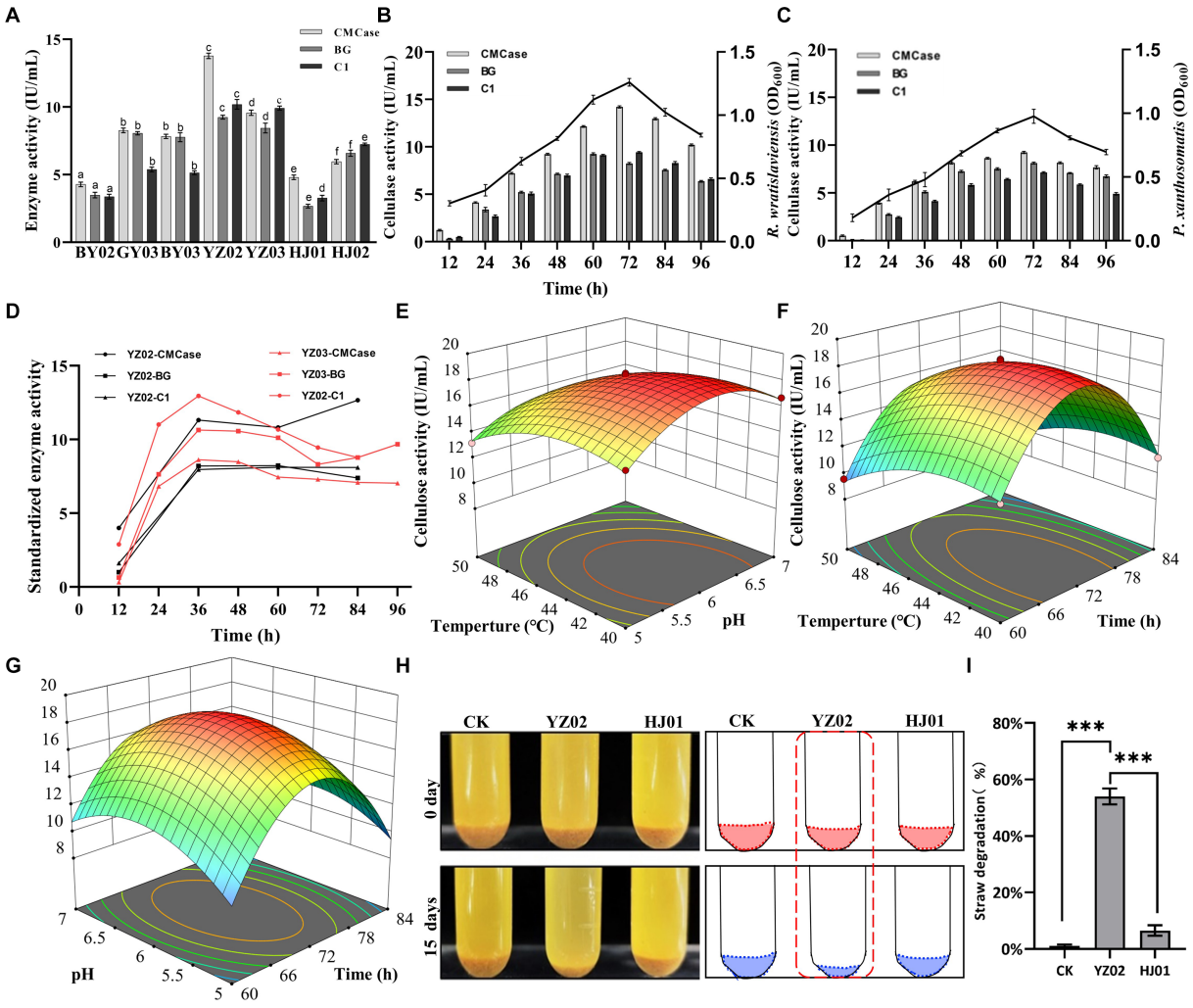

FIGURE 3
Determination of cellulase activity of the isolated strains. **(A)** CMCase, BG, and C1 enzymes represent endo-1,4-β-glucanase, β-glucosidase, and endoglucanase, respectively, using CMC, salicin, and absorbent cotton as reaction substrates Enzyme activity was measured at 12 h intervals. The values represent the means of three biological replicates, and the error bars indicate the standard error of the mean. The cellulase activity of each isolate was monitored over a 72 h fermentation period using the 3,5-dinitrosalicylic acid (DNS) method. Different letters indicate significant differences between groups ($p < 0.05$) **(B)** Trend of CMCase, BG, and C1 enzyme activities of strain YZ02 over time. The left Y-axis represents enzyme activity, and the right Y-axis represents the bacterial OD600 value. **(C)** Trend of CMCase, BG, and C1 enzyme activities of strain YZ03 over time. The left Y-axis represents enzyme activity, and the right Y-axis represents the bacterial OD600 value. **(D)** The CMCase, BG, and C1 enzyme activity data of strains YZ02 and YZ03 were normalized. The normalized enzyme activity data were obtained by dividing the cellulase activity by the bacterial OD600.The Y-axis represents the relative cellulase activity. **(E)** Response surface diagram of temperature and pH effect on the CMCase activity of strain YZ02. **(F)** Response surface diagram of temperature and time effect on the CMCase activity of strain YZ02. **(G)** Response surface diagram of Ph and time effect on the CMCase activity of strain YZ02.To assess the straw powder degradation capability of *R. wratislaviensis* YZ02, the fermentation medium devoid of bacteria served as a blank control, while the degradation efficacy of strain HJ01 acted as a positive control. **(H)** Using straw powder as a carbon source, inoculated with cellulolytic bacteria and fermented for 15 days. **(I)** The degradation rate of straw powder by strain YZ02 and strain HJ01 was obtained by subtracting the weight of the original straw powder in the test tube from the weight of the straw powder remaining after 15 days of fermentation and dividing by the weight of the original straw powder.

and *P. xanthosomatis YZ03* was performed based on the Nanopore triple sequencing technology platform and the second-generation sequencing technology platform. The genome size of *R. wratislaviensis* YZ02 was 8.51 Mb, encompasses 8,466 genes, including 4 23S rRNAs, 4 16S rRNAs, and 4 5S rRNAs, of these, 3,776, 8,308, 6,253, 7,080, and 6,975 genes were, respectively, annotated in the KEGG, Nr, GO, COG, and Pfam databases (Supplementary Table S2). The genome of *P. xanthosomatis*, sized at 6.66 Mb, comprises 5,745 genes with 6 23S rRNAs, 6 16S rRNAs, and 7 5S rRNAs. These were annotated in the KEGG, Nr, GO, COG, and Pfam databases, with annotations numbering 3,385, 5,703, 3,940, 4,758, and 4,830, respectively (Supplementary Table S2). Genomic data, including genome structure annotations, GC content, and COG functional annotations, were synthesized using an R package to depict the genomic circle (Figures 4A,B). The results demonstrated that *R. wratislaviensis* YZ02 exhibited a genome size of 8.51 Mb and a GC content of 67.41% (Figure 4A), while *P. xanthosomatis* exhibited a genome size of 6.66 Mb and a GC content of 64.05% (Figure 4B), and clearly showed the relationship between genome components and genome positions.

10.3389/fmicb.2024.1409697

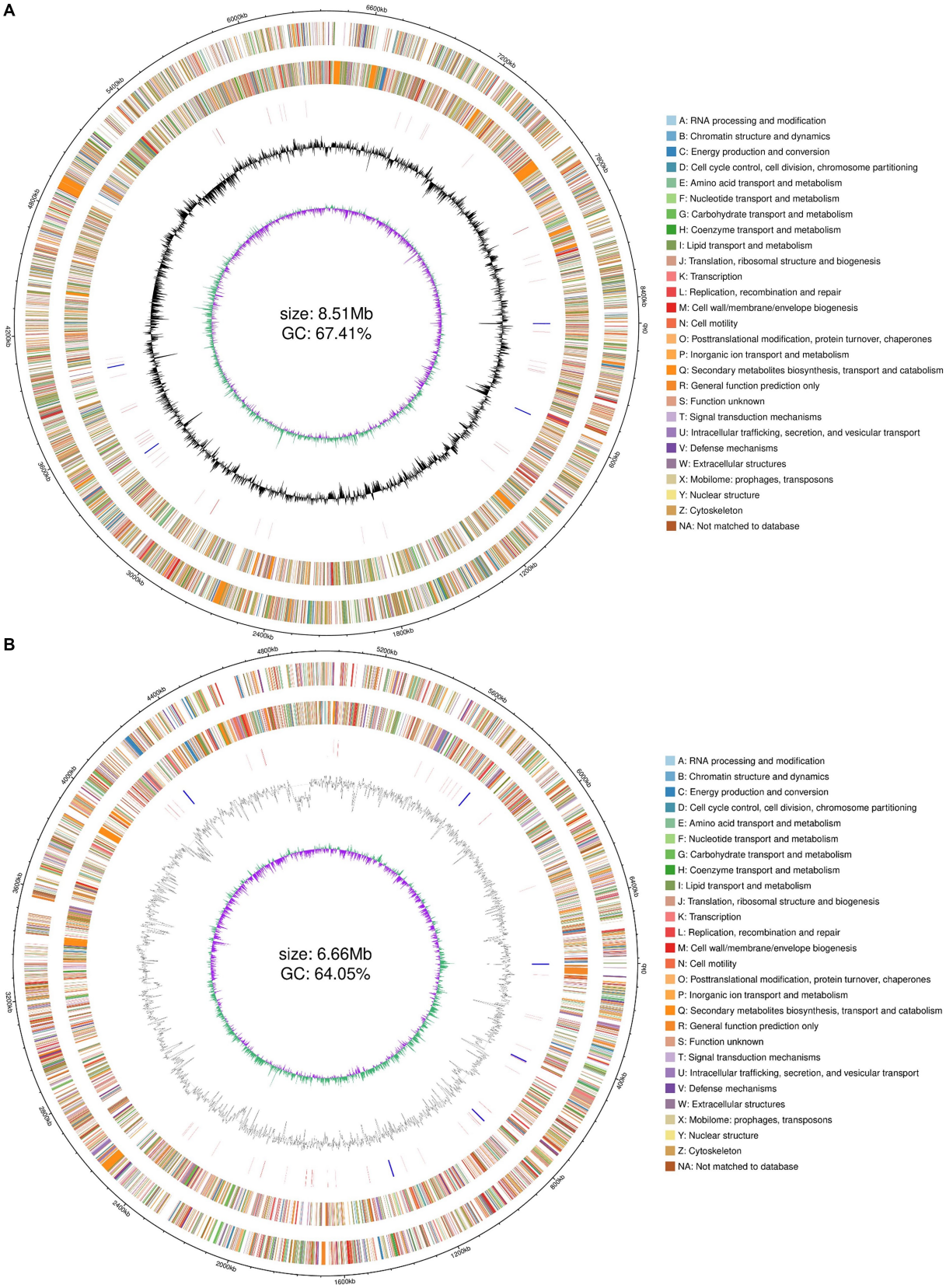

FIGURE 4
Whole-genome visualization map of *Rhodococcus wratislaviensis* YZ02 and *Pseudomonas xanthosomatis* YZ03. From the outer circle to the inner circle, ring 1, genomic coordinates; ring 2, genes on the positive strand of the genomic sequence, with different colors representing different COG functional classifications; ring 3, genes on the negative strand of the genomic sequence, with different colors representing different COG functional classifications; ring 4, rRNAs and tRNAs on the genomic sequence, with the rRNAs in blue and the tRNAs in red; ring 5, GC content of the genomic sequence; ring 6, GC skew profile of the genomic sequence.

Homologous gene clusters involved in glucose metabolism in genome annotation

To delve deeper into the cellulolytic capabilities of *R. wratislaviensis* YZ02 and *P. xanthosomatis* YZ03at the genetic level, these strains were annotated in the COG database, revealing 7,080 and 4,758 genes, respectively (Figures 5A,B). These annotations facilitated an analysis of genes associated with carbohydrate metabolism. For amino acid transport and metabolism, *R. wratislaviensis* YZ02 and *P. xanthosomatis* YZ03 possessed 830 (11.72%) and 614 (12.91%) genes, respectively. In terms of carbohydrate transport and metabolism, the gene counts were 584 (8.25%) for *R. wratislaviensis* YZ02 and 289 (6.07%) for *P. xanthosomatis* YZ03. Among the identified genes, strains YZ02 harbor COG2723 (β-glucosidase), COG3507 (beta-xylosidase), and COG1427 (exoglucanase) (Figure 5A). *P. xanthosomatis* possessed COG1427 (exoglucanase) (Figure 5B). The presence of a considerable number of genes related to carbohydrate metabolism and transport indicates that and *P. xanthosomatis* YZ03 possess the genetic basis for cellulose degradation.

KEGG and go database annotations

The Kyoto Encyclopedia of Genes and Genomes (KEGG) serves as a pivotal database for the comprehensive annotation of enzymes catalyzing reactions across diverse metabolic stages, facilitating an in-depth understanding of enzyme roles within metabolic pathways during bacterial cellulose degradation. The genomes of *R. wratislaviensis* YZ02 and *P. xanthosomatis* YZ03 were annotated utilizing KEGG and subsequently categorized based on their involvement in specific KEGG metabolic pathways. KEGG pathway analyses uncovered notable disparities in gene involvement across 15 metabolic pathways between strains YZ02 and YZ03, particularly within carbohydrate pathways, enumerating 447 and 272 genes, respectively, (Figures 6A,C). Moreover, the glycolysis/gluconeogenesis pathway involved 53 and 34 genes in *R. wratislaviensis* YZ02 and *P. xanthosomatis* YZ03, respectively (Figures 6A,C).

Gene Ontology (GO) annotation results indicated that genes within *R. wratislaviensis* YZ02 and *P. xanthosomatis* YZ03 were predominantly enriched in molecular functions, while cellular components and biological processes were less represented (Figures 6B,D). Within biological processes, *R. wratislaviensis* YZ02 and *P. xanthosomatis* YZ03 harbored 295 and 122 genes, respectively, associated with transcription regulation. Furthermore, analysis revealed 656 and 301 genes related to DNA binding and 491 and 361 genes associated with ATP binding in strains YZ02 and YZ03, respectively (Figures 6B,D). Subsequent analysis of genes involved in carbohydrate metabolism and transport yielded 57 and 32 carbohydrate metabolism-related genes in strains YZ02 and YZ03, respectively, encompassing GO terms such as GO:0005975 (carbohydrate metabolic process), GO:0030246 (carbohydrate binding), and GO:0008643 (carbohydrate transport). These findings suggest that the abundance of carbohydrate metabolism-related genes in *R. wratislaviensis* YZ02 and *P. xanthosomatis* YZ03 underpins their cellulolytic capabilities.

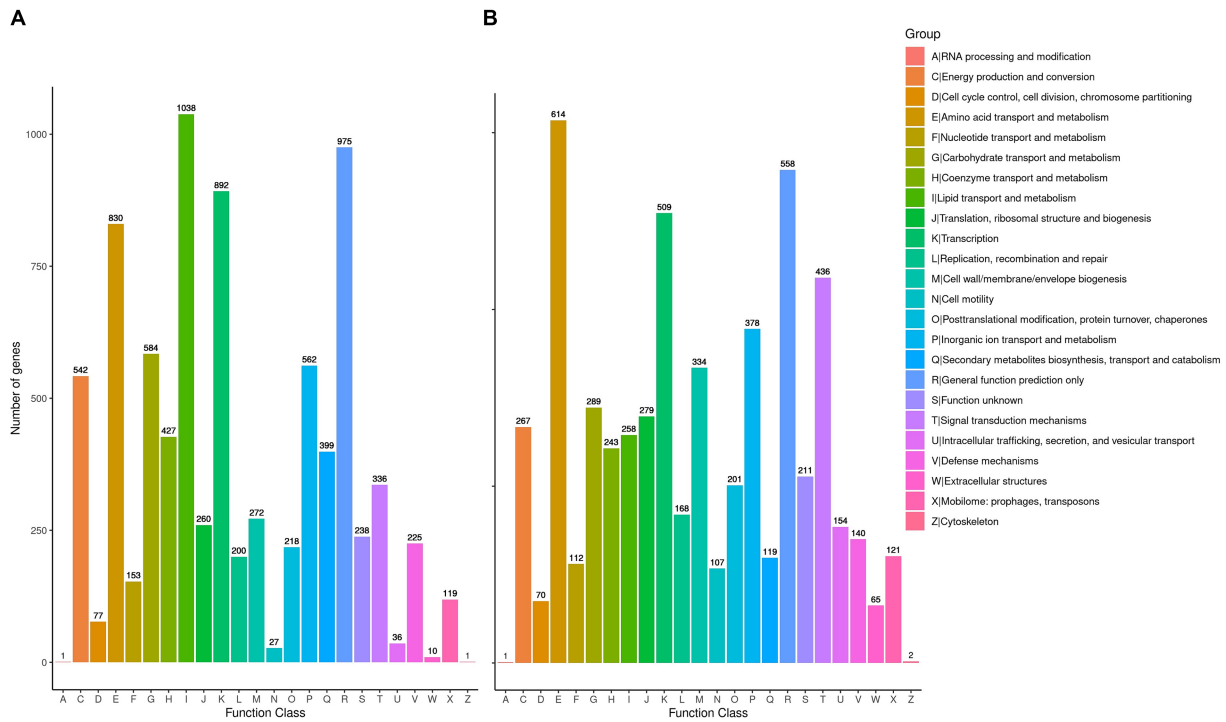

FIGURE 5
Clusters of Orthologous Groups annotation analysis. **(A,B)** It illustrates the distribution of genes within the genomes of strains YZ02 and YZ03, respectively, according to their predicted functional categories. Vertical axis is the number of genes annotated under COG classification while the horizontal axis is the content of each COG classification.

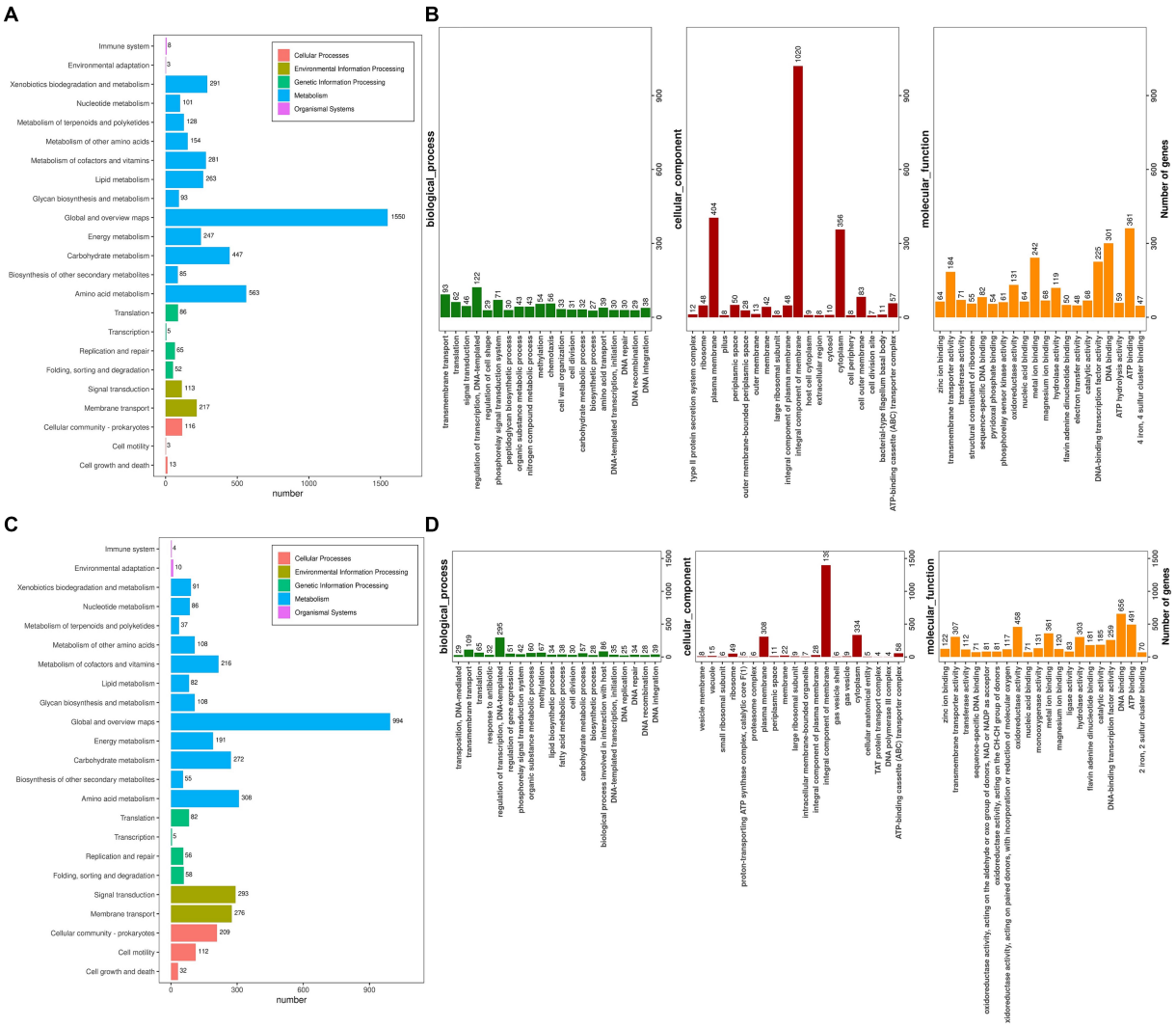

FIGURE 6
KEGG pathway analysis and Gene ontology cluster analysis of *Rhodococcus wratislaviensis* YZ02 and *Pseudomonas xanthosomatis* YZ03. **(A)** The KEGG annotation analysis of *R. wratislaviensis* YZ02and **(C)** The KEGG annotation analysis of *P. xanthosomatis* YZ03 The horizontal axis is the number of genes annotated under KEGG pathway classification. The vertical axis is KEGG pathway classification, and different colors represent different classifications. **(B)** The GO annotation analysis of *R. wratislaviensis* YZ02. **(D)** The GO annotation analysis of *P. xanthosomatis*. The horizontal axis generally represents the count or proportion of genes within each GO term, showing the extent to which certain functions or processes are represented in the organism's genome. The vertical axis lists the GO terms that have been assigned to the genes. This axis would be divided into the main GO domains (Biological Process, Molecular Function, and Cellular Component), each potentially further subdivided into more specific terms.

CAZyme annotations

Figure 7 illustrates the statistics of carbohydrate enzyme-related genes in strains YZ02 and YZ03, as annotated in the CAZy database. The glycoside hydrolase (GH) family and glycosyltransferase (GT) family account for the largest proportions. In *R. wratislaviensis* YZ02, there were 37 GH family genes and 54 GT family genes, whereas *P. xanthosomatis* YZ03 harbored 23 GH family genes and 30 GT family genes. Moreover, for *R. wratislaviensis* YZ02 and *P. xanthosomatis* YZ03 respectively, 30 and 2 CE genes, 1 and 2 PL genes, and 27 and 9 AA genes were identified (Figure 7). The genome of *R. wratislaviensis* YZ02 was found to contain 37 annotated cellulase-related genes, including 25 genes of the GH family. (Figure 7). These genes encode proteins such as β-glucosidase, which mainly belong to the GH1, GH2, GH3, and GH16 families, and endoglucanase, which mainly belongs to the GH5 family (EC 3.2.1.4). Furthermore, proteins encoded by the glucan-1,4-α- glucosidase (EC 3.2.1.3) gene mainly belongs to the GH15 family, and proteins encoded by the α-glucosidase (EC 3.2.1.20) gene mainly belong to the GH13, GH63, and GH76 families. *P. xanthosomatis's* genome was found to possess 27 annotated cellulose-related genes, including those from the GH3, GH13, and GH15 families, which are pivotal in cellulose degradation. The presence of these genes enables bacteria to decompose cellulose efficiently and also responds to the ability of *R. wratislaviensis* YZ02 and *P. xanthosomatis* YZ03 to degrade cellulose at the genetic level.

Discussion

Cellulose enzymes from bacteria are considered promising candidates for the conversion of lignocellulosic biomasses into fermentable sugars. Soil bacteria can produce various hydrolytic

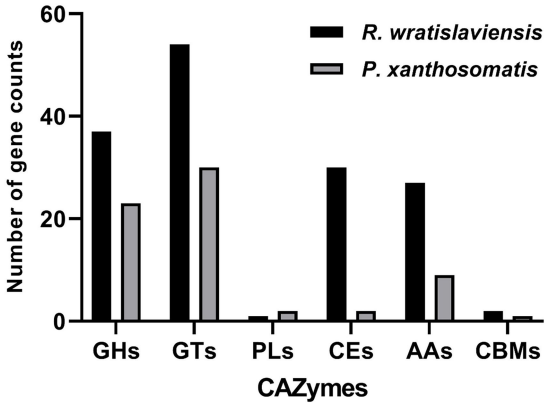

FIGURE 7
Carbohydrate-active enzymes family distribution in *Rhodococcus wratislaviensis* YZ02 and *Pseudomonas xanthosomatis* YZ03. The vertical axis (quantity of genes) represents the number of genes associated with each CAZyme family. A higher count indicates a greater potential capacity of the organism to engage in certain types of carbohydrate metabolism. The horizontal axis (types of genes/CAZyme families) categorizes the genes according to the specific CAZyme family they belong to, such as GH, GT, PL, CE, AA, and CBM.

enzymes that play a crucial role in cellulose degradation (Hentges and Smith, 2018). In recent years a number of microorganisms with cellulose-degrading potential have been isolated from the soil, *B. subtilis K1*, isolated from soil, exhibits significant cellulose-degrading activity under cold conditions(He et al., 2023). Similarly, *Raoultella* sp. S12 (Bao, 2016) is known to degrade lignocellulose, and *Xanthomonas translucens*, isolated from rice straw, can be used in fuel cells (Khoirunnisa et al., 2020). *Bosea* sp. FBZP-16 (Houfani et al., 2017), *Paenibacillus lautus* strain BHU3 (Yadav and Dubey, 2018), *Cellulomonas gilvus* sp. (Christopherson et al., 2013), these strains are all considered excellent cellulase-producing bacteria. However, a significant gap in the literature exists regarding the cellulose-degrading capabilities of *Rhodococcus wratislaviensis* and Pseudomonas xanthosomatis. We tested the enzymatic activities of the three most critical cellulases in cellulose degradation using carboxymethyl cellulose CMC, salicin, and cotton as substrates, and for the first time, discovered that *Rhodococcus wratislaviensis* and *Pseudomonas xanthosomatis* exhibit excellent cellulose-degrading abilities (Figure 3A). Additionally, we identified several rarely reported cellulose-degrading bacteria, including *Pseudomonas mosselii*, *Pseudomonas putia*, *Pseudomonas straminea*, and *Priestia qingshengii* as potential cellulase-producing strains (Figures 1C, 3A). These newly discovered cellulolytic bacteria expand the known range of cellulose-degrading bacteria and open up new avenues for industrial applications.

The cellulase activities of both strains YZ02 and YZ03 peaked after 60 to 72 h of fermentation, significantly surpassing those reported for several other cellulose-degrading bacteria. (Figures 3B,C). For instance, *Bacillus cereus*, as reported by Nema et al. (2015), exhibited a maximum cellulase activity of 0.213 IU/mL, and *Bacillus megaterium* isolated by Bhagat and Kokitkar (2021). Interestingly, we observed that the variations in cellulase activity closely mirrored the dynamic changes in bacterial cell numbers, elucidating the initial increase followed by a subsequent decrease in cellulase activity of the strains (Figures 3B,C). After standardizing the data to account for bacterial cell numbers, we observed an initial increase in cellulase activity, followed by a decrease and then a subsequent increase. This pattern is likely due to the accumulation and adsorption of reaction products inhibiting enzyme activity after it reaches its peak. Over time, the enzymes may desorb from the cellulose surface, alleviating the "clogging" effect and partially restoring their activity.(Andric et al., 2010). These findings not only demonstrate the high cellulase activity of strain YZ02 and YZ03 but also provide insights into the enzymatic dynamics during cellulose degradation, which can inform future industrial applications. Furthermore, we investigated the factors influencing the cellulase activity of *R. wratislaviensis* YZ02. Our results indicated that the highest cellulase activity was observed at a pH of 6 and a reaction temperature of 45°C (Figures 3D–F). This suggests that the cellulase from *R. wratislaviensis* YZ02 exhibits thermal stability and retains high activity across a broad pH range. Such characteristics are advantageous for industrial applications, as they have the potential to significantly reduce production costs. Moreover, there are very few studies that use rice straw powder as carbon source to investigate the utilization of straw cellulose by these strains. Our results demonstrate that *Rhodococcus wratislaviensis* can effectively degrade rice straw powders (Figures 3G,H). Rice straw, being a cheap and abundant cellulose substrate, has become a key raw material for cellulase production due to its high cellulose content and wide availability (Goodman, 2020). *Rhodococcus wratislaviensis* YZ02 may be highly effective in processing waste straw from Yangzhou, thereby enabling the recycling and utilization of agricultural waste. The ability of *R. wratislaviensis* YZ02 to process waste straw from Yangzhou highlights its potential for agricultural waste recycling, further underlining the practical implications of our findings.

The composition of fungal cellulase is less complex than that of bacteria, which can produce large amounts of cellulase extracellularly (Sukumaran et al., 2005). Among various fungi, *Aspergillus mushrooms* have higher cellulase activity compared to other genera. Although fungi have high enzyme-producing activity, bacteria is also efficient in cellulose degradation, with a wide range of cellulose-degrading enzymes and a strong organic matter degradation capacity. For example, Auffret et al. showed through transcriptomic analysis that *Rhodococcus wratislaviensis* can participate in the degradation of hydrocarbons, gasoline, and diesel fuel (Auffret et al., 2014), and Suresh *Rhodococcus Subashchandrabose* et al. showed that *R. wratislaviensis* is capable of degrading p-nitrophenol (Subashchandrabose et al., 2018), and Paola Grenni isolated *Rhodococcus* strains capable of degrading S-triazine from groundwater (Grenni et al., 2009). Compared with fungi, bacteria have the advantages of rapid growth, high application potential, short generation time and low cost for cellulase production (Westers et al., 2004), so cellulose conversion by bacteria is a highly efficient production strategy. Currently, *Fibrosomonas aeruginosa* and *Thermomonas brownii* have been widely studied and used for cellulase production.

Through whole-genome sequencing and analysis, we improved our understanding of the genomes and cellulose degradation pathways of cellulose-degrading bacteria. This knowledge provides a theoretical basis for the future engineering of *R. wratislaviensis* YZ02 and *P. xanthosomatis* YZ03 into cellulose-degrading microorganisms. Therefore, we selected *Rhodococcus wratislaviensis* YZ02 and *Pseudomonas Xanthosomatis* YZ03 for whole genome sequencing and analysis to obtain valuable genetic information. Through annotation in the COG, KEGG and GO database, it was found that *R. wratislaviensis* YZ02 and *P. xanthosomatis* YZ03 are equipped with a large number of

genes essential for the metabolism of carbohydrates and other nutrients (Figures 5–7). Notably, *R. wratislaviensis* YZ02 had a significantly higher number of genes for metabolizing carbohydrates, starch, and sucrose compared to *P. xanthosomatis* YZ03. This suggests that *R. wratislaviensis* YZ02 is more efficient in carbohydrate metabolism than *P. xanthosomatis* YZ03. These genetic insights not only enhance our understanding of these bacteria but also lay the groundwork for their potential biotechnological applications. The glycoside hydrolase family is a crucial enzyme in bacterial polysaccharide degradation and promotes bacterial growth and catalytic efficiency alongside CBM glycohydrolase-active enzymes (Hervé et al., 2010). Studies have shown that bacterial genomes are typically enriched in genes encoding glycoside hydrolases (Berlemont et al., 2015). Therefore, we analyzed the carbohydrate utilization ability of two bacterial strains using the Carbohydrate Active Enzymes Database (CAZy).[2] The study found that *R. wratislaviensis* YZ02 and *P. xanthosomatis* YZ03 both possess genes encoding enzymes critical to the cellulose degradation pathway, including GH, GT, CE, PL, AA and CBM. *R. wratislaviensis* YZ02 and *P. xanthosomatis* YZ03 possess extensive GH family genes (Figure 7), which enable them to utilize a wide range of polysaccharides. This suggests that these strains have excellent cellulolytic capabilities. In addition, we identified genes encoding cellulases such as GH1 and GH5 as well as β-glucosidase genes (Koeck et al., 2014). Differences in gene number led to variations in the expression of CMCase, C1 and BGase between strains. These findings were consistent with our preliminary enzyme activity measurements, which indicated that *R. wratislaviensis* YZ02 had higher activity levels for all three enzymes compared to *P. xanthosomatis* YZ03. The synergistic action of these three enzymes plays an important role in the hydrolysis of cellulose and its derivatives to glucose (Henrissat et al., 1985). Additionally, we also identified genes encoding CBM family protein in both strains. These proteins can specifically bind polysaccharides, thereby increasing the catalytic efficiency of carbohydrase (Wei et al., 2022). Our results provide valuable genetic insights into the mechanisms of cellulose degradation by these bacteria, suggesting implications for their application in biomass conversion and waste recycling efforts. Our study is unique in identifying and characterizing these genetic attributes, thereby providing a comprehensive understanding of the cellulolytic mechanisms in *R. wratislaviensis* YZ02 and *P. xanthosomatis* YZ03.

Data availability statement

The datasets presented in this study can be found in online repositories. The names of the repository/repositories and accession number(s) can be found in the article/Supplementary material.

Author contributions

DM: Writing – original draft, Software, Writing – review & editing, Data curation, Formal analysis, Investigation, Methodology, Resources. HC: Data curation, Formal analysis, Investigation, Methodology, Software, Validation, Visualization, Writing – original draft, Writing – review & editing. DL: Data curation, Formal analysis, Investigation, Software, Validation, Visualization, Writing – original draft. CF: Data curation, Formal analysis, Investigation, Methodology, Project administration, Resources, Software, Validation, Writing – original draft. YH: Formal analysis, Investigation, Methodology, Software, Writing – original draft. TG: Data curation, Formal analysis, Investigation, Software, Writing – original draft. XG: Writing – original draft, Formal analysis, Investigation, Software. YZ: Writing – original draft, Data curation, Formal analysis, Investigation, Software. HW: Writing – original draft, Data curation, Methodology, Software. GT: Data curation, Formal analysis, Methodology, Software, Writing – original draft. HL: Writing – review & editing, Conceptualization, Data curation. KZ: Writing – review & editing, Conceptualization, Data curation, Formal analysis, Funding acquisition, Investigation, Methodology, Project administration, Resources, Software, Supervision, Validation, Visualization, Writing – original draft.

Funding

The author(s) declare that financial support was received for the research, authorship, and/or publication of this article. This work was supported by the National Natural Science Foundation of China (32372486), Excellent Youth Fund of Jiangsu Natural Science Foundation (BK20220116), the Yangzhou Modern Agriculture Key R&D Project (YZ2021032), and the Chinese Government Scholarship (China Scholarship Council, CSC) (File No. 202108320223), and Young and Middle-aged Academic Leaders of the "Qinglan Project" of Yangzhou University.

Acknowledgments

We are grateful to each member in plant pathology laboratory of Yangzhou University for their constructive and critical suggestions.

Conflict of interest

The authors declare that the research was conducted in the absence of any commercial or financial relationships that could be construed as a potential conflict of interest.

Publisher's note

Supplementary material

The Supplementary material for this article can be found online at: https://www.frontiersin.org/articles/10.3389/fmicb.2024.1409697/full#supplementary-material

2 http://www.cazy.org

References

Andric, P., Meyer, A. S., Jensen, P. A., and Dam-Johansen, K. (2010). Reactor design for minimizing product inhibition during enzymatic lignocellulose hydrolysis: I. Significance and mechanism of cellobiose and glucose inhibition on cellulolytic enzymes. *Biotechnol. Adv.* 28, 308–324. doi: 10.1016/j.biotechadv.2010.01.003

Asgher, M., Wahab, A., Bilal, M., and Iqbal, H. M. N. (2017). Delignification of lignocellulose biomasses by alginate–chitosan immobilized laccase produced from Trametes versicolor IBL-04. *Waste Biomass Valorizat.* 9, 2071–2079. doi: 10.1007/s12649-017-9991-0

Aswini, K., Gopal, N. O., and Uthandi, S. (2020). Optimized culture conditions for bacterial cellulose production by *Acetobacter senegalensis* MA1. *BMC Biotechnol.* 20:46. doi: 10.1186/s12896-020-00639-6

Auffret, M. D., Yergeau, E., Labbé, D., Fayolle-Guichard, F., and Greer, C. W. (2014). Importance of Rhodococcus strains in a bacterial consortium degrading a mixture of hydrocarbons, gasoline, and diesel oil additives revealed by metatranscriptomic analysis. *Appl. Microbiol. Biotechnol.* 99, 2419–2430. doi: 10.1007/s00253-014-6159-8

Baldrian, P., and Valášková, V. (2008). Degradation of cellulose by basidiomycetous fungi. *FEMS Microbiol. Rev.* 32, 501–521. doi: 10.1111/j.1574-6976.2008.00106.x

Bao, W. (2016). Screening and genomic analysis of a lignocellulose degrading bacterium. *Acta Microbiol. Sin.* 56, 765–777. doi: 10.13343/j.cnki.wsxb.20150293

Berlemont, R., Martiny, A. C., and Kivisaar, M. (2015). Genomic potential for polysaccharide deconstruction in Bacteria. *Appl. Environ. Microbiol.* 81, 1513–1519. doi: 10.1128/AEM.03718-14

Bhagat, S. A., and Kokitkar, S. S. (2021). Isolation and identification of bacteria with cellulose-degrading potential from soil and optimization of cellulase production. *J. Appl. Biol. Biotechnol.* 9, 154–161. doi: 10.7324/JABB.2021.96020

Campano, C., Balea, A., Blanco, A., and Negro, C. (2015). Enhancement of the fermentation process and properties of bacterial cellulose: a review. *Cellulose* 23, 57–91. doi: 10.1007/s10570-015-0802-0

Capella-Gutiérrez, S., Silla-Martínez, J. M., and Gabaldón, T. (2009). trimAl: a tool for automated alignment trimming in large-scale phylogenetic analyses. *Bioinformatics* 25, 1972–1973. doi: 10.1093/bioinformatics/btp348

Chen, H. (2011). Biotechnology of lignocellulose. Beijing: Chemical Industry Press.

Christopherson, M. R., Suen, G., Bramhacharya, S., Jewell, K. A., Aylward, F. O., Mead, D., et al. (2013). The genome sequences of Cellulomonas fimi and "Cellvibrio gilvus" reveal the cellulolytic strategies of two facultative anaerobes, transfer of "Cellvibrio gilvus" to the genus Cellulomonas, and proposal of Cellulomonas gilvus sp. nov. *PLoS One* 8:e53954. doi: 10.1371/journal.pone.0053954

Dashtban, M., Schraft, H., and Qin, W. (2009). Fungal bioconversion of lignocellulosic residues; opportunities & perspectives. *Int. J. Biol. Sci.* 5, 578–595. doi: 10.7150/IJBS.5.578

Du, J., Zhang, X., Li, X., Zhao, J., Liu, G., Gao, B., et al. (2018). The cellulose binding region in Trichoderma reesei cellobiohydrolase I has a higher capacity in improving crystalline cellulose degradation than that of Penicillium oxalicum. *Bioresour. Technol.* 266, 19–25. doi: 10.1016/j.biortech.2018.06.050

Eveleigh, D. E., Mandels, M., Andreotti, R., and Roche, C. (2009). Measurement of saccharifying cellulase. *Biotechnol. Biofuels* 2:21. doi: 10.1186/1754-6834-2-21

Goodman, B. A. (2020). Utilization of waste straw and husks from rice production: A review. *J. Bioresour. Bioprod.* 5, 143–162. doi: 10.1016/j.jobab.2020.07.001

Grenni, P., Gibello, A., Barra Caracciolo, A., Fajardo, C., Nande, M., Vargas, R., et al. (2009). A new fluorescent oligonucleotide probe for in situ detection of s-triazine-degrading *Rhodococcus wratislaviensis* in contaminated groundwater and soil samples. *Water Res.* 43, 2999–3008. doi: 10.1016/j.watres.2009.04.022

Han, Y., Zhang, Z., Li, T., Chen, P., Nie, T., Zhang, Z., et al. (2023). Straw return alleviates the greenhouse effect of paddy fields by increasing soil organic carbon sequestration under water-saving irrigation. *Agric. Water Manag.* 287:108434. doi: 10.1016/j.agwat.2023.108434

He, Z., Ding, B., Ali, Q., Liu, H., Zhao, Y., Wang, X., et al. (2023). Screening and isolation of cold-adapted cellulose degrading bacterium: A candidate for straw degradation and De novo genome sequencing analysis. *Front. Microbiol.* 13:1098723. doi: 10.3389/fmicb.2022.1098723

Henrissat, B., Driguez, H., Viet, C., and Schülein, M. (1985). Synergism of Cellulases from Trichoderma reesei in the degradation of cellulose. *Bio/Technology* 3, 722–726. doi: 10.1038/nbt0885-722

Hentges, D. J., and Smith, L. D. (2018). Hydrolytic enzymes as virulence factors of anaerobic bacteria. *Bacterial Enzymes and Virulence.* (pp. 105–120). CRC Press.

Hervé, C., Rogowski, A., Blake, A. W., Marcus, S. E., Gilbert, H. J., and Knox, J. P. (2010). Carbohydrate-binding modules promote the enzymatic deconstruction of intact plant cell walls by targeting and proximity effects. *Proc. Natl. Acad. Sci.* 107, 15293–15298. doi: 10.1073/pnas.1005732107

Houfani, A. A., Vetrovsky, T., Baldrian, P., and Benallaoua, S. (2017). Efficient screening of potential cellulases and hemicellulases produced by Bosea sp. FBZP-16 using the combination of enzyme assays and genome analysis. *World J. Microbiol. Biotechnol.* 33:29. doi: 10.1007/s11274-016-2198-x

Hui-juan, Y., and Xia-li, G. (2018). Screening of straw-degrading Bacteria and study on their cellulose-degrading Performanes. *Biotechnol. Bull.* 35, 58–63. doi: 10.13560/j.cnki.biotech.bull.1985.2018-0731

Iizuka, H., and Komagata, K. (1963). New species of Pseudomonas belonged to fluorescent group. *J. Agric. Chem. Soc. Japan* 37, 137–141. doi: 10.1271/NOGEIKAGAKU1924.37.137

Jesus, R. B. d., Omori, W. P., Lemos, E. G. D. M., and Souza, J. A. M. d. (2015). <b>bacterial diversity in bovine rumen by metagenomic 16S rDNA sequencing and scanning electron microscopy. *Acta Sci. Anim. Sci.* 37:251. doi: 10.4025/actascianimsci.v37i3.26535

Jia, J., Wang, X., Deng, P., Ma, L., Baird, S. M., Li, X., et al. (2020). Pseudomonas glycinae sp nov. isolated from the soybean rhizosphere. *MicrobiologyOpen* 9:1101. doi: 10.1002/mbo3.1101

Jin, S., and Chen, H. (2007). Near-infrared analysis of the chemical composition of rice straw. *Ind. Crop. Prod.* 26, 207–211. doi: 10.1016/j.indcrop.2007.03.004

Kazeem, M. O., Shah, U. K. M., Baharuddin, A. S., and AbdulRahman, N. A. (2017). Prospecting agro-waste cocktail: supplementation for Cellulase production by a newly isolated thermophilic *B. licheniformis* 2D55. *Appl. Biochem. Biotechnol.* 182, 1318–1340. doi: 10.1007/s12010-017-2401-z

Khoirunnisa, N. S., Syaiful, A., and Dwi Andreas, S. (2020). Isolation and selection of cellulolytic bacteria from rice straw for consortium of microbial fuel cell. *Biodiv. J. Biol. Divers.* 21:450. doi: 10.13057/biodiv/d210450

Kim, D., and Ku, S. (2018). Bacillus Cellulase molecular cloning, expression, and surface display on the outer membrane of *Escherichia coli*. *Molecules* 23:503. doi: 10.3390/molecules23020503

Koeck, D. E., Pechtl, A., Zverlov, V. V., and Schwarz, W. H. (2014). Genomics of cellulolytic bacteria. *Curr. Opin. Biotechnol.* 29, 171–183. doi: 10.1016/j.copbio.2014.07.002

Ladeira, S. A., Cruz, E., Delatorre, A. B., Barbosa, J. B., and Martins, M. L. L. (2015). Cellulase production by thermophilic Bacillus sp. SMIA-2 and its detergent compatibility. *Electron. J. Biotechnol.* 18, 110–115. doi: 10.1016/j.ejbt.2014.12.008

Lakshmi, A., and Narasimha, G. (2012). Production of cellulases by fungal cultures isolated from forest litter soil. *Ann. For. Res.* 55, 85–92. doi: 10.15287/afr.2012.80

Li, J. (2010). Study on the mode of straw resources collection, storage and transportation in China.

Liu, S., and Han, L. (2021). The current situation and development strategy of corn straw returning in Heilongjiang Province. *China Seed Industry* 11, 20–22.

Lu, T., Gao, H., Liao, B., Wu, J., Zhang, W., Huang, J., et al. (2020). Characterization and optimization of production of bacterial cellulose from strain CGMCC 17276 based on whole-genome analysis. *Carbohydr. Polym.* 232:115788. doi: 10.1016/j.carbpol.2019.115788

Ma, L., Lu, Y., Yan, H., Wang, X., Yi, Y., Shan, Y., et al. (2020). Screening of cellulolytic bacteria from rotten wood of Qinling (China) for biomass degradation and cloning of cellulases from *Bacillus methylotrophicus*. *BMC Biotechnol.* 20:2. doi: 10.1186/s12896-019-0593-8

Ma, L., Yang, W., Meng, F., Ji, S., Xin, H., and Cao, B. (2015). Characterization of an acidic cellulase produced by *Bacillus subtilis* BY-4 isolated from gastrointestinal tract of Tibetan pig. *J. Taiwan Inst. Chem. Eng.* 56, 67–72. doi: 10.1016/j.jtice.2015.04.025

Manuel, M. (2013). A new semi-subterranean diving beetle of the *Hydroporus normandi* complex from South-Eastern France, with notes on other taxa of the complex (Coleoptera: Dytiscidae). *Zootaxa* 3652:4. doi: 10.11646/zootaxa.3652.4.4

McDonald, J. E., Rooks, D. J., and McCarthy, A. J. (2012). Methods for the isolation of cellulose-degrading microorganisms. *Cell* 510, 349–374. doi: 10.1016/B978-0-12-415931-0.00019-7

Miller, G. L. (2002). Use of Dinitrosalicylic acid reagent for determination of reducing sugar. *Anal. Chem.* 31, 426–428. doi: 10.1021/ac60147a030

Mondal, S., Halder, S. K., and Mondal, K. C. (2021). Tailoring in fungi for next generation cellulase production with special reference to CRISPR/CAS system. *Syst. Microbiol. Biomanufact.* 2, 113–129. doi: 10.1007/s43393-021-00045-9

Nema, N., Alamir, L., and Mohammad, M. (2015). Production of cellulase from *Bacillus cereus* by submerged fermentationusing corn husks as substrates. *Int. Food Res. J.* 22, 1831–1836.

Parks, D. H., Rinke, C., Chuvochina, M., Chaumeil, P.-A., Woodcroft, B. J., Evans, P. N., et al. (2017). Recovery of nearly 8,000 metagenome-assembled genomes substantially expands the tree of life. *Nat. Microbiol.* 2, 1533–1542. doi: 10.1038/s41564-017-0012-7

Paudel, L., Ghimire, N., Han, S.-R., Park, H., Jung, S.-H., and Oh, T.-J. (2022). Complete genome of Nakamurella sp. PAMC28650: genomic insights into its environmental adaptation and biotechnological potential. *Funct. Integr. Genomics* 23:6. doi: 10.1007/s10142-022-00937-6

Pollegioni, L., Tonin, F., and Rosini, E. (2015). Lignin-degrading enzymes. *FEBS J.* 282, 1190–1213. doi: 10.1111/febs.13224

Shi, W., Fang, Y. R., Chang, Y., and Xie, G. H. (2023). Toward sustainable utilization of crop straw: greenhouse gas emissions and their reduction potential from 1950 to 2021 in China. *Resour. Conserv. Recycl.* 190:106824. doi: 10.1016/j.resconrec.2022.106824

Somogyi, M. (1952). Notes on sugar determination. *J. Biol. Chem.* 195, 19–23. doi: 10.1016/S0021-9258(19)50870-5

Subashchandrabose, S. R., Venkateswarlu, K., Krishnan, K., Naidu, R., Lockington, R., and Megharaj, M. (2018). *Rhodococcus wratislaviensis* strain 9: an efficient p -nitrophenol degrader with a great potential for bioremediation. *J. Hazard. Mater.* 347, 176–183. doi: 10.1016/j.jhazmat.2017.12.063

Sukumaran, R. K., Singhania, R. R., and Pandey, A. (2005). Microbial cellulases — production, applications and challenges. *J. Sci. Ind. Res.* 64, 832–844.

Uzuner, S., and Cekmecelioglu, D. (2019). Enzymes in the beverage industry. *Enzymes in Food Biotechnology*, 29–43. doi: 10.1016/B978-0-12-813280-7.00003-7

Wang, Y., Liu, Q., Yan, L., Gao, Y., Wang, Y., and Wang, W. (2013). A novel lignin degradation bacterial consortium for efficient pulping. *Bioresour. Technol.* 139, 113–119. doi: 10.1016/j.biortech.2013.04.033

Wang, J., Walker, B. J., Abeel, T., Shea, T., Priest, M., Abouelliel, A., et al. (2014). Pilon: an integrated tool for comprehensive microbial variant detection and genome assembly improvement. *PLoS One* 9:2963. doi: 10.1371/journal.pone.0112963

Wang, J., Zhang, Z., and Liu, Y. (2018). Spatial shifts in grain production increases in China and implications for food security. *Land Use Policy* 74, 204–213. doi: 10.1016/j.landusepol.2017.11.037

Wei, X. F., Fan, H., Ma, J., Wang, J. Q., and Li, P. W. (2022). Research progress of carbohydrate-binding modules. *J. Qilu Univ. Technol.* 36, 13–19.

Westers, L., Westers, H., and Quax, W. J. (2004). *Bacillus subtilis* as cell factory for pharmaceutical proteins: a biotechnological approach to optimize the host organism. *Biochim. Biophys. Acta* 1694, 299–310. doi: 10.1016/j.bbamcr.2004.02.011

Wood, T. M., and Garcia-Campayo, V. (1990). Enzymology of cellulose degradation. *Biodegradation* 1, 147–161. doi: 10.1007/BF00058833

Xi, J., He, L. Y., Huang, Z., and Sheng, X. F. (2014). Bacillus qingshengii sp. nov., a rock-weathering bacterium isolated from weathered rock surface. *nt J Syst Evol Microbiol* 64, 2473–2479. doi: 10.1099/ijs.0.061929-0

Xie, X., Chen, L., Shi, Y., Chai, A., Fan, T., Li, L., et al. (2022). The calcium cyanamide and polyethylene blocks the secondary transmission and infection of vegetable leaf diseases. *Frontiers. Plant Sci.* 13:1027584. doi: 10.3389/fpls.2022.1027584

Xin-Yu, M., LI-Na, S., Shan, L., Peng, H., Yi-Ping, Z., and Xing-Yi, L. (2020). Screening of straw degrading microbial strains and their degradation effects. *Chin. J. Ecol.* 39, 1198–1205. doi: 10.13292/j.1000-4890.202004.012

Xu, J., Gao, Z., Wu, B., and He, B. (2017). Lactose-inducted production of a complete lignocellulolytic enzyme system by a novel bacterium Bacillus sp. BS-5 and its application for saccharification of alkali-pretreated corn cob. *Cellulose* 24, 2059–2070. doi: 10.1007/s10570-017-1247-4

Yadav, S., and Dubey, S. K. (2018). Cellulose degradation potential of *Paenibacillus lautus* strain BHU3 and its whole genome sequence. *Bioresour. Technol.* 262, 124–131. doi: 10.1016/j.biortech.2018.04.067

Yadav, S., Reddy, B., and Dubey, S. K. (2019). De novo genome assembly and comparative annotation reveals metabolic versatility in cellulolytic bacteria from cropland and forest soils. *Funct. Integr. Genomics* 20, 89–101. doi: 10.1007/s10142-019-00704-0

Yang, W., Li, X. H., and Zhang, Y. T. (2022). Research Progress and the development trend of the utilization of crop straw biomass resources in China. *Front. Chem.* 10:904660. doi: 10.3389/fchem.2022.904660

Zhang, D.-F., He, W., Shao, Z., Ahmed, I., Zhang, Y., Li, W.-J., et al. (2023). EasyCGTree: a pipeline for prokaryotic phylogenomic analysis based on core gene sets. *BMC Bioinformat.* 24:390. doi: 10.1186/s12859-023-05527-2

Zhang, Z., Liu, J.-L., Lan, J.-Y., Duan, C.-J., Ma, Q.-S., and Feng, J.-X. (2014). Predominance of Trichoderma and Penicillium in cellulolytic aerobic filamentous fungi from subtropical and tropical forests in China, and their use in finding highly efficient β-glucosidase. *Biotechnol. Biofuels* 7:107. doi: 10.1186/1754-6834-7-107

frontiers | Frontiers in Microbiology

TYPE Original Research
PUBLISHED 04 September 2024
DOI 10.3389/fmicb.2024.1433092

OPEN ACCESS

EDITED BY
Qi Zhang,
Nanchang University, China

REVIEWED BY
Kun Zhang,
Yangzhou University, China
Vidya De Gannes,
The University of the West Indies St. Augustine, Trinidad and Tobago
Shanfei Fu,
Chinese Academy of Sciences (CAS), China

*CORRESPONDENCE
Xiangwei You
youxiangwei@caas.cn
Yiqiang Li
liyiqiang@caas.cn

†These authors have contributed equally to this work

RECEIVED 15 May 2024
ACCEPTED 21 August 2024
PUBLISHED 04 September 2024

CITATION
Xie C, Wang X, Zhang B, Liu J, Zhang P, Shen G, Yin X, Kong D, Yang J, Yao H, You X and Li Y (2024) Co-composting of tail vegetable with flue-cured tobacco leaves: analysis of nitrogen transformation and estimation as a seed germination agent for halophyte.
Front. Microbiol. 15:1433092.
doi: 10.3389/fmicb.2024.1433092

Co-composting of tail vegetable with flue-cured tobacco leaves: analysis of nitrogen transformation and estimation as a seed germination agent for halophyte

Chenghao Xie[1†], Xiao Wang[1,2†], Benqiang Zhang[3], Jiantao Liu[1], Peng Zhang[4], Guangcai Shen[5], Xingsheng Yin[5], Decai Kong[3], Junjie Yang[3], Hui Yao[1,2], Xiangwei You[1,2*] and Yiqiang Li[1,2*]

[1]Marine Agriculture Research Center, Tobacco Research Institute, Chinese Academy of Agricultural Sciences, Qingdao, China, [2]National Center of Technology Innovation for Comprehensive Utilization of Saline-Alkali Land, Dongying, China, [3]Tobacco Shandong Industrial Co., Ltd., Jinan, China, [4]Plant Functional Component Research Center, Tobacco Research Institute, Chinese Academy of Agricultural Sciences, Qingdao, China, [5]Tobacco Baoshan Industrial Co., Ltd., Baoshan, China

Resource utilization of tail vegetables has raised increasing concerns in the modern agriculture. However, the effect and related mechanisms of flue-cured tobacco leaves on the product quality, phytotoxicity and bacterially-mediated nitrogen (N) transformation process of tail vegetable composting were poorly understood. Amendments of high-dosed (5% and 10% w/w) tobacco leaves into the compost accelerated the heating process, prolonged the time of thermophilic stage, increased the peak temperature, thereby improving maturity and shortening composting duration. The tobacco leaf amendments at the 10% (w/w) increased the N conservation (TN and NH_4-N content) of compost, due to the supply of N-containing nutrient and promotion of organic matter degradation by tobacco leaves. Besides, tobacco leaf amendments promoted the seed germination and root development of wild soybean, exhibiting the feasibility of composting product for promoting the growth of salt-tolerant plants, but no dose-dependent effect was found for tobacco leaf amendments. Addition of high dosed (5% and 10% w/w) tobacco leaves shifted the bacterial community towards lignocellulosic and N-fixing bacteria, contributing to increasing the compost maturity and N retention. PICRUSt 2 functional prediction revealed that N-related bacterial metabolism (i.e., hydroxylamine oxidation and denitrifying process) was enhanced in the tobacco leaf treatments, which contributed to N retention and elevated nutrient quality of composting. To the best knowledge, this was the first study to explore the effect of tobacco waste additives on the nutrient transformation and halophyte growth promotion of organic waste composting. These findings will deepen the understanding of microbially-mediated N transformation and composting processes involving flue-cured tobacco leaves.

KEYWORDS

organic waste, tail vegetable, wild soybean, phytotoxicity, nitrogen conversion

1 Introduction

With the rapid improvement of people living standard, the requirements for food health and nutrition have increased. As a result, the demand for meat, eggs, milk, and fresh vegetables are constantly increasing (Jin et al., 2021). Accordingly, the scale of livestock and poultry breeding in China is expanding and standardization is strengthened. However, the related pollution prevention and resource treatment work is lagging behind. Owing to the poor post-disposal (e.g., direct return to field and incineration), the enormous quantities of agricultural organic waste (e.g., livestock manure and tail vegetables) exceeded the bearing capacity of nearby natural ecosystem, posing a serious threat to environment and human health (Xie et al., 2023). Therefore, to utilize agricultural organic waste in a recycling and green manner has become an urgent issue to be addressed (He X. et al., 2022).

Agricultural waste contained a large amount of organic matter and nutrient elements such as nitrogen, phosphorus, and potassium, which can be converted into fertilizers via various technologies (Zheng et al., 2022). Tail vegetables were commonly generated from the agricultural production. It was estimated that the generation amount of tail vegetable in China reached 384 million tons in 2021 (Qian et al., 2022). Tail vegetables, characterized as low nitrogen content and high carbon content, were mostly the root, stems and leaves after the crop harvest. Most of tail vegetables were cellulose, hemicellulose, lignin, and other organic substances that were difficult to be decomposed (Zheng et al., 2022). Besides, tail vegetables commonly carried heavy metals and pathogens, increasing the ecological risks (Hoang et al., 2022). Therefore, for resource utilization and environment protection, it was very crucial to properly treat and dispose of tail vegetables. Resource utilization technologies of tail vegetables popularized in China mainly included direct return to field, incineration and aerobic composting (Qiao et al., 2023). Compared with other treatment methods, composting was an efficient and environmentally benign technology that converted solid wastes into a safer product and/or organic fertilizer (Li et al., 2023; Qian et al., 2022). Aerobic composting could maximize the material cycle and carbon capture, posing a series of positive effects (Huang et al., 2022; Shan et al., 2021). However, there were many challenges with composting, such as large N losses and greenhouse gas emissions. N loss could not only cause atmospheric pollution, but also reduce the quality of compost product. TN amount was generally lost accompanied with N-containing gas emissions (Shan et al., 2021). Hence, mitigating N loss during the composting is particularly important to improve composting quality and reduce environmental pollution. Several studies have demonstrated that application of additives into the compost could be one of highly effective methods to reduce N loss and enhance N conservation during composting (Huang et al., 2022). Adding biochar, salts (e.g., $MgCl_2$, $FeSO_4$) or acid–base additives [e.g., $Mg(OH)_2$, H_3PO_4] into compost could reduce NH_3 emission, increase NH_4^+ content, and reduce TN loss (Ba et al., 2020; Ye et al., 2023). Essentially, composting was a process of degradation of organic matter under the action of microorganisms. However, microbially-mediated nutrient transformation process (especially for N conservation) in the compost and related ecological impacts have not been clearly illustrated.

Tobacco was cultivated in more than 4 million hectares of land area globally. China is one of the main tobacco growers in the world (Lisuma et al., 2020). Discarded tobacco leaf was a representative of tobacco waste. A large amount of tobacco waste with high water content were produced in farmland, and it may cause environmental pollution if it was not properly treated. Tobacco waste was not easily collected and transported, resulting in its centralized treatment was expensive. However, tobacco leaves were rich in nutrients, with protein accounting for about 10% of dry matter and minerals accounting for 5–10%, of which K accounts for 0.44–0.53% (Zittel et al., 2020). It will be beneficial to solve environmental pollution, recover parts of nutrients, and increase organic matter content in the soil, if the tobacco waste can be effectively reused (Wang et al., 2020). However, the effect of tobacco leaves on the N transformation process, product quality, and phytotoxicity of tail vegetable composting and related microbially-mediated mechanisms were poorly understood. Moreover, lack of studies addressing on the nitrogen loss issues during the tail vegetable composting has motivated the investigation of the present study.

Therefore, the flue-cured leaves of tobacco (*Nicotiana tabacum* L.) were collected aerobiotic composting was conducted using mixture of tomato tail vegetable, cattle manure and rice husk as compost raw materials, different doses of flue-cured tobacco leaves as additives. The specific objectives were (1) to investigate the variation in physicochemical properties and N-transformation process during composting amended with different doses of tobacco leaves; (2) to explore how the addition of tobacco leaves influence the bacterial community structure and metabolic functions; and (3) to evaluate the promotion efficiency of composting leachate on the seed germination of salt-tolerant halophytes. This study will offer guidelines for the development of composting technology used for resource utilization of tail vegetables and application of related composting products into promoting growth of halophytes in the salt-affected soils.

2 Materials and methods

2.1 Description of compost material

Tomato tail vegetable was collected from a conventional tomato farm located in Jimo District, Qingdao. Cattle manures were obtained from the local dairy farm in the Jimo District, Qingdao, Shandong Province, China. The husk of rice (*Oryza sativa* L.) was provided by Beisenmiao Energy Company, Henan. Ultrapure water was prepared using the Milli-Q water purification system (Advantage A10, Millipore, United States). The flue-cured leaves of tobacco (*Nicotiana tabacum* L.) were provided by Tobacco Research Institute, Chinese Academy of Agricultural Sciences, Qingdao. Prior to mixing, the rice husks were cut into 0.5 cm pieces and flue-cured tobacco leaves were passed through 2 mm sieve.

2.2 Composting process and sampling

Rice husk, tomato tail vegetable and cattle manure were mixed evenly at 5:4:1 (wet weight) to ensure the C/N ratio around 30. Composting in each treatment was conducted in three sealed 40 L-cylindrical rotary drum composters for 50 days. Each treatment was replicated three times. The proper amount of ultrapure water was

added into the mixture in each rotary drum composter to maintain the moisture content at the 65%. Temperature was monitored every day between 9:00 and 10:00 a.m. The adding ratio of tobacco leaves with raw material mixture (RM), including 0 (%w/w), 2 (%w/w), 5 (%w/w) and 10 (%w/w). Therefore, four composting treatments were set up (1) RM: tomato tail vegetable + cattle manure + rice husk (CKT); (2) RM + 2% (w/w) tobacco leaves (LT); (3) RM + 5% (w/w) tobacco leaves (MT); (4) RM + 10% (w/w) tobacco leaves (HT). Samples weighting about 200 g were collected from each rotary drum composter after mixing thoroughly from top to bottom layers in the composters on day 3, 7, 9, 14, 28, and 50 for the analysis of physiochemical properties. During the compost sampling, all the instruments were sterilized. About 0.5 g of fresh compost from each drum composter on day 3, 9, 14, and 50 were sampled and stored at −80°C for microbial community analysis.

2.3 Physicochemical property analysis of compost

During the composting period, various physicochemical parameters including temperature, pH, electrical conductivity (EC), total carbon (TC), total nitrogen (TN), ammonia nitrogen (NH_4^+-N), available phosphorus, emissions of ammonia (NH_3) and greenhouse gases (CH_4, CO_2, and N_2O) were measured. The fresh compost sample was supplemented with deionized water at a ratio of 1:10 (w/v) and shaken at 200 rpm for 30 min to determine pH and EC using a digital pH meter (S-3C, Leici, China) and a conductivity meter (DDS-307A, Leici, China). TC and TN content of compost were measured by an Elemental analyzer (Thermo Fisher FlashSmart, United States). To determine NH_4^+-N content, the sampled compost product was extracted with 2 mol/L KCl solution at solid-to-lipid ratio of 1:5 (w/v). Available phosphorus (AP) content of compost was determined by a continuous flow analysis (SA 4000, Skalar San++, France) after extracting with 0.5 M sodium bicarbonate ($NaHCO_3$) (Luo et al., 2024; Wang X. et al., 2023). For the gas collection and analysis, a 50 mL gas sample was collected by a syringe and pulled back three times to ensure the sampled gas homogeneous at each sampling timepoint. Then, the gas sample was transferred into 25 mL pre-evacuated headspace flasks (Vial, crimp, FB, Agilent, United States). During each gas collection, the time and temperature were recorded, and gases were sampled every 10 min. The concentrations of ammonia (NH_3) and greenhouse gases (CH_4, CO_2, and N_2O) were measured with a gas chromatography (GC, Agilent 7890, United States). After the sampling, fresh air was pump-flushed into the flasks for 5 min to supplement air. Wild soybean (*Glycine soja*), one of representative salt-tolerant halophytes widely distributed in the Yellow River Delta, China (Yin et al., 2023), was used as the tested plant to evaluate the promotion efficiency of tail vegetable compost as a seed germination agent. Seed germination index (GI) was calculated as follows:

$$GI(\%) = \frac{\text{Seed germination rate of treatment}(\%) \times \text{Root length of treatment}}{\text{Seed germination rate of control}(\%) \times \text{Root length of control}} \times 100\%$$

2.4 Microbial analysis of compost

To investigate the effect of tobacco leaf amendments on the diversity and composition of compost bacterial community, PCR amplification of 16S rRNA high-throughput sequencing analysis was conducted. Total DNA was extracted from 0.5 g of fresh compost using the FastDNA SPIN Kit (MP Biomedicals, Santa Ana, CA, United States) according to manufacturer's instructions. DNA quality and quantity were determined using a NanoDrop 2000 UV–vis spectrophotometer (Thermo Scientiffc, Wilmington, United States), and 1% agarose gel electrophoresis, respectively. The V3–V4 region of 16S rRNA genes was amplified using the primers 338F (5′-barcode-ACTCCTACGGGAGGCAGCAG-3′) and 806R (5′-GGACTACHV GGGTWTCTAAT-3′). The PCR products were purified and quantified, subsequently, library was constructed and sequenced at the MiSeq® Illumina 2000 platform by Majorbio Bio-Pharm Technology Co., Ltd. (Shanghai, China) (Wang X. et al., 2023). The sequencing reads were analyzed by QIIME (version 2.0.0). Operational taxonomic units (OTUs) were clustered with 97% identify. Taxonomic classification of each OTU was conducted using the RDP classifier against the SILVA database. PICRUSt 2 was used for functional profile prediction of bacterial 16S rRNA based on the Kyoto Encyclopedia of Genes and Genomes (KEGG) database (Wang et al., 2024).

2.5 Statistical analysis

All the data were expressed as mean values. Each treatment was replicated three times. Statistical analyses were conducted using the Statistical Product and Service Solutions Software 22 (SPSS Inc., Chicago, United States). Significant differences among different treatments were analyzed by the one-way analysis of variance (ANOVA) using the Duncan's multiple-comparison test ($p < 0.05$). Prior to the ANOVA analysis, the normality and homogeneity of data was assessed by the Shapiro–Wilk tests and Levene test, respectively. All the data were analyzed using the SPSS Statistics 20.0 at a "$p < 0.05$" level. The OTU richness and Shannon diversity index of bacterial community were determined using the R vegan package. Nonmetric multidimensional scaling (NMDS) analysis was conducted to visualize the similarity of bacterial community structures among different treatments.

3 Results and discussion

3.1 Changes in the physicochemical properties of compost

The four treatment groups went through three typical temperature change stages (mesophilic, thermophilic, and cooling) during the aerobic composting (Figure 1A). Temperature was a crucial indicating parameter of composting, directly reflecting composting progress, maturation extent, and microbial growth and metabolic activities (Kong et al., 2022; Sun et al., 2022). The similar change trends of temperature during composting were found in all treatments, which contained heating, thermophilic, cooling and maturity stages (Figure 1A). Due to rapid decomposition of organic matter by microbes (exothermic reaction), the temperature of

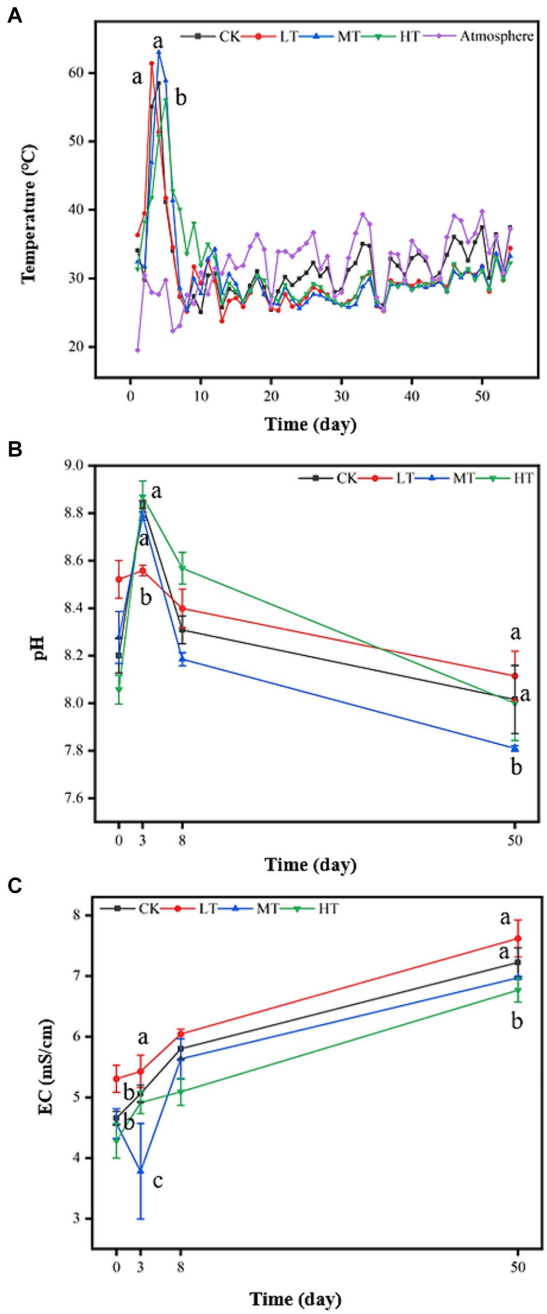

FIGURE 1
Effects of tobacco leaf amendments of basic physicochemical properties of tomato tail vegetable composting; **(A)** temperature, **(B)** pH and **(C)** electrical conductivity. CK: tomato tail vegetable + cattle manure + rice husk; LT: tomato tail vegetable + cattle manure + rice husk + 2% (w/w) tobacco leaves; MT: tomato tail vegetable + cattle manure + rice husk + 5% (w/w) tobacco leaves; HT: tomato tail vegetable + cattle manure + rice husk + 10% (w/w) tobacco leaves. The different lowercase letters on day 3 and 50 represent significant difference between different treatments (Duncan's multiple-comparison test, $p < 0.05$).

compost increased sharply to 50°C–60°C at the beginning stage (day 5–7) of composting in all the treatments. Compared with CK treatment, medium and high-dosed amendments of tobacco leaf generally lengthened the thermophilic stage of composting to 1–2 days, following HT > MT. However, the low-dosed addition of tobacco leaves had little effect on the duration time of thermophilic stage (Figure 1A). While for the peak temperature of composting, MT treatment occupied the highest temperature (63°C), followed by LT treatment (62°C) and CK (59°C). The results showed that tobacco leaf amendment accelerated the compost degradation at the thermophilic stage. In this stage, the anaerobic microorganisms and aerobic microorganisms could efficiently participate in the decomposition and transformation of organic matter at 40°C–60°C (Huang et al., 2022; Li et al., 2023). Therefore, the increased compost temperature at the thermophilic stage could accelerate the decomposition rate of organic matter in the compost. This could speed up the composting process and shorten the composting cycle, elevating the compost quality (Sun et al., 2022). Additionally, the high temperature (>50°C) can kill the pathogenic microorganisms and decompose toxic substances in the compost efficaciously, increasing the environmental safety of composting products (Huang et al., 2022). After the thermophilic stage, readily-decomposed organic matter and available carbon sources are gradually exhausted with the decreasing microbial activity, so the temperature gradually decreased (Li et al., 2023). Notably, MT and HT treatments put off the decrease of temperature, but LT had little impact on it, exhibiting the dose-dependent effect. The effects of tobacco leaf amendments on compost temperature could be ascribed to that the supply of N-containing nutrients from tobacco leaves promoted microbial metabolism and accelerated the organic matter degradation, resulting in the generation of more heat (Kurt and Kinay, 2021; Li et al., 2023).

The pH was an indicator of compost maturity, which affected many biological processes, including the degradation of organic matter. Variation of pH during composting was related with ammonification, nitrification, NH_3emission and microbe-mediated N transformation. During composting, the pH increased gradually and reached the peak at day 3, LT treatment decreased the compost pH, while MT and HT treatments did not show the similar effect on pH (Figure 1B). The compost pH then decreased from day 3 to 50. This was ascribed to volatilization of NH_3, emission of CO_2 and production of organic acids (Wong et al., 2017). Moreover, the pH was highest in HT treatment during composting on day 8. This result is probably because high-dosed amount addition of tobacco leaves promoted the decomposition of organic nitrogen compounds and the production of ammonia as a result of promoted microbial activities (Huang et al., 2022; Li et al., 2023), strongly agreed with the higher compost temperature after HT treatment (Figure 1A). At the end of composting, pH in all the treatments was 7.8–8.2, which was within the required standards (5.5–8.5) of the Chinese Industry Standard (Wang N. et al., 2022). The EC reflected the degradation of organic matter, which could be used to evaluate the supply of nutrient elements in the compost (Wang et al., 2021). The EC values in all treatments increased at the inception stage of the composting (Figure 1C). This was mainly attributed to microbial decomposition of organic matter, which produced the large number of small molecular fatty acids and other small molecular substances (Wang et al., 2021; Xi et al., 2016). However, in the initial phase of composting, the EC values of compost treated with MT were significantly lower by 7.69% than that of control (Figure 1C) due to the precipitation and adsorption of mineral salts by the lignocellulose resulted from the increased compost pH after the addition of tobacco leaves (Li et al., 2023; Wang G. et al., 2022).

3.2 Nutrient condition of compost

The C/N ratios reflected the maturation degree of compost (Chen et al., 2021). With the extension of composting time, the C/N ratios increased sharply by 130–300% in all the treatments possibly due to rapid decomposition of nitrogenous compounds by microbes and emission of NH_3 at the thermophilic stage (Figure 2A). On day 3 and 8, HT treatment increased the C/N ratios of compost compared with CK treatment. This could be ascribed to input of high-amount of N-containing in tobacco leaves to compost (Wang G. et al., 2022). However, tobacco amendments had little effect on C/N ratios. After the thermophilic stage of composting, the C/N ratios in all the treatments decreased and eventually were under 20, which meet the standard of compost maturity (Chen et al., 2021). After day 3, the microbial activity was enhanced, which could lead to the increased consumption of carbon-containing substrates (e.g., sugars and organic acids) in the compost, thereby resulting in the decrease of compost TC content (Figure 2B). However, till to the ending of composting, the TC content of compost amended with tobacco leaves was significantly higher than CK. However, the TN content exhibited the increasing tread as the time longed (Figure 2C), perhaps owing to the mass reduction (Li et al., 2023). Relative to CK treatment, the TN content of the final composting product in HT, MT and LT treatments were increased by 11.40, 20.44, and 34.35%, respectively (Figure 2A).

NH_4^+-N content in all treatments firstly decreased from day 1 to 2 and subsequently increased from day 2 to 4 (Figure 2D). The increase of NH_4^+-N concentration in the early stage of composting may be due to the decomposition of organic matter and ammoniation of organic N by microorganisms (Wang G. et al., 2022). Compared with CK treatment, tobacco leaf amendments increased NH_4^+-N content of compost on day 3 and 4, with the order of HT (1.39 g/kg) > MT (0.70 g/kg) > LT (0.30 g/kg), exhibiting the obvious dose-dependent effect (Figure 2D). On day 50, the NH_4^+-N content of MT (0.80 g/kg), LT (0.70 g/kg) and HT (0.57 g/kg) were generally higher than that of CK treatment, and met the mature requirements of compost (more than 400.0 mg/kg) (Zhang et al., 2021). This result

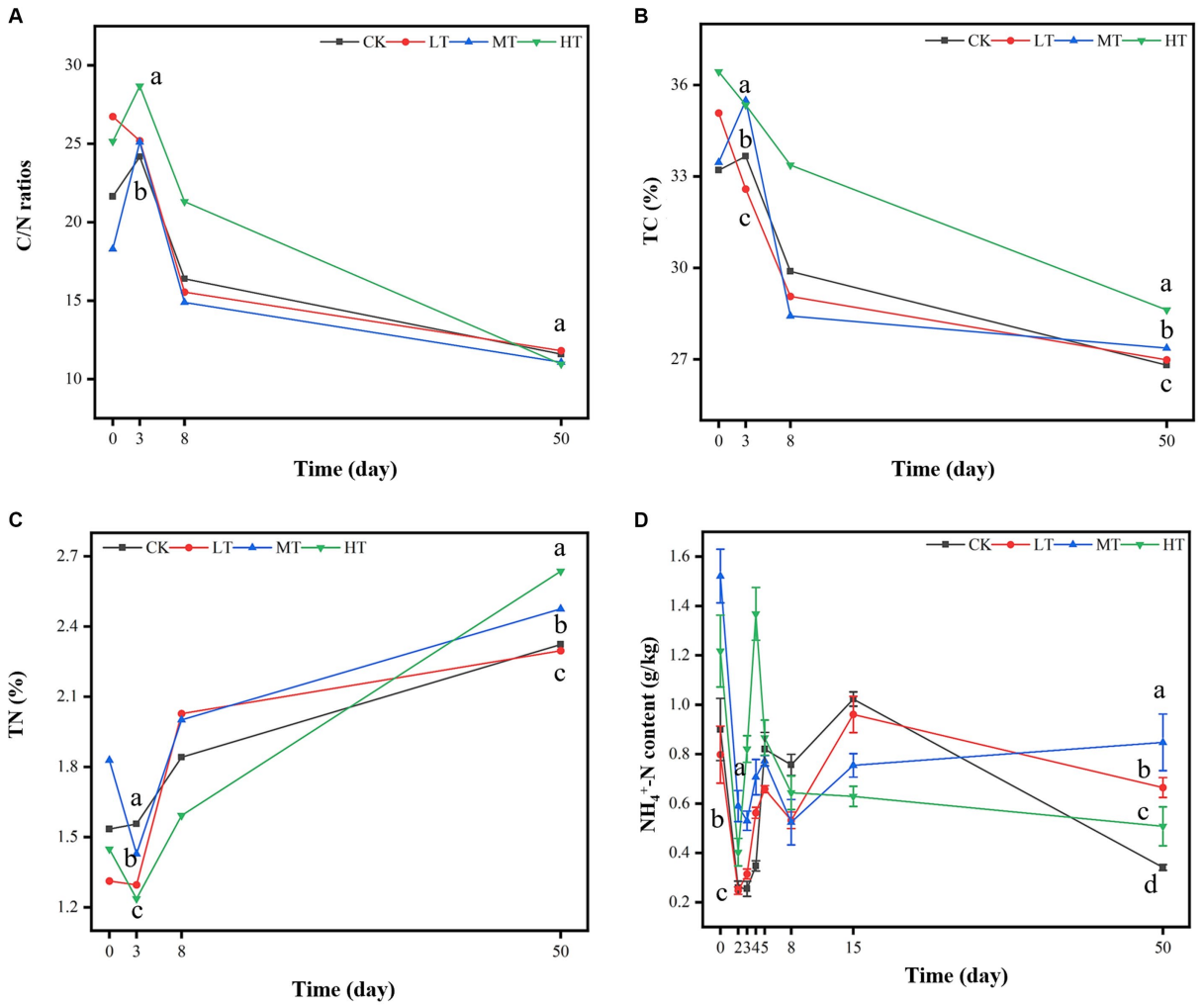

FIGURE 2
Effects of tobacco leaf amendments of nutrient parameters of tomato tail vegetable composting; **(A)** C/N ratios, **(B)** total carbon content (TC) content, **(C)** total nitrogen (TN) content, **(D)** ammonia nitrogen (NH_4^+-N) content. CK: tomato tail vegetable + cattle manure + rice husk; LT: tomato tail vegetable + cattle manure + rice husk + 2% (w/w) tobacco leaves; MT: tomato tail vegetable + cattle manure + rice husk + 5% (w/w) tobacco leaves; HT: tomato tail vegetable + cattle manure + rice husk + 10% (w/w) tobacco leaves. The different lowercase letters on day 3 and 50 represent significant difference between different treatments (Duncan's multiple-comparison test, $p < 0.05$).

indicated that N-containing organic matter and mineral salts in tobacco leaves was converted into inorganic N during the thermophilic stage of composting. Notably, TN and NH_4^+-N content of compost in tobacco leaf treatments were generally higher than that of CK (Figure 2D), indicating that tobacco leaf amendments enhanced the N retention in compost product (Li et al., 2023).

3.3 Change of bacterial community diversity and structure in the compost

Tobacco leaf amendments affected bacterial α-diversity of compost during the different stages of composting, which was evaluated based on ACE richness and Simpson diversity index (Figures 3A,B). For the ACE index, MT and HT treatments increased it in the compost on day 1. However, the ACE index underwent a sharp decrease on day 3 relative to it on day 1 (Figure 3A). This could be ascribed to the non-suitable microenvironment (e.g., oxygen and labile nutrient deficiency) of compost for microbial growth at the initial stage of composting (Qian et al., 2022). Similar results were also observed for Simpson index (Figure 3B). As the composting process progressed, the microorganisms gradually adapted and grew, resulting in the increased microbial diversity (Chen et al., 2022). Moreover, tobacco leaf amendments had non-significant effect on the ACE index on day 3, 7 and 50. These results indicated that amendments of tobacco leaves did not increase the number of bacterial species in the composting system. MT and HT treatments elevated the Simpon index of composting on day 3 and 50 (Figure 3B), which could be resulted from the input of nutrients (e.g., N-containing organic matter and mineral salts) from tobacco leaves into the compost

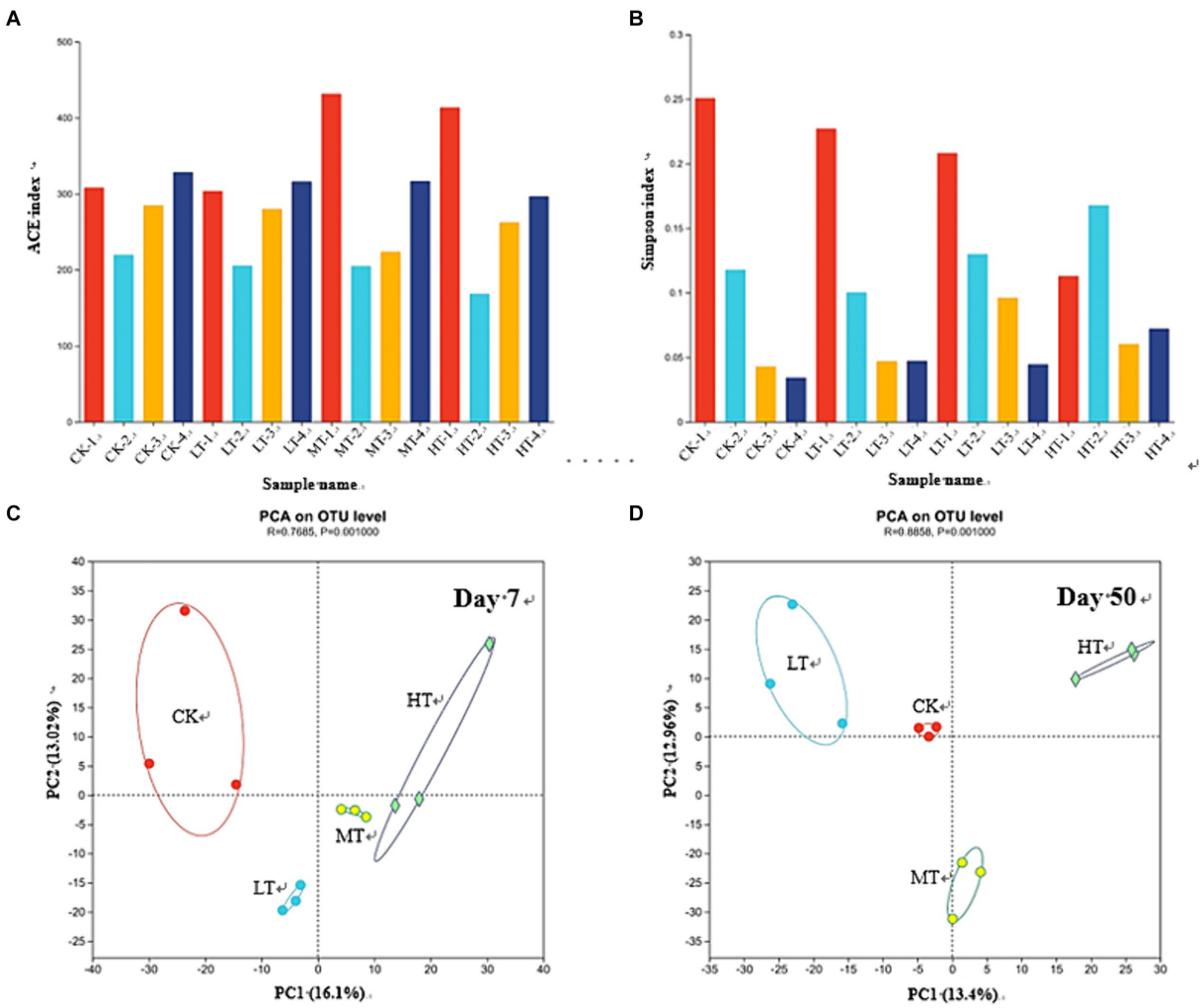

FIGURE 3
Effects of tobacco leaf amendments of bacterial community diversity and structure in the compost with or without tobacco leaf amendments. **(A)** The richness index of bacterial community (ACE index). **(B)** The diversity index of bacterial community (Shannon index). **(C)** Principal component analysis (PCA) of bacterial community composition according to the Bray–Curtis similarity at day 7. **(D)** PCA of bacterial community composition according to the Bray–Curtis similarity at day 50. CK: tomato tail vegetable + cattle manure + rice husk; LT: tomato tail vegetable + cattle manure + rice husk + 2% (w/w) tobacco leaves; MT: tomato tail vegetable + cattle manure + rice husk + 5% (w/w) tobacco leaves; HT: tomato tail vegetable + cattle manure + rice husk + 10% (w/w) tobacco leaves. -1, -2, -3, and -4 in the panels **A**,**B** represented the samples collected from the compost on day 1, 3, 7, and 50, respectively.

promoted microbial metabolism and accelerated the organic matter degradation (Kurt and Kinay, 2021; Li et al., 2023).

The Bray–Curtis based PCA (Figures 3C,D) showed that tobacco leaves changed the bacterial community composition. During the thermophilic stage, the tobacco leaf amendments remarkably changed the bacterial community composition of compost compared with CK treatment, revealed by the distinct clustering features between CK and tobacco leaf treatments (LT, MT, and HT). Among the tobacco leaf treatments, the MT treatment was located close to HT treatment (Figure 3C). However, at the ending of composting on day 50, every tobacco leaf treatment moved far from CK treatment, showing distinctly different clustering features of bacterial community between each other (Figure 3D). These results indicated that susceptibility of bacterial community of compost to different doses of tobacco leaves changed with different composting stages.

3.4 Change of bacterial community composition in the compost

The bacterial community in the composting system at different compost stage were analyzed using 16S rRNA high-throughput sequencing. Figures 4A,B showed the changes in bacterial abundance at the phylum level and the top 30 bacterial genera. Firmicutes, Proteobacteria, Actinobacteria, Bacteroidota, Chloroflexi, and Gemmatimonadota were the dominant bacteria throughout the entire aerobic composting process. These bacterial phyla accounted for 85.08–98.35% of the total bacterial 16S rRNA gene sequences (Figure 4A). The bacterial community was dominated by Firmicutes at the initial stage of composting (day 1 and 3), although the proportion varied among different treatments (35.4%–87.5%). During the thermophilic period, the relative abundance of Firmicutes in the MT and HT group increased relative to the CK (CK-1 and CK-2) group. Proteobacteria and Bacteroidota were enriched in the higher-doses of tobacco leaf treatments (MT-1, -2 and HT-1, -2) at the initial stage of thermophilic period compared with the CK group. However, at the peak of thermophilic period (day 7), LT-3 treatment showed little effect on bacterial community at the phylum level relative to CK, despite the relative abundance of Proteobacteria and Firmicutes increased in the MT-3 and HT-3 treatments (Figure 4A). It was reported that some members of phylum Bacteroidota and Firmicutes could degrade lignocellulosic polymers, which can be fermented into short chain volatile fatty acids (Wang C. et al., 2022). Actinobacteriota could survive in tough environments, such as high temperatures, effectively degrade organic matter and lignocelluloses (He J. et al., 2022; Zhao et al., 2016). Proteobacteria was associated with compost nitrogen transformation and was dominant during thermophilic and cooling periods. Proteobacteria, recognized as N-fixing bacteria, could be beneficial for mitigating N loss and N retention in the compost (Wang Z. et al., 2023). Therefore, the tobacco leaf induced response changes of bacterial community in the compost could contribute to increasing the compost maturity and N retention.

The taxonomic composition during composting at the genus level was also investigated (Figure 4B). In the CK treatment, the dominant genera in the initial stage of composting were *Staphylococcus* and *Corynebacterium*. However, after tobacco leaf amendments, the compost was dominantly occupied by *Staphylococcus* and *Weissella*. At the thermophilic stage, the relative abundance of *Bacillaceae*, *Weissella* and *Cellvibrio* generally increased after the tobacco leaf amendments in the MT-2/3 and HT-2/3 treated composts compared with the CK treatment (Figure 4B). As a member of Firmicutes, *Bacillaceae* is a typical sporulating and heat resist species (Wang C. et al., 2022). Many other functional bacteria, such as *Weissella*, a thermophilic bacterium that can hydrolyze phenolic compounds, existing with *Bacillaceae*, improving the community stability (Wang et al., 2019). A previous study also found that *Luteimonas*, *Cellvibrio* and *Pseudomonas* were the main bacterial genera in the maturation stage of composting (Yin et al., 2021). *Cellvibrio*, a cellulose-degrading bacteria with low tolerance to high temperature (Wang Z. et al., 2022), were found to be more abundant in the late stage of compost in the MT and HT treatments, indicating that tobacco leaf amendments facilitated the compost humification.

3.5 Analysis of functional genes related to nitrogen transformation in the compost

The bacterial metabolic function prediction was carried out using the PICRUSt 2 based on KEGG pathway database. The expression profiles of N conversion-associated genes were further investigated to elucidate the mechanism of N transformation in the compost (Figure 5). As for nitrification process of compost, *amoA*, *amoB*, and *amoC* are three key genes encoding subunits of ammonia monooxygenase, whose relative abundance was generally higher in tobacco leaf groups than in CK group. Moreover, the promotion effect followed the order of HT > MT > LT, showing the dose-dependent effect. This result suggested tobacco leaf amendments elevated the activity and abundance of ammonia oxidizing bacteria, which could be resulted from changes of environmental factors such as composting temperature and oxygen content (Xiong et al., 2022). Similarly, the relative abundance of hydroxylamine oxidase (*hao*) gene in the tobacco leaf treatments was higher than CK treatments. Taken together, the addition of tobacco leaves promoted the nitrification process, converting more NH_4^+-N to NO_3^--N. However, as the composting time going, the relative abundance of ammonia oxidizing genes exhibited no significant difference in tobacco leaf treatments from CK treatment, implying that ammonia oxidation in compost was inhibited possibly due to the decreased activity and abundance of nitrifying bacteria after thermophilic and maturation phases (Figure 5).

For the denitrifying bacterial genes such as *nirA*, *nirS* and *nirK*, the tobacco leaf amendments elevated their relative abundance at the early stage, but decreased their relative abundance during the thermophilic and maturation phases. The different effect of tobacco leaf amendments on denitrifying bacterial gene at different composting stages could be explained by biodegradation extent and O_2 content (Zhong et al., 2020). At the early stages of composting, strong biodegradation occurred and O_2 was rapidly consumed, providing a favorable anaerobic environment for denitrifying bacteria (Tian et al., 2024; Zhong et al., 2020). With the constant consumption of easily degradable organic matter in the compost, the composting was gradually stabilized (Xiong et al., 2022). These could explain the variable responses of bacterial genes in the compost to tobacco leaf amendments at the different composting stages (Figure 5). The *norB* gene was responsible for the denitrification step in the conversion of NO into N_2O. A

10.3389/fmicb.2024.1433092

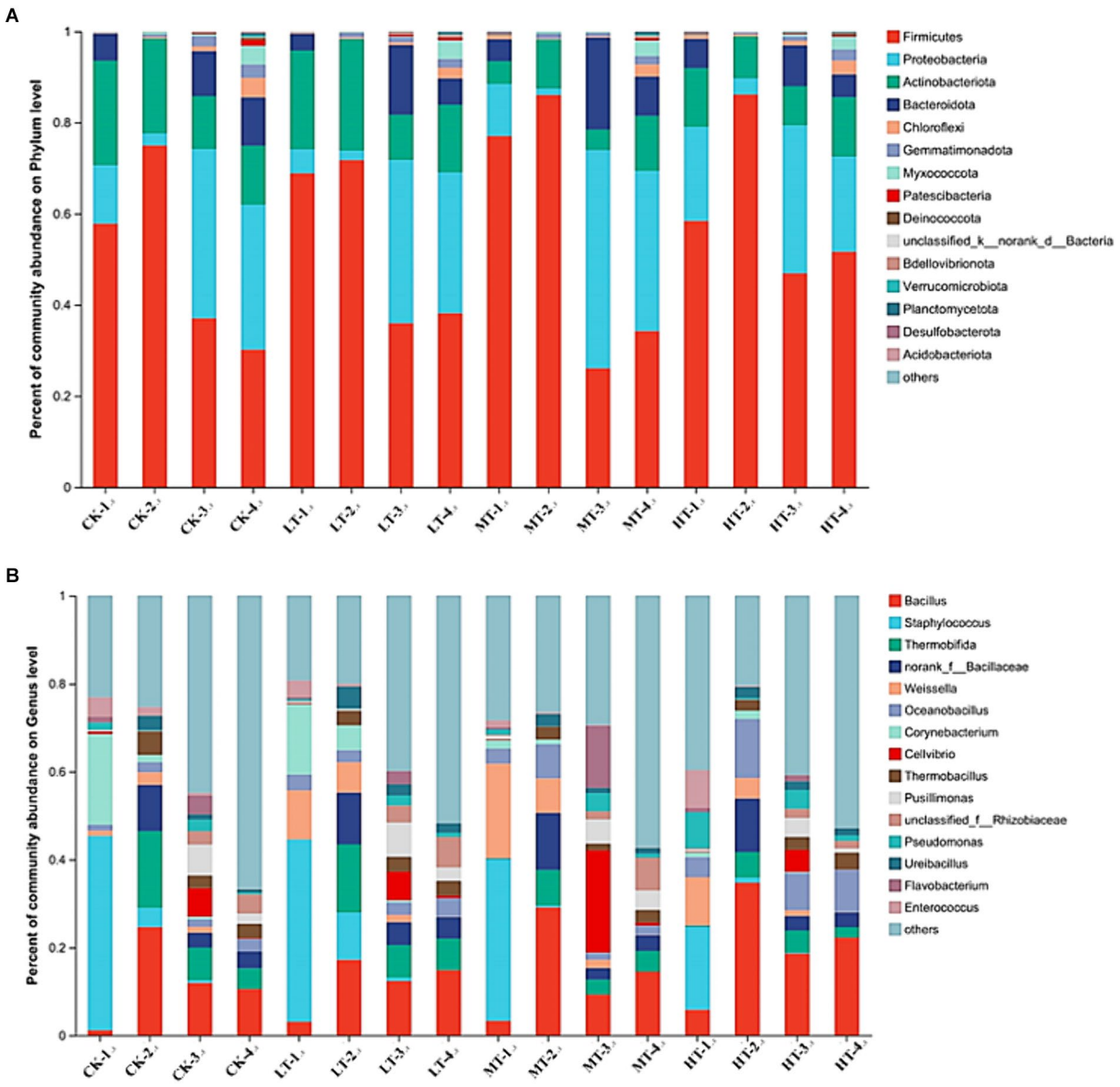

FIGURE 4
Profiles of bacterial community composition in the compost with or without tobacco leaf amendments on day 50. **(A)** Cumulative histogram showing the relative abundance of top 15 bacterial phyla. **(B)** Cumulative histogram showing the relative abundance of top 30 bacterial genera. CK: tomato tail vegetable + cattle manure + rice husk; LT: tomato tail vegetable + cattle manure + rice husk + 2% (w/w) tobacco leaves; MT: tomato tail vegetable + cattle manure + rice husk + 5% (w/w) tobacco leaves; HT: tomato tail vegetable + cattle manure + rice husk + 10% (w/w) tobacco leaves. -1, -2, -3, and -4 in the panels **A,B** represented the samples collected from the compost on day 1, 3, 7, and 50, respectively.

significantly higher *norB* gene relative abundance was observed on day 1 and 7 in tobacco leaf treatments than CK, but the difference became smaller as the composting proceeded except for the MT-3 treatment. The relative abundance of *nosZ* gene in the HT-1 treatment was higher than that in the CK-1 treatment. However, the relative abundance of *nosZ* gene remained constant in individual tobacco leaf treatment during the thermophilic and maturation phases. The reason behind this observation might be that the *nosZ* gene is associated with bacteria with an extreme tolerance to high temperatures. These results strongly agreed with a previous study showing that the temperature was one of the main factors affecting the denitrifier bacterial community in the compost (Zhou et al., 2022).

3.6 Evaluation of tail vegetable compost as a seed germination agent for halophyte

The composting leachate in all the treatments was also prepared to evaluate the effect of compost products on seed germination and root development of local halophyte, i.e., wild soybean (*Glycine soja*). On day 3, the germination rate of wild soybean in the MT treatment was significantly higher than those in other treatments (Figure 6A). Similarly, all the tobacco leaf treatments occupied the obviously higher seed germination rate compared with CK at the thermophilic and cooling periods (from day 8 to 15), following the order of MT > HT > LT. While the seed germination rate in the LT treatment was higher than that of CK

10.3389/fmicb.2024.1433092

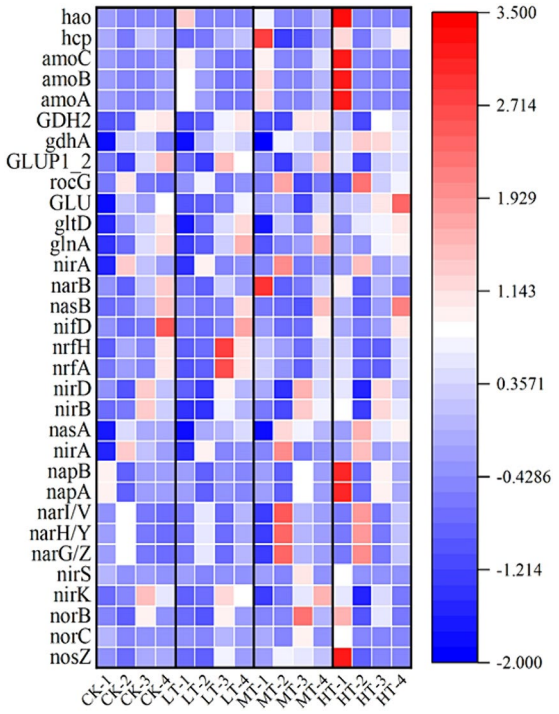

FIGURE 5
Heatmap showing expression profiles of N-transformation functional genes in the compost. CK: tomato tail vegetable + cattle manure + rice husk; LT: tomato tail vegetable + cattle manure + rice husk + 2% (w/w) tobacco leaves; MT: tomato tail vegetable + cattle manure + rice husk + 5% (w/w) tobacco leaves; HT: tomato tail vegetable + cattle manure + rice husk + 10% (w/w) tobacco leaves. -1, -2, -3, and -4 represented composted which was collected on day 1, 3, 7, and 50, respectively. Color intensity of the scale indicated the relative abundance of each gene based on the log2 (fold change) values.

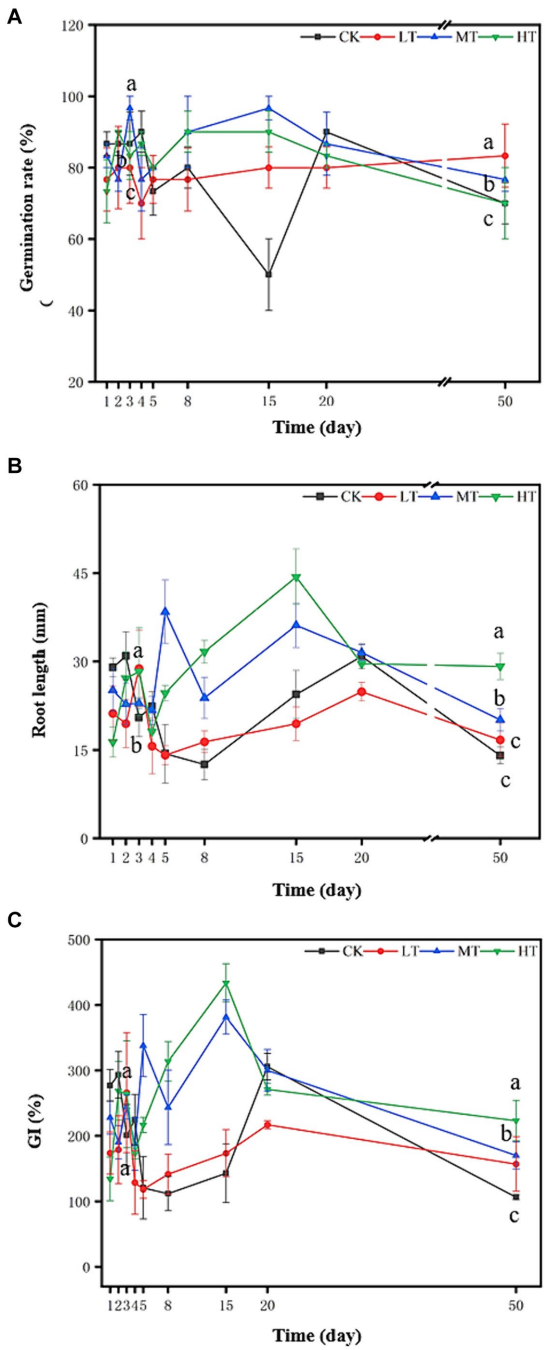

FIGURE 6
Effect of tail vegetable compost leachate on the seed germination of wild soybean (*Glycine soja*). **(A)** Germination rate; **(B)** root length and **(C)** germination index (GI). CK: tomato tail vegetable + cattle manure + rice husk; LT: tomato tail vegetable + cattle manure + rice husk + 2% (w/w) tobacco leaves; MT: tomato tail vegetable + cattle manure + rice husk + 5% (w/w) tobacco leaves; HT: tomato tail vegetable + cattle manure + rice husk + 10% (w/w) tobacco leaves. The different lowercase letters on day 3 and 50 represent significant difference between different treatments (Duncan's multiple-comparison test, $p < 0.05$).

treatment, but no similar results were found in other tobacco leaf treatments (Figure 6A). These results showed that tobacco leaf amendments elevated the efficiency of composting products in promoting seed germination of halophyte. For the root length, the higher doses of tobacco leaf amendments (MT and HT treatments) increased it, with the order of MT > HT, but the root length of wild soybean in the LT treatment exhibited non-significant difference from that in the CK (Figure 6B). At the cooling and ending stages (from day 15 to 50) of composting, tobacco leaf amendments generally increased the root length of wild soybean relative to CK, following HT (101%) > MT (33.4%) > LT (13.3%). The result suggested the dose-dependent promotion effect of tobacco leaf amendments on seed germination and root development of halophyte. This can be explained by the supply of water soluble N-containing nutrients from tobacco leaf treated composts (Yuan et al., 2019).

The germination index (GI) can be used to assess the phytotoxicity and maturity of compost (Yang et al., 2021). When the GI is lower than 50.0%, there are more toxic substances in the heap, which has an inhibitory effect on plant growth. When the GI is greater than 70.0%, the heap is decomposed and non-toxic, and can be used for fertilizer application, which is conducive to plant growth and development (Wang G. et al., 2022). As shown in Figure 6C, GI index gradually increased with the composting processed in all the four treatments. On day 5, all the compost treatments reached the maturity standard (80%). Compared with CK treatment, the GI in the MT and HT treatments were significantly higher on day 8 and 15, showing an obvious

enhancement on the compost maturity (Figure 6C). This could be attributed to the higher nutrient content and temperature in tobacco leaf treated compost. When the final composts were subjected to phytotoxicity tests on day 50, the GI were significantly higher in the treatments with tobacco leaf additives than in CK, but did not differ significantly among the three treatments (Figure 6C). Seed germination is inhibited by phytotoxic substances such as low molecular weight organic acids, heavy metals, and inorganic nitrogen in the aqueous extracts of composts (Chen et al., 2021). Composting can decrease phytotoxicity by degradation, transformation, thereby reducing toxin bioavailability (Li et al., 2023; Wang G. et al., 2022). Therefore, the increased GI in the compost after tobacco leaf treatment could be resulted from the higher peak temperature and increased nutrient supply in the compost with tobacco leaf (Figure 1A), which can effectively kill the pathogenic microorganisms and elevate the compost quality.

4 Conclusion

Resource utilization of tail vegetables has become an urgent issue to be addressed in the modern agriculture. In the present study, the effect of different doses of tobacco leaf amendments on the N transformation, compost quality and microbial regulation of tomato tail vegetable composting was firstly investigated. The results showed that high-doses (5% w/w and 10% w/w) of tobacco leaves elevated the maturity of compost, enhanced N conservation, changed bacterial community structure during the composting. Moreover, owing to supply of N-containing nutrients from tobacco leaves and promoted organic matter degradation, the population diversity and N-related microbial metabolism (i.e., hydroxylamine oxidase and denitrifying bacterial gene) of compost was enhanced after flue-cured tobacco leaf amendments. Besides, tobacco leaf amendments promoted the seed germination and root development of wild soybean, representative of halophyte. These findings showed the great potential of flue-cured tobacco leaves as additives during the aerobiotic composting of tail vegetables. Furthermore, tobacco leaf amendments increased the efficiency of composting product into promoting salt-tolerant plant growth and elevating the primary productivity of salt-affected soils. Therefore, it could be a promising field remediation method to enhance the soil health and primary productivity for the salt-affected wetland ecosystems using the tobacco-modified composting products. Considering the significant role of tobacco leaf-modified compost properties, quality and induced microbial N transformation responses, it could be a good choice to screen and inoculate N-transforming functional bacterial taxa with higher performance in stimulating ammonifying process to further enhance labile N retention and availability in the compost.

Data availability statement

The raw data supporting the conclusions of this article will be made available by the authors, without undue reservation.

Author contributions

CX: Writing – original draft, Formal analysis, Investigation, Methodology, Software. XW: Resources, Validation, Writing – review & editing, Formal analysis. BZ: Conceptualization, Supervision, Writing – review & editing. JL: Investigation, Software, Writing – review & editing. PZ: Methodology, Supervision, Writing – review & editing. GS: Methodology, Software, Writing – review & editing. XYi: Investigation, Software, Validation, Writing – review & editing. DK: Project administration, Validation, Writing – review & editing. JY: Methodology, Supervision, Validation, Writing – review & editing. HY: Investigation, Software, Writing – review & editing. XYo: Conceptualization, Formal analysis, Funding acquisition, Investigation, Project administration, Resources, Software, Validation, Visualization, Writing – review & editing. YL: Conceptualization, Funding acquisition, Resources, Visualization, Writing – review & editing.

Funding

The author(s) declare that financial support was received for the research, authorship, and/or publication of this article. This work was funded by the Agricultural Science and Technology Innovation Program of China (ASTIP-TRIC06, ASTIP No. CAASZDRW202201) and the Central Government Guides Local Science and Technology Development Projects (24-1-8-cspz-17-nsh).

Conflict of interest

BZ, DK, and JY were employed by Tobacco Shandong Industrial Co., Ltd. GS and XYi were employed by Tobacco Baoshan Industrial Co., Ltd.

The remaining authors declare that the research was conducted in the absence of any commercial or financial relationships that could be construed as a potential conflict of interest.

Publisher's note

All claims expressed in this article are solely those of the authors and do not necessarily represent those of their affiliated organizations, or those of the publisher, the editors and the reviewers. Any product that may be evaluated in this article, or claim that may be made by its manufacturer, is not guaranteed or endorsed by the publisher.

References

Ba, S., Qu, Q., Zhang, K., and Groot, J. C. J. (2020). Meta-analysis of greenhouse gas and ammonia emissions from dairy manure composting. *Biosyst. Eng.* 193, 126–137. doi: 10.1016/j.biosystemseng.2020.02.015

Chen, Z., Fu, Q., Cao, Y., Wen, Q., and Wu, Y. (2021). Effects of lime amendment on the organic substances changes, antibiotics removal, and heavy metals speciation transformation during swine manure composting. *Chemosphere* 262:128342. doi: 10.1016/j.chemosphere.2020.128342

Chen, Y., Tang, P., Li, Y., Chen, L., Jiang, H., Liu, Y., et al. (2022). Effect of attapulgite on heavy metals passivation and microbial community during co-composting of river sediment with agricultural wastes. *Chemosphere* 299:134347. doi: 10.1016/j.chemosphere.2022.134347

He, X., Zhang, T., Niu, Y., Xue, Q., Ali, E. F., Shaheen, S. M., et al. (2022). Impact of catalytic hydrothermal treatment and Ca/Al-modified hydrochar on lability, sorption, and speciation of phosphorus in swine manure: microscopic and spectroscopic investigations. *Environ. Pollut.* 299:118877. doi: 10.1016/j.envpol.2022.118877

He, J., Zhu, N., Xu, Y., Wang, L., Zheng, J., and Li, X. (2022). The microbial mechanisms of enhanced humification by inoculation with *Phanerochaete chrysosporium* and *Trichoderma longibrachiatum* during biogas residues composting. *Bioresour. Technol.* 351:126973. doi: 10.1016/j.biortech.2022.126973

Hoang, H. G., Thuy, B. T. P., Lin, C., Vo, D.-V. N., Tran, H. T., Bahari, M. B., et al. (2022). The nitrogen cycle and mitigation strategies for nitrogen loss during organic waste composting: a review. *Chemosphere* 300:134514. doi: 10.1016/j.chemosphere.2022.134514

Huang, D., Gao, L., Cheng, M., Yan, M., Zhang, G., Chen, S., et al. (2022). Carbon and N conservation during composting: a review. *Sci. Total Environ.* 840:156355. doi: 10.1016/j.scitotenv.2022.156355

Jin, S., Zhang, B., Wu, B., Han, D., Hu, Y., Ren, C., et al. (2021). Decoupling livestock and crop production at the household level in China. *Nat. Sustain.* 4, 48–55. doi: 10.1038/s41893-020-00596-0

Kong, Y., Ma, R., Li, G., Wang, G., Liu, Y., and Yuan, J. (2022). Impact of biochar, calcium magnesium phosphate fertilizer and spent mushroom substrate on humification and heavy metal passivation during composting. *Sci. Total Environ.* 824:153755. doi: 10.1016/j.scitotenv.2022.153755

Kurt, D., and Kinay, A. (2021). Effects of irrigation, nitrogen forms and topping on sun cured tobacco. *Ind. Crop. Prod.* 162:113276. doi: 10.1016/j.indcrop.2021.113276

Li, D., Manu, M. K., Varjani, S., and Wong, J. W. C. (2023). Role of tobacco and bamboo biochar on food waste digestate co-composting: nitrogen conservation, greenhouse gas emissions, and compost quality. *Waste Manag.* 156, 44–54. doi: 10.1016/j.wasman.2022.10.022

Lisuma, J., Mbega, E., and Ndakidemi, P. (2020). Influence of tobacco plant on macronutrient levels in sandy soils. *Agronomy* 10:418. doi: 10.3390/agronomy10030418

Luo, X., Chen, W., Liu, Q., Wang, X., Miao, J., Liu, L., et al. (2024). Corn straw biochar addition elevated phosphorus availability in a coastal salt-affected soil under the conditions of different halophyte litter input and moisture contents. *Sci. Total Environ.* 908:168355. doi: 10.1016/j.scitotenv.2023.168355

Qian, X., Bi, X., Xu, Y., Yang, Z., Wei, T., Xi, M., et al. (2022). Variation in community structure and network characteristics of spent mushroom substrate (SMS) compost microbiota driven by time and environmental conditions. *Bioresour. Technol.* 364:127915. doi: 10.1016/j.biortech.2022.127915

Qiao, Y., Tie, J., Wang, X., Wei, B., Zhang, W., Liu, Z., et al. (2023). Comprehensive evaluation on effect of planting and breeding waste composts on the yield, nutrient utilization, and soil environment of baby cabbage. *J. Environ. Manag.* 341:117941. doi: 10.1016/j.jenvman.2023.117941

Shan, G., Li, W., Gao, Y., Tan, W., and Xi, B. (2021). Additives for reducing nitrogen loss during composting: a review. *J. Clean. Prod.* 307:127308. doi: 10.1016/j.jclepro.2021.127308

Sun, S., Abdellah, Y. A. Y., Miao, L., Wu, B., Ma, T., Wang, Y., et al. (2022). Impact of microbial inoculants combined with humic acid on the fate of estrogens during pig manure composting under low-temperature conditions. *J. Hazard. Mater.* 424:127713. doi: 10.1016/j.jhazmat.2021.127713

Tian, X., Qin, W., Zhang, Y., Liu, Y., Lyu, Q., Chen, G., et al. (2024). The inoculation of thermophilic heterotrophic nitrifiers improved the efficiency and reduced ammonia emission during sewage sludge composting. *Chem. Eng. J.* 479:147237. doi: 10.1016/j.cej.2023.147237

Wang, X., Kong, Q., Cheng, Y., Xie, C., Yuan, Y., Zheng, H., et al. (2024). Cattle manure hydrochar posed a higher efficiency in elevating tomato productivity and decreasing greenhouse gas emissions than plant straw hydrochar in a coastal soil. *Sci. Total Environ.* 912:168749. doi: 10.1016/j.scitotenv.2023.168749

Wang, G., Kong, Y., Liu, Y., Li, D., Zhang, X., Yuan, J., et al. (2020). Evolution of phytotoxicity during the active phase of co-composting of chicken manure, tobacco powder and mushroom substrate. *Waste Manag.* 114, 25–32. doi: 10.1016/j.wasman.2020.06.034

Wang, X., Li, Z., Cheng, Y., Yao, H., Li, H., You, X., et al. (2023). Wheat straw hydrochar induced negative priming effect on carbon decomposition in a coastal soil. *iMeta* 2:e134. doi: 10.1002/imt2.134

Wang, M., Liu, Y., Wang, S., Wang, K., and Zhang, Y. (2021). Development of a compound microbial agent beneficial to the composting of Chinese medicinal herbal residues. *Bioresour. Technol.* 330:124948. doi: 10.1016/j.biortech.2021.124948

Wang, J., Liu, Z., Xia, J., and Chen, Y. (2019). Effect of microbial inoculation on physicochemical properties and bacterial community structure of citrus peel composting. *Bioresour. Technol.* 291:121843. doi: 10.1016/j.biortech.2019.121843

Wang, C., Wu, M., Peng, C., Yan, F., Jia, Y., Li, X., et al. (2022). Bacterial dynamics and functions driven by a novel microbial agent to promote kitchen waste composting and reduce environmental burden. *J. Clean. Prod.* 337:130491. doi: 10.1016/j.jclepro.2022.130491

Wang, Z., Xu, Y., Yang, T., Liu, Y., Zheng, T., and Zheng, C. (2023). Effects of biochar carried microbial agent on compost quality, greenhouse gas emission and bacterial community during sheep manure composting. *Biochar* 5:3. doi: 10.1007/s42773-022-00202-w

Wang, G., Yang, Y., Kong, Y., Ma, R., Yuan, J., and Li, G. (2022). Key factors affecting seed germination in phytotoxicity tests during sheep manure composting with carbon additives. *J. Hazard. Mater.* 421:126809. doi: 10.1016/j.jhazmat.2021.126809

Wang, N., Zhao, K., Li, F., Peng, H., Lu, Y., Zhang, L., et al. (2022). Characteristics of carbon, nitrogen, phosphorus and sulfur cycling genes, microbial community metabolism and key influencing factors during composting process supplemented with biochar and biogas residue. *Bioresour. Technol.* 366:128224. doi: 10.1016/j.biortech.2022.128224

Wang, Z., Zhao, M., Xie, J., Wang, Z., Tsui, T.-H., Ren, X., et al. (2022). Insight into the fraction variations of selenium and their effects on humification during composting. *Bioresour. Technol.* 364:128050. doi: 10.1016/j.biortech.2022.128050

Wong, J. W. C., Karthikeyan, O. P., and Selvam, A. (2017). Biological nutrient transformation during composting of pig manure and paper waste. *Environ. Technol.* 38, 754–761. doi: 10.1080/09593330.2016.1211747

Xi, B., Zhao, X., He, X., Huang, C., Tan, W., Gao, R., et al. (2016). Successions and diversity of humic-reducing microorganisms and their association with physical-chemical parameters during composting. *Bioresour. Technol.* 219, 204–211. doi: 10.1016/j.biortech.2016.07.120

Xie, S., Tran, H.-T., Pu, M., and Zhang, T. (2023). Transformation characteristics of organic matter and phosphorus in composting processes of agricultural organic waste: research trends. *Mater. Sci. Energy Technol.* 6, 331–342. doi: 10.1016/j.mset.2023.02.006

Xiong, J., Su, Y., He, X., Han, L., Guo, J., Qiao, W., et al. (2022). Effects of functional-membrane covering technique on nitrogen succession during aerobic composting: metabolic pathways, functional enzymes, and functional genes. *Bioresour. Technol.* 354:127205. doi: 10.1016/j.biortech.2022.127205

Yang, Y., Wang, G., Li, G., Ma, R., Kong, Y., and Yuan, J. (2021). Selection of sensitive seeds for evaluation of compost maturity with the seed germination index. *Waste Manag.* 136, 238–243. doi: 10.1016/j.wasman.2021.09.037

Ye, P., Fang, L., Song, D., Zhang, M., Li, R., Awasthi, M. K., et al. (2023). Insights into carbon loss reduction during aerobic composting of organic solid waste: a meta-analysis and comprehensive literature review. *Sci. Total Environ.* 862:160787. doi: 10.1016/j.scitotenv.2022.160787

Yin, Y., Ren, Z., Zhang, L., Qin, L., Chen, L., Liu, L., et al. (2023). *In situ* proteomic analysis of herbicide-resistant soybean and hybrid seeds via matrix-assisted laser desorption/ionization-mass spectrometry imaging. *J. Agric. Food Chem.* 71, 7140–7151. doi: 10.1021/acs.jafc.3c00301

Yin, Y., Yang, C., Tang, J., Gu, J., Li, H., Duan, M., et al. (2021). Bamboo charcoal enhances cellulase and urease activities during chicken manure composting: roles of the bacterial community and metabolic functions. *J. Environ. Sci.* 108, 84–95. doi: 10.1016/j.jes.2021.02.007

Yuan, Y., Zou, P., Zhou, J., Geng, Y., Fan, J., Clark, J., et al. (2019). Microwave-assisted hydrothermal extraction of non-structural carbohydrates and hemicelluloses from tobacco biomass. *Carbohydr. Polym.* 223:115043. doi: 10.1016/j.carbpol.2019.115043

Zhang, Z., Liu, D., Qiao, Y., Li, S., Chen, Y., and Hu, C. (2021). Mitigation of carbon and nitrogen losses during pig manure composting: a meta-analysis. *Sci. Total Environ.* 783:147103. doi: 10.1016/j.scitotenv.2021.147103

Zhao, Y., Lu, Q., Wei, Y., Cui, H., Zhang, X., Wang, X., et al. (2016). Effect of actinobacteria agent inoculation methods on cellulose degradation during composting based on redundancy analysis. *Bioresour. Technol.* 219, 196–203. doi: 10.1016/j.biortech.2016.07.117

Zheng, X., Zou, D., Wu, Q., Wang, H., Li, S., Liu, F., et al. (2022). Review on fate and bioavailability of heavy metals during anaerobic digestion and composting of animal manure. *Waste Manag.* 150, 75–89. doi: 10.1016/j.wasman.2022.06.033

Zhong, X.-Z., Zeng, Y., Wang, S.-P., Sun, Z.-Y., Tang, Y.-Q., and Kida, K. (2020). Insight into the microbiology of nitrogen cycle in the dairy manure composting process revealed by combining high-throughput sequencing and quantitative PCR. *Bioresour. Technol.* 301:122760. doi: 10.1016/j.biortech.2020.122760

Zhou, L., Li, J., Pokhrel, G. R., Zhao, Y., Zhang, C., Chu, W., et al. (2022). Effects of monoculture regime on the soil nirK- and nosZ-denitrifying bacterial communities of *Casuarina equisetifolia*. *Appl. Soil Ecol.* 171:104326. doi: 10.1016/j.apsoil.2021.104326

Zittel, R., da Silva, C. P., Domingues, C. E., Seremeta, D. C. H., da Cunha, K. M., and de Campos, S. X. (2020). Availability of nutrients, removal of nicotine, heavy metals and pathogens in compounds obtained from smuggled cigarette tobacco compost associated with industrial sewage sludge. *Sci. Total Environ.* 699:134377. doi: 10.1016/j.scitotenv.2019.134377

frontiers | Frontiers in Microbiology

TYPE Original Research
PUBLISHED 12 September 2024
DOI 10.3389/fmicb.2024.1438878

OPEN ACCESS

EDITED BY
Qi Zhang,
Nanchang University, China

REVIEWED BY
Haoxin Lv,
Henan University of Technology, China
Zhigang Yu,
The University of Queensland, Australia

*CORRESPONDENCE
Gang Jia
✉ jiagang700510@163.com

†These authors have contributed equally to this work

RECEIVED 26 May 2024
ACCEPTED 21 August 2024
PUBLISHED 12 September 2024

CITATION
Xie Y, Liu D, Liu Y, Tang J, Zhao H, Chen X, Tian G, Liu G, Cai J and Jia G (2024) The microbiota and metabolome dynamics and their interactions modulate solid-state fermentation process and enhance clean recycling of brewers' spent grain. *Front. Microbiol.* 15:1438878. doi: 10.3389/fmicb.2024.1438878

The microbiota and metabolome dynamics and their interactions modulate solid-state fermentation process and enhance clean recycling of brewers' spent grain

Yueqin Xie†, Dongyun Liu†, Yang Liu, Jiayong Tang, Hua Zhao, Xiaoling Chen, Gang Tian, Guangmang Liu, Jingyi Cai and Gang Jia*

Key Laboratory for Animal Disease-Resistance Nutrition of China, Ministry of Education, Institute of Animal Nutrition, Sichuan Agricultural University, Chengdu, Sichuan, China

The massive yield of brewers' spent grain (BSG) waste inevitably threaten environmental health. Here, solid-state fermentation (SSF) technology featuring multi-strain (MS) inoculation and high-throughput sequencing technology were employed to facilitate the sustainable and clean recycling of BSG waste while revealing the associated underlying microbiological and metabolic mechanisms. MS inoculation displayed a lower pH value (3.91 vs. 4.12) and neutral detergent fiber content (446.24 vs. 476.23 g/kg DM), a higher levels of lactic acid (86.64 vs. 33.07 g/kg DM), acetic acid (6.13 vs. 4.87 g/kg DM), propionic acid (2.78 vs. 2.18 g/kg DM) and crude protein (307.5 vs. 289.15 g/kg DM) than those in the control group. Moreover, MS inoculation inhibited the formation of non-protein-N and ammonia-N, and spoilage microorganism resuscitation, while enhanced substrate preservation. Microbiologically, during the SSF, the group treated with MS inoculation exhibited an increase in the relative abundance of *Leuconostoc* (0.58%∼6.60%), *Weissella* (6.22%∼15.42%), *Enterococcus* (3.15%∼9.08%), *Bacillus* (17.63%∼31.29%), *Lactobacillus* (12.89%∼8.29%), *Pseudoalteromonas* (12.87%∼16.29%), and a decrease in the relative abundance of *Acinetobacter* (0.79%∼0.02%) and *Enterobacteriaceae* (0.78%∼0.24%). Metabolically, starch and sucrose metabolism, arginine and proline metabolism, and phenylalanine metabolism significantly influenced the quality of extruded BSG fermented by MS during SSF. The examination of the correlation between the microbiota, metabolites, and fermentation parameters revealed that complex interactions between microbes and the environment factors impact metabolite production. Collectively, inoculating with MS improved fermentation quality and stability, facilitated the clean recycling of BSG, which is linked to complex interactions among microbes, the environment factors and metabolite production.

KEYWORDS

Brewer's spent grain waste, metabolome-microbiome interactions, solidstate fermentation technology, multi-strain inoculation, environmental factor analysis

1 Introduction

Beer is the fifth most consumed beverage worldwide, after tea, coffee, sodium bicarbonate, and milk (Eliopoulos et al., 2022). The annual beer production is increasing continuously, stimulated by economic development and the transition of consumption structure, especially in China. At present, the beer industry has become an important field with the most potential and development prospects in China's beverage industry, with an annual production of 35.555 million kiloliters in 2022 (Fan et al., 2024). However, a substantial amount of waste is generated during the brewing process, with the primary by-product being brewers' spent grain (BSG) constituting 80–85% of the total waste produced (Jayant et al., 2018). The annual production of BSG surpasses 30 million tons, with each hectoliter of beer resulting in 15–20 kg of BSG (Radosavljević et al., 2018). It is reported that BSG wastes pose an environmental hazard as they demand around 30–60% of oxygen for complete oxidation (Hang et al., 1975). And BSG waste is rich in essential nutrients, making it an ideal substrate for harmful microorganisms. This can lead to groundwater pollution, greenhouse gas emissions, and pathogen proliferatio (Kavalopoulos et al., 2021). Furthermore, the ultra-high demand for livestock feed causes an inevitable conflict between food production levels for humans and livestock, directly placing food security at risk (Herrero et al., 2015). The adverse impacts stemming from these challenges can stimulate the development of new sustainable livestock feed resources (Newbold et al., 2015). Through the lens of cleaner production, transforming BSG waste into livestock feed has the potential to transition from a linear economy to a circular economy, thereby easing the strain on food supply and environmental conservation (de Mello Santos et al., 2022). This strategy aligns with the European Strategy and Action Plan for the Circular Economy in 2015, highlighting its positive response to current environmental initiatives (Eliopoulos et al., 2022).

However, the key issues for converting BSG waste into livestock feed are its high moisture content of around 70% and the anti-degradation barrier formed by high fiber (cellulose, hemicellulose and lignin), which results in nutrient loss and low nutrient efficiency, respectively (Roth et al., 2019). Our previous study demonstrated that drying BSG to 28% moisture and utilizing extrusion pretreatment can effectively address these challenges by disrupting the cellulosic structure and increasing the accessibility of microorganisms (unpublished). Solid-state fermentation (SSF) has been proposed as a feasible approach to recycle waste into livestock feed by employing solid waste as substrates for cultivating microorganisms to enhance the nutritional quality within the solid wastes (Huang et al., 2023). Microbes and their metabolites significantly influence the quality of the final feed in SSF (Kumar et al., 2021). Studies have highlighted that interactions between microorganisms and metabolites impact ecosystem stability and offer valuable insights for predicting ecological functions (Wang et al., 2022). In addition, studying the relationship between the microbiome, metabolome, and fermentation parameters characterizes the specific microbes and metabolites, helping to understand the potential mechanism (Huang et al., 2023; Xu et al., 2021; Gu et al., 2024). Unfortunately, the microbial and metabolite information related to BSG waste recycling, particularly how composite microbial fermentation impacts the quality of BSG waste feed, remains elusive. Therefore, a reasonable hypothesis suggests that the use of multiple strains (*Bacillus safensis* SCYA3, *Candida tropicalis* SCYA4 and *Bacillus subtilis* SCYA6) can enhance fermentation efficiency, minimize nutrient loss, and decrease pollution production during the SSF of BSG waste. So the effectiveness of multi-strain (MS) on fermentation performance, microbial profiles, and chemical composition were evaluated for feasibility (Yan et al., 2024). 16S rRNA gene sequencing and liquid chromatography–mass spectrometry (LC-MS) were used to investigate the dynamic alterations in the microbiome and metabolome of the extruded BSG inoculated with compound fermentation bacteria. Subsequently, the correlation among environmental factors, microbiome, and metabolome were investigated to unveil the underlying regulatory mechanisms. These findings are instrumental in developing a clean SSF system with enhanced performance, reduced pollution, and for the production of high-quality fermentative feed from BSG waste. Additionally, this research contributes to advancing our understanding of strategies to enhance the quality of fermented extruded BSG waste feed.

2 Materials and methods

2.1 Fermentative materials preparation

Firstly, BSG (Sichuan Nuke Teide Biotechnology Co., Ltd. Chengdu, China) was pretreated by using DSE32 twin-screw extruder with the extrusion parameters of moisture content 27%, extrusion temperature 106°C and screw speed 16 Hz to obtain extruded brewers' spent grain (EBSG) (unpublished). Subsequently, EBSG was combined with wheat bran (mass ratio, 9:1) to create a fermentation substrate that would establish a stable fermentation system, as determined through preliminary experiments. Furthermore, the fermentation substrate were randomly divided into 24 individual subsamples, including 4 time durations × 2 treatments × 3 replicates. Two treatment groups were established: one as a control without inoculation (Con), and the other receiving inoculation with a multi-strain (MS) combination comprising *Bacillus safensis* SCYA3 (NCBI accession no. PQ138514), *Candida tropicalis* SCYA 4 (CCTCC NO: M20241049), and *Bacillus subtilis* SCYA6 (NCBI accession no. PQ138515). *Bacillus safensis* SCYA3 and *Bacillus subtilis* SCYA6 were cultured in liquid LB medium at 34°C with agitation at 150 r/min on an orbital shaker and *Candida tropicalis* SCYA 4 was cultured in Yeast extract peptone dextrose medium at 30°C with agitation at 150 r/min on an orbital shaker. After the fermentation substrate was prepared and sterile water was added to achieve a feed to water ratio of 1:1 (w/v), the mixed MS was inoculated into the fermentation substrate at a total inoculation size of 15% (v/w). The fermentation conditions of the inoculation treatment group were as follows: *Bacillus safensis* SCYA3, *Bacillus subtilis* SCYA6 and *Candida tropicalis* SCYA4 were mixed in a volume ratio of 3:2:1, the concentration (MS combination) of 1.0×10^7 CFU/mL, total inoculation size of 15% (v/w), temperature of 34°C, and feed to water ratio of 1:1 (w/v). The fermentation conditions of the Con were the same as those of the treatment group except that the total inoculation size of the MS was replaced by sterile water

with the equal volume, and other conditions such as fermentation temperature and feed to water ratio remained consistent. Following treatment, each fermentation bag containing 300 g of subsamples was prepared using polyethylene bags sized at 30 cm × 20 cm, equipped with a one-way breathing valve (only exhaust but not intake). These bags were then stored at ambient temperature (34°C), with samples collected after 1, 3, 5 and 7 days of SSF.

2.2 Chemical composition, fermentation parameters and microbial profiles

Samples were ground, passed through a 0.3-mm screen, and analyzed for dry matter (DM), crude protein (CP), neutral detergent fiber (NDF) and acid detergent fiber (ADF) according to standard procedures described by Navarro et al. (2018). And the total nitrogen (TN) content was determined by dividing the CP by 6.25 (AOAC, 1990). Additionally, the water-soluble carbohydrate (WSC) was measured according to the method described by Murphy (Murphy, 1958). The sample (20 g) was blended with 180 mL of deionized water for 60 s using a blender, then filtered through 4 layers of cheesecloth and filter paper. The pH of the filtrate was immediately measured using a glass electrode pH meter. The filtrate was centrifuged at 18,000 × g for 15 min and then the supernatant was collected. Subsequently, the levels of lactic acid (LA), acetic acid (AA) and propionic acid (PA) were determined according to the method described by Li et al. (2023b). 10 g fresh sample were mixed with 90 mL of sterile 0.85% sodium chloride solution and shaken at 150 rpm for 30 min to create a homogenate. Subsequently, lactic acid bacteria (LAB), coliform bacteria, and yeast and yeast were counted according to the method of Li et al. (2023a).

2.3 Nitrogen distribution assays

The levels of nonprotein nitrogen (nonprotein-N) were calculated from true protein and crude protein using the method described by Licitra et al. (1996) for the precipitate procedure of true protein. The content of ammonia nitrogen (ammonia-N) was determined according to Broderick and Kang's method (Broderick and Kang, 1980).

2.4 DNA extraction, PCR amplification, sequencing and bioinformatics analysis

Total DNA was extracted from fermentative products using the E.Z.N.A.® soil DNA kit (Omega Bio-tek, Norcross, GA, U.S). The DNA content and quality were assessed. The primer pair 338F (5′-ACTCCTACGGGAGGCAGCAG-3′) and 806R (5′-GGACTACHVGGGTWTCTAAT-3′) were used to amplify the V3-V4 regions of the 16S rRNA gene. The polymerase chain reaction was conducted according to standardized research procedures (Tan et al., 2021). The purified and quantified samples were sequenced for 16S rRNA amplicons using the Illumina NovaSeq PE250 platform (Sanshu biotechnology Co., Ltd, Shanghai, China). The raw Illumina FASTQ files underwent demultiplexing and quality filtering prior to analysis with QIIME (version 1.9.1). Simultaneously, the raw FASTQ files were quality filtered with Trichromatic and then merged using FLASH. Following this, OTUs were clustered at a 97% similarity cutoff utilizing UPARS. The taxonomic classification of each 16S rRNA gene sequence was determined using the RDP Classifier algorithm with a confidence threshold of 70% against the Greengenes 16S rRNA databas. The sequences were submitted to NCBI's Sequence Read Archive for open access (PRJNA1148331). Diversity values for the samples were assessed using rarefaction analysis with the Chao1 and Shannon indexes. To analyze community dissimilarities in different treatments and fermentation time, we calculated unweighted or weighted UniFrac distances and visualized the results with coordinates obtained from principal coordinates analysis (PCoA). Furthermore, we utilized the Linear Discriminant Analysis Effect Size (LEfSe) method to detect the main genera showing differential abundance. Additionally, we also used the Phylogenetic Investigation of Communities by Reconstruction of Unobserved States (PICRUSt) tool to examine functional differences in bacterial community during EBSG fermentation (Fu et al., 2022).

2.5 Non-targeted metabolite analysis

The metabolites were extracted following the method outlined by Xiang et al. (2021). To maintain stability and consistency in instrument analysis for LC-MS, quality control samples were created by pooling 10 μL from each sample. The QC samples were inserted and analyzed in every 10 samples using a UPLC-Orbitrap-MS system (UPLC, Vanquish; MS, HFX). The UPLC analysis conditions are based on earlier methods (Liu et al., 2022). The HRMS data were recorded on a Q Exactive HFX Hybrid Quadrupole Orbitrap mass spectrometer with a heated ESI source, employing the Full-ms-ddMS2 MS acquisition methods. The raw MS data were acquired on the Q-Exactive using Xcalibur 4.1 (Thermo Fisher Scientific) and processed with Progenesis QI (Waters Corporation, Milford, USA). All untargeted metabolomic data used in this publication have been deposited to the EMBL-EBl MetaboLights database with the identifier MTBLS2733. The quantified data analysis using the R package, where they were subjected to multivariate data analysis such as principal component analysis (PCA). The significance of each variable in the classification process was assessed through the calculation of its Variable Importance in Projection (VIP) value. Metabolites were identified through KEGG annotation and enrichment analysis, and the results were then mapped to the KEGG Pathway database.

2.6 Statistical analysis

The data for fermentation parameters, nitrogen distribution, chemical composition, and microbial profiles were analyzed using a two-way analysis of variance (ANOVA). Statistical difference between the two treatment groups was determined using Student's t-tests, and the different fermentation times was analyzed through one-way ANOVA followed by Duncan's multiple-range test. $P < 0.05$ suggest statistically significant differences. The Pearson

10.3389/fmicb.2024.1438878

TABLE 1 Fermentation parameters of EBSG during the solid state fermentation.

Item [1]	Days	Treatment [2]		SEM [c]	*P*-value [4]		
		Con	MS		A	T	A x T
pH	1	5.14^{a}	5.10^{a}	0.10	< 0.05	< 0.05	< 0.05
	3	4.78^{Ab}	4.39^{Bb}				
	5	4.62^{Ac}	4.13^{Bc}				
	7	4.12^{Ad}	3.91^{Bd}				
LA (g/kg DM)	1	24.22^{d}	24.50^{d}	4.11	< 0.05	< 0.05	< 0.05
	3	24.17^{Bc}	29.91^{Ac}				
	5	27.76^{Bb}	36.37^{Ab}				
	7	33.07^{Ba}	86.64^{Aa}				
AA (g/kg DM)	1	3.18^{c}	3.40 ^{d}	0.20	< 0.05	< 0.05	< 0.05
	3	3.38^{Bc}	4.61^{Ac}				
	5	3.97^{Bb}	5.27^{Ab}				
	7	4.87^{Ba}	6.13^{Aa}				
PA (g/kg DM)	1	1.12^{b}	1.17 ^{b}	0.12	< 0.05	< 0.05	< 0.05
	3	1.39^{b}	1.41 ^{b}				
	5	1.95^{Ba}	2.26^{Aa}				
	7	2.18^{Ba}	2.78^{Aa}				
WSC (g/kg DM)	1	15.56^{a}	16.02^{a}	0.56	< 0.05	< 0.05	< 0.05
	3	12.45^{Bb}	15.32^{Aab}				
	5	10.07^{Bc}	13.96^{Ab}				
	7	9.00^{Bc}	11.33^{Ac}				

[1]DM, dry matter; LA, lactic acid; AA, acetic acid; PA, propionic acid; WSC, water-soluble carbohydrates. [2]Con, control; MS, multi-strain. The data with different capital letters in the same row are significantly different ($P < 0.05$). The data with different lowercase letters in the same column are significantly different ($P < 0.05$). [3]SEM, standard error of means. [4]A, the application of MS; T, fermentation time; A × T, the interaction between MS and fermentation time.

correlation among the microbiota, fermentation parameters, and metabolites was examined with SPSS 22.0 software.

3 Results and discussion

3.1 Fermentation parameters during the solid state fermentation

Table 1 shows that there was an interaction between the application of MS and fermentation time on all fermentation parameters. The MS group had a significant decrease in pH value compared to the Con group from days 3 to 7 ($P < 0.05$). Furthermore, the LA levels in both the Con and MS groups increased throughout the SSF process. However, the LA level in the MS group was significantly higher ($P < 0.05$) than that in the Con group from days 3–7. And the MS group showed a significant increase ($P < 0.05$) in AA level from days 3 to 7 when compared to the Con group. No significant difference in PA level was found between the Con and MS groups ($P > 0.05$), except at 5 and 7 days of fermentation. Moreover, the MS group had significantly higher WSC levels than the Con group from days 3 to 7 ($P < 0.05$), with no significant differences in WSC levels observed between the Con and MS groups on day 1 ($P > 0.05$).

3.2 Microbial cultivation profiles during the SSF

An interaction between the application of MS and fermentation time was observed in the microbial cultivation profiles displayed in Table 2. The MS group showed significant increases in LAB counts from days 3 to 7 compared to the Con group ($P < 0.05$). Additionally, the MS group showed significant reductions in coliform bacteria counts compared to the Con group during the SSF process ($P < 0.05$). Moreover, MS group possessed significantly higher yeast counts than Con from days 3–7 ($P < 0.05$). No significant differences in yeast counts on day 1 were observed between the Con and MS groups ($P > 0.05$).

3.3 Nitrogen distribution and chemical composition during the SSF

Table 3 demonstrates that the interactions of applying MS and fermentation time were significant for all parameters except ADF content. A higher ($P < 0.05$) CP level than Con was observed in MS from days 3–7. The contents of non-protein-N and ammonia-N were significantly reduced ($P < 0.05$) by MS compared to Con from days 1–7. Additionally, the NDF content of the MS group was

TABLE 2 Microbial cultivation profiles of EBSG during the solid state fermentation.

Item [1]	Days	Treatment [2]		SEM [3]	*P* value [4]		
		Con	MS		A	T	A x T
LAB (log_{10} CFU/g FM)	1	5.73^{b}	5.81^{b}	0.11	< 0.05	< 0.05	< 0.05
	3	5.98^{Bab}	6.14^{Ab}				
	5	6.12^{Ba}	6.94^{Aa}				
	7	6.25^{Ba}	7.22^{Aa}				
Coliform bacteria (log_{10} CFU/g FM)	1	3.73^{Aa}	3.03^{Ba}	0.12	< 0.05	< 0.05	< 0.05
	3	3.56^{Ab}	2.62^{Ba}				
	5	3.47^{Ac}	2.29^{Bab}				
	7	3.37^{Ad}	2.13^{Bb}				
Yeast (log_{10} CFU/g FM)	1	3.83^{c}	3.91^{b}	0.16	< 0.05	< 0.05	< 0.05
	3	3.89^{Bc}	4.59^{Ab}				
	5	3.98^{Bb}	5.23^{Aab}				
	7	4.08^{Ba}	6.10^{Aa}				

[1]FM, fresh matter; LAB, lactic acid bacteria; CFU, colony-forming unit. [2]Con, control; MS, multi-strain. The data with different lowercase letters in the same column are significantly different ($P < 0.05$). The data with different capital letters in the same row are significantly different ($P < 0.05$). [3]SEM, standard error of means. [4]A, the application of MS; T, fermentation time; A × T, the interaction between MS and fermentation time.

lower than that of Con from days 3–7 ($P < 0.05$), with no significant difference observed between them on day 1.

3.4 Microbial community composition during the SSF

The Illumina MiSeq sequencing analysis revealed variations in microbial composition and temporal dynamics during SSF between the Con group and the MS group, highlighting spatiotemporal changes in microbial fermentation. The principal coordinates analysis (PCoA) was used with unweighted and weighted UniFrac distances to determine the factors that shape the differences between EBSG microbiomes (β diversity). The results showed a significant succession of bacterial species over time during fermentation (Figures 1A, B). Three distinct clusters were identified in EBSG fermentation after 1, 3–5, and 7 days. Particularly, the microbial diversity of EBSG fermented for 7 days was distinctly separated from that of the other durations. MS group significantly increased the Shannon index and Chao1 index during fermentation from days 3–7 when compared to the control group in the alpha diversity analysis ($P < 0.05$). However, the bacterial α diversity of both Con and MS groups decreased with the extension of fermentation time (Figure 1C).

Solid state fermentation is a dynamic process. Conducting microbiological analysis at multiple time points offers a more accurate depiction of microbial dynamics compared to analyzing at a single time point. The microbiota composition dynamics are exhibited in Figures 2A, B. Overall, over eight bacterial phyla were present in each sample (Figure 2A). In the Con group, *Cyanobacteria* and *Proteobacteria* accounted for approximately 76.67% of the sequences at fermentation times of 1 days. As fermentation advanced, *Firmicutes* increasingly became the dominant members, while the relative abundance of *Cyanobacteria* and *Proteobacteria* gradually decreased. While in the MS group, *Firmicutes* increasingly became the dominant members, while the relative abundance of *Proteobacteria* gradually decreased. Continuous variations were detected in the microbial community (genus level) throughout the 4 time points (Figure 2B). *Leuconostoc* (0.58%∼6.60%), *Weissella* (6.22%∼15.42%), *Enterococcus* (3.15%∼9.08%), Bacillus (17.63%∼31.29%), *Lactobacillus* (12.89%∼8.29%), *Pseudoalteromonas* (12.87%∼16.29%) were the dominant bacteria in MS group. The Con group exhibited an ecological imbalance with the dominant bacteria being *Acinetobacter*, *Enterobacteriaceae* and *Acidaminococcus*. While *Acinetobacter* and *Enterobacteriaceae* are types of spoilage bacteria. Interestingly, the abundance of these pathogens was very low in the MS group. These results demonstrated that MS application effectively inhibits the growth of harmful microorganisms in fermented products, enhancing their safety. The LEfSe results showed significant differences in taxonomy between the two groups at different fermentation time points (Figures 2C, D). On day 1, many harmful bacteria, including *Acinetobacter*, *Enterobacteriaceae*, *Proteobacteria*, and *Gammaproteobacteria*, were found in abundance in the Con group.

The functional changes of bacterial communities in Con and MS groups during different fermentation time shown in Figure 3A were obtained based on the KEGG pathway database. At four time points across 6 metabolic functions, most predicted protein sequences in Con group and MS group ranged from 80.29% to 0.34% and 78.75% to 0.29%, respectively, which represented different pathways. Interestingly, Carbohydrate and amino acid metabolism comprised over 20% of the enriched pathways during SSF, exhibiting significant changes across various time points in the Con and MS groups (Supplementary Figure 1A). It can be revealed that the metabolic interaction between bacteria and compounds,

10.3389/fmicb.2024.1438878

TABLE 3 Nitrogen distribution and chemical composition of EBSG during the solid state fermentation.

Item [1]	Days	Treatment [2]		SEM [3]	*P*-value [4]		
		Con	MS		A	T	A x T
Crude protein (g/kg DM)	1	280.46^{b}	282.91^{b}	1.79	< 0.05	< 0.05	< 0.05
	3	280.34^{Bb}	290.20^{Aab}				
	5	285.78^{Bab}	295.96^{Aa}				
	7	289.15^{Ba}	307.54^{Aa}				
Nonprotein-N (g/kg TN)	1	659.83^{Aa}	640.59^{Ba}	23.76	< 0.05	< 0.05	< 0.05
	3	655.63^{Aa}	510.88^{Bb}				
	5	650.87^{Aab}	408.73^{Bc}				
	7	637.01^{Ab}	366.25^{Bd}				
Ammonia-N (g/kg TN)	1	131.51^{Aa}	128.25^{Ba}	4.73	< 0.05	< 0.05	< 0.05
	3	129.61^{Aa}	101.35^{Bb}				
	5	127.29^{Aab}	80.63^{Bc}				
	7	125.67^{Ab}	71.41^{Bc}				
NDF (g/kg DM)	1	489.68^{a}	489.48^{a}	2.98	< 0.05	< 0.05	< 0.05
	3	486.49^{Aa}	471.93^{Bb}				
	5	480.09^{Aab}	460.61^{Bc}				
	7	476.23^{Ab}	446.24^{Bd}				
ADF (g/kg DM)	1	163.17	162.92	0.38	0.15	0.14	0.77
	3	162.70	162.26				
	5	162.92	160.82				
	7	161.40	159.79				

[1]DM, dry matter; TN, total nitrogen; Nonprotein-N, nonprotein nitrogen; Ammonia-N, ammonia nitrogen; NDF, neutral detergent fiber; ADF, acid detergent fiber. [2]Con, control; MS, multi-strain. The data with different lowercase letters in the same column are significantly different ($P < 0.05$). The data with different capital letters in the same row are significantly different ($P < 0.05$). [3]SEM, standard error of means. [4]A, the application of MS; T, fermentation time; A × T, the interaction between MS and fermentation time.

so we speculate that the change in substrate composition during fermentation alters the change of metabolic function of bacterial community. We observed some efficiency differences during SSF at microbial gene function level 3 (Figure 3B and Supplementary Figure 1B), particularly in the MS group (Figure 3B). The majority of genes related to amino acid metabolism (glycine, serine and threonine metabolism, lysine degradation, arginine and proline metabolism, cysteine and methionine metabolism), carbohydrate metabolism (starch and sucrose metabolism) and lipid metabolism (fatty acid biosynthesis) in the MS group showed increasing upregulation during SSF ($P < 0.05$). While the abundances of glycan biosynthesis and metabolism, as well as the metabolism of cofactors and vitamins, showed a decrease.

3.5 Metabolomic profiles during the SSF

To assess the metabolome changes in fermented EBSG, we used the untargeted metabolomic approach. A total of 1,517 metabolites were detected across all samples. Unsupervised PCA can reflect variation within and between groups, showing distribution tendency and possible discrete points. PCA with a total cumulative variance of 82.70% comprised of PCA-1 (52.8%) and PCA-2 (29.9%) showed differences in metabolites formation among samples (Supplementary Figure 2). Metabolome analysis indicated that amino acids and nitrogen compounds, lipids and lipid-like molecules, carbohydrates, and nucleosides, nucleotides, and analogues were predominant in Con and MS groups during SSF. Among them, the abundance of carbohydrates, and amino acids, nutrigen compounds during SSF constantly upregulated from days 1 to 5. Contrastingly, the levels of nucleosides, nucleotides, analogs, lipids, and lipid-like molecules constantly declined from days 1 to 7. The MS group showed a higher relative abundance of amino acids and carbohydrates than the Con group at all four time points (Figure 4A). We further analyzed the next level of the top 20 metabolites to identify specific changes in related metabolite (Figure 4B). Figure 5A displayed the VIP values for the top 20 metabolites, indicating their unique metabolic characteristics at various time points following fermentation. Glutamate, gamma-methyl ester, gamma-Diosphenol, Ile-Val-Gly, and Brachystemidine F were the dominant substances in the Con group. While the relative concentration of L-Tyrosine, phenylacetaldehyde, ferulic acid, D-phenylalanine, D-Tryptophan and 5-aminopentanoic acid persistently increased in MS group during the whole fermentation stage.

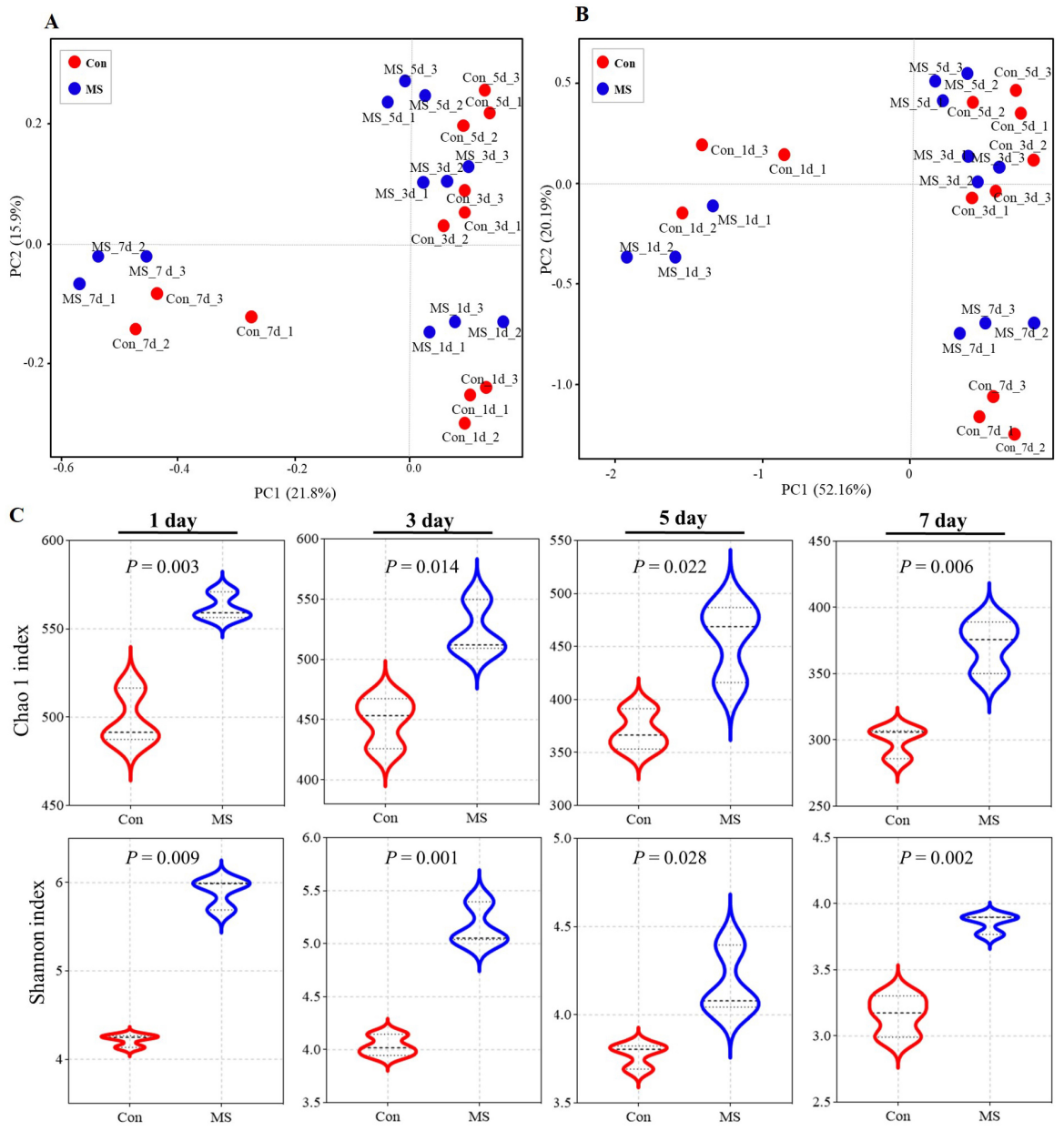

FIGURE 1
(A) The community dissimilarities in different treatments and fermentation time, calculated by unweighted UniFrac distances, with coordinates calculated by principal coordinates analysis (PCoA). **(B)** The community dissimilarities in different treatments and fermentation time, calculated by weighted UniFrac distances, with coordinates calculated by principal coordinates analysis (PCoA). **(C)** The variations of community alpha-diversities (Chao1 richness and Shannon index). Con, control; MS, multi-strain.

The pathways were annotated and enrichment analysis was carried out based on the results of differential metabolites. The first 20 metabolic pathways were displayed in Figure 5B. In the MS group, the metabolic pathways most affected during the fermentation process were arginine and proline metabolism, starch and sucrose metabolism, and phenylalanine metabolism when compared to the Con group. On day 1 of SSF, the enrichment of arginine and proline metabolism, and citrate cycle (TCA cycle) decreased throughout the fermentation process. On day 3, the Con group showed significant upregulation of fructose and mannose metabolism as well as porphyrin and chlorophyll metabolism. On day 5 of SSF, the Con group exhibited a notable increase in 6 different metabolic pathways. On day 7 of SSF, the Con group exhibited a notable increase in 7 different metabolic pathways, such as starch and sucrose metabolism, ABC transport and tryptophan metabolism, among others. Whereas, glycerophospholipid metabolism and glycerolipid metabolism were significantly upregulated in the MS group on day 5 of SSF. 16 different metabolic pathways, such as starch and sucrose metabolism, glycine, serine and threonine metabolism, phenylalanine metabolism, tyrosine metabolism, lysine degradation, and tryptophan metabolism etc., were markedly increased in the MS group on day 7 of SSF. The results showed that

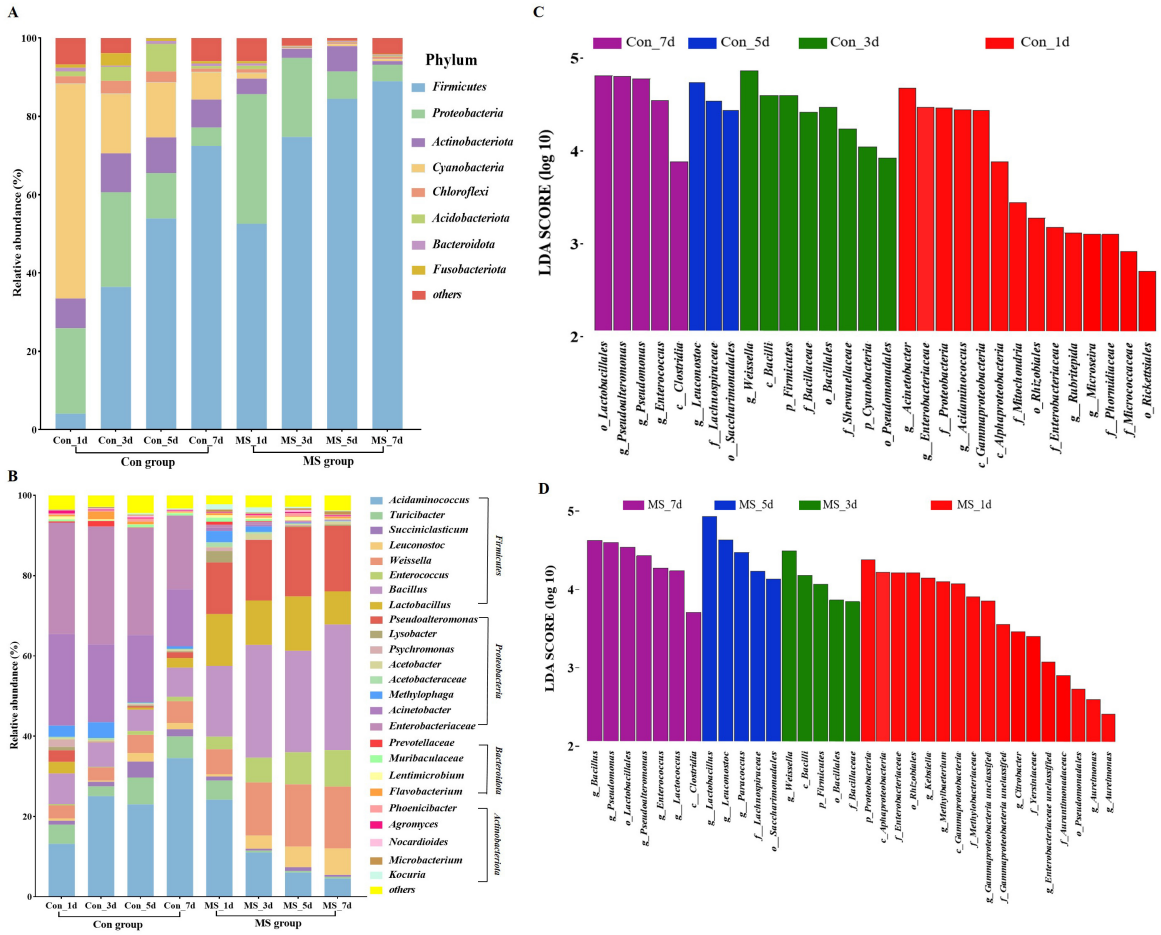

FIGURE 2
(A) Relative abundance of bacteria at the genus level. **(B)** Relative abundance of bacteria at the top 25 species level. **(C)** Linear discriminant analysis effect sizes (LEfSe) analysis of bacterial communities at different fermentation time points in Con group. **(D)** Linear discriminant analysis effect sizes (LEfSe) analysis of bacterial communities at different fermentation time points in MS group. Con, control; MS, multi-strain.

amino acid metabolism was robust and the quantity of amino acids rose during SSF in the MS group.

3.6 The correlations among microbiota, fermentation parameters, and metabolites during the SSF

Correlation analyses were conducted to further investigate the relationship between the changes in microbes (genus level), fermentation parameters, and metabolites (Figure 6A). In the Con group, the relative abundance of *Weissella* and *Enterococcus* showed positive correlations ($P < 0.05$) with LA, AA, PA and CP, and negative correlations ($P < 0.05$) with pH, WSC, ammonia-N, nonprotein-N, NDF and nucleosides, nucleotides, and analogues. While the abundance of *Acinetobacter* and *Enterobacteriaceae* were negatively ($P < 0.05$) related to LA, AA, PA and CP, and positively ($P < 0.05$) correlated with pH, WSC, ammonia-N, nonprotein-N, NDF and nucleosides, nucleotides, and analogues. In the MS group, *Leuconostoc*, *Weissella*, *Enterococcus*, and *Bacillus* showed a significant positive relationship ($P < 0.05$) with AA, PA, CP, amino acids, nutrigen compounds, and carbohydrates. Conversely, they exhibited a negative correlation ($P < 0.05$) with pH, WSC, ammonia-N, nonprotein-N, NDF, lipids, lipid-like molecules, organoheterocyclic compounds, and nucleosides, nucleotides, and analogues. These microbial groups contributed to enhancing the fermentation quality of the substrates (Figure 6B). Furthermore, *Lactobacillus* exhibited a significant positive correlation ($P < 0.05$) with LA and AA, and a significant negative correlation ($P < 0.05$) with NDF. *Pseudoalteromonas* was positively ($P < 0.05$) related to AA, PA, amino acids and nutrigen compunds and carbohydrates, and negatively ($P < 0.05$) related to pH, WSC, ammonia-N, nonprotein-N, NDF, organoheterocyclic compounds, and lipids and lipid-like molecules.

3.7 Integrated microbiomic and metabolomic changes in functional pathways during SSF

To further explain the differences of these metabolites resulting from MS inoculation and explore the metabolic mechanism, we integrated microbiomic and metabolomic pathways by combining 16S data and metabolic data (Figure 7). We identified 5 microbial

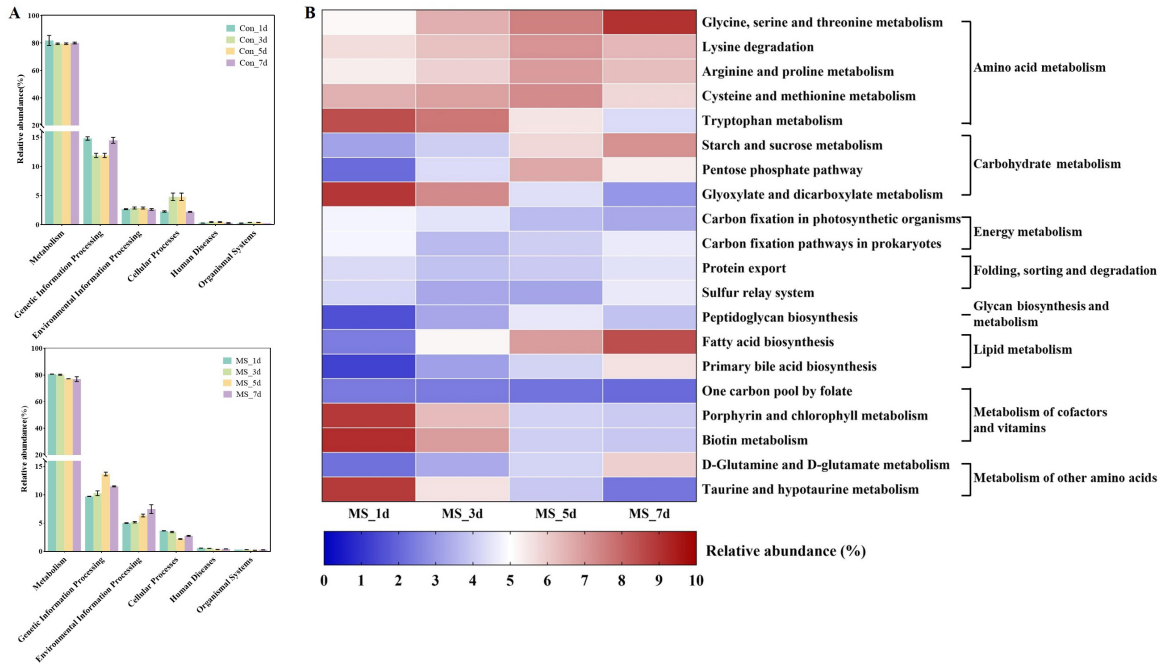

FIGURE 3
(A) Dynamics of bacterial functional profiles during SSF processes analyzed by PICRUSt in level 1 metabolic pathways; **(B)** Dynamics of bacterial functional profiles during SSF processes analyzed by PICRUSt in level 3 KEGG ortholog functional predictions of the relative abundances of the top 20 metabolic functions. Con, control; MS, multi-strain.

metabolic pathways at level 2 of the KEGG database, which include amino acid metabolism, carbohydrate metabolism, metabolism of other amino acids, metabolism of cofactors and vitamins, and lipid metabolism. Amino acid, carbohydrate, and lipid metabolism increased consistently from days 1 to 7, whereas cofactors and vitamins metabolism decreased. Metabolism of other amino acids were enriched at 5 day. At level 3, glycine, serine and threonine metabolism, D-glutamine and D-glutamate metabolism, primary bile acid biosynthesis, starch and sucrose metabolism, and fatty acid biosynthesis showed a continuous increase in expression. While porphyrin and chlorophyll metabolism, tryptophan metabolism, biotin metabolism, and glyoxylate and dicarboxylate metabolism showed a continuous decrease in expression. Arginine and proline metabolism, cysteine and methionine metabolism, and lysine degradation were enriched at 5 day. C-lysine was the product of amino acid, other amino acids, lipid, and carbohydrate metabolism, and then it could be metabolized by Porphyrin and chlorophyll metabolism to produce 5- amino-levulinic acid. L-cysteine and taurocholate levels were upregulated. And α-ketoglutaric acid was produced from D-Glutamine and D-glutamate metabolism. It can then form Acetyl-CoA through TCA cycle, which was involved in fatty acid biosynthesis.

4 Discussion

In the process of SSF, the ideal pH value of fermented feed is 3.8–4.2, which is crucial for inhibiting the metabolism of most undesired microbes and ensuring excellent fermentation quality (Ren et al., 2020). Furthermore, LA with a lower dissociation constant causes a quicker decline in pH value compared to other organic acids (Li et al., 2023b). In this study, the MS group exhibited higher LA concentration and lower pH value, likely attributed to the synergistic antimicrobial effects of metabolites produced by MS inoculation, which led to the suppression of undesirable microbes. Additionally, AA and PA play crucial roles as microbial metabolites in anaerobic fermentation (Li et al., 2023a). MS group showed a significant increase in AA and PA levels, which helped to reduce the pH value of fermentation substrate, thus improving fermentation stability and preventing feed deterioration. Additionally, we also observed a decrease in WSC in both Con and MS groups, indicating that microbial fermentation needs to consume a certain amount of soluble carbohydrates during fermentation, but the level of WSC content in the MS group remained higher than that in the Con group, indicating that MS inoculation enhanced the preservation of fermentation substrates. Collectively, the inoculation of MS boosted fermentative efficiency and improved substrate preservation. The culturable microbial community plays a vital role in evaluating the fermentation efficiency of a fermentation system. Among them, LAB is prominent in the microbiome, indicating successful anaerobic fermentation (Li et al., 2022). Hereon, the MS group displayed high levels of lactic acid bacteria (LAB), suggesting LAB dominance. Coliform bacteria such as *Pseudomonas*, *Enterobacteriaceae*, and *Aeromonas* are consistently associated with energy and dry matter losses (He et al., 2020). The coliform bacteria reduction in the MS group may be attributed to higher levels of short-chain fatty acids or antimicrobial metabolites produced by MS inoculants (Ham et al., 2003). Yeast can thrive in anaerobic conditions and remains unaffected within the pH range of 2–8, leading to increased CP production (Du et al., 2021).

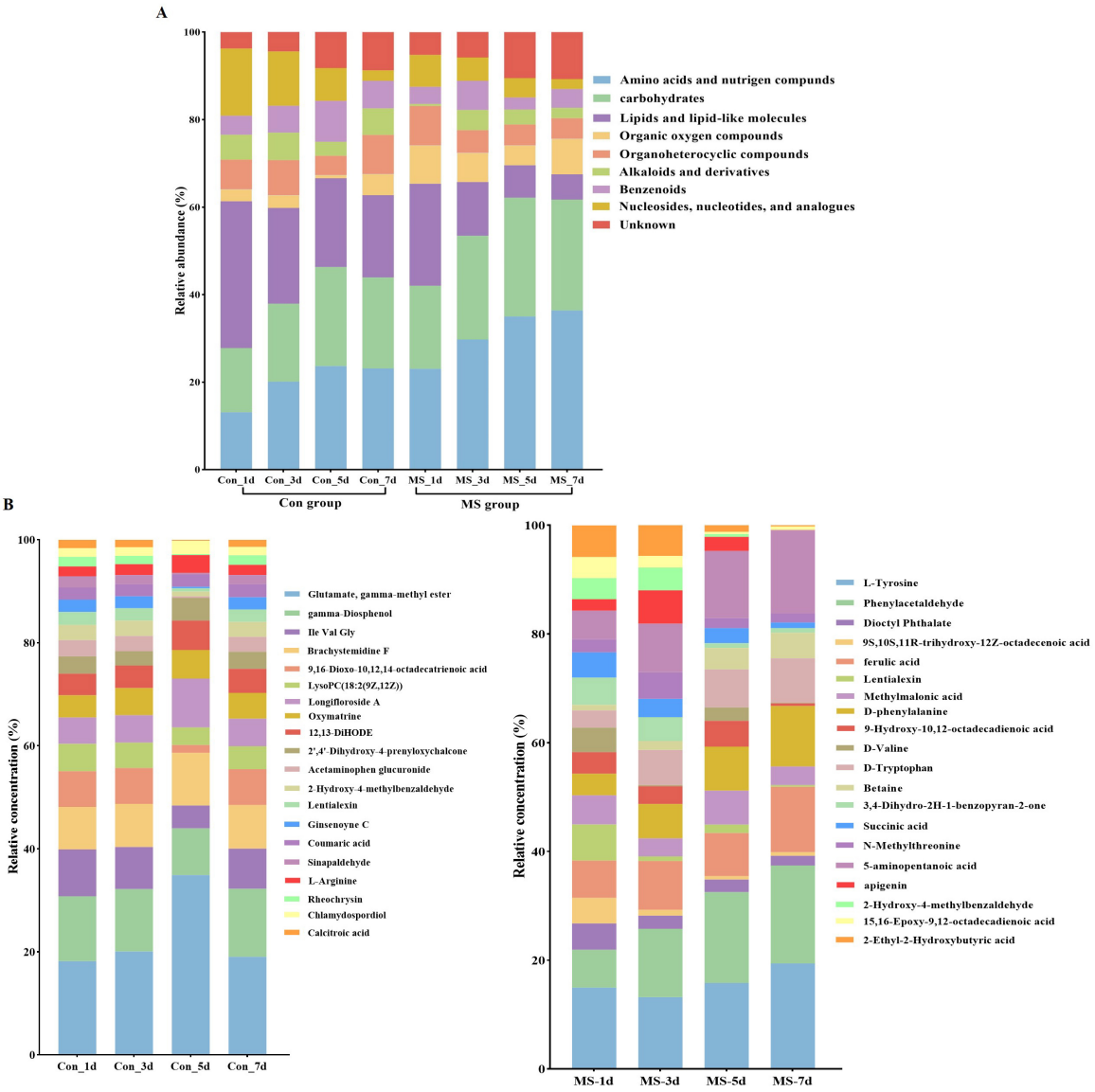

FIGURE 4
(A) Relative compositions of the main metabolites for different fermentation time. **(B)** Top 20 metabolites at different fermentation times. Con, control; MS, multi-strain.

However, in this study, MS group showed a high yeast count, which may be due to the change of interaction within the microbial group, which built beneficial conditions for yeast (Li et al., 2022). Hence, the inoculation of MS is beneficial for creating an environment that inhibits the growth of harmful microorganisms.

Assessing fermentative product quality requires careful consideration of nitrogen distribution. Elevated nonprotein-N levels diminish nitrogen availability, resulting in increased nitrogen emissions and environmental worries (Li et al., 2022). The low levels of nonprotein-N in MS can be attributed to the degradation of nonprotein-N-containing substances by microorganisms into ammonia through enzyme activities. Subsequently, the ammonia is further assimilated into amino acids catalyzed by enzyme activities, and these and amino acids are finally metabolized to produce bacterial proteins (He et al., 2019). The increase in CP level provides an explanation for this result. Ammonia-N is a more precise parameter compared to nonprotein-N for reflecting the deamination of amino acids or peptides. Furthermore, ammonia emissions, closely connected to ammonia nitrogen, can potentially transport over long distances in the atmosphere, posing a significant threat to animal and human health, as well as the health of natural ecosystems (Li et al., 2022). As such, the mitigation of ammonia-N levels is a significant national and global concern. Findings from this study show that using MS application can reduce ammonia-N formation. A plausible reason may be that the reduction of undesirable microbes caused by MS treatment is beneficial to reduce the content of ammonia nitrogen. Collectively, MS application can reduce the pollution generation and promote the production of bacterial protein during SSF. Moreover, the inclusion of MS inoculants led to a reduction in NDF levels with no effect on ADF levels. This indicates that the inoculant treatments raised organic acid levels through the degradation of hemicellulose

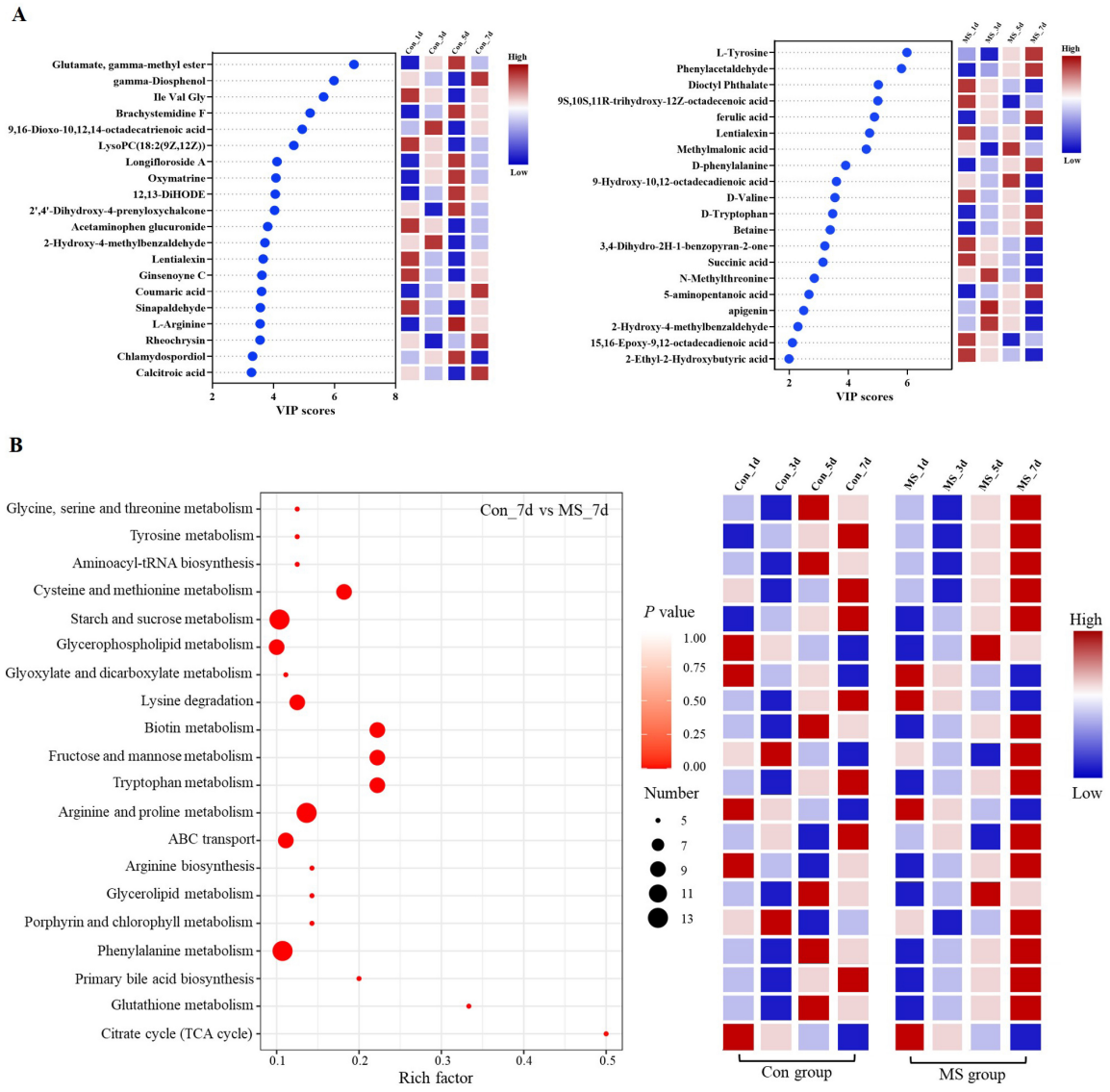

FIGURE 5
(A) A scatter plot of the top 20 distinct metabolites was identified by applying variable importance projection (VIP). **(B)** Enrichment analysis of pathways. Number (dot), number of metabolites annotated to pathways. Con, control; MS, multi-strain.

and cellulose (Li et al., 2023b). This results may be attributed to the (hemi)cellulase-producing characteristics of *Bacillus safensis* SCYA3 and *Bacillus subtilis* SCYA6.

Microbial diversity is indicated by the beta and alpha diversity analysis, which represent the richness and uniformity of sample microbiomes (Shang et al., 2022). In this study, the bacterial α diversity of both Con and MS groups decreased with the extension of fermentation time, which may be due to the interaction between metabolic environment and microorganisms, leading to the inhibition of some microbiota in late fermentation (Wang et al., 2023). Additionally, solid state fermentation is a dynamic process. On day 1, many harmful bacteria, including *Acinetobacter*, *Enterobacteriaceae*, *Proteobacteria*, and *Gammaproteobacteria*, were found in abundance in the Con group. The most possible explanation lies in the high pH value in Con group during fermentation (Liao et al., 2023). While *Bacillus*, *Pseudomonas*, *Enterococcus*, *Lactococcus*, *Leuconostoc* and *Weissella* were enriched in MS group. de Gannes et al. (2013) reported that *Bacillus* genus members efficiently degraded protein and cellulose in SSF because of their robust hydrolytic capacity. *Enterococcus* belongs to a mesophilic bacterium that produces LA (Yuan et al., 2018). *Pseudomonas* have been confirmed for their potential role as biocontrol agents to enhance fermentation quality in SSF (Ventorino et al., 2016). *Weissella*, *Leuconostoc*, and *Lactococcus* can produce beneficial metabolites like bacteriocins and exopolysaccharides, as well as enzymes like amylases, proteases, esterases, and glucosidases to break down macromolecules (Zhao et al., 2020). Furthermore, these bacteria play a crucial role in providing flavor precursors for alcohols and esters. Yang et al. (2021) emphasized that the absence of these precursors could lead to a lack of flavor. These dominant genera are a specialized community with characteristic including large-molecule catabolism traits and their ability to produce LA, which is achieved by inoculating with MS. The bacterial structure evolved

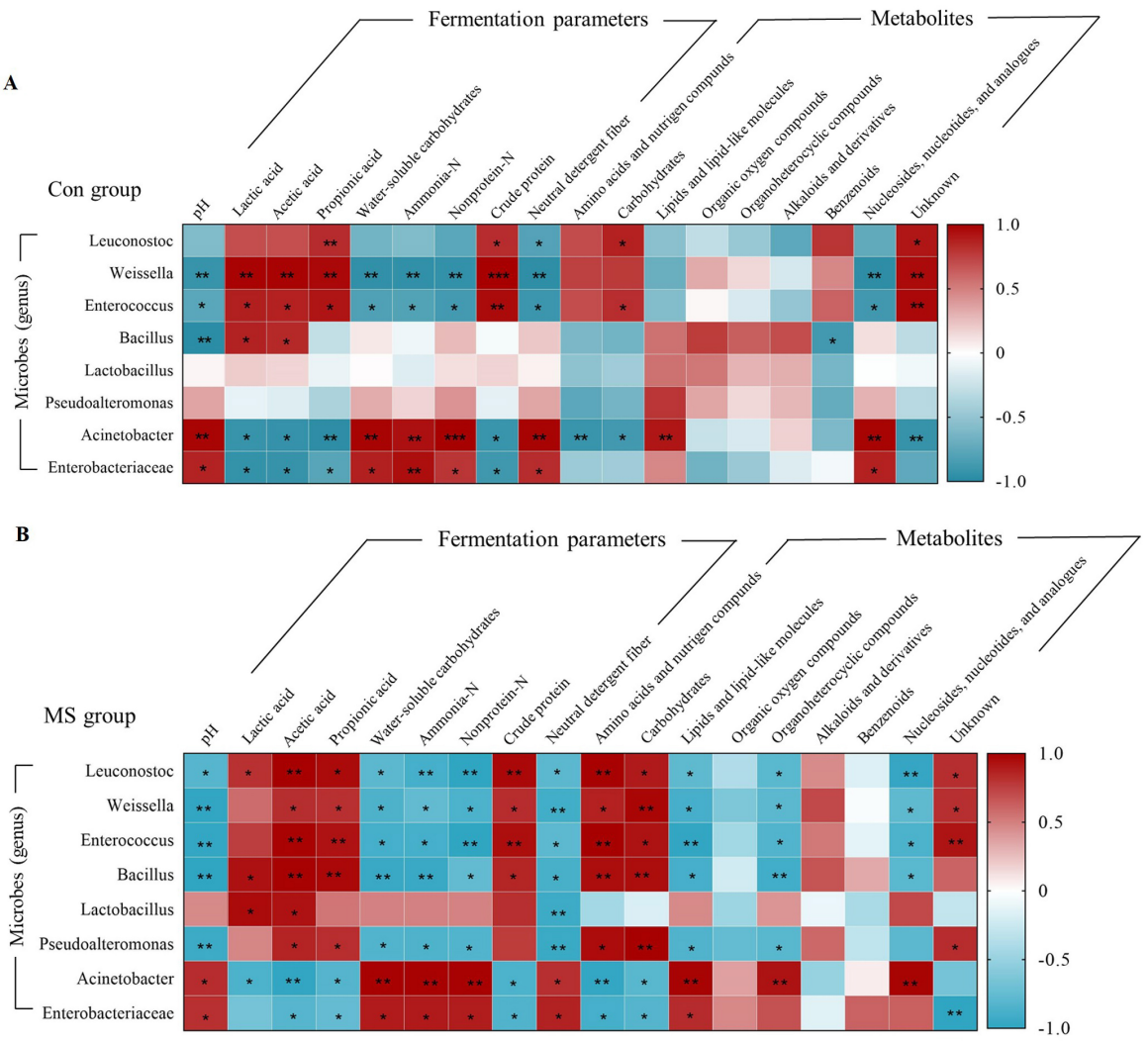

FIGURE 6
Relationships among the microbiota, metabolites and fermentation quality. **(A)** Relationships among the microbiota, metabolites, and fermentation parameters in Con group during SSF. **(B)** Relationships among the microbiota, metabolites, and fermentation parameters in MS group during SSF. **$0.001 < P < 0.01$, *$0.01 < P < 0.05$, respectively. Con, control; MS, multi-strain.

to show that MS enhanced certain functional bacteria that could establish a symbiotic relationship with the MS. Further, analyzing KEGG gene functions at levels 1 to 3 shows a gradual increase in genes related to carbohydrate and amino acid metabolism during the progression of SSF. Metabolizing cellulose and hemicellulose generates compounds that enhance bacterial growth (Toledo et al., 2017). And amino acids can provide energy and carbon sources for bacteria (López-González et al., 2015). Our findings showed that the degradation of carbohydrates and proteins leads to higher levels of saccharides and amino acids, which are used by the microbial community in fermented EBSG.

The fluctuating metabolite levels during fermentation process are a direct result of microorganisms either producing them or transforming nutrients present in the raw materials used in fermentation. Consequently, the dynamic changes of microorganisms in the fermentation process directly impact the dynamic changes of metabolites. In our study, the MS group showed a higher relative abundance of amino acids and carbohydrates than the Con group at all four time points. The analysis of the top 20 metabolites showed that MS group increased the relative concentration of L-Tyrosine, phenylacetaldehyde, ferulic acid, D-phenylalanine, D-Tryptophan and 5-aminopentanoic acid. Proteins' nutritional value relies heavily on their amino acid composition, particularly the essential amino acids in animal diets. According to Wang et al. (2022), fermentation has been shown to increase amino acid levels, such as lysine, phenylalanine, isoleucine, and valine. Additionally, phenylamine metabolism is directly linked to the production of flavor compounds during fermentation. Phenylalanine is converted to cinnamic acid by the phenylalanine ammonia lyase, which is further metabolized into various aromatic organic acids by cinnamate 4-hydroxylase. 5-aminopentanoic acid, a biomarker, contributes to the protective and therapeutic effects against hyperlipidemia in animal. The increase in 5-aminopentanoic acid levels indicates that fermentation enhances the potential benefits of the substrates (Zeng et al., 2020). Ferulic acid exhibits

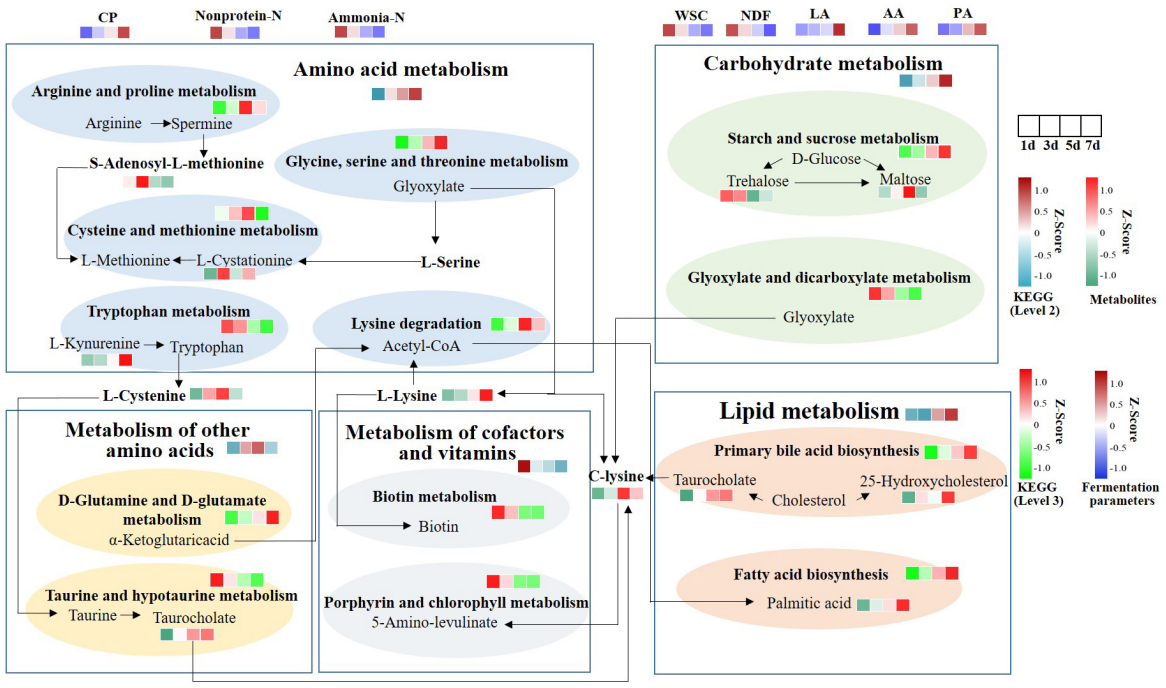

FIGURE 7
Functional pathway changes of integrated microbiome and metabolomics. KEGG level 2 was selected based on significantly different metabolic data. Using 16S data to predict the abundance of KEGG levels 2 and 3. CP, crude protein; Non-protein-N, non-protein nitrogen; Ammonia-N, ammonia nitrogen; WSC, water-soluble carbohydrates; NDF, neutral detergent fiber; LA, lactic acid; AA, acetic acid; PA, propionic acid.

prebiotic effects by enhancing the host's antioxidant capacity and modulating inflammatory responses (Zhang et al., 2022). These results indicate that inoculation with MS improved the production of key flavor compounds and beneficial substances in EBSG fermentation. Metabolites are the final products of an intricate biochemical reaction network that is controlled by different biological processes, such as mRNA, enzymes, genes, and other metabolites. Metabolic pathways, comprising complex metabolic reactions and their regulation, are crucial for understanding metabolic activities and dynamics (Xu et al., 2020). The metabolic pathways analysis showed that amino acid metabolism was robust and the quantity of amino acids rose during SSF in the MS group, including glycine, serine and threonine metabolism, phenylalanine metabolism, tyrosine metabolism, lysine degradation, and tryptophan metabolism. The threonine, phenylalanine, and lysine are essential amino acids, which animals cannot synthesize (Dong et al., 2022). The upregulation of metabolism and the downregulation in degradation of these essential amino acids in fermented EBSG suggest its enhanced nutritional value.

Complex interactions between microbes and the environment factors impact metabolite production. Correlation analyses showed that *Leuconostoc*, *Weissella*, *Enterococcus*, and *Bacillus* showed a significant positive relationship with AA, PA, CP, amino acids, nutrigen compounds, and carbohydrates, while exhibited a negative correlation with pH, WSC, ammonia-N, nonprotein-N, NDF, lipids, lipid-like molecules, organoheterocyclic compounds, and nucleosides, nucleotides, and analogues. It can be seen that *Leuconostoc*, *Weissella*, *Enterococcus* and *Bacillus* were the most dominant genus in the SSF process of MS group. Studies show that *Bacillus* is the main fermentation bacteria, which can promote the natural fermentation of foods rich in protein, produce flavor compounds, and decompose complex food compounds into smaller components during fermentation (Wang et al., 2022). Furthermore, many enzymes secreted by Bacillus can promote the degradation of complex carbohydrates and proteolysis, which also explains the positive correlation between *Bacillus* bacteria and carbohydrates, amino acids, and nitrogen compounds during SSF. *Enterococcus*, *Weissella* and *Leuconostoc* are lactate-producing bacteria that improve taste and flavor by breaking down proteins, fats, and carbohydrates, and by producing aromatic compounds (Yang et al., 2021). The relationships of microbiota, fermentation parameters and metabolites further confirmed the addition of MS promoted the degradation of protein and carbohydrates by *Leuconostoc*, *Weissella*, *Enterococcus* and *Bacillus*, and finally improved the fermentation quality. Finally, based on the results of metabolic pathway integration, we speculate that it may be due to the proliferation of dominant bacteria such as *Leuconostoc*, *Weissella*, *Enterococcus* and *Bacillus* after inoculation with MS, which directly or indirectly participate in amino acid metabolism, carbohydrate metabolism, metabolism of other amino acids, and lipid metabolism, leading to increased metabolic capacity. Consequently, the dominant metabolic function during varying fermentation times after inoculation with MS was further elucidated. The consistency of fermentation parameters and metabolites confirms the metabolic differences resulting from distinct microbial compositions in SSF. However, the detailed metabolic mechanism of the identified metabolites in this study is still not fully unclear, indicating the complexity of the metabolic process of fermented EBSG. In order to address this knowledge gap, future research efforts should prioritize the investigation

of secondary metabolites and work towards establishing a standardized metabolic spectrum for fermentation studies.

5 Conclusion

Herein, this study systematically studied the dynamic changes of fermentation characteristics, microbial community and metabolites of EBSG during SSF, and revealed that MS inoculation was beneficial in establishing a clean SSF system that is highly efficient, of high quality, and low in pollution. This helps in producing high-quality fermented feed from BSG waste, resulting in low pH and ammonia nitrogen levels, as well as high WSC content. Microbiologically, MS inoculation enhances the competitiveness of *Leuconostoc*, *Weissella*, *Enterococcus* and *Bacillus* in microbial community and promotes metabolic ability. Metabonomics, starch and sucrose metabolism, arginine and proline metabolism, and phenylalanine metabolism are important metabolic pathways that influence the quality of EBSG fermentation by MS. Moreover, studying the correlation among microbial community, metabolites and environmental factors provides valuable clues for constructing an efficient, high-quality and low-pollution fermentation system. The basic fermentation mechanism of obtaining high-quality fermented feed based on BSG waste was guided by exploring the comprehensive changes of microbiology and metabonomics of functional pathways in SSF. Collectively, MS is suitable for the SSF system utilizing EBSG waste, leading to a clean, efficient, high-quality, and environmentally friendly SSF system.

Data availability statement

The original contributions presented in the study are publicly available. This data can be found at the NCBI with accession number: PRJNA1148331.

Author contributions

YX: Writing – original draft, Visualization, Software, Project administration, Methodology, Formal analysis, Data curation, Conceptualization. DL: Writing – original draft, Visualization, Software, Project administration, Data curation. YL: Writing – original draft, Project administration, Data curation. JT: Writing – review and editing. HZ: Writing – review and editing, Project administration. XC: Writing – review and editing, Resources, Investigation. GT: Writing – review and editing, Formal analysis. GL: Writing – review and editing, Validation, Methodology. JC: Writing – review and editing, Validation, Methodology. GJ: Writing – review and editing, Visualization, Validation, Methodology, Funding acquisition, Conceptualization.

Funding

The author(s) declare financial support was received for the research, authorship, and/or publication of this article. This work was supported by the Sichuan Science and Technology Program (No. 2021ZDZX0009).

Conflict of interest

The authors declare that the research was conducted in the absence of any commercial or financial relationships that could be construed as a potential conflict of interest.

Publisher's note

All claims expressed in this article are solely those of the authors and do not necessarily represent those of their affiliated organizations, or those of the publisher, the editors and the reviewers. Any product that may be evaluated in this article, or claim that may be made by its manufacturer, is not guaranteed or endorsed by the publisher.

Supplementary material

The Supplementary Material for this article can be found online at: https://www.frontiersin.org/articles/10.3389/fmicb.2024.1438878/full#supplementary-material

References

AOAC (1990). *Official methods of analysis*, 15th Edn. Rockville, MD: Association of Official Analytical Chemists.

Broderick, G., and Kang, J. (1980). Automated simultaneous determination of ammonia and total amino acids in ruminal fluid and in vitro media. *J. Dairy Sci.* 63, 64–75. doi: 10.3168/jds.S0022-0302(80)82888-8

de Gannes, V., Eudoxie, G., and Hickey, W. J. (2013). Prokaryotic successions and diversity in composts as revealed by 454-pyrosequencing. *Bioresour. Technol.* 133, 573–580. doi: 10.1016/j.biortech.2013.01.138

de Mello Santos, V. H., Campos, T. L. R., Espuny, M., and de Oliveira, O. J. (2022). Towards a green industry through cleaner production development. *Environ. Sci. Pollut. R.* 29, 349–370. doi: 10.1007/s11356-021-16615-2

Dong, Z., Li, J., Wang, S., Dong, D., and Shao, T. (2022). Time of day for harvest affects the fermentation parameters, bacterial community, and metabolic characteristics of sorghum-sudangrass hybrid silage. *Msphere* 7:e00168–22. doi: 10.1128/msphere.00168-22

Du, G., Shi, J., Zhang, J., Ma, Z., Liu, X., Yuan, C., et al. (2021). Exogenous probiotics improve fermentation quality, microflora phenotypes, and trophic modes of fermented vegetable waste for animal feed. *Microorganisms* 9:644. doi: 10.3390/microorganisms9030644

Eliopoulos, C., Arapoglou, D., Chorianopoulos, N., Markou, G., and Haroutounian, S. A. (2022). Conversion of brewers' spent grain into proteinaceous animal feed using solid state fermentation. *Environ. Sci. Pollut. R.* 29, 29562–29569. doi: 10.1007/s11356-021-15495-w

Fan, M., Zhou, T., Zhao, Z., Du, Y., Liu, S., Bi, Z., et al. (2024). Characteristics analysis of solid waste generation and carbon emission of beer production in China. *Environ. Res.* 245:118017. doi: 10.1016/j.envres.2023.118017

Fu, S.-C., Lee, C.-H., Hsieh, Y.-C., Wu, P.-H., Lin, S.-H., and Wang, H. (2022). A Pilot Study exploring the association of entacapone, gut microbiota, and the subsequent side effects in patients with Parkinson's disease. *Front. Cell. Infect. Microbiol.* 12:837019. doi: 10.3389/fcimb.2022.837019

Gu, Z., Yan, H., Zhang, Q., Wang, Y., Liu, C., Cui, X., et al. (2024). Elimination of copper obstacle factor in anaerobic digestion effluent for value-added utilization: Performance and resistance mechanisms of indigenous bacterial consortium. *Water Res.* 252:121217. doi: 10.1016/j.watres.2024.121217

Ham, J., Kim, H., Hong, K., Kim, J., Jeong, S., Chae, H., et al. (2003). Inhibitiory activity of lactic acid bacteria against hazardous microbes. *Asian Aust. J. Animal. Sci.* 16, 1550–1554. doi: 10.5713/ajas.2003.1550

Hang, Y., Splittstoesser, D., and Woodams, E. (1975). Utilization of brewery spent grain liquor by *Aspergillus niger*. *J. Appl. Microbiol.* 30, 879–880. doi: 10.1128/am.30.5.879-880.1975

He, L., Wang, C., Xing, Y., Zhou, W., Pian, R., Yang, F., et al. (2019). Dynamics of proteolysis, protease activity and bacterial community of *Neolamarckia cadamba* leaves silage and the effects of formic acid and *Lactobacillus farciminis*. *Bioresour. Technol.* 294:122127. doi: 10.1016/j.biortech.2019.122127

He, L., Zhou, W., Xing, Y., Pian, R., Chen, X., and Zhang, Q. (2020). Improving the quality of rice straw silage with *Moringa oleifera* leaves and propionic acid: Fermentation, nutrition, aerobic stability and microbial communities. *Bioresour. Technol.* 299:122579. doi: 10.1016/j.biortech.2019.122579

Herrero, M., Wirsenius, S., Henderson, B., Rigolot, C., Thornton, P., Havlík, P., et al. (2015). Livestock and the environment: What have we learned in the past decade? *Annu. Rev. Env. Resour.* 40, 177–202. doi: 10.1146/annurev-environ-031113-093503

Huang, J., Dai, Y., Zhang, Y., Liu, G., Peng, F., Xie, M., et al. (2023). Dynamics of bacterial community, metabolites profile and physicochemical characteristics during solid-state fermentation of soybean meal and corn mixed substrates inoculated with *Bacillus pumilus* and *Limosilactobacillus fermentum*. *J. Sci. Food Agric.* 103, 5588–5599. doi: 10.1002/jsfa.12639

Jayant, M., Hassan, M., Srivastava, P., Meena, D., Kumar, P., Kumar, A., et al. (2018). Brewer's spent grains (BSGs) as feedstuff for striped catfish, *Pangasianodon hypophthalmus* fingerlings: An approach to transform waste into wealth. *J. Clean. Prod.* 199, 716–722. doi: 10.1016/j.jclepro.2018.07.213

Kavalopoulos, M., Stoumpou, V., Christofi, A., Mai, S., Barampouti, E. M., Moustakas, K., et al. (2021). Sustainable valorisation pathways mitigating environmental pollution from brewers' spent grains. *Environ. Pollut.* 270:116069. doi: 10.1016/j.envpol.2020.116069

Kumar, V., Ahluwalia, V., Saran, S., Kumar, J., Patel, A. K., and Singhania, R. R. (2021). Recent developments on solid-state fermentation for production of microbial secondary metabolites: Challenges and solutions. *Bioresour. Technol.* 323:124566. doi: 10.1016/j.biortech.2020.124566

Li, J., Ma, D., Tian, J., Sun, T., Meng, Q., Li, J., et al. (2023b). The responses of organic acid production and microbial community to different carbon source additions during the anaerobic fermentation of Chinese cabbage waste. *Bioresour. Technol.* 371:128624. doi: 10.1016/j.biortech.2023.128624

Li, J., Jia, S., Ma, D., Deng, X., Tian, J., Wang, R., et al. (2023a). Effects of citric acid and heterofermentative inoculants on anaerobic co-fermentation of Chinese cabbage waste and wheat bran. *Bioresour. Technol.* 377:128942. doi: 10.1016/j.biortech.2023.128942

Li, J., Meng, Q., Xing, J., Wang, C., Song, C., Ma, D., et al. (2022). Citric acid enhances clean recycling of Chinese cabbage waste by anaerobic fermentation. *J. Clean. Prod.* 348:131366. doi: 10.1016/j.jclepro.2022.131366

Liao, H., Luo, Y., Huang, X., and Xia, X. (2023). Dynamics of quality attributes, flavor compounds, and microbial communities during multi-driven-levels chili fermentation: Interactions between the metabolome and microbiome. *Food Chem.* 405:134936. doi: 10.1016/j.foodchem.2022.134936

Licitra, G., Hernandez, T., and Van Soest, P. (1996). Standardization of procedures for nitrogen fractionation of ruminant feeds. *Anim. Feed Sci. Technol.* 57, 347–358. doi: 10.1016/0377-8401(95)00837-3

Liu, J., Wang, J., Zhou, Y., Han, H., Liu, W., Li, D., et al. (2022). Integrated omics analysis reveals differences in gut microbiota and gut-host metabolite profiles between obese and lean chickens. *Poultry Sci.* 101:102165. doi: 10.1016/j.psj.2022.102165

López-González, J. A., Suárez-Estrella, F., Vargas-García, M., López, M., Jurado, M., and Moreno, J. (2015). Dynamics of bacterial microbiota during lignocellulosic waste composting: Studies upon its structure, functionality and biodiversity. *Bioresour. Technol.* 175, 406–416. doi: 10.1016/j.biortech.2014.10.123

Murphy, R. (1958). A method for the extraction of plant samples and the determination of total soluble carbohydrates. *J. Sci. Food. Agric.* 9, 714–717. doi: 10.1002/jsfa.2740091104

Navarro, D., Bruininx, E., de Jong, L., and Stein, H. (2018). Analysis for low-molecular-weight carbohydrates is needed to account for all energy-contributing nutrients in some feed ingredients, but physical characteristics do not predict in vitro digestibility of dry matter. *J. Anim. Sci.* 96, 532–544. doi: 10.1093/jas/sky010

Newbold, T., Hudson, L. N., Hill, S. L., Contu, S., Lysenko, I., Senior, R. A., et al. (2015). Global effects of land use on local terrestrial biodiversity. *Nature* 520, 45–50. doi: 10.1038/nature14324

Radosavljević, M., Pejin, J., Kocić-Tanackov, S., Mladenović, D., Djukić-Vuković, A., and Mojović, L. (2018). Brewers' spent grain and thin stillage as raw materials in l-(+)-lactic acid fermentation. *J. Inst. Brew.* 124, 23–30. doi: 10.1002/jib.462

Ren, H., Feng, Y., Liu, T., Li, J., Wang, Z., Fu, S., et al. (2020). Effects of different simulated seasonal temperatures on the fermentation characteristics and microbial community diversities of the maize straw and cabbage waste co-ensiling system. *Sci. Total Environ.* 708:135113. doi: 10.1016/j.scitotenv.2019.135113

Roth, M., Jekle, M., and Becker, T. (2019). Opportunities for upcycling cereal byproducts with special focus on Distiller's grains. *Trends Food Sci. Technol.* 91, 282–293. doi: 10.1016/j.tifs.2019.07.041

Shang, Z., Ye, Z., Li, M., Ren, H., Cai, S., Hu, X., et al. (2022). Dynamics of microbial communities, flavor, and physicochemical properties of pickled chayote during an industrial-scale natural fermentation: Correlation between microorganisms and metabolites. *Food Chem.* 377:132004. doi: 10.1016/j.foodchem.2021.132004

Tan, G., Liu, Y., Peng, S., Yin, H., Meng, D., Tao, J., et al. (2021). Soil potentials to resist continuous cropping obstacle: Three field cases. *Environ. Res.* 200:111319. doi: 10.1016/j.envres.2021.111319

Toledo, M., Gutiérrez, M., Siles, J., García-Olmo, J., and Martín, M. (2017). Chemometric analysis and NIR spectroscopy to evaluate odorous impact during the composting of different raw materials. *J. Clean. Prod.* 167, 154–162. doi: 10.1016/j.jclepro.2017.08.163

Ventorino, V., Parillo, R., Testa, A., Viscardi, S., Espresso, F., and Pepe, O. (2016). Chestnut green waste composting for sustainable forest management: Microbiota dynamics and impact on plant disease control. *J. Environ. Manag.* 166, 168–177. doi: 10.1016/j.jenvman.2015.10.018

Wang, C., Wei, S., Jin, M., Liu, B., Yue, M., and Wang, Y. (2022). Integrated microbiomic and metabolomic dynamics of fermented corn and soybean by-product mixed substrate. *Front. Nutr.* 9:831243. doi: 10.3389/fnut.2022.831243

Wang, Y., Zhang, C., Liu, F., Jin, Z., and Xia, X. (2023). Ecological succession and functional characteristics of lactic acid bacteria in traditional fermented foods. *Crit. Rev. Food Sci.* 63, 5841–5855. doi: 10.1080/10408398.2021.2025035

Xiang, S., Ye, K., and Li, M. (2021). Xylitol enhances synthesis of propionate in the colon via cross-feeding of gut microbiota. *Microbiome* 9:62. doi: 10.1186/s40168-021-01029-6

Xu, D., Ding, Z., Wang, M., Bai, J., Ke, W., Zhang, Y., et al. (2020). Characterization of the microbial community, metabolome and biotransformation of phenolic compounds of sainfoin (*Onobrychis viciifolia*) silage ensiled with or without inoculation of *Lactobacillus plantarum*. *Bioresour. Technol.* 316:123910. doi: 10.1016/j.biortech.2020.123910

Xu, D., Wang, N., Rinne, M., Ke, W., Weinberg, Z. G., Da, M., et al. (2021). The bacterial community and metabolome dynamics and their interactions modulate fermentation process of whole crop corn silage prepared with or without inoculants. *Microb. Biotechnol.* 14, 561–576. doi: 10.1111/1751-7915.13623

Yan, H., Gu, Z., Zhang, Q., Wang, Y., Cui, X., Liu, Y., et al. (2024). Detoxification of copper and zinc from anaerobic digestate effluent by indigenous bacteria: Mechanisms, pathways and metagenomic analysis. *J. Hazard. Mater.* 469:133993. doi: 10.1016/j.jhazmat.2024.133993

Yang, Y., Niu, C., Shan, W., Zheng, F., Liu, C., Wang, J., et al. (2021). Physicochemical, flavor and microbial dynamic changes during low-salt doubanjiang (broad bean paste) fermentation. *Food Chem.* 351:128454. doi: 10.1016/j.foodchem.2020.128454

Yuan, S.-F., Hsu, T.-C., Wang, C.-A., Jang, M.-F., Kuo, Y.-C., Alper, H. S., et al. (2018). Production of optically pure l (+)-lactic acid from waste plywood chips using an isolated thermotolerant *Enterococcus faecalis* SI at a pilot scale. *J. Ind. Microbiol. Biotechnol.* 45, 961–970. doi: 10.1007/s10295-018-2078-5

Zeng, W., Huang, K. E., Luo, Y., Li, D. X., Chen, W., Yu, X. Q., et al. (2020). Nontargeted urine metabolomics analysis of the protective and therapeutic effects of Citri Reticulatae Chachiensis *Pericarpium* on high-fat feed-induced hyperlipidemia in rats. *Biomed. Chromatogr.* 34:e4795. doi: 10.1002/bmc.4795

Zhang, Z., Yang, P., and Zhao, J. (2022). Ferulic acid mediates prebiotic responses of cereal-derived arabinoxylans on host health. *Anim. Nutr.* 9, 31–38. doi: 10.1016/j.aninu.2021.08.004

Zhao, N., Yang, B., Lu, W., Liu, X., Zhao, J., Ge, L., et al. (2020). Divergent role of abiotic factors in shaping microbial community assembly of paocai brine during aging process. *Food Res. Int.* 137:109559. doi: 10.1016/j.foodres.2020.109559

frontiers | Frontiers in Microbiology

TYPE Original Research
PUBLISHED 25 October 2024
DOI 10.3389/fmicb.2024.1472922

OPEN ACCESS

EDITED BY
Xiang Wang,
Jinan University, China

REVIEWED BY
Jian-Wei Zheng,
Foshan University, China
Peter Pristas,
Pavol Jozef Šafárik University in Košice, Slovakia
Ting Zhou,
University of Technology Sydney, Australia
Nikolaos Remmas,
Democritus University of Thrace, Greece

*CORRESPONDENCE
Xiaofang Li
xfli@sjziam.ac.cn
Likun Wang
lkwang@sjziam.ac.cn

RECEIVED 30 July 2024
ACCEPTED 15 October 2024
PUBLISHED 25 October 2024

CITATION
Wang L, Li Y and Li X (2024) Microbe-aided thermophilic composting accelerates manure fermentation.
Front. Microbiol. 15:1472922.
doi: 10.3389/fmicb.2024.1472922

Microbe-aided thermophilic composting accelerates manure fermentation

Likun Wang[1,2]*, Yan Li[1,3] and Xiaofang Li[1]*

[1]Center for Agricultural Resources Research, Institute of Genetics and Developmental Biology, Chinese Academy of Sciences, Shijiazhuang, China, [2]Yancheng Institute of Soil Ecology, Yancheng, China, [3]College of Advanced Agricultural Sciences, University of Chinese Academy of Sciences, Beijing, China

Aerobic composting is a key strategy to the sustainable use of livestock manure, which is however constrained by the slow kinetics. Microbe-aided thermophilic composting provides an attractive solution to this problem. In this study, we identified key thermophilic bacteria capable of accelerating manure composting based on the deciphering of manure bacterial community evolution in a thermophilic system. High-throughput sequencing showed a significant evolution of manure bacterial community structure with the increasing heating temperature. Firmicutes were substantially enriched by the heating, particularly some known thermotolerant bacterial species, such as *Novibacillus thermophiles*, *Bacillus thermolactis*, and *Ammoniibacillus agariperforans*. Correspondingly, through function prediction, we found bacterial taxa with cellulolytic and xylanolytic activities were significantly higher in the thermophilic process relative to the initial stage. Subsequently, a total of 47 bacteria were isolated *in situ* and their phylogenetic affiliation and degradation capacity were determined. Three isolates were back inoculated to the manure, resulting in shortened composting process from 5 to 3 days with Germination Index increased up to 134%, and improved compost quality particularly in wheat growth promoting. Comparing to the mesophilic and thermophilic *Bacillus*, the genomes of the three isolates manifested some features similar to the thermophiles, including smaller genome size and mutation of specific genes that enhance heat tolerance. This study provide robust evidence that microbe-aided thermophilic composting is capable to accelerate manure composting and improve the quality of compost, which represents a new hope to the sustainable use of manure from the meat industry.

KEYWORDS

manure, thermophilic composting, microbe-aided, thermophiles, comparative genomics

Introduction

Waste recycling and reuse to achieve carbon neutrality is a goal that many countries are striving for (Burnley et al., 2011). Among the most common wastes, livestock manure from the growing livestock and poultry breeding industries becomes one of the primary contributors to non-point source environmental contamination (Sun et al., 2012). Correct treatment of livestock manure is thus crucial to addressing these challenges.

Landfill, incineration, anaerobic digestion, and aerobic composting are widely implemented technologies for organic solid waste treatment (Wainaina et al., 2020; De la Cruz et al., 2021; Vlaskin and Vladimirov, 2018), among which aerobic composting is currently one of the most widely used approaches for treating livestock and poultry manure (Pajura, 2023). Aerobic composting is a self-heating, dynamic, and complex biochemical process, during

which the successful biotransformation of organic substrates is completed by many different microorganisms. Aerobic composting is considered as an effective technique for waste management and production of organic fertilizers that can significantly increase soil fitness (Chaurasia et al., 2018). However, a mature compost product that produced by traditional composting is usually completed in 90–270 days (Khalil et al., 2008; Zhang et al., 2013). Besides, numerous greenhouse gasses (GHG) were usually released during this process, including carbon dioxide (CO_2) from organic carbon digestion and methane (CH_4) from poor air circulation and low moisture inside the pile (Lin et al., 2022).

Different from the conventional composting, thermophilic composting provides the benefit of improving biotransformation efficiency and suppressing the proliferation of pathogenic microbes by continuously sustaining high substrate temperatures through external heating. For instance, Zaman et al. (2022) developed a procedure of thermophilic composting with auxiliary heating to 55°C, resulting in a significantly rapid composting process and lower CH_4 emission (Zaman et al., 2022). Aerobic composting bio-reactors can be used to quickly heat up and maintain a high temperature state, which leads to shortened fermentation period to within 10 days, high efficiency, regulated reaction conditions, and centralized exhaust gas treatment.

In most enhancement approaches for livestock manure treatment, biological methods, either the addition of co-substrate or microbial inoculation technology, are often considered as the less expensive and environmental-friendly option (Dong et al., 2023; Niu et al., 2022). A growing body of experimental and observational literature is providing evidence that microbial inoculum has enhanced the composting process and improved maturity of waste and manure (Liu et al., 2023a). Microbial inoculation technique enhances the composting process by increasing the microbial population or ensuring that the appropriate microbial population is present to provide the required enzyme for digesting organic compounds. Cellulases and xylanases generated by microbes in compost catalyze the breakdown of about half of the available xylan and cellulose during the thermophilic phases of composting (Jurak et al., 2015). The addition of cellulose, starch and protein-degraded bacteria in swine manure and rice straw was reported to hasten composting by enhancing compost maturation (Wang and Liang, 2021). On the other hand, a number of studies have found that microbial inoculant has little to no substantial effect on compost maturity, due primary to the incompatibility of the exogenous microbial inoculums with the characteristics of the feedstock and the less-than-ideal operating conditions for composting. Thus, use of *in situ* isolated functional microbes will better adapt to the target environment (Gu et al., 2024), can be one of the strategies to improve the application efficiency of aerobic composting. Ma et al. (2022) indicated that the coupling effect of high temperature and thermophilic bacteria expedited the decomposition of organic materials and promoted the humification process. However, the information on the microbial dynamics during the thermophilic composting process are still missing. Such information is essential to isolate extreme heat-tolerant microbial strains that can be applied in thermophilic composting process, reduce the energy consumption and to increase the production rate of compost within a short time.

In the current study, high-throughput amplicon sequencing analysis was used to obtain a deep understanding of bacterial population dynamics during thermophilic composting process of consortia with cattle dung and chicken manure. Heat-tolerant bacterial strains with cellulose and lignin degrading properties were isolated indigenously based on microbial community dynamics. These isolates were used as microbial additives to enhance the composting kinetics of livestock manure. Physiochemical features of the compost and the fertilizer effect of the compost on wheat growth were evaluated to derive the degree of decomposition at various stage and quality of the matured compost. These results were expected to help identify core microbial species in strengthen fermentation in a livestock manure thermophilic composting system and provide valuable insights for the industrial-scale application of fermentation promoting microbes.

Materials and methods

Thermophilic composting process and sampling

Raw organic materials used for composting consisted of chicken manure and cow dung at a rate of 1:1 collecting from local farm of Yancheng, China. The raw materials were mixed with straw at a rate of approximately 15% (weight/weight). The properties of the raw materials are given in Supplementary Table S1. After thorough mixing, 1 kg of raw materials were sealed in a 2 L Mason jar and incubated in electro heating standing temperature cultivator (DH3600II, Taisite, Tianjin, China) with eight replicate jars for each treatment. A rapid heating composting strategy was adopted in this study to simulate the internal conditions of bioreactor. The composting process lasted a total of 6 days, including 5 days of heating-up and thermophilic process and 1 day of cooling process. The temperature in the incubator was gradually elevated by 5°C per hour from the initial 25°C to the highest temperature 60°C. Raw materials were subsequently incubated under 60°C for 5 days before gradually cooling down. Samples were collected at the initial stage (0 d), heating-up stage (1 d), thermophilic stage (3 d), and cooling stage (6 d). Aliquote of the manure samples were stored immediately in −70°C for molecular characterizations.

Metagenomic sequencing and microbial community analysis

Eight compost samples from each of the four composting steps were collected and sent to Shanghai Majorbio Bio-pharm Technology Co., Ltd. for amplicon sequencing (Yan et al., 2024). Following the manufacturer's instructions, the E.Z.N.A.® soil DNA Kit (Omega Bio-tek, Norcross, GA, United States) was used to extract microbial community genomic DNA from composting samples. The hypervariable region V3-V4 of the bacterial 16S rRNA gene were amplified with primer pairs 338F (5'-ACTCCTACGGG AGGCAGCAG-3′) and 806R (5'-GGACTACHVGGGTWTCT AAT-3′). Purified amplicons were pooled in equimolar and performed paired-end sequencing on an Illumina MiSeq PE300 platform (Illumina, San Diego, United States) in accordance to the standard protocols by Majorbio. The raw reads were deposited into the NCBI Sequence Read Archive (SRA) database (Accession number: SRP513095).

The raw 16S rRNA gene sequencing reads were demultiplexed, quality-filtered by fastp version 0.20.0 (Chen et al., 2018) and merged by FLASH version 1.2.7 (Magoc and Salzberg, 2011). The direction of the sequences were adjusted and barcodes were extracted. Operational taxonomic units (OTUs) with 97% similarity cutoff (Edgar, 2013) were clustered using UPARSE version 7.1 (Edgar, 2013), and chimeric sequences were identified and removed. The taxonomy of each OTU representative sequence was analyzed by RDP Classifier version 2.2 (Wang et al., 2007) against the 16S rRNA database Silva v138 with a confidence threshold of 0.7.

The Majorbio online analysis platform was used to calculate the alpha diversity indices (Richness, Shannon, Chao1, Simpson index) and beta diversity metrics based on the shared presence (Jaccard distance) or abundance (Bray-Curtis distance) of taxa. These metrics were then ordinated via Principal Coordinates Analysis (PCoA). Direct gradient analysis, distance-based redundancy analysis, and permutative ANOVA were used to test for separation (10,000 permutations). The taxonomy differential analysis was conducted using non parametric Kruskal Wallis sum-rank test among each two pairs of the four steps. Random forest analysis was used to identify the key OTUs that can distinguish differences between the two groups of composting steps, as well as their impact on the model. The network analysis of bacterial community was conducted though Random Matrix Theory (RMT)-based network construction methods (Deng et al., 2012).[1] The prediction of community metagenomic functional abundance was performed using PICRUSt1 and FAPROTAX.

Microbial isolation

Microbes were isolated from thermophilic and maturated stage samples. Three separate 1 g compost sub-samples were obtained from each sample and individually placed in tubes containing 10 mL sterile distilled water. Compost suspensions were prepared by mixing on a vortex mixer for 60s, serially diluted, and spread onto nutrition agar (Aoboxing Bio-tech Co., Ltd., Beijing, China) plates for isolating bacteria. Culturing plates were incubated at 45°C and 60°C for isolating heat tolerant and extreme heat tolerant microorganisms. Colonies that can grow at 45 or 60°C were transferred to new media and morphologically redundant ones were removed. The left colonies were subjected to DNA extraction and molecular identification based on 16S sequences. The 16S rDNA sequences of the bacterial isolates were deposited into NCBI GenBank database with the Accession Numbers of PQ462071 to PQ462113 and PQ459755-PQ459762.

Enzymatic assessment

For cellulase assay, the bacterial isolates were incubated on sodium carboxymethyl cellulose medium at 45°C for 18 h. Congo red [0.1% (volume/volume); Macklin, Shanghai, China] staining was performed for 5 min, and then the destaining process was carried out by soaking the stained sample in 1.0 M NaCl for 10 min. Ligninase production activity was assessed by incubating bacterial isolates on nutrient agar medium containing aniline blue (Solarbio, Beijing, China), and the results were assessed 18 h post incubation. The enzyme activity and enzyme-degrading ability could be assessed by the size of the clear zone on the medium around the bacterial colonies (Teather and Wood, 1982).

Microbial inoculation for thermophilic composting enhancement

Three bacterial inocula with targeted properties were selected for microbial-aided thermophilic composting experiment as previous described. The selected strains were incubated in liquid LB medium and shaken at 45°C, 150 r/min overnight. The inocula were collected by centrifuging, and fresh cells were inoculated individually in manure at a ratio of 1: 100 (weight/weight) with 3 replicates for each microbial treatment. A non-microbial inoculation control (NI) with 3 replicates was included in this experiment. Compost samples were collected at 3 days and 5 days post heat treatment.

Analysis of compost's physicochemical properties

Composting temperatures were recorded using a temperature sensor. Moisture was measured by drying fresh solid samples at 105°C for approximately 8 h to achieve a constant weight. Total carbon and total nitrogen were determined using an elemental analyzer (FlashSMART, Thermo Fisher Scientific Inc., MA, United States). Fresh solid samples were mixed with deionized water at a mass ratio of 1:10 and shaken for 1 h to obtain the water extract for the measurement of pH, electrical conductivity (EC), and seed Germination Index (GI). The pH and EC values were determined using a FiveEasy Plus™ pH/EC meter (Mettler Toledo, Shanghai, China). The GI was measured following the methods described previously by Wang et al. (2023) and Liu et al. (2023b). The GI values were measured using 10 cucumber seeds cultured in the water extract at 25°C for 48 h in darkness. Deionized water was used as a control. Organic matter content in the compost was determined by potassium dichromate volumetric method. In addition, total soluble phosphorus and total potassium contents were determined using UV-1900i spectrophotometers (Shimadzu Co., Ltd, Shanghai, China) and TAS-990 atomic absorption spectroscopy (Beijing Puxi General Instrument Co., Ltd, Beijing, China), respectively.

Testing of manure quality by a wheat growth test

Composted manure was subjected to wheat growth tests to examine the quality of the fermentation products. After fermentation, composts from different treatments were thoroughly mixed with growing substrates at a volume ratio of 2:1. The growing substrates contained vermiculite and potting mix (Klasmann-Deilmann, Germany) at a ratio of 7:1 to create a barren nutritional environment. Wheat seeds were transplanted in the culture mix after germinating in Petri dish using distilled water. Five pots were applied for each compost sample with 2 seeds in each pot. Pots were arranged in a completely randomized design in an artificial climate growth chamber (PRX-800D-F, Ningbo, China). Plants were grown in the greenhouse

1 http://ieg2.ou.edu/MENA

at 25–28°C with a 14-h photoperiod, watered at 3-day intervals, and harvested 1 month after planting. Wheat seedlings shoot height, shoot, and root dry weight were measured at harvest.

Bacterial whole genome sequencing

Genome sequencing was conducted at Shanghai Majorbio Bio-pharm Technology Co., Ltd. Genomic DNA was extracted using Bacterial DNA extraction kit (magnetic beads) (BioDynami, Alabama, United States) according to the manufacture's protocol. Paired-end Illumina sequencing (2 × 150 bp) on Illumina Novaseq 6,000 (Illumina Inc., SanDiego, CA, United States) was used to sequence the whole-genome of FSB24, FSB30 and FSB35. The raw reads were deposited into the NCBI SRA database (Accession number: SRP513345).

The low-quality reads were filtered to obtain clean data using fastp 0.20.0 (Chen et al., 2018). After quality control, clean reads were *de novo* assembled to obtain genome draft using short sequence assembly software SOAP denovo2 (Luo et al., 2012), resulting in the optimal contigs assembly. Then, aligned contigs were locally assembled and optimized base on the paired-end and overlap relationships of reads to construct scaffold. Glimmer3 (Delcher et al., 2007), GeneMarkS-2 (Lomsadze et al., 2018), and Prodigal v2.6.3 (Hyatt et al., 2010) were used to predict the coding sequence (CDS) on the genome. tRNAscan-SE v2.0 (Chan and Lowe, 2019), Barrnap,[2] and Tandem Repeats Finder v 4.09 (Benson, 1999) were used to predict tRNAs, rRNAs, and tandem repeat sequences, respectively. Genes were annotated against Gene Ontology (GO),[3] Kyoto Encyclopedia of Genes and Genomes (KEGG),[4] Cluster of Orthologous Groups of proteins (COG),[5] KOG, evolutionary genealogy of genes: Non-supervised Orthologous Groups (eggNOG), Non-Redundant Protein Database (NR), Transporter Classification Database (TCDB), Swiss-Prot,[6] Carbohydrate-Active enZYmes Database (CAZy) databases using diamond v2.1.9 (Buchfink et al., 2021) with an cutoff *E*-value of 1.0 e-5. Secondary metabolism gene cluster analysis was performed using antiSMASH v2.0.2 (Blin et al., 2013).

Comparative genomics

Based on the genome maps of three isolates, their genes on genomes were compared to understand the functions, expression mechanisms, and evolution process. OrthoMCL v2.0 (Li et al., 2003) was used to obtain homologous gene families, as well as gene number and information in each gene family. The genomes of the three isolates FSB24, FSB30 and FSB35 were then screened for core genes (genes included in all isolates) and unique genes (genes included only in a specific isolate).

Genomic collinearity analysis and phylogenomic analysis were conducted by Mauve 2.4.0 (Darling et al., 2004). Isolates FSB24, FSB30 and FSB35 were aligned to 12 other *Bacillus* species, and also individually mapped to the known thermophile *Bacillus thermotolerans* (GCF_000812025.2) and mesophile *Bacillus cereus* (GCF_000007825.1) using BLAST+ with an E value ≤1e-5. Genes with identity <80% were considered as non-homolog genes. The phylogenetic relationship of the selected genes was constructed with MEGA 7.0 (Kumar et al., 2016) using the maximum likelihood method and 1,000 bootstrap replicates. Multiple sequence alignment was performed using ClustalW (Thompson et al., 1994), and p-distance was calculated.

Statistical analysis

Plant growth and physicochemical compost properties data were subjected to ANOVA using SAS (Version 9.4; SAS Institute, Cary, NC) GLM model for a completely randomized design. Data were subjected to analysis of variance and means separation using Fisher's least significant test, with $p \leq 0.05$ considered significant.

Results

Succession in bacterial diversity during thermophilic composting process

The heat treatment resulted in decreasing Chao 1 indices of bacterial communities than the initial stage (Control). The Chao 1 indices of bacterial communities were not different between thermophilic (TC) and cooling (CL) steps, but they both significantly lower than heat-up (HT) step and the Control. In addition, the bacterial abundance, indicated by the Chao 1 index, in HT step was significantly higher than that in the Control (Figure 1a). PCoA analysis indicated that bacterial community compositions of the TC and CL steps were more similar to each other but distinct from that of the Control and HT (Figure 1b), additionally, the bacterial community compositions of Control and HT were more similar to each other. A total of 726 bacterial OTUs presented in all the composting steps, and individually, 24, 1, 33 and 49 OTUs were only presented in the Control, HT, TC and CL steps (Figure 1c). Among the 49 unique OTUs detected in CL process, OTU596 from the Genus of *Paenibacillus* (15.01%), OTU918 from the Genus of *Thermobacillus* (9.12%) and OTU556 from the Family of Limnochordaceae (8.71%) represented the greatest proportion among the unique OTUs. While among the unique OTUs in the Control, OTU63 from the Genus of *Brumimicrobium* (17.31%), OTU392 from the Family of Sphingobacteriaceae (9.62%), and the OTU47 from the Order of Peptostreptococcales-Tissierellales (9.62%) represented the greatest proportion.

Among bacterial phyla, Firmicutes, Actinobacteriota, Proteobateria, Bacteroidota, Gemmatimonadota, Deinococcota, Halanaerobiaeota, Myxococcota, Chloroflexi, and Desulfobacterota were detected at greater abundance in TC and CL processes (Figure 1d). The bacterial phylum that was significantly altered in abundance during the composting process was Firmicutes (Figure 1d), with about 2.5 fold increase in TC (67.21 ± 9.60%) and CL (62.5 ± 7.35%) steps relative to the Control (25.71 ± 14.27%). The abundance of Actinobacteriota was first increased and then decreased during the whole composting process. The abundances of

2 https://github.com/tseemann/barrnap
3 http://geneontology.org/
4 http://www.genome.jp/kegg/
5 http://www.ncbi.nlm.nih.gov/COG/
6 http://www.ebi.ac.uk/uniprot/

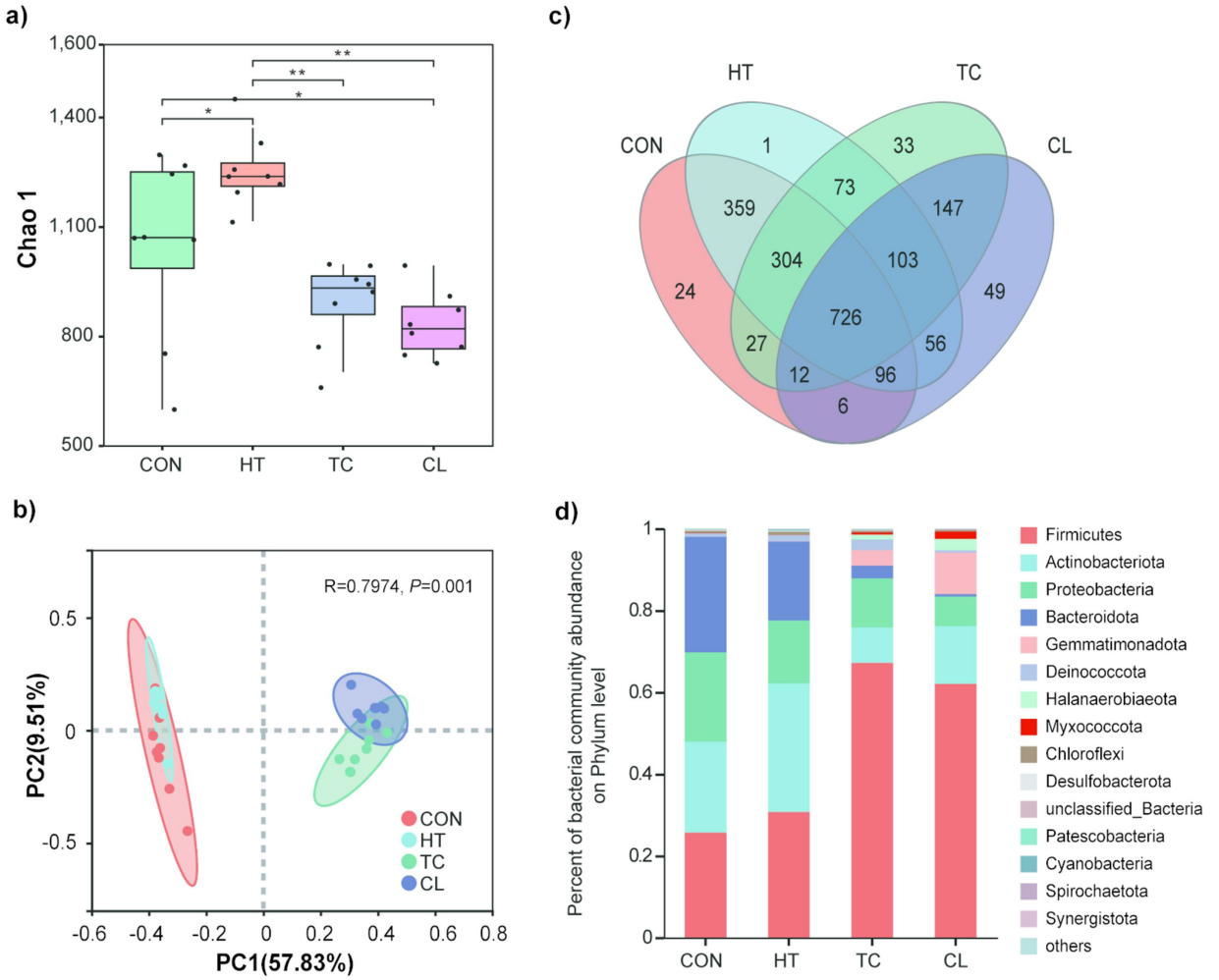

FIGURE 1
Abundance and diversity alteration of bacterial communities across the thermophilic composting process. **(a)** Chao 1 index of bacterial community across thermophilic composting processes. **(b)** Principal coordinates analysis of Bray-Curtis distances based on bacterial species abundance profiles across thermophilic composting. **(c)** Numbers of common and unique bacterial species across thermophilic composting showed by Venn diagram. **(d)** Relative abundance of bacteria in phylum level in the four steps of thermophilic composting.

Proteobacteria and Bacteroidota were decreased during composting, whereas the abundance of Gemmatimonadota was dramatically increased with the rising temperature (Figure 1d). Besides, the phyla Gemmatimonadota and Halanaerobiaeota were only in the top 10 abundant bacterial phyla of TC and CL, but not in HT or the Control.

Differential analysis of bacterial taxonomy among the fermentation steps

Random forest analysis showed that the top 50 differentially abundant bacterial OTUs among the four fermentation steps were mainly in the phyla of Firmicutes, Proteobacteria, Bacteroidota, and Myxococcota (Supplementary Figure S2). Among them, the thermophilic bacteria *Ammoniibacillus agariperforans* (Sakai et al., 2015), *Novibacillus thermophiles* (Yang et al., 2015), and *Ureibacillus thermosphaericus* (Jia et al., 2017) were significantly abundant in the TC and CL steps. Whereas *Facklamia tabacinasalis* (Collins et al., 1999) and *Aerococcus urinaeequi* (Rasmussen, 2016), two potential human pathogens, were more abundant in HT step and the Control (Supplementary Figure S2).

Since bacterial communities in the TC and CL steps were similar to each other (so were HT and the Control) based on diversity and taxonomy analysis, samples from TC and CL (thermophilic group), as well as the Control and HT (control group) were combined to conduct the pairwise comparison. Through differential analysis of control group and thermophilic group, 464 differentially abundant bacterial OTUs were obtained. The top 50 significantly abundant bacteria in thermophilic group were mainly in the Phyla of Firmicutes, including the thermotolerant bacteria *Sinibacillus soli* (Yang and Zhou, 2014), *Bacillus thermolactis* (Coorevits et al., 2011), and *A. agariperforans* (Sakai et al., 2015) (Figure 2a). Besides, several bacteria in the Phyla of Gemmatimonadota, Myxococcota, and Proteobacteria were also significantly abundant in the thermophilic group (Figure 2a). The top 50 significantly abundant bacteria in the control group were mainly in the Phyla of Firmicutes, Bacteroidota, and Proteobacteria. Among them, *Streptococcus equinus* (Park et al., 2023), *F. tabacinasalis* (Collins et al., 1999), *A. urinaeequi* (Rasmussen, 2016), and

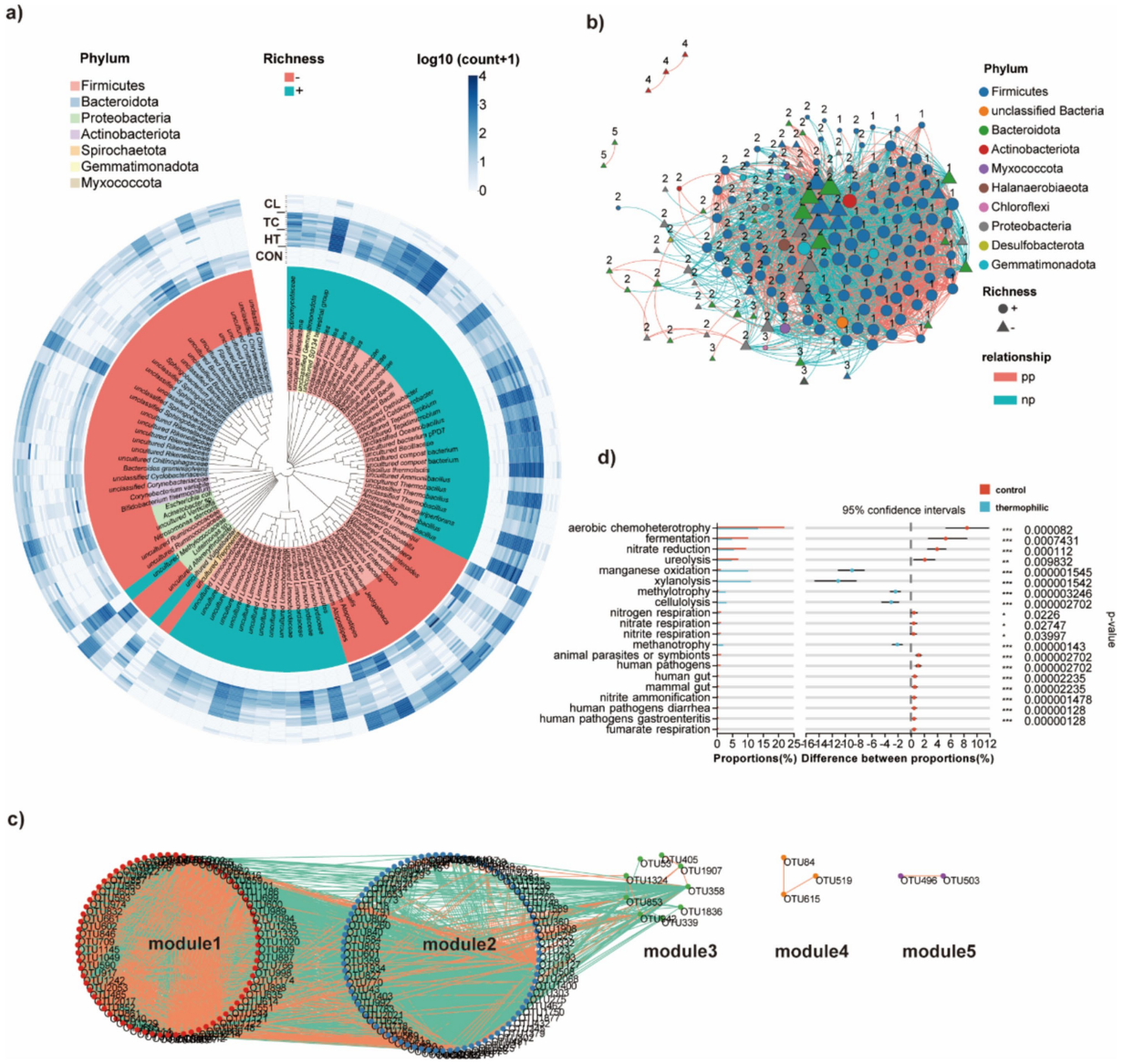

FIGURE 2
Pairwise comparison of bacterial taxonomy between the two groups (thermophilic group vs. control group). **(a)** The top 50 bacterial species that significantly altered in abundance comparing between thermophilic and control group. **(b)** Network of bacterial OTUs with significantly altered abundance, comparing between thermophilic and control group. **(c)** Modules of bacteria with significantly altered abundance, comparing between thermophilic and control group based on molecular ecological network (MENs) analysis. **(d)** Significantly different bacterial metabolites comparing between thermophilic and control group that analyzed through FAPROTAX.

Enterococcus faecalis (Kristich et al., 2014) from the Phylum of Firmicutes, and *Escherichia coli* from the Phylum of Proteobacteria are reported human/animal pathogens (Figure 2a).

Molecular ecological network (MENs) through RMT-based methods was constructed for all the differentially abundant bacterial OTUs between the thermophilic and control group, resulting in 172 nodes and 2,616 edges (Figure 2b). The 172 OTUs were classified into 5 modules, and OTU1379 (Firmicutes), OTU432 (Bacteroidota), and OTU491 (Bacteroidota) were in the centre of the network (Figure 2b). There were 72 bacterial OTUs classified to module 1 with 64 of them were significantly abundant in the thermophilic group, while eight of them were significantly abundant in the control group (Figure 2c). Among the 64 bacterial OTUs enriched in the thermophilic group, the slow growing species *Thermobifida fusca*, which was reported to promote the growth of other bacteria by sharing cobalamin in a quasi-natural composting system (Zhao et al., 2023), was related to 75 OTUs, and all the relationships were positive. There were 85 bacterial OTUs classified to module 2 with 44 of them were significantly abundant in the thermophilic group, while 41 of them were significantly abundant in the control group. The thermophilic species *Clostridiales bacterium* and *Bacillus thermocloacae* that significantly abundant in the thermophilic group had 1 negative and 3 positive connections with other OTUs, respectively. There were only three and two OTUs classified to module 4 and 5, respectively, and they were all significantly more abundant in the control group (Figure 2c).

FAPROTAX was used to map bacterial taxonomy to metabolic related functions. Through Wilcoxon rank-sum test, we found that the abundance of bacteria with metabolic functions of cellulolysis, xylanolysis, methanotrophy and manganese oxidation were significantly higher in the thermophilic group, while functions related to animal/plant pathogenesis were significantly higher in the control group (Figure 2d). Besides, functions related to nitrogen cycle, such as nitrite ammonification and nitrate reduction, were significantly decreased with temperature increasing (Figure 2d), suggesting the functions of bacterial community converted during the thermophilic composting process. It was consistent with previous reports (Song et al., 2016).

High-throughput culturing of thermophilic fermentation strains

A total of 47 bacterial isolates were obtained from the plate culture based on colony morphology, color and shape. The 47 bacterial isolates were identified through 16S rDNA sequencing (Supplementary Table S3). A maximum likelihood dendrogram was generated with the 16S rDNA sequences of the bacteria and representative sequences from the databases. Phylogenetic analysis of the 47 isolates mainly matched with the genera of *Bacillus*, *Ureibacillus*, *Geobacillus*, *Acinetobacter*, *Sphingomonas*, *Lactobacillus*, *Staphylococcus*, and *Burkholderia*. Among the 47 bacterial isolates, 11 isolates produced the cellulose enzyme. A clear halo zone was found around the colonies in the Congo red agar plates (Figure 3a; Supplementary Figure S4). Nine of the isolates were able to produce lignin peroxidase, as clear halo zones were observed around the colonies in the aniline blue agar plates (Figure 3a; Supplementary Figure S5).

Influence of microbial inoculum on manure compost maturity

According to the 16S rDNA conserved region taxonomy identification and enzyme production, three isolates FSB24, FSB30, and FSB35, were selected as microbial inocula, and they were classified to *Bacillus stercoris*, *B. stercoris*, and *Bacillus licheniformis*, respectively, wherein *B. stercoris* is the sub-species of *Bacillus subtilis* (Figures 3b–d). In fact, through our subsequent whole genome sequencing, the taxonomy of FSB24 and FSB30 were closer to *Bacillus spizizenii* (Figure 4a).

Generally, compost is considered mature when the GI value of seed germination is >50%, and it is considered completely mature when GI is >80% (Zucconi et al., 1981). The compost inoculated with microbial agents FSB24 and FSB30 had GI values higher than 90% after 3 days of fermentation, which were significantly higher than those inoculated with FSB35 and no inoculation (NI) (Figure 5a). After 5 days of fermentation, the compost inoculated with microbial agents all possessed GI values significantly higher than the NI, among which the GI of FSB35 and NI were significantly increased comparing to 3 days' fermentation (Figure 5a).

It is generally believed that compost is considered mature when its carbon to nitrogen (C/N) ratio close to 16, which is the C/N ratio of microorganisms (Li et al., 2022). The C/N ratios of compost inoculated with microbial agents FSB24, FSB30 and FSB35 after 3 days of fermentation were 13.97, 13.64, and 13.10 respectively, which were significantly higher than that of the NI (Figure 5b). The C/N values of compost inoculated with microbial inoculation after 5 days of fermentation were 13.97, 14.49, and 13.07, respectively, which were again significantly higher than that of the NI (Figure 5b). Additionally, the C/N ratios of FSB30 was closer to 16, indicating this treatment possessed higher degree of maturity than others (Figure 5b).

The initial organic matter content (OMC) of the raw manure materials was 54.38% (Supplementary Table S1). After fermentation, the OMC of all the treatments decreased, while the OMC of the composts with microbial inoculations were significantly lower than that of the NI regardless of the fermentation days, indicating that the microbial inoculation did a good job in decomposing the organic matter in the manure (Figure 5c). The OMC were not significantly different from each other among the three inoculation treatments regardless of the fermentation days (Figure 5c).

The total soluble phosphorus content of compost inoculated with microbial agents were all significantly higher than that of the NI after fermentation for 3 days. In addition, phosphorus content of the compost inoculated with FSB35 was significantly higher than that inoculated with FSB24 at 3 days of fermentation (Supplementary Figure S6a). At 5 days post fermentation, the phosphorus content of compost inoculated with microbial agents FSB35 was significantly higher than the NI, whereas the phosphorus content were not different among composts inoculated with FSB24, FSB30, and the NI (Supplementary Figure S6a).

The total potassium content of compost inoculated with microbial agents FSB35 was significantly higher than that inoculated with FSB24 after 3 days of fermentation, however, the potassium content in the composts inoculated with FSB24, FSB30 and the NI were not significantly different among each other (Supplementary Figure S6b). The total potassium content of compost after 5 days of fermentation were not significantly different among each other (Supplementary Figure S6b).

The conductivity of all the treatments were not significantly different among each other at 3 days of fermentation (Supplementary Figure S6c). However, the conductivity of the NI significantly decreased at 5 days of fermentation comparing to 3 days, resulting in a significantly lower value than the composts with microbial inoculations (Supplementary Figure S6c).

Effect of fermented manure with microbial inoculation on wheat growth

Overall, the wheat cultivated in substrates mixed with composts grew better comparing to no treatment control (NTC) (Figures 6a,b). The root dry weight of wheat cultivated in 3-day-fermentation compost inoculated with microbial agents FSB24 was greater than other microbial inoculation treatments and the NI (Figure 6c). The root dry weight of wheat cultivated in 5-day-fermentation compost that inoculated with FSB24 and FSB30 were greater than those of the FSB35 and the NI treatments, whereas FSB35 and NI were not significantly different from each other (Figure 6c).

The shoot dry weight of wheat cultivated in 3-day-fermentation compost that inoculated with microbial agents were greater than that of the NI, and the wheat cultivated in compost inoculated with FSB24 performed the best in shoot growth (Figure 6d). Likewise, the shoot dry weight of wheat cultivated in 5-day-fermentation compost that

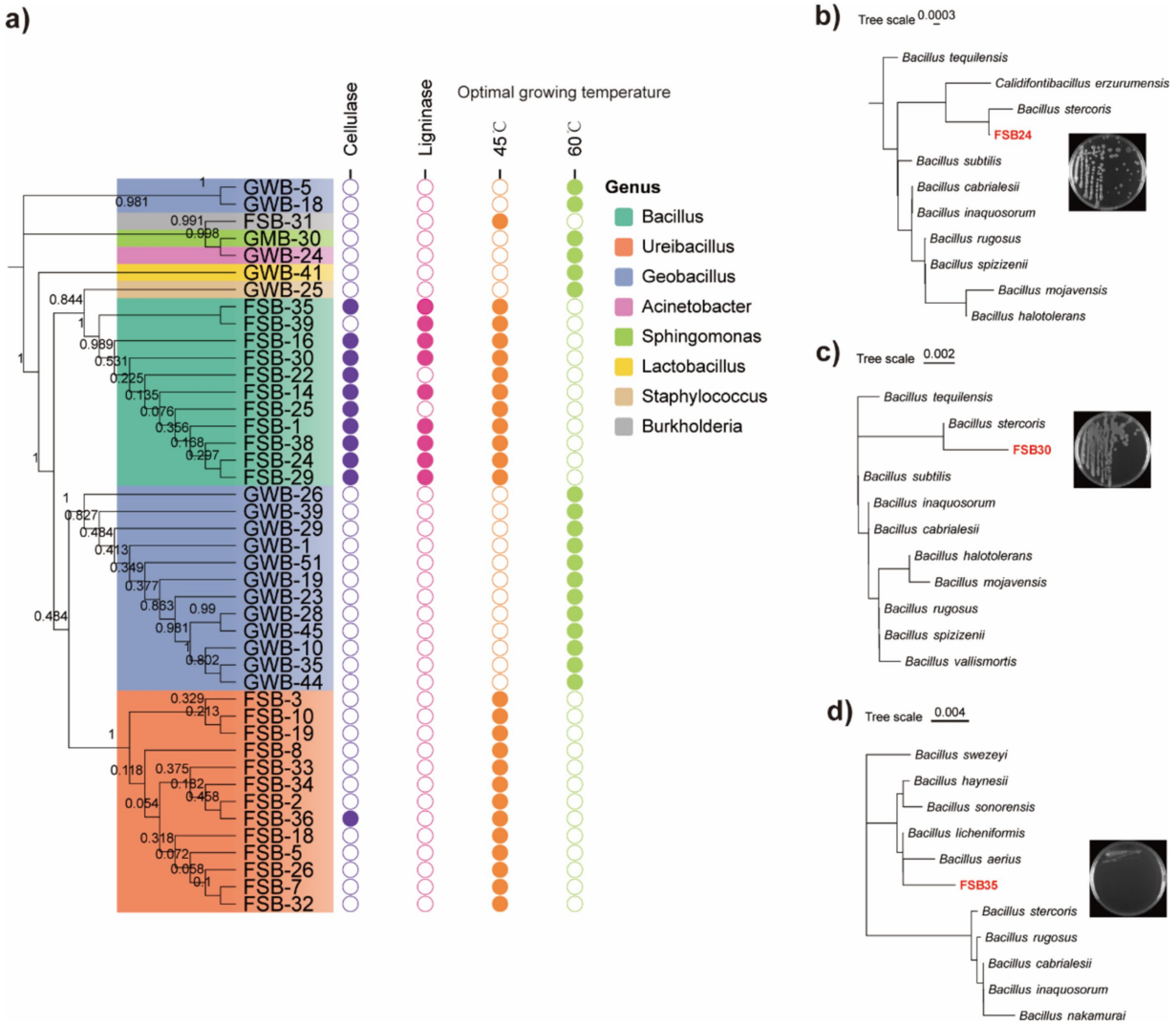

FIGURE 3
Thermophilic bacteria isolated through high-throughput culturing. **(a)** Phylogenetic tree of the 47 isolated bacterial strains assessed through 16S rDNA region using the maximum likelihood method and 1,000 bootstrap replicates in MEGA 7.0, their enzymatic production activities, and optimum incubation temperature. **(b)** Morphology and classification of isolate FSB24 assessed through 16S rDNA conserved region. **(c)** Morphology and classification of isolate FSB30 assessed through 16S rDNA conserved region. **(d)** Morphology and classification of isolate FSB35 assessed through 16S rDNA conserved region.

inoculated with microbial agents were greater than that of the NI, and the wheat cultivated in compost inoculated with FSB24 performed significantly greater shoot growth than that of the FSB30 (Figure 6d).

The shoot height of wheat cultivated in 3-day-fermentation compost that inoculated with FSB24 and FSB35 were significantly greater than that of the FSB30 and NI (Figure 6e). The shoot height of wheat cultivated in 5-day-fermentation compost that inoculated with microbial agents were all significantly greater than that of the NI (Figure 6e). Wheat cultivated in 5-day-fermentation compost inoculated with FSB35 had the greatest shoot height among all the treatments (Figure 6e).

Genome sequencing and comparative genomics

The genome sequence of the three bacteria generated about 1.2 Gb clean data, and the coverage base on reads mapping of FSB24, FSB30, and FSB35 were 98.70, 98.76, and 98.81%, respectively. Comparing to the genome of mesophilic bacterium *B. cereus*, the genome sizes of the three isolates, FSB24, FSB30, and FSB35 were smaller, but they all larger than the genomes of thermophilic bacterium *B. thermotolerans* (Table 1). The genomes of FSB24, FSB30, and FSB35 comprised of 8, 21, and 23 scaffolds, with GC contents of 43.38, 43.93, and 45.88%, respectively (Table 1), which were consistent with their (species) conformis genomes *B. spizizenii* (GCF_000227465.1) and *B. licheniformis* (GCF_000011645.1), but higher than the mesophilic bacterium *B. cereus* (Table 1).

There were 4,292, 4,118, and 4,482 protein coding genes (CDS) recognized on the genomes of FSB24, FSB30, and FSB35, respectively, which were more than that on the conformis genomes of *B. spizizenii* and *B. licheniformis* as well as the thermophilic bacterium *B. thermotolerans* (Table 2). Whereas the numbers of CDS on the genome of the three isolates were smaller than the mesophilic bacterium *B. cereus* (Table 1). Among the three isolates, FSB30 and

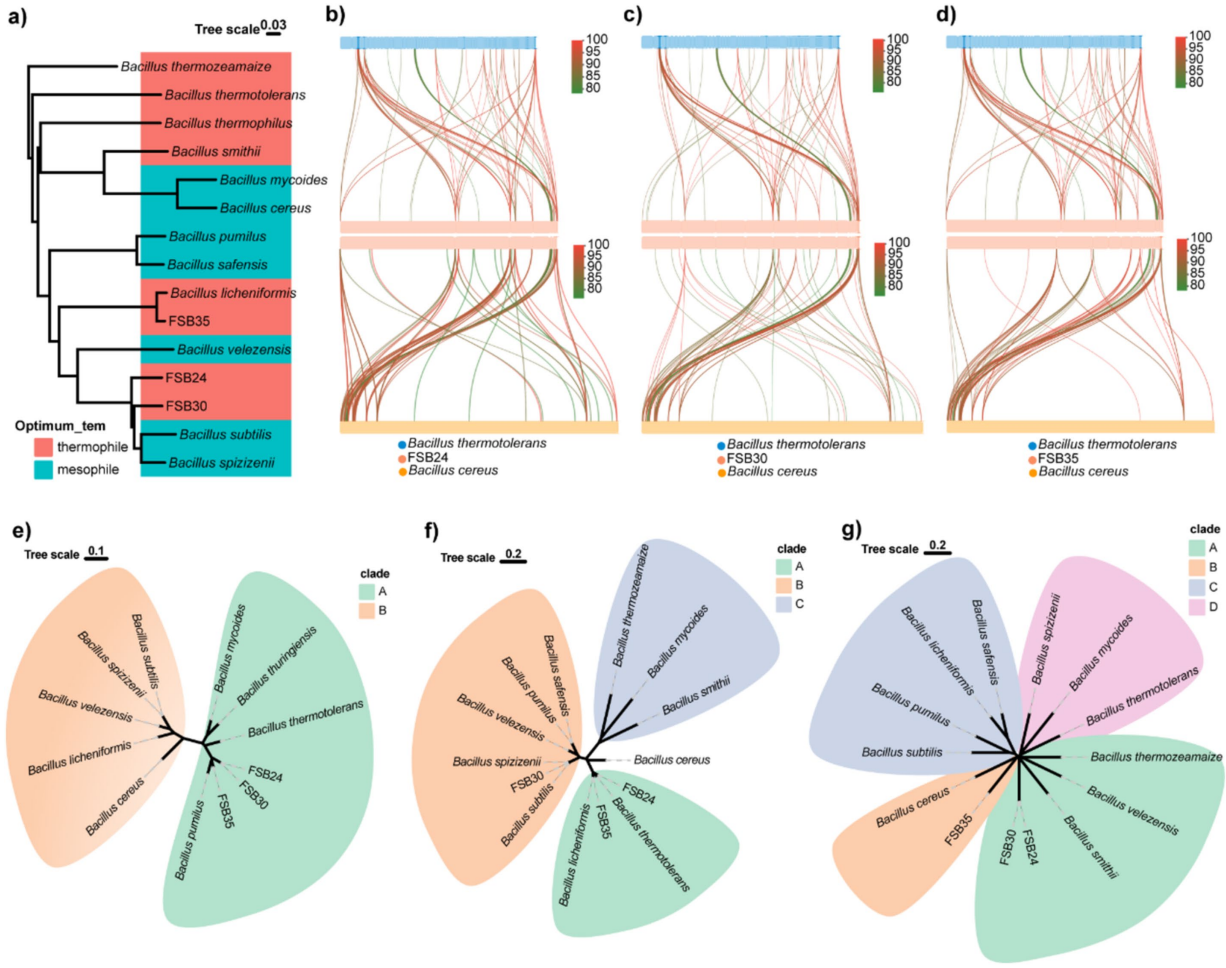

FIGURE 4
Genomic comparison of typical thermophiles and mesophiles in the genus of *Bacillus*. **(a)** Phylogenome analysis of the three isolates used in this study and 9 known *Bacillus* thermophiles and mesophiles were conducted by Mauve 2.4.0 and visualized through ggtree in R v4.3.2. **(b)** Genomic collinearity analysis of FSB24 with thermophile *Bacillus thermotolerans* and mosophile *Bacillus cereus*. **(c)** Genomic collinearity analysis of FSB30 with thermophile *B. thermotolerans* and mosophile *B. cereus*. **(d)** Genomic collinearity analysis of FSB35 with thermophile *B. thermotolerans* and mosophile *B. cereus*. **(e)** Phylogenetic analysis of small acid-soluble protein (SASP) sequences in various *Bacillus* species. **(f)** Phylogenetic analysis of fatty acid desaturase (DesE) sequences in various *Bacillus* species. **(g)** Phylogenetic analysis of transcription factor LysR sequences in various *Bacillus* species.

FSB35 comprised of plasmids (Table 2). Additionally, the tandem repeat number in isolates FSB24 and FSB30 were much lower than that in FSB35 (Table 2).

There were 3,026 genes commonly found in the three isolates, while there were 266, 461, and 1,114 unique genes found in FSB24, FSB30 and FSB35, respectively (Figure 7d). In total 3,932 homologous gene families were found through OrthoMCL annotation, including 33 of them possessed homologous genes ≥5. The 33 homologous gene families contain genes functioning in some basic life activities, such as non-ribosomal peptide synthesis, cell wall synthesis (LTA synthase family protein) and glycosyl transfer (Figure 7e). Besides, there are also homologous genes that explain why the three strains of bacteria are suitable for survival under stress (NADP-malic enzyme) (Chen et al., 2019). In addition, there are more than 5 homologous genes annotated to phosphotransferase system (PTS), which is a well-documented microbial system with a prominent role in carbohydrates transportation (Xu et al., 2023).

CAZymes play a significant role in degradation of complex carbohydrates. In the six categories of CAZymes, number of genes in carbohydrate esterases and glycosyl transferases presented obvious differences among the three isolates (Figure 7f). In carbohydrate esterases group, acetylxylan esterase plays an important role in the hydrolysis of xylan and possess 16, 20 and 22 genes in FSB24, FSB30 and FSB35, respectively (Figure 7f). Pectin methylesterase, which plays a critical role in modifying pectins, was only found in FSB35 (Figure 7f). In glycosyl transferases group, lipid-A-disaccharide synthase, which function in lipopolysaccharide biosynthesis, was only found in FSB24 and FSB35. The genes annotated to sucrose synthase in FSB24, FSB30, and FSB35 were 8, 6, and 7, respectively (Figure 7f).

Phylogenomics analysis of the three isolates together with 12 bacteria in the genus of *Bacillus* revealed that their genomes was classified by evolutionary relationships rather than heat tolerance (Figure 4a). Comparing to the genome of thermophilic bacterium *B. thermotolerans*, 7.45, 5.53, and 5.74% of genes on the genomes of FSB24, FSB30 and FSB35 were homologous (with identity ≥80%), respectively (Figures 4b–d).

Targeted to specific genes, we found that some genes in the three isolates homologous to *B. thermotolerans* were not homolog to

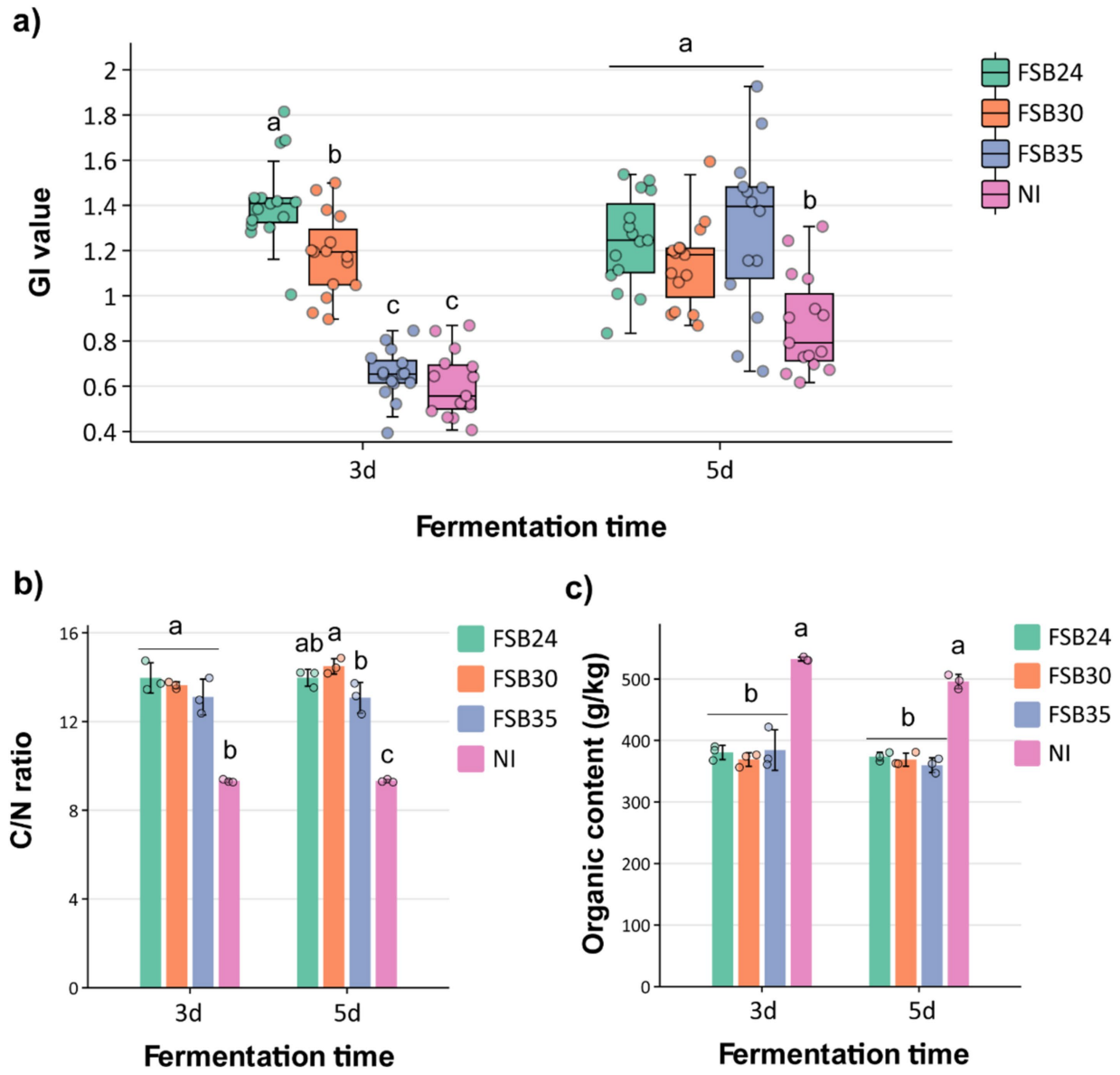

FIGURE 5
Influence of microbial inoculation on compost physiochemical characteristics after 3 days and 5 days of thermophilic composting. **(a)** Germination index (GI) index of the composts inoculated by the three bacterial isolates, individually. **(b)** C/N ratio of the composts inoculated by the three bacterial isolates, individually. **(c)** Organic content of the compost inoculated by the three bacterial isolates, individually. Bars indicate standard errors of the means. For a given duration of heat treatment, bars designated with the same letter indicate means that are not significantly different based on Fisher's LSD analysis. NI: no inoculation.

mesophile *B. cereus*. The genes annotated to small acid-soluble protein (SASP) in the three isolates were more similar to *B. thermotolerans* according to the phylogenetic analysis than to the mesophiles *B. subtilis*, *B. velezensis*, *B. cereus* and their conformis genomes (Figure 4e). SASP are double-stranded DNA-binding proteins that contribute to the dormant spore's high resistance to UV radiation by protecting the DNA backbone from enzymatic and chemical cleavage. The genes in FSB24 and FSB35 that encoded fatty acid desaturase were more similar to that in the thermophiles *B. thermotolerans* and *B. licheniformis* rather than the mesophiles (Figure 4f). Fatty acid desaturase catalyzes the desaturation reactions of saturated fatty acids thereby accelerate the metabolism of fatty acid. In addition, through phylogenetic analysis we found that transcriptional factor LysR of these three isolates were distantly away from their respective reference genomes but close to the thermophiles *B. thermozeamaize* and *B. smithii* (Figure 4g). LysR-type transcriptional regulators (LTTRs) regulate a diverse set of genes, including those involved in virulence, metabolism, quorum sensing and motility (Maddocks and Oyston, 2008).

Discussion

Both thermophilic and lignocellulolytic microbe inoculations are cutting-edge strategies for expediting fecal fermentation and improve the production efficiency of organic fertilizer. Through 16S rRNA

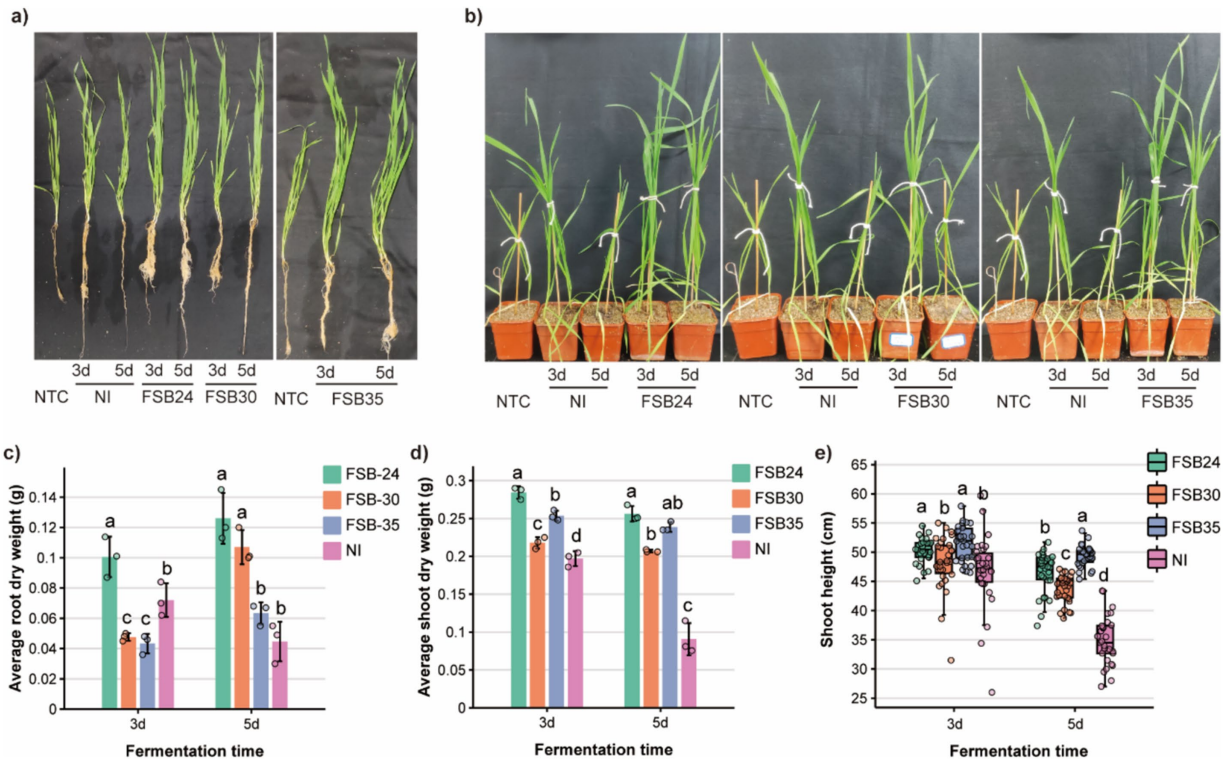

FIGURE 6
Quality of composts from microbe-aided thermophilic composting tested on wheat growth. **(a)** Root and shoot phenotypes of wheat fertilized by composts. **(b)** Phenotypes of wheat in pots fertilized by composts. **(c)** Root dry weight of wheat fertilized by composts treated with different microbial inoculum. **(d)** Shoot dry weight of wheat fertilized by composts treated with different microbial inoculum. **(e)** Shoot height of wheat fertilized by composts treated with different microbial inoculum.

TABLE 1 Genomic features of the three isolates used in this study and four other published *Bacillus* species.

Sample name	Genome size (Mb)	Total scarf no.	Scaffold N50 (Mb)	G + C (%)	Gene no.	Protein-coding
FSB24	4.04	8	2.13	43.38	4,560	4,292
FSB30	3.99	21	0.51	43.93	4,395	4,118
FSB35	4.14	23	2.12	45.88	4,832	4,482
Bacillus spizizenii	4.20	2	4.20	44.00	4,286	4,045
Bacillus cereus	5.40	1	5.00	35.50	5,497	5,255
Bacillus licheniformis	4.30	2	4.10	45.50	4,492	4,384
Bacillus thermotolerans	3.80	124	0.07	44.50	4,019	4,019

TABLE 2 Gene features of the three isolates used in this study.

Sample name	tRNAs no.	rRNAs no.	sRNA no.	Tandem repeat no.	Transposon no.	Plasmid no.
FSB24	80	9	92	18	4	0
FSB30	84	6	91	34	3	5
FSB35	79	11	96	81	3	8

amplicon sequencing, we studied the microbial community evolution during livestock manure thermophilic composting. A clear microbial community alteration occurred mainly during the TC step. The abundance of thermotolerant bacterial species, such as *B. thermolactis*, significantly increased during composting, and correspondingly through function prediction, we found the abundance of cellulolysis and xylanolysis species were significantly higher in thermophilic process relative to the control. On the basis of the microbial succession and functional prediction, a total of 47 bacteria were *in situ* isolated and three of them with cellulose and lignin degradation ability were

10.3389/fmicb.2024.1472922

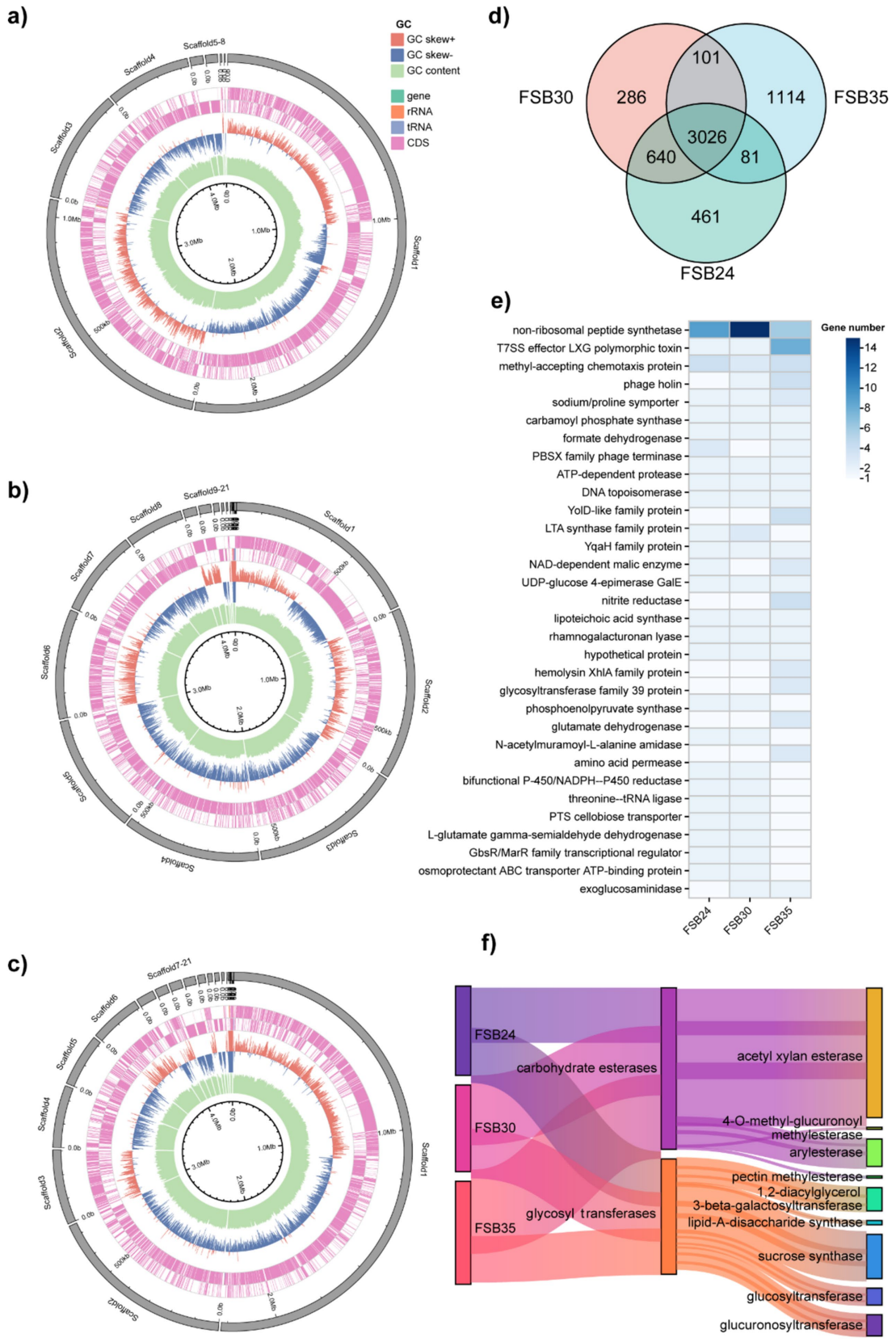

FIGURE 7
Comparative genomic analysis of the bacterial isolates FSB24, FSB30, and FSB35. **(a–c)** Circos display of the genomes of FSB24, FSB30, and FSB35, respectively. **(d)** Common and unique genes on the genome of FSB24, FSB30, and FSB35 as displayed through Venn diagram. **(e)** Homologous gene families with more than 5 homologous genes that obtained through comparing the genomes of FSB24, FSB30, and FSB35. **(f)** The abundance of two carbohydrate active enzyme classes, carbohydrate esterases and glycosyl transferases, on the genomes of FSB24, FSB30, and FSB35.

back inoculated to the manure, resulting in improved compost maturity and enhanced manure quality. Through comparative genomics analysis, it was demonstrated that, thermophilic feature is not a result of large-scale genomic alterations, but the changes in specific features and genes, such as the genome reduction, high GC content, and specific gene mutations.

The microbial dynamics in conventional manure waste composting has been well-studied (Chandrashekhar Parab and Prajapati, 2023; Wang et al., 2020), whereas the microbial community in the rapid thermophilic composting process that used in the present study is not very clear. Same as conventional aerobic composting, microbial community in rapid thermophilic composting has also undergone a succession from mesophiles-dominated to thermophiles-dominated, whereas the speed of community dynamic was faster and the community composition was more stable after TC step (Figures 1–3). For instance, though the HT stage in our fermentation system occurred within only 10 h, there have been significantly changes in α diversity (Figures 1a,b) and taxonomy abundance (Figures 1e,f) of the bacterial communities. High temperature is a kind of selection pressure, in which taxa with thermophilic or thermotolerant features become active as the process of composting continued, while those not well adapted to environmental changes either died out or entered a dormant state (Meng et al., 2019), resulting in a significantly simpler structure of the community with a lower total microbial diversity. Indeed, the α diversity of bacterial community was significantly decreased during the thermophilic step in the current study, which was in line with the findings of earlier researches (Xie et al., 2021; Cruz-Paredes et al., 2021). Additionally, we found the bacterial phylum of Firmicutes, which consist of the genus *Bacillus* with high tolerance to multiple stresses, was significantly increased in TC and CL steps (Figure 1e). These results suggested that the succession and formation of microbial communities can occur in a heterogeneous and targeted way due to niche differentiation and changes in the fundamental characteristics of composts, such as temperature and nutrient availability (Wei et al., 2018; Zhong et al., 2020).

In the current study, the microbe-aided thermophilic composting method required just 3 days to produce a mature and stable compost with the ideal addition of microbial inocula, which was much superior to the traditional composting, indicating that the inocula significantly shortened the time needed to produce a mature compost. There are two principal traits for sifting an effective composting microbial additive, thermotolerant and biomass degradation. Different composting piles were dominated by different microbial species, and each of which was adapted to a particular environmental state that varied during each composting stage (Zhao et al., 2018; Qiao et al., 2019; Wu et al., 2020). In a farm wastes and food wastes composting system, the prevalent bacteria were mainly from the genera of *Bacillus*, *Halobacillus* and *Staphylococcus* (Girish Chander et al., 2018), which was consistent with that of our rapid thermophilic composting. Species from the genus *Bacillus* have been reported to survive in various abiotic and biotic stresses through germination of spores, and possess the ability to secret kinds of enzymes. Therefore, they are often used in industry to produce highly active and high-purity amylase and protease (Gardener, 2004). Agro-industrial wastes generated from livestock manure consist of a large amount of animal proteins, as well as cellulose, hemicelluloses, and lignin originated from their feeds. Bacteria in the manure can promote refractory organic matter decomposition and nutrient transformation by increasing their own metabolic activity and extracellular enzyme production, and thus finally affect the compost maturity (Xie et al., 2021; Liu et al., 2023b). *Bacillus*, *Ureibacillus*, and *Geobacillus* are all in the family of Bacillaceae and reported to have various traits including N-fixation, P-solubilization, plant growth promotion, biological control and bio-fertilization (Singh et al., 2008; Richardson and Simpson, 2011; Sharma et al., 2013). Among the 47 bacteria isolated from TC and CL steps, 11 of them were in the genus of *Bacillus* in the current study (Figure 3a), and eight of them were able to degrade both cellulose and lignin (Supplementary Figures 4, 5).

Organisms that can live at temperature above 60°C are known as thermophiles. Research on the survival strategies of the thermophiles has gained a lot of attention because it sheds light on how life can thrive under extreme temperatures, and the potential applications in biotechnology. The majority of studies have concentrated on the characteristics of particular molecules, such as stability of protein structures (Bezsudnova et al., 2012) and/or the activity of thermophiles enzymes (Hakulinen et al., 2003). High temperature can no doubt induce genomic evolution, which in turn provides the bacteria with thermal-tolerant ability. Gene loss, gene mutations, or horizontal gene transfer (HGT) could all lead to such evolutionary alterations (Averhoff and Müller, 2010).

Comparative analysis on hundreds of genomes demonstrated that more than 20% of the bacterial genes and 40% of the archaeal genes are horizontally transferred (Gu and Hilser, 2009; Pang and Allemann, 2007). In the current study, we explored the common features among the three thermophile isolates that related to thermal adaptability. The random movement of transposon can create gene mutations that result in obtaining of new functions. In this study, the transposon helitron and long interspersed nuclear elements (LINE) were shared in all the three isolates, which was similar to geminiviruses, a virus that endemic to tropical and subtropical climates (Feschotte and Wessler, 2001). Besides, several homologous genes among the three isolates were reported to play a role in stress adaptation, such as the gene encoded NADP-malic enzyme. In plant, NADP-malic enzyme is essential to break down malate, which is necessary for maintaining the cytoplastic pH, regulating stomatal aperture, and boosting defenses against pathogens and excess aluminum (Chen et al., 2019).

The genome size of thermophiles are usually smaller than those of non-thermophiles (Wang et al., 2015). It was demonstrated that species that live at temperatures >60°C have genomes smaller than 4 Mb, whereas all species with genomes larger than 6 Mb live at temperatures lower than 45°C (van Noort et al., 2013). Likewise, in the current study, genome size of the three MI isolates were smaller than the mesophilic bacterium *B. cereus* and their reference genome *B. spizizenii* and *B. licheniformis*, but larger than the thermophile *B. thermotolerans* (Table 1). A possible explanation is that thermophiles used a cost-minimizing mechanism to adjust to external temperature changes by reducing the functional complexity of their genomes (Burra et al., 2010; Das et al., 2006). It is still up to dispute though, if thermophiles could delete genes that encode proteins with low thermo-stabilities during evolution (Sabath et al., 2013).

In addition to the changes in typical genomic features, the three MI isolates were genetically classified by their taxonomy, indicating that the acquisition of heat tolerance is not a global alteration on the genome, but a variation in specific heat-sensitive genes. Temperature is expected to dictate cell membrane lipid composition, such as fatty acid chain

length and types of lipid headgroups, which in turn regulates the uptake and dissipation of ion gradients across biological membranes (Sollich et al., 2017). The mutation of *fabA* gene in *Escherichia coli* increased the degree of saturation in membrane lipids, resulting in enhanced adaptation to elevated temperatures (Blaby et al., 2012). In this study, the gene encoded fatty acid desaturase (*DesE*) in FSB24 and FSB35, which catalyzes the desaturation reactions of saturated fatty acids, were classified with those in thermophiles *B. thermotolerans* and *B. licheniformis* rather than the mesophiles (Figure 4f), suggesting the fatty acid saturation in the membrane of thermopiles may altered.

In recent years, due to the increase in conventional bedding material costs, an increasing number of farmers choose to use harmless recycled manure as bedding. Manure bedding treatment of farms can solve the problem of not only manure pollution, but also resource utilization. Under the decomposition of microorganisms, organic matter in manure is largely transferred into bio-available nitrogen, phosphorus, and potassium that can be absorbed by plants. In the current study, the addition of microbial inoculum has significant technical and economic advantages in promoting rapid composting, and shortening the fermentation cycles (Figures 5, 6). We observed significant decreasing of organic matter content in compost with microbial inoculation relative to NI, indicating inocula played an important role in consuming the organic matter in manure (Figure 5c). In addition, the growth-promoting effect of compost inoculated with microbial inoculation were highly improved relative to the compost without inoculation (Figure 6). Intriguingly, in our study, FSB35 (*B. licheniformis*) did a better job in releasing bio-available phosphorus and potassium comparing to the other two isolates (*B. spizizenii*) (Supplementary Figures 6a,b). *B. licheniformis* has been regarded as an outstanding microbial cell factory for the production of biochemicals and enzymes (Zhan et al., 2020), including cellulose, hemicellulose and various thermo-tolerant proteinases, and it is also used as a plant growth promoter (Nunes et al., 2023), thus has widely application value.

Conclusion

Different from the conventional aerobic composting, the composting process in a bio-reactor is more rapid and efficient. Mimicking the conditions of tank composting, we found that the bacterial community has also undergone a succession from mesophiles-dominated to thermophiles-dominated, but the community changed at an accelerated pace, with a decline in diversity and a trend toward simplified structure. Majority of the bacteria isolated through high throughput cultivation method were identified as *Bacillus*, *Ureibacillus*, and *Geobacillus*, which are in the phylum of Firmicutes. Three *Bacillus* isolates with cellulose and lignin degradation ability were back inoculated to the manure, resulting in 3-day fast maturity and improved compost quality as fertilizers, especially in terms of promoting wheat growth. Comparing to the genomes of mesophilic and thermophilic *Bacillus*, the genomes of the three isolates manifested some features closer to the thermophiles, not only including the typical genomic features such as shrunken genome size, but also particular genes' mutation that related to heat tolerance, such as membrane saturation. The current study indicated that in the microbe-aided thermophilic composting system, the improvement of composting efficiency was due to the prevalence of thermophiles with specific functions. This study has crucial implications for the resource utilization of livestock manure.

Data availability statement

The datasets presented in this study can be found in online repositories. The names of the repository/repositories and accession number(s) can be found in the article/Supplementary material.

Author contributions

LW: Writing – original draft, Methodology, Funding acquisition, Formal analysis, Data curation. YL: Writing – review & editing, Methodology. XL: Supervision, Funding acquisition, Conceptualization, Writing – review & editing.

Funding

The author(s) declare that financial support was received for the research, authorship, and/or publication of this article. This work was funded by the National Natural Science Foundation of China (nos. U21A2024 and 32250015) and the Natural Science Foundation of Hebei Province (C2022503014).

Acknowledgments

We would like to thank Furong Li for her contribution in performing the wheat culturing trial and providing the wheat cultivation protocol. We would also like to thank all the persons who contributed to this project.

Conflict of interest

Zhongke Houtu Runze Environmental Science and Technology (Jiangsu), Inc. may join Center for Agricultural Resources Research, Institute of Genetics and Developmental Biology, Chinese Academy of Sciences and Yancheng Institute of Soil Ecology on the development of patents and the potential products based on the result of these research. The authors have developed an approved plan to manage any potential conflicts that may arise from the patents/products development.

Publisher's note

Supplementary material

The Supplementary material for this article can be found online at: https://www.frontiersin.org/articles/10.3389/fmicb.2024.1472922/full#supplementary-material

References

Averhoff, B., and Müller, V. (2010). Exploring research frontiers in microbiology: recent advances in halophilic and thermophilic extremophiles. *Res. Microbiol.* 161, 506–514. doi: 10.1016/j.resmic.2010.05.006

Benson, G. (1999). Tandem repeats finder: a program to analyze DNA sequences. *Nucleic Acids Res.* 27, 573–580. doi: 10.1093/nar/27.2.573

Bezsudnova, E. Y., Boyko, K. M., Polyakov, K. M., Dorovatovskiy, P. V., Stekhanova, T. N., Gumerov, V. M., et al. (2012). Structural insight into the molecular basis of polyextremophilicity of short-chain alcohol dehydrogenase from the hyperthermophilic archaeon. *Biochimie* 94, 2628–2638. doi: 10.1016/j.biochi.2012.07.024

Blaby, I. K., Lyons, B. J., Wroclawska-Hughes, E., Phillips, G. C. F., Pyle, T. P., Chamberlin, S. G., et al. (2012). Experimental evolution of a facultative thermophile from a mesophilic ancestor. *Appl. Environ. Microb.* 78, 144–155. doi: 10.1128/Aem.05773-11

Blin, K., Medema, M. H., Kazempour, D., Fischbach, M. A., Breitling, R., Takano, E., et al. (2013). Anti SMASH 2.0-a versatile platform for genome mining of secondary metabolite producers. *Nucleic Acids Res.* 41, W204–W212. doi: 10.1093/nar/gkt449

Buchfink, B., Reuter, K., and Drost, H. G. (2021). Sensitive protein alignments at tree-of-life scale using DIAMOND. *Nat. Methods* 18, 366–368. doi: 10.1038/s41592-021-01101-x

Burnley, S., Phillips, R., Coleman, T., and Rampling, T. (2011). Energy implications of the thermal recovery of biodegradable municipal waste materials in the United Kingdom. *Waste Manag.* 31, 1949–1959. doi: 10.1016/j.wasman.2011.04.015

Burra, P. V., Kalmar, L., and Tompa, P. (2010). Reduction in structural disorder and functional complexity in the thermal adaptation of prokaryotes. *PLoS One* 5:e12069. doi: 10.1371/journal.pone.0012069

Chan, P. P., and Lowe, T. M. (2019). tRNAscan-SE: searching for tRNA genes in genomic sequences. *Methods Mol. Biol.* 1962, 1–14. doi: 10.1007/978-1-4939-9173-0_1

Chandrashekhar Parab, K. D. Y., and Prajapati, V. (2023). Genomics and microbial dynamics in green waste composting: a mini review. *Ecol. Genet. Genom.* 29:100206. doi: 10.1016/j.egg.2023.100206

Chaurasia, A., Meena, B. R., Tripathi, A. N., Pandey, K. K., Rai, A. B., and Singh, B. (2018). Actinomycetes: an unexplored microorganisms for plant growth promotion and biocontrol in vegetable crops. *World J. Microb. Biot.* 34:132. doi: 10.1007/s11274-018-2517-5

Chen, Q. Q., Wang, B. P., Ding, H. Y., Zhang, J., and Li, S. C. (2019). Review: the role of NADP-malic enzyme in plants under stress. *Plant Sci.* 281, 206–212. doi: 10.1016/j.plantsci.2019.01.010

Chen, S. F., Zhou, Y. Q., Chen, Y. R., and Gu, J. (2018). Fastp: an ultra-fast all-in-one FASTQ preprocessor. *Bioinformatics* 34, i884–i890. doi: 10.1093/bioinformatics/bty560

Collins, M. D., Hutson, R. A., Falsen, E., and Sjödén, B. (1999). *Facklamia tabacinasalis* sp. nov., from powdered tobacco. *Int. J. Syst. Bacteriol.* 49, 1247–1250. doi: 10.1099/00207713-49-3-1247

Coorevits, A., Logan, N. A., Dinsdale, A. E., Halket, G., Scheldeman, P., Heyndrickx, M., et al. (2011). *Bacillus thermolactis* sp. nov., isolated from dairy farms, and emended description of *Bacillus thermoamylovorans*. *Int. J. Syst. Evol. Micr.* 61, 1954–1961. doi: 10.1099/ijs.0.024240-0

Cruz-Paredes, C., Tájmel, D., and Rousk, J. (2021). Can moisture affect temperature dependences of microbial growth and respiration? *Soil Biol. Biochem.* 156:108223. doi: 10.1016/j.soilbio.2021.108223

Darling, A. C. E., Mau, B., Blattner, F. R., and Perna, N. T. (2004). Mauve: multiple alignment of conserved genomic sequence with rearrangements. *Genome Res.* 14, 1394–1403. doi: 10.1101/gr.2289704

Das, S., Paul, S., Bag, S. K., and Dutta, C. (2006). Analysis of Nanoarchaeum equitans genome and proteome composition: indications for hyperthermophilic and parasitic adaptation. *BMC Genomics* 7:186. doi: 10.1186/1471-2164-7-186

De la Cruz, F. B., Cheng, Q. W., Call, D. F., and Barlaz, M. A. (2021). Evidence of thermophilic waste decomposition at a landfill exhibiting elevated temperature regions. *Waste Manag.* 124, 26–35. doi: 10.1016/j.wasman.2021.01.014

Delcher, A. L., Bratke, K. A., Powers, E. C., and Salzberg, S. L. (2007). Identifying bacterial genes and endosymbiont DNA with glimmer. *Bioinformatics* 23, 673–679. doi: 10.1093/bioinformatics/btm009

Deng, Y., Jiang, Y. H., Yang, Y. F., He, Z. L., Luo, F., and Zhou, J. Z. (2012). Molecular ecological network analyses. *BMC Bioinf.* 13. doi: 10.1186/1471-2105-13-113

Dong, W., Zhou, R., Li, X., Yan, H., Zheng, J., Peng, N., et al. (2023). Effect of simplified inoculum agent on performance and microbiome during cow manure-composting at industrial-scale. *Bioresour. Technol.* 393:130097. doi: 10.1016/j.biortech.2023.130097

Edgar, R. C. (2013). UPARSE: highly accurate OTU sequences from microbial amplicon reads. *Nat. Methods* 10, 996–998. doi: 10.1038/Nmeth.2604

Feschotte, C., and Wessler, S. R. (2001). Treasures in the attic: rolling circle transposons discovered in eukaryotic genomes. *P. Natl. Acad. Sci. U. S. A.* 98, 8923–8924. doi: 10.1073/pnas.171326198

Gardener, B. B. M. (2004). Ecology of Bacillus and *Paenibacillus* spp. in agricultural systems. *Phytopathology* 94, 1252–1258. doi: 10.1094/Phyto.2004.94.11.1252

Girish Chander, S. P. W., Gopalakrishnan, S., Mahapatra, A., Swati Chaudhury, C. S., Pawar, M. K., and Rao, A. V. R. K. (2018). Microbial consortium culture and vermi-composting technologies for recycling on-farm wastes and food production. *Int. J. Recycl. Org. Waste Agricult.* 7, 99–108. doi: 10.1007/s40093-018-0195-9

Gu, J., and Hilser, V. J. (2009). Sequence-based analysis of protein energy landscapes reveals nonuniform thermal adaptation within the proteome. *Mol. Biol. Evol.* 26, 2217–2227. doi: 10.1093/molbev/msp140

Gu, Z. Q., Yan, H. B., Zhang, Q., Wang, Y. P., Liu, C. X., Cui, X., et al. (2024). Elimination of copper obstacle factor in anaerobic digestion effluent for value-added utilization: performance and resistance mechanisms of indigenous bacterial consortium. *Water Res.* 252:121217. doi: 10.1016/j.watres.2024.121217

Hakulinen, N., Turunen, O., Jänis, J., Leisola, M., and Rouvinen, J. (2003). Three-dimensional structures of thermophilic β-1,4-xylanases from *Chaetomium thermophilum* and *Nonomuraea flexuosa*: comparison of twelve xylanases in relation to their thermal stability. *Eur. J. Biochem.* 270, 1399–1412. doi: 10.1046/j.1432-1033.2003.03496.x

Hyatt, D., Chen, G. L., LoCascio, P. F., Land, M. L., Larimer, F. W., and Hauser, L. J. (2010). Prodigal: prokaryotic gene recognition and translation initiation site identification. *BMC Bioinf.* 11:119. doi: 10.1186/1471-2105-11-119

Jia, X. B., Lin, X. J., Tian, Y. D., Chen, J. C., and You, M. S. (2017). High production, purification, biochemical characterization and gene analysis of a novel catalase from the thermophilic bacterium FZSF03. *Int. J. Biol. Macromol.* 103, 89–98. doi: 10.1016/j.ijbiomac.2017.05.034

Jurak, E., Punt, A. M., Arts, W., Kabel, M. A., and Gruppen, H. (2015). Fate of carbohydrates and lignin during composting and mycelium growth of *Agaricus bisporus* on wheat straw based compost. *PLoS One* 10:e0138909. doi: 10.1371/journal.pone.0138909

Khalil, A., Domeizel, M., and Prudent, P. (2008). Monitoring of green waste composting process based on redox potential. *Bioresour. Technol.* 99, 6037–6045. doi: 10.1016/j.biortech.2007.11.043

Kristich, C. J., Rice, L. B., and Arias, C. A. (2014). "Enterococcal infection-treatment and antibiotic resistance" in Enterococci: From commensals to leading causes of drug resistant infection. eds. M. S. Gilmore, D. B. Clewell, Y. Ike and N. Shankar (Boston, MA: Elsevier).

Kumar, S., Stecher, G., and Tamura, K. (2016). MEGA7: molecular evolutionary genetics analysis version 7.0 for bigger datasets. *Mol. Biol. Evol.* 33, 1870–1874. doi: 10.1093/molbev/msw054

Li, L., Stoeckert, C. J., and Roos, D. S. (2003). OrthoMCL: identification of ortholog groups for eukaryotic genomes. *Genome Res.* 13, 2178–2189. doi: 10.1101/gr.1224503

Li, D. Y., Yuan, J., Ding, J. T., Wang, H. H., Shen, Y. J., and Li, G. X. (2022). Effects of carbon/nitrogen ratio and aeration rate on the sheep manure composting process and associated gaseous emissions. *J. Environ. Manag.* 323:116093. doi: 10.1016/j.jenvman.2022.116093

Lin, X., Wang, N. Y., Li, F. H., Yan, B. H., Pan, J. T., Jiang, S. L., et al. (2022). Evaluation of the synergistic effects of biochar and biogas residue on CO_2 and CH_4 emission, functional genes, and enzyme activity during straw composting. *Bioresour. Technol.* 360:127608. doi: 10.1016/j.biortech.2022.127608

Liu, X., Rong, X., Yang, J., Li, H., Hu, W., Yang, Y., et al. (2023b). Community succession of microbial populations related to CNPS biological transformations regulates product maturity during cow-manure-driven composting. *Bioresour. Technol.* 369:128493. doi: 10.1016/j.biortech.2022.128493

Liu, G. L., Yang, Y., Ma, R. N., Jiang, J. H., Li, G. X., Wang, J. N., et al. (2023a). Thermophilic compost inoculating promoted the maturity and mature compost inoculating reduced the gaseous emissions during co-composting of kitchen waste and pig manure. *Environ. Technol. Inno.* 32:103427. doi: 10.1016/j.eti.2023.103427

Lomsadze, A., Gemayel, K., Tang, S. Y. Y., and Borodovsky, M. (2018). Modeling leaderless transcription and atypical genes results in more accurate gene prediction in prokaryotes. *Genome Res.* 28, 1079–1089. doi: 10.1101/gr.230615.117

Luo, R. B., Liu, B. H., Xie, Y. L., Li, Z. Y., Huang, W. H., Yuan, J. Y., et al. (2012). SOAPdenovo2: an empirically improved memory-efficient short-read assembler. *Gigascience* 1:18. doi: 10.1186/2047-217x-1-18

Ma, F., Zhu, T., Yao, S., Quan, H. Y., Zhang, K., Liang, B. R., et al. (2022). Coupling effect of high temperature and thermophilic bacteria indirectly accelerates the humification process of municipal sludge in hyperthermophilic composting. *Process Saf. Environ.* 166, 469–477. doi: 10.1016/j.psep.2022.08.052

Maddocks, S. E., and Oyston, P. C. F. (2008). Structure and function of the LysR-type transcriptional regulator (LTTR) family proteins. *Microbiol. SGM* 154, 3609–3623. doi: 10.1099/mic.0.2008/022772-0

Magoc, T., and Salzberg, S. L. (2011). FLASH: fast length adjustment of short reads to improve genome assemblies. *Bioinformatics* 27, 2957–2963. doi: 10.1093/bioinformatics/btr507

Meng, Q. X., Yang, W., Men, M. Q., Bello, A., Xu, X. H., Xu, B. S., et al. (2019). Microbial community succession and response to environmental variables during cow manure and corn straw composting. *Front. Microbiol.* 10:529. doi: 10.3389/fmicb.2019.00529

Niu, K. F., Chao, C., Zhang, X. X., An, Z. G., Zhou, J. Y., and Yang, L. G. (2022). Effects of different microbial agents on bedding treatment of ectopic fermentation of buffalo manure. *Front. Microbiol.* 13:1080650. doi: 10.3389/fmicb.2022.1080650

Nunes, P. S. D., de Medeiros, F. H., de Oliveira, T. S., Zago, J. R. D., and Bettiol, W. (2023). Bacillus subtilis and *Bacillus licheniformis* promote tomato growth. *Braz. J. Microbiol.* 54, 397–406. doi: 10.1007/s42770-022-00874-3

Pajura, R. (2023). Composting municipal solid waste and animal manure in response to the current fertilizer crisis - a recent review. *Sci. Total Environ.* 912:169221. doi: 10.1016/j.scitotenv.2023.169221

Pang, J. Y., and Allemann, R. K. (2007). Molecular dynamics simulation of thermal unfolding of *Thermatoga maritima* DHFR. *Phys. Chem. Chem. Phys.* 9, 711–718. doi: 10.1039/b611210b

Park, S. Y., Kwon, H., Kim, S. G., Park, S. C., Kim, J. H., and Seo, S. (2023). Characterization of two lytic bacteriophages, infecting complex (SBSEC) from Korean ruminant. *Sci. Rep.* 13:9110. doi: 10.1038/s41598-023-36306-x

Qiao, C. C., Penton, C. R., Liu, C., Shen, Z. Z., Ou, Y. N., Liu, Z. Y., et al. (2019). Key extracellular enzymes triggered high-efficiency composting associated with bacterial community succession. *Bioresour. Technol.* 288:121576. doi: 10.1016/j.biortech.2019.121576

Rasmussen, M. (2016). Aerococcus: an increasingly acknowledged human pathogen. *Clin. Microbiol. Infec.* 22, 22–27. doi: 10.1016/j.cmi.2015.09.026

Richardson, A. E., and Simpson, R. J. (2011). Soil microorganisms mediating phosphorus availability. *Plant Physiol.* 156, 989–996. doi: 10.1104/pp.111.175448

Sabath, N., Ferrada, E., Barve, A., and Wagner, A. (2013). Growth temperature and genome size in bacteria are negatively correlated, suggesting genomic dtreamlining during thermal adaptation. *Genome Biol. Evol.* 5, 966–977. doi: 10.1093/gbe/evt050

Sakai, M., Deguchi, D., Hosoda, A., Kawauchi, T., and Ikenaga, M. (2015). *Ammoniibacillus agariperforans* gen. Nov., sp. nov., a thermophilic, agar-degrading bacterium isolated from compost. *Int. J. Syst. Evol. Micr.* 65, 570–577. doi: 10.1099/ijs.0.067843-0

Sharma, A., Shankhdhar, D., and Shankhdhar, S. C. (2013). Enhancing grain iron content of rice by the application of plant growth promoting rhizobacteria. *Plant Soil Environ.* 59, 89–94. doi: 10.17221/683/2012-Pse

Singh, N., Pandey, P., Dubey, R. C., and Maheshwari, D. K. (2008). Biological control of root rot fungus *Macrophomina phaseolina* and growth enhancement of *Pinus roxburghii* (Sarg.) by rhizosphere competent *Bacillus subtilis* BN1. *World J. Microb. Biot.* 24, 1669–1679. doi: 10.1007/s11274-008-9680-z

Sollich, M., Yoshinaga, M. Y., Häusler, S., Price, R. E., Hinrichs, K. U., and Bühring, S. I. (2017). Heat stress dictates microbial lipid composition along a thermal gradient in marine sediments. *Front. Microbiol.* 8:1550. doi: 10.3389/fmicb.2017.01550

Song, C. H., Li, M. X., Wei, Z. M., Jia, X., Xi, B. D., Liu, D. M., et al. (2016). Effect of inoculation with multiple composite microorganisms on characteristics of humic fractions and bacterial community structure during biogas residue and livestock manure co-composting. *J. Chem. Technol. Biot.* 91, 155–164. doi: 10.1002/jctb.4554

Sun, B., Zhang, L. X., Yang, L. Z., Zhang, F. S., Norse, D., and Zhu, Z. L. (2012). Agricultural non-point source pollution in China: causes and mitigation measures. *Ambio* 41, 370–379. doi: 10.1007/s13280-012-0249-6

Teather, R. M., and Wood, P. J. (1982). Use of Congo red polysaccharide interactions in enumeration and characterization of cellulolytic bacteria from the bovine rumen. *Appl. Environ. Microb.* 43, 777–780. doi: 10.1128/Aem.43.4.777-780.1982

Thompson, J. D., Higgins, D. G., and Gibson, T. J. (1994). Clustal-W-improving the sensitivity of progressive multiple sequence alignment through sequence weighting, position-specific gap penalties and weight matrix choice. *Nucleic Acids Res.* 22, 4673–4680. doi: 10.1093/nar/22.22.4673

van Noort, V., Bradatsch, B., Arumugam, M., Amlacher, S., Bange, G., Creevey, C., et al. (2013). Consistent mutational paths predict eukaryotic thermostability. *BMC Evol. Biol.* 13:7. doi: 10.1186/1471-2148-13-7

Vlaskin, M. S., and Vladimirov, G. N. (2018). Hydrothermal carbonization of organic components from municipal solid waste. *Theor. Found. Chem. Eng.* 52, 996–1003. doi: 10.1134/S0040579518050421

Wainaina, S., Awasthi, M. K., Sarsaiya, S., Chen, H. Y., Singh, E., Kumar, A., et al. (2020). Resource recovery and circular economy from organic solid waste using aerobic and anaerobic digestion technologies. *Bioresour. Technol.* 301:122778. doi: 10.1016/j.biortech.2020.122778

Wang, Q. H., Cen, Z., and Zhao, J. J. (2015). The survival mechanisms of thermophiles at high temperatures: an angle of omics. *Physiology* 30, 97–106. doi: 10.1152/physiol.00066.2013

Wang, Q., Garrity, G. M., Tiedje, J. M., and Cole, J. R. (2007). Naive Bayesian classifier for rapid assignment of rRNA sequences into the new bacterial taxonomy. *Appl. Environ. Microb.* 73, 5261–5267. doi: 10.1128/Aem.00062-07

Wang, W. K., and Liang, C. M. (2021). Enhancing the compost maturation of swine manure and rice straw by applying bioaugmentation. *Sci. Rep.* 11:6103. doi: 10.1038/s41598-021-85615-6

Wang, T. T., Sun, Z. Y., Wang, S. P., Tang, Y. Q., and Kida, K. (2020). Succession of total and active microbial community during the composting of anaerobic digested residue. *Waste Biomass Valori* 11, 4677–4689. doi: 10.1007/s12649-019-00779-7

Wang, L. Q., Zhao, Y., Xie, L. A., Zhang, G. G., Wei, Z. M., Li, J., et al. (2023). The dominant role of cooperation in fungal community drives the humification process of chicken manure composting under addition of regulatory factors. *Environ. Res.* 232:116358. doi: 10.1016/j.envres.2023.116358

Wei, H. W., Wang, L. H., Hassan, M., and Xie, B. (2018). Succession of the functional microbial communities and the metabolic functions in maize straw composting process. *Bioresour. Technol.* 256, 333–341. doi: 10.1016/j.biortech.2018.02.050

Wu, N., Xie, S. Y., Zeng, M., Xu, X. Y., Li, Y., Liu, X. Y., et al. (2020). Impacts of pile temperature on antibiotic resistance, metal resistance and microbial community during swine manure composting. *Sci. Total Environ.* 744:140920. doi: 10.1016/j.scitotenv.2020.140920

Xie, G. X., Kong, X. L., Kang, J. L., Su, N., Luo, G. W., and Fei, J. C. (2021). Community-level dormancy potential regulates bacterial beta-diversity succession during the co-composting of manure and crop residues. *Sci. Total Environ.* 772:145506. doi: 10.1016/j.scitotenv.2021.145506

Xu, T., Tao, X. Y., He, H. X., Kempher, M. L., Zhang, S. P., Liu, X. C., et al. (2023). Functional and structural diversification of incomplete phosphotransferase system in cellulose-degrading clostridia. *ISME J.* 17, 823–835. doi: 10.1038/s41396-023-01392-2

Yan, H. B., Gu, Z. Q., Zhang, Q., Wang, Y. P., Cui, X., Liu, Y. H., et al. (2024). Detoxification of copper and zinc from anaerobic digestate effluent by indigenous bacteria: mechanisms, pathways and metagenomic analysis. *J. Hazard. Mater.* 469:133993. doi: 10.1016/j.jhazmat.2024.133993

Yang, G. Q., Chen, J. H., and Zhou, S. G. (2015). *Novibacillus thermophilus* gen. Nov., sp. nov., a gram-staining-negative and moderately thermophilic member of the family Thermoactinomycetaceae. *Int. J. Syst. Evol. Micr.* 65, 2591–2597. doi: 10.1099/ijs.0.000306

Yang, G. Q., and Zhou, S. G. (2014). *Sinibacillus soli* gen. Nov., sp. nov., a moderately thermotolerant member of the family Bacillaceae. *Int. J. Syst. Evol. Micr.* 64, 1647–1653. doi: 10.1099/ijs.0.055608-0

Zaman, B., Hardyanti, N., and Purwono, R. B. S. (2022). An innovative thermal composter to accelerate food waste decomposition at the household level. *Biores. Technol. Rep.* 19:101203. doi: 10.1016/j.biteb.2022.101203

Zhan, Y. Y., Xu, Y., Zheng, P. L., He, M., Sun, S. H., Wang, D., et al. (2020). Establishment and application of multiplexed CRISPR interference system in *Bacillus licheniformis*. *Appl. Microbiol. Biot.* 104, 391–403. doi: 10.1007/s00253-019-10230-5

Zhang, L., Sun, X. Y., Tian, Y., and Gong, X. Q. (2013). Effects of brown sugar and calcium superphosphate on the secondary fermentation of green waste. *Bioresour. Technol.* 131, 68–75. doi: 10.1016/j.biortech.2012.10.059

Zhao, Y., Liu, Z., Zhang, B., Cai, J., Yao, X., Zhang, M., et al. (2023). Inter-bacterial mutualism promoted by public goods in a system characterized by deterministic temperature variation. *Nat. Commun.* 14:5394. doi: 10.1038/s41467-023-41224-7

Zhao, X. Y., Wei, Y. Q., Fan, Y. Y., Zhang, F., Tan, W. B., He, X. S., et al. (2018). Roles of bacterial community in the transformation of dissolved organic matter for the stability and safety of material during sludge composting. *Bioresour. Technol.* 267, 378–385. doi: 10.1016/j.biortech.2018.07.060

Zhong, X. Z., Li, X. X., Zeng, Y., Wang, S. P., Sun, Z. Y., and Tang, Y. Q. (2020). Dynamic change of bacterial community during dairy manure composting process revealed by high-throughput sequencing and advanced bioinformatics tools. *Bioresour. Technol.* 306:123091. doi: 10.1016/j.biortech.2020.123091

Zucconi, F., Monaco, A., and Debertoldi, M. (1981). Biological evaluation of compost maturity. *Biocycle* 22, 27–29.

frontiers | Frontiers in Microbiology

TYPE Original Research
PUBLISHED 03 January 2025
DOI 10.3389/fmicb.2024.1498653

OPEN ACCESS

EDITED BY
Qi Zhang,
Nanchang University, China

REVIEWED BY
Obaid Ur Rehman,
Zhejiang University, China
Ting Zhou,
University of Technology Sydney, Australia

*CORRESPONDENCE
Yongqiang Tian
✉ tianyq@mail.lzjtu.cn

RECEIVED 19 September 2024
ACCEPTED 08 November 2024
PUBLISHED 03 January 2025

CITATION
Zheng Y, Liu T, Wang Z, Wang X, Wang H, Li Y, Zheng W, Wei S, Leng Y, Li J, Yang Y, Liu Y, Li Z, Wang Q and Tian Y (2025) Whole-genome sequencing and secondary metabolite exploration of the novel *Bacillus velezensis* BN with broad-spectrum antagonistic activity against fungal plant pathogens.
Front. Microbiol. 15:1498653.
doi: 10.3389/fmicb.2024.1498653

Whole-genome sequencing and secondary metabolite exploration of the novel *Bacillus velezensis* BN with broad-spectrum antagonistic activity against fungal plant pathogens

Yanli Zheng[1], Tongshu Liu[1], Ziyu Wang[1], Xu Wang[1], Haiyan Wang[1], Ying Li[1], Wangshan Zheng[1], Shiyu Wei[1], Yan Leng[1], Jiajia Li[1], Yan Yang[1], Yang Liu[1], Zhaoyu Li[1], Qiang Wang[2,3] and Yongqiang Tian[1]*

[1]School of Biological and Pharmaceutical Engineering, Lanzhou Jiaotong University, Lanzhou, Gansu, China, [2]State Key Laboratory of Crop Stress Adaptation and Improvement, School of Life Sciences, Henan University, Kaifeng, China, [3]Academy for Advanced Interdisciplinary Studies, Henan University, Kaifeng, China

The utilization of chemical pesticides recovers 30%–40% of food losses. However, their application has also triggered a series of problems, including food safety, environmental pollution, pesticide resistance, and incidents of poisoning. Consequently, green pesticides are increasingly seen as viable alternatives to their chemical counterparts. Among these, Plant Growth-Promoting Rhizobacteria (PGPR), which are found within plant rhizosphere, stand out for their capacity to stimulate plant growth. Recently, we isolated a strain, BN, with broad-spectrum antimicrobial activity from the rhizosphere of *Lilium brownii*. Identification revealed that this strain belongs to the species *Bacillus velezensis* and exhibits significant inhibitory effects against various fungal plant pathogens. The complete genome sequence of *B. velezensis* BN consists of a circular chromosome with a length of 3,929,791 bp, includes 3,747 protein-coding genes, 81 small RNAs, 27 rRNAs, and 86 tRNAs. Genomic analysis revealed that 29% of the genes are directly involved in plant growth, while 70% of the genes are indirectly involved. In addition, 12 putative biosynthetic gene clusters were identified, responsible for the synthesis of secondary metabolites, such as non-ribosomal peptides, lanthipeptides, polyketides, siderophores, and terpenes. These findings provide a scientific basis for the development of efficient antimicrobial agents and the construction of biopesticide production platforms in chassis cells.

KEYWORDS

green pesticides, food safety, Plant Growth-Promoting Rhizobacteria (PGPR), antimicrobial agents, non-ribosomal peptides

1 Introduction

The increasing frequency and severity of plant diseases present growing threats to global food security, biodiversity and agricultural production. These diseases reduced crop yields and caused ecological damage, with pathogens and pests alone accounting for up to 41% of global crop losses, costing the global economy over $220 billion annually (Savary et al., 2019; Singh B. K. et al., 2023). Crops are vulnerable to infections from a diverse array of pathogens, encompassing bacteria, fungi, oomycetes, viruses, and nematodes. Historically, pesticides have been the predominant method for managing plant diseases. Nevertheless, the rising resistance of these pathogens, coupled with the substantial environmental pollution caused by chemical usage, poses a grave risk to public health (Tang et al., 2021). In the rhizosphere of terrestrial plants, a diverse array of indigenous beneficial bacteria engage in close interactions with plant roots. These bacteria contribute to plant growth and bolster stress resistance through diverse mechanisms (Liu et al., 2020), presenting a promising alternative to traditional pesticides.

Indigenous bacteria consortia have a wide range of applications across multiple fields. Through isolation and optimization, they can eliminate heavy metals from wastewater, enhance soil ecological functions, and promote plant growth (Gu et al., 2024; La et al., 2024; Yan et al., 2024). However, the complex interactions among these microorganisms, along with strong environmental dependencies, make artificial regulation challenging. As a result, synthetic microbial communities (SynCom) have gained considerable attention in plant protection (Qiao et al., 2024; Wang et al., 2024).

SynCom are artificially created by combining two or more bacteria with distinct classifications, genetic traits, and functional characteristics. Research has shown that a SynCom, SSC8, composed of eight *Pseudomonas* can enhance the growth and disease resistance of watermelon (Qiao et al., 2024). A SynCom-mix7 was developed using seven *Pseudomonas*, significantly improving the resistance of *S. babylonica* to *P. versicolora* (Wang et al., 2024). These indicates that SynCom primarily consist of infraspecies, as interspecies combinations may lead to competition among microbes, making stable coexistence difficult.

To address this issue, researchers have proposed strategies and methods for artificial spatial isolation, successfully achieving interspecies microbial communities involving *E. coli*, *S. cerevisiae*, and *C. glutamicum* (Wang L. et al., 2022). Additionally, genome analysis of individual Plant Growth-Promoting Rhizobacteria (PGPR) can be employed to construct engineered strains with clear pathways that are artificially controllable, which can then be mixed with other strains. By designing the engineered strains, it becomes possible to create adjustable and stable dual- or multi-strain combinations (Fedorec et al., 2021).

Bacillus species, known as PGRP, are renowned for their abundant secretion of biologically active molecules, predominantly secondary metabolites with molecular weights under 2.5 KDa, which possess the ability to suppress the growth of plant pathogens (Jayakumar et al., 2011; Ruparelia et al., 2022). Although these molecules are not essential for bacterial growth or replication, they provide a substantial selective advantage upon the producing strain. This repertoire of bioactive molecules includes lipopeptides, antibiotics, enzymatic degraders, iron chelators, polyketides, non-ribosomal peptides, ribosomal peptides, volatile organic compounds (VOC), and specific plant hormones, all of which demonstrate antifungal, antibacterial, and antiviral properties, concurrently promoting plant growth (Grady et al., 2016; Ruparelia et al., 2022). Furthermore, the spore-forming ability of *Bacillus* species renders ideal candidate for developing highly efficacious biopesticide products (Ongena and Jacques, 2008; Zhao et al., 2023). To date, a number of *Bacillus* strains have been successfully commercialized as biocontrol agents, such as *Bacillus velezensis* FZB42 (ABiTEP, GmbH, Berlin, Germany), and *Bacillus pumilus* (QST2808; AgraQuest, Inc., Davis, California, USA) (Hèlène et al., 2011; Pérez-García et al., 2011).

Between 1999 and 2000, researchers successfully isolated two strains, CR-14b and CR-502^T, from soil samples collected at the mouth of the Vélez River at Torre del mar in the province of Málaga, southern Spain (Ruiz-García et al., 2005). Phenotypic and phylogenetic analyses suggested a close relationship of these strains to *Bacillus subtilis* and *Bacillus amyloliquefaciens*. However, digital DNA-DNA hybridization (dDDH) revealed <20% sequence similarity with any known species within the *Bacillus* genus, which warranted their classification as a novel species, *Bacillus velezensis* (*B. velezensis*) (Dunlap et al., 2016; Ruiz-García et al., 2005; Wang et al., 2008). *B. velezensis*, an aerobic, Gram-positive bacterium, is capable of forming endospores and producing a wide range of secondary metabolites with broad-spectrum antibacterial activity, as well as its capacity to promote plant growth (Rabbee et al., 2019). Consequently, *B. velezensis* has seen widespread application in the biological control of plant diseases. At present, various strains of *B. velezensis* are being employed in the management of plant diseases. For instance, *B. velezensis* JB0319 helps lettuce to overcome salt stress and promote growth by enriching nitrogen-fixing bacteria (Bai et al., 2023). Another strain, *B. velezensis* BAC03, enhances the growth of several crops, including beets, carrots and cucumbers (Meng et al., 2016).

Among plant-associated *Bacillus* species, *B. velezensis* stands out as a paradigmatic organism due to its significant role in promoting plant growth and suppressing plant pathogens. Its primary mechanisms include producing antimicrobial substances to antagonize pathogens, competing for ecological niches and nutrients, and activating induced systemic resistance (ISR) of plants, offering a multifaceted approach to enhance plant growth and yield (Ongena and Jacques, 2008). Notably, *B. velezensis* allocates over 10% genome content to the synthesis of specialized secondary metabolites. These secondary metabolites have a unique ability to detect signaling molecules released by soil competitors, such as the siderophore pyochelin produced by *Pseudomonas aeruginosa*, which allows it to modulate its metabolic activities and deploy a range of defensive strategies (Andrić et al., 2023). Furthermore, the metabolites can significantly enrich plant-beneficial indigenous bacteria, for instance, *Pseudomonas stutzeri* in the cucumber rhizosphere, promoting the formation of stable mixed biofilms in the crop rhizosphere and conferring beneficial effects to the crops (Sun et al., 2022).

In this study, we introduce the complete genome sequence of the *B. velezensis* BN for the first time and demonstrate its broad resistance to various fungal plant pathogens. Our

work not only elucidated the structural features of the *B. velezensis* BN genome but also delves into its functional genes, particularly those associated with promoting plant growth, utilizing rigorous whole-genome sequencing and analytical approaches. Furthermore, we have identified a suite of pivotal antimicrobial secondary metabolites. These findings have laid the foundation for the developing efficient microbial agents and constructing high-yield cell factories for value-added products.

2 Materials and methods

2.1 Isolation and culture of BN strain

The bulbs of *Lilium brownii* (lily) were collected from Lintao County, Gansu Province. First, the bulbs were rinsed with sterile water for 1 min, repeating the process two to three times, and allowed to air dry. Second, the bulbs underwent disinfection with 75% ethanol and 3% sodium hypochlorite, followed by three rinses with sterile water to eliminate any residual ethanol and sodium hypochlorite. Third, the disinfected bulbs were crushed into a fine powder using a sterilized mortar. One gram sample was mixed with 9 mL sterile water and vortexed to ensure homogeneity. Fourth, the mixture was serially diluted to achieve concentrations of 10^{-6}, 10^{-7}, 10^{-8}, and 10^{-9}, and 100 μL aliquots of each dilution was spread onto solid Luria-Bertani (LB) medium. Finally, these LB plates were incubated at 30°C for 48 h. Distinct single colonies were selected for further isolation and purification, culminating in the successful isolation of the *B. velezensis* BN.

The culture conditions for the *B. velezensis* BN were as follows: LB medium with the NaCl concentration adjusted to 0.17 M, the pH maintained at 7.0, and the temperature at 30°C. The cells were observed using a fluorescence microscope (Yongxing N-800F, China).

2.2 Antifungal activity of BN strains

To evaluate the antifungal activity of *B. velezensis* BN against diverse fungal pathogens, a dual-culture experiment was conducted, as previously described (Liu et al., 2024). The study encompassed six distinct fungal species: *Colletotrichum gloeosporioides* (*C. gloeosporioides*), *Fusarium oxysporum* (*F. oxysporum*), *Rhizoctonia solani* (*R. solani*), *Phytophthora infestans* (*P. infestans*), *Fusarium graminearum* (*F. graminearum*) and *Fusarium tricinctum* (*F. tricinctum*). Following a 7 days incubation, the pathogens were inoculated at the center of the Potato Dextrose Agar (PDA) plates. The PDA medium was prepared with 200 g L^{-1} potato, 20 g L^{-1} glucose, and 20 g L^{-1} agar, with the pH adjusted to 7.0. *B. velezensis* BN was inoculated ~1 cm from the edge of each plate, with control plates containing only the pathogens. Each experiment was replicated three times to ensure statistical robustness. All plates were incubated at 28°C until the fungal growth in the control plates extended to the edges.

2.3 DNA extraction and 16s rRNA analysis

The genomic DNA of *B. velezensis* BN was extracted using a bacterial DNA extraction kit (General, Shanghai, China). The 16S rRNA gene was amplified using primers 27F (5′-AGAGTTTGATCMTGGCTCAG-3′) and 1492R (5′-GGYTACCTTGTTACGACTT-3′). Sequencing of the PCR products was performed by Sangon Biotech Co., Ltd., (China). The phylogenetic analysis of the 16S rRNA was conducted using the Type (Strain) Genome Server (TYGS) (https://tygs.dsmz.de/) (Le Han et al., 2022; Meier-Kolthoff and Göker, 2019).

2.4 Whole genome sequencing and analysis

Whole-genome sequencing of *B. velezensis* BN was performed at Majorbio Laboratory (Shanghai, China) and involved both Scaffolding and completing genome assemblies. For scaffolding, an Illumina paired-end (PE) library with an average insert size of ~400 bp was constructed and sequenced using the Illumina HiSeq platform. This process included *de novo* genome assembly to obtain preliminary genomic sequences and functional annotation. To refine the genome assemblies, a PacBio RS II library with a read length of ~10 kb was generated and sequenced on the PacBio RS II platform, followed by comprehensive bioinformatics analysis. Scaffolding was performed using SOAPdenovo2 software for the assembly of multiple short reads, while completion of genome assemblies were achieved with Unicycler v0.4.8 and Pilon v1.22 for sequence polishing.

Phylogenetic analysis of the *gyrA* gene and whole-genome sequences were conducted using the TYGS server (Le Han et al., 2022; Meier-Kolthoff and Göker, 2019). Average nucleotide identity (ANI) analysis was performed using the JSpeciesWS53 web server (https://jspecies.ribohost.com/jspeciesws/) (Richter et al., 2016). dDDH analysis was conducted using the Genome-to-Genome Distance Calculator 3.0 (GGDC) web server (https://ggdc.dsmz.de/ggdc.php#) (Meier-Kolthoff et al., 2013). Collinearity analysis of the four strains was carried out with Mauve software. Core and pan-genome analyses were performed using BPGA v1.3 software.

2.5 Genome annotation and metabolite analysis

Functional annotation of the predicted coding genes was accomplished through a dual-pronged approach. Initially, we aligned the predicted genomic data with the genomes of the *B. velezensis* species, selected as reference genomes based on a phylogenetic analysis of 16S rRNA. This analysis facilitated the identification of homologous genes and their subsequent functional annotation. Subsequently, a database comparison method was employed, leveraging six major databases (NR, Swiss-Prot, Pfam, EggNOG, GO, and KEGG) to enhance the precision of functional descriptions for gene annotation.

Carbohydrate active enzymes were identified by the CAZy database (http://www.cazy.org/). Genes implicated

in plant growth-promoting traits were analyzed by PGPT-Pred (https://plabase.cs.uni-tuebingen.de/pb/form.php?var=PGPT-Pred) (Patz et al., 2021). Furthermore, AntiSMASH 7.0 (https://antismash.secondarymetabolites.org/) (Blin et al., 2023) was employed to identify and characterize the biosynthetic gene clusters of secondary metabolites with molecular weights <2.5 kDa.

3 Results

3.1 Isolation, characterization and preliminary dentification of strain BN

A bacterial strain isolated from the rhizosphere of *Lilium brownii* (lily) was designated as BN. Lily is widely recognized for its various health benefits, such as having calming properties, skin soothing effects, moisturizing dryness, and relieving cough. Additionally, research has shown that Lilium polysaccharides exhibit a variety of pharmacological activities, including antitumor, immunomodulatory, hypoglycemic, and radioprotective properties (Guo et al., 2024). The optimal culture conditions of BN were determined to be a temperature of 30°C, pH 7.0, and 0.17 M NaCl. BN is a Gram-positive bacterium, rod-shaped bacterium with length of 1–3 μm (Supplementary Figure S1A). It is characterized the formation of a substantial biofilm, which may potentially facilitate the colonization in the plant rhizosphere (Paula et al., 2020) (Supplementary Figure S1B).

Our study shown that BN exhibits a broad-spectrum antagonistic activity against several fungal plant pathogens, including *C. gloeosporioides*, *F. oxysporum*, *R.solani*, *P. infestans*, *F. graminearum* and *F. tricinctum* (Figure 1). *C. gloeosporioides* is a globally widespread plant pathogen that causes anthracnose in various plants, including wolfberry, legumes, and strawberries, leading to lesions on fruit and leaf surfaces (Dean et al., 2012). *F. oxysporum* is a destructive soil-borne pathogen that causes fusarium wilt and ceitocybe bescens in over 100 crops, including those in the Musaceae, Rosaceae, and Cucurbitaceae families (Berrocal-Lobo and Molina, 2008; Edel-Hermann and Lecomte, 2019). *R. solani* is a challenging pathogen to control which causes significant damage to a wide range of vegetables, fruits, and crops like potatoes, rice, corn, and cotton, leading to substantial yield and economic losses (Singh A. et al., 2023). *P. infestans* is responsible for causing the serious solanaceous plant disease known as late blight, particularly affecting potatoes, and was a major culprit in the 1840s European (Nowicki et al., 2012). *F. graminearum* is the primary causative agent of Fusarium head blight (FHB), one of the most destructive diseases affecting cereal crops worldwide (Dash et al., 2012; Lu et al., 2022). *F. tricinctum* is a ubiquitous and significant plant pathogen and mycotoxin producer that affects a variety of crops, notably causing Fusarium head blight (FHB) and ceitocybe bescens. In lilies, *F. tricinctum* can result in root rot, bulbs rot, and the yellowing and shedding of basal leaves (Li et al., 2013; Wang Y. et al., 2022). In summary, the BN strain shows promising potential as a highly effective broad-spectrum biocontrol agent.

We performed a phylogenetic analysis on the 16S rRNA gene sequence of the BN strain (Figure 2). The result revealed that BN exhibited the highest similarity with *B. velezensis* FZB 42, with a 16S rRNA sequence identity of 99.74%. *B. velezensis* FZB 42 serves as the model strain for promoting plant growth and biocontrol rhizosphere (Fan et al., 2018). Additionally, BN shared a sequence identity of 98.84% with *B. velezensis* B19. In summary, based on the sequence similarity of the 16S rRNA genes, coupled with the clustering patterns observed on the phylogenetic tree, BN was preliminarily identified as *B. velezensis*. The complete genome of BN was sequenced to further explore the antimicrobial capabilities and identify additional resistance genes, laying a foundation for developing engineered biocontrol strains.

3.2 Genome sequencing of BN and comparative genomics

The circular genome map of BN was constructed using the GC view program, as shown in Figure 3A (Grant and Stothard, 2008; Le Han et al., 2022). The whole genome sequence of BN consists of a circular chromosome spanning 3,929,791 bp, with a G+C content of 46.5%, and no plasmid sequences were detected. A total of 3,747 protein-coding genes (CDS) were predicted, accounting for 88.44% of the genome. These CDS genes have an average G+C content of 47.34% and an average length of 928 bp, inclusive of 281 pseudogenes. Additionally, the genome contains 81 small RNAs (sRNAs), 27 rRNAs (nine copies each of 5S, 16S, and 23S rRNAs), and 86 tRNAs.

The ANI and dDDH analyses are widely used to evaluate the similarity across bacterial strains based on whole-genome sequences. According to studies by Zhang et al. (2016), the compared strains exhibiting ANI values of ≥96% and DDH values of ≥70% are typically classified within the same species. In this study, the ANI values between BN and *B. velezensis* FZB 42, *B. velezensis* B19, and *B. velezensis* JS25R were 98.3%, 98.1%, and 98.2%, respectively (Figure 3B). Correspondingly, the DDH values were 85.4%, 83.4%, and 84.5% (Figure 3B).

The phylogeny based on the *gyrA* gene sequence from whole-genome sequences (Supplementary Figure S2), revealing that BN exhibited 98.76% and 98.33% sequence identity with the *gyrA* sequences of *B. velezensis* FZB 42 and *B. velezensis* B19, respectively. The *gyrA* gene, a highly conserved housekeeping gene in the *Bacillus* genus, exists as a single copy across all bacterial species, providing a higher resolution for *Bacillus* identification than the 16S rRNA gene, which may exhibit heterogeneity due to the multicopy (Liu et al., 2022). Furthermore, a phylogenomic tree was constructed based on the complete genome of BN and the published whole-genome sequences of other strains (Figure 3C). Collectively, these data fully confirmed the classification of the BN strain as a member of *B. velezensis* (Figures 2, 3, Supplementary Figure S2).

Comparative genomic analysis using whole genome sequencing with the Mauve program demonstrated that *B. velezensis* BN shares a high degree of homology with the majority of genes from *B. velezensis* FZB 42, *B. velezensis* B19, and *B. velezensis* JS25R. However, compared to *B. velezensis* FZB 42 and *B. velezensis* JS25R, certain genes were found to be absent in *B. velezensis* BN. Additionally, in comparison to *B. velezensis* B19,

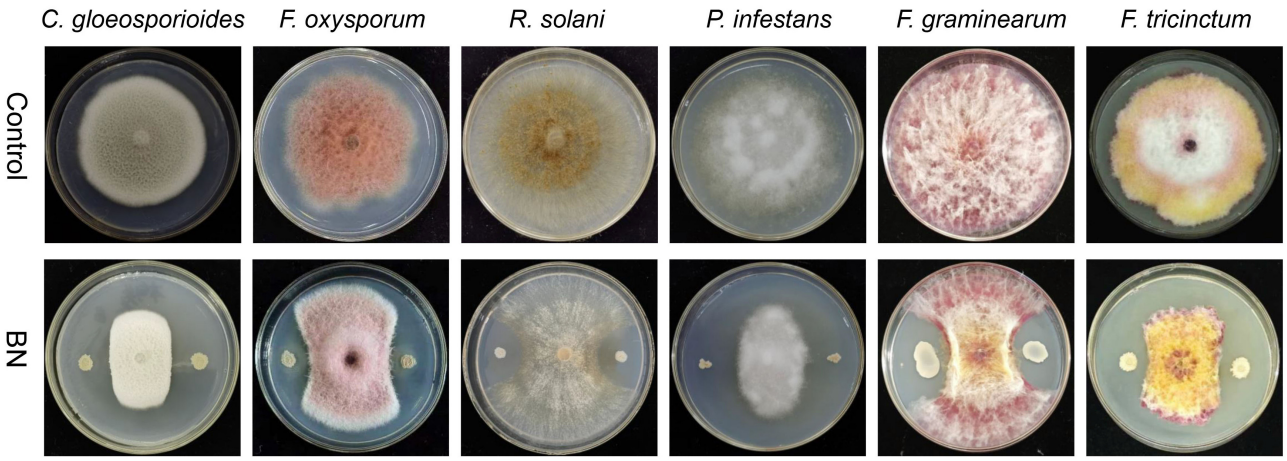

FIGURE 1
The dual confrontation between BN strain and five fungal pathogens. *C. gloeosporioides*, *Colletotrichum gloeosporioides*; *F. oxysporum*, *Fusarium oxysporum*; *R. solani*, *Rhizoctonia solani*; *P. infestans*, *Phytophthora infestans*; *F. graminearum*, *Fusarium graminearum*; *F. tricinctum*, *Fusarium tricinctum*.

both deletion and inversion of specific genes were observed in *B. velezensis* BN (Supplementary Figure S3A). Core pan-genomic analysis revealed that the four strains collectively possess 3,266 core genes, constituting 87.2% of the total gene count of *B. velezensis* BN, further substantiating the high similarity between *B. velezensis* BN and the other three strains. Additionally, *B. velezensis* BN contains 111 unique genes (Supplementary Figure S3B).

3.3 Metabolite analysis of *B. velezensis* BN

COG (Clusters of Orthologous Groups) gene annotation reveals that the largest proportion of genes fall into three categories: Amino acid transport and metabolism, Transcription, and Carbohydrate transport and metabolism (Supplementary Figure S4A). Notably, genes associated with secondary metabolite biosynthesis, transport, and catabolism constitute 2.1% of the total coding genes.

Carbohydrate active enzymes (CAZy) are a crucial class of enzymes, classified into glycoside hydrolases (GHs), glycosyl transferases (GTs), polysaccharide lyases (PLs), carbohydrate esterases (CEs), Carbohydrate-Binding Modules (CBMs) and Auxiliary Activities (AAs). These enzymes are responsible for degrading, modifying, and generating glycoside bonds. The ability of CAZy to degrade carbohydrates not only provides a competitive advantage against other bacteria but also activates the immunity of host cell (Bu et al., 2023; Wardman et al., 2022). For instance, endophyte-derived α-mannosidase can activate the host immunity by degrading the rice cell wall and releasing oligosaccharides as DAMPs (damage-associated molecular patterns), thereby enhancing the rice's disease resistance (Bu et al., 2023). The function of the *B. velezensis* BN gene was annotated based on the CAZy database (Supplementary Figure S4B). The analysis identified 128 of CAZy, including 41 GHs, 42 GTs, two CBMs, 31 CEs, three PLs, and nine AAs.

PGPT-Pred is an analytical tool designed to predict plant growth-promoting traits within single bacterial genomes (Patz et al., 2021). As of the analysis conducted in August 2024, PGPT-Pred indicates that the gene distribution within *B. velezensis* BN is as follows: 26% are associated with plant colonization systems, 22% with competitive exclusion, 22% with stress control mechanisms, 12% with bio-fertilization, 10% with phytohormones, 7% with bioremediation, and 2% with plant immune response stimulation (Figure 4A). Notably, genes involved in plant colonization, competitive exclusion, and stress control, as well as plant immune response stimulation, indirectly influence plant growth, while those associated with bio-fertilization, phytohormone, and bio-remediation have a direct effect on promoting plant growth (Figure 4B, Supplementary Figure S5).

3.4 Secondary metabolites analysis of *B. velezensis* BN

Biocontrol strains can produce a variety of secondary metabolites with diverse properties and structures, exhibiting a broad range of activities. These secondary metabolites include antibiotics, pigments, plant growth promoters, effectors of ecological competition, enzyme inhibitors, and pheromones (Chaabouni et al., 2012). Among them, compounds with a molecular weight below 2.5 kDa, produced during the stationary phase, represent the most important class of secondary metabolites for the control of plant diseases (Jayakumar et al., 2011; Ruparelia et al., 2022). They exhibit a wide range of antibacterial properties, triggering systemic acquired resistance, and promoting biofilm formation which facilitates the colonization for the producing strains. The antiSMASH platform is the leading resource for identifying and analyzing the biosynthetic gene clusters (BGCs) responsible for compounds with a molecular weight below 2.5 kDa in both archaea and bacteria (Blin et al., 2023).

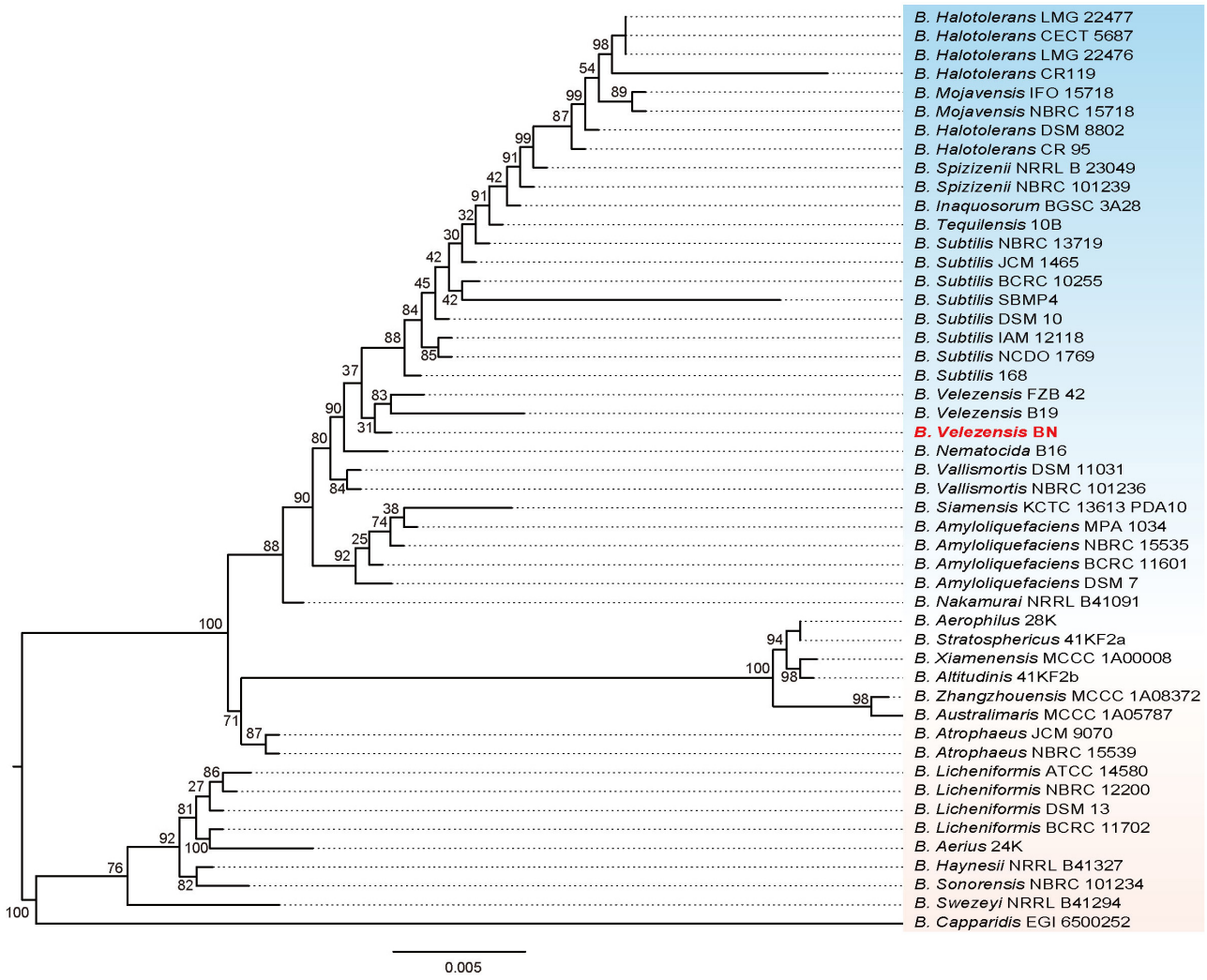

FIGURE 2
The phylogenetic tree based on 16S rRNA genes illustrates the relationship between the BN strain and other related strains. The scale bar represents 0.005 substitutions per nucleotide position. Additionally, the tree is midpoint-rooted.

The antiSMASH was employed to predict the BGCs in *B. velezensis* BN, aiming to assessing its capacity to suppress pathogenic activity. The analysis revealed a total of 12 BGCs dedicated to the production of compounds with a molecular weight below 2.5 kDa (Table 1), spanning a combined length of 754.8 kb, which constitutes a significant 19.2% of the genome's total length. Among the identified BGCs are two encoding nonribosomal peptide synthetases (NRPS), two trans-Acyl transferase polyketide synthases (transAT-PKS), one type III polyketide synthase (T3PKS), two transAT-PKS-NRPS hybrid systems, one lanthipeptides, one putative polyketide synthase (PKS), two terpene clusters, and one cluster of an undetermined type (Table 1).

Further analysis revealed that seven BGCs in *B. velezensis* BN exhibit a high degree of similarity to those found in the model strains *B. velezensis* FZB 42 and *B. subtilis* 168. The sequences of macrolactin H, bacillaene, fengycin, difficidin, bactillihactin, and bacilysin are 100% homologous with the reference strains, while surfactin show 82% similarity based on alignment with the public database (Table 1). Additionally, we compared the sequence differences of seven compounds among four strains: *B. velezensis* BN, *B. velezensis* FZB 42, *B. velezensis* JS25R, and *B. velezensis* B19. The results demonstrate that the four strains possess similar core biosynthetic genes, but *B. velezensis* B19 exhibits some differences compared to the other three (Figure 5), which aligns with the findings of the collinearity analysis (Supplementary Figure S3A). These differences may be attributed to the distinct environmental in which these strains evolved, leading to the development of unique metabolic pathways as adaptive mechanisms.

In this study, we conducted an antiSMASH analysis to provide a detailed summary of several key compound biosynthetic pathways (Figure 5). The biosynthetic gene cluster for surfactins is composed of four open reading frames (ORFs): *licA*, *licB*, *licC*, and *srfATE*, with a total length of 26.1 kb. In other species, the gene cluster ORFs related to surfactin biosynthesis are named *srfAA*, *srfAB*, *srfAC*, and *srfAD* (Ongena and Jacques, 2008). The synthesis of macrolactin H is catalyzed by a PKS encoded by seven genes, *pksE*, *mlnB*, *mlnC*, *mlnD*, *mlnE*, *mlnF*, and *mlnG*, totaling 48.2 kb. The biosynthesis

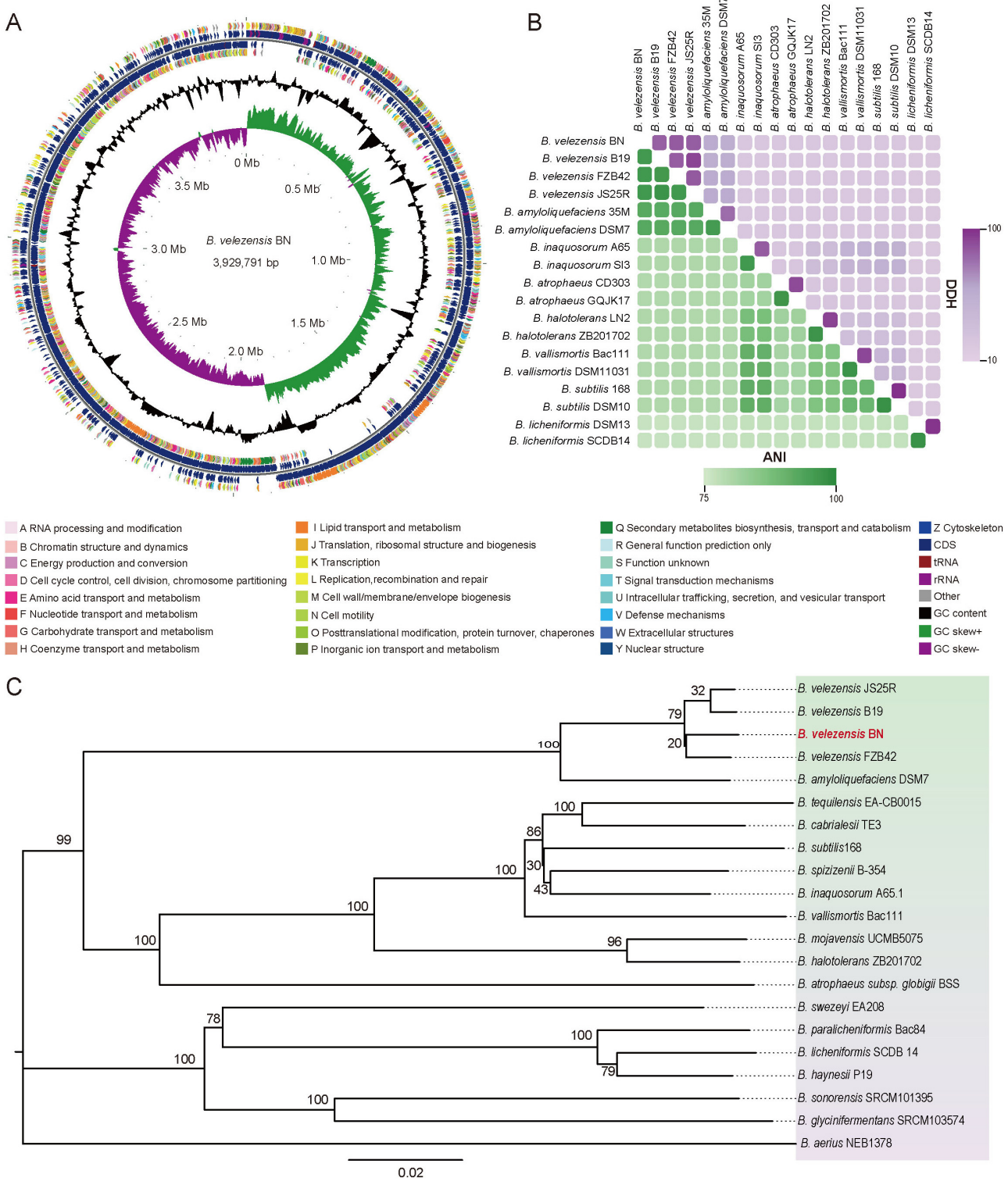

FIGURE 3
The whole-genome sequencing of BN strain and comparative analysis. **(A)** The circular representation of the BN strain genome. From outer to inner, the first and fourth circles represent the CDS on the positive and negative strands, respectively, with different colors denoting various COG functional. The second and third circles illustrate the CDS, tRNA, and rRNA on the positive and negative strands, respectively. The fifth circle displays the GC content, with outward-facing sections indicating regions where the GC content exceeds the average. The sixth circle illustrates the GC-Skew values. **(B)** The comparisons of ANI and dDDH values of BN strain and other related strains. Green, ANI. Purple, DDH. **(C)** The phylogenetic tree generated from whole-genome sequencing. The scale bar indicates 0.02 substitutions per nucleotide position, and the tree is midpoint-rooted for clarity.

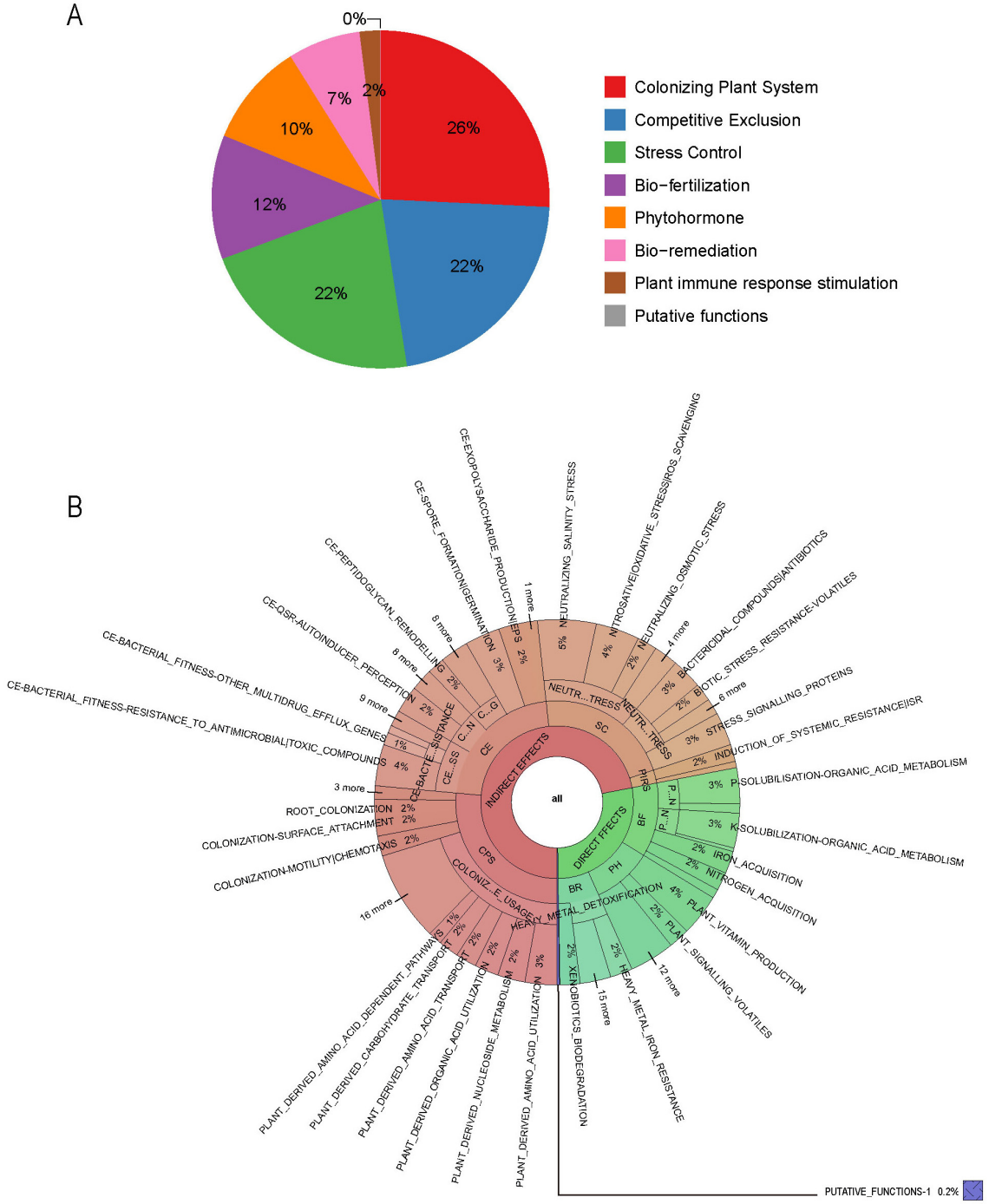

FIGURE 4
The functional genes of *B. velezensis* BN associated with plant growth-promoting traits. **(A)** The proportion of various functional genes in the genome. **(B)** Function genes that directly or indirectly affect plant growth. CPS, colonizing plant system; CE, competitive exclusion; SC, stress control; PIRS, plant immune response stimulation; BF, bio-fertilization; PH, phytohormone; BR, bio-remediation.

of bacillaene involves a PKS composed of *pksC*, *pksD*, *pksE*, *acpK*, *pksG*, *pksH*, *pksI*, and *pksL*, along with a NRPS composed of *pksJ*, *pksN*, and *pksR*, resulting in a total gene cluster length of 70.1 kb. Fengycin is catalyzed by a NRPS composed of *ppsA-E*, with a total gene cluster length of 37.7 kb. Difficidin is catalyzed by a PKS composed of *dfnD-J*, totaling 60 kb. Bactillihactin comprises five ORFs, *entA*, *entC*, *entE*, *entB*, and *dhbF*, with a total length of 11.7 kb. In addition, bacillibactin is a siderophore that can absorb iron elements at extremely low iron concentrations. Given that iron atoms in nature primarily exist as ferric iron, which has low bioavailability at physiological pH, the role of bacillibactin is particularly crucial (Jia et al., 2021; Ma et al., 2017). The bacilysin is primarily catalyzed by a series of enzymes encoded by *bacA-G*, each performing distinct functions. The biosynthetic pathways of these

10.3389/fmicb.2024.1498653

TABLE 1 Prediction of biosynthetic gene clusters of secondary metabolites in *B. velezensis* BN using antiSMASH 7.0.

Region	Type	Start	End	Most similar known cluster	Similarity	Formula	MIBiG accession	Gene cluster from organisms
Region 1	NRPS	322,199	387,606	Surfactin	82	$C_{52}H_{91}N_7O_{13}$	BGC0000433	*Bacillus velezensis* FZB42
Region 2	PKS-like	924,056	965,300	Butirosin A/ButirosinB	7	$C_{21}H_{41}N_{15}O_{12}$	BGC0000693	*Bacillus circulans*
Region 3	Terpene	1,047,344	1,068,084					
Region 4	Lanthipeptide-class-II	1,188,577	1,217,465					
Region 5	TransAT-PKS	1,384,028	1,472,261	Macrolactin H	100	$C_{24}H_{34}O_5$	BGC0000181	*Bacillus velezensis* FZB42
Region 6	TransAT-PKS, T3PKS, NRPS	1,690,940	1,801,045	Bacillaene	100	$C_{34}H_{50}N_2O_6$	BGC0001089	*Bacillus velezensis* FZB42
Region 7	NRPS, TransAT-PKS, betalactone	1,865,676	2,003,477	Fengycin	100	$C_{72}H_{110}N_{12}O_{20}$	BGC0001095	*Bacillus velezensis* FZB42
Region 8	Terpene	2,028,704	2,050,587					
Region 9	T3PKS	2,113,905	2,155,005					
Region 10	TransAT-PKS	2,269,991	2,376,173	Difficidin	100	$C_{31}H_{45}O_6P_1$	BGC0000176	*Bacillus velezensis* FZB42
Region 11	NRP-metallophore, NRPS, RiPP-like	3,000,877	3,052,668	Bactillihactin	100	$C_{39}H_{42}N_6O_{18}$	BGC0000309	*Bacillus subtilis* 168
Region 12	Other	3,588,978	3,630,396	Bacilysin	100	$C_{12}H_{18}N_2O_5$	BGC0001184	*Bacillus velezensis* FZB42

natural active substances not only reveal their roles in microbial metabolism but also provide a potential for constructing artificial biocontrol engineering strains.

4 Discussion

The PGPR confer benefits to plants by inhibiting pathogenic invasion and facilitating the acquisition of soil nutrients, thereby serving as an effective alternative to chemical agents in the prevention and control of diseases and pests (Ling et al., 2022). *Bacillus* species are characterized by their exuberant metabolism, production of diverse secondary metabolites, high fermentation density, and strong resistance and adaptability, which render an important group of beneficial biocontrol strains in nature environment (Fira et al., 2018). In recent years, there has been a notable increase in the discovery of *B. velezensis*. As of August 2024, the genomes from 928 strains of *B. velezensis*, either fully or partially, have been submitted to the National Center for Biotechnology Information (NCBI) database. This repository is pivotal for the exploration of antimicrobial compounds and the development of biocontrol engineering strains that can be artificially controlled.

In this study, we isolated a novel PGPR from the rhizosphere of lily, which thrives at growth temperature of 30°C, pH 7.0, and 0.17 M NaCl. Phylogenetic analysis based on 16S rRNA, *gyrA* gene and whole genome sequence revealed that this strain is a member of the *B. velezensis* species (Figures 2, 3C, Supplementary Figure S2). We found that it exhibits significant antimicrobial activity against various phytopathogenic fungi, including *C. gloeosporioides*, *F. oxysporum*, *R. solani*, *P. infestans*, *F. graminearum*, and *F. tricinctum* (Figure 1). Therefore, *B. velezensis* BN emerges as a promising candidate for biopesticide applications, offering a potential solution for the prevention and management of plant diseases caused by fungal pathogens.

In PGPR, secondary metabolites with molecular weights below 2.5 kDa are identified as the most critical antagonistic substance. Among these compounds, fengycins and surfactins, which are cyclic lipopeptides, distinguished by their unique composition of both amino acid and hydroxy fatty acid chains (Supplementary Figures S6A, B). Their exhibit significant heterogeneity, which can be attributed to the diversity in the type and sequence of amino acid residues, the unique feature of peptide fragment cyclization, and the unique characteristics of hydroxy fatty acid chains regarding their length, branching, and the specific synthetic pathways involved. The broad-spectrum antibacterial properties of fengycins and surfactins have positioned them as potent agents in the management of plant disease (Ongena and Jacques, 2008). In recent study, we found that elevating surfactins levels in *B. velezensis* BN not only thickens biofilm formation but also enhances its colonization capacity on plant roots (unpublished data).

10.3389/fmicb.2024.1498653

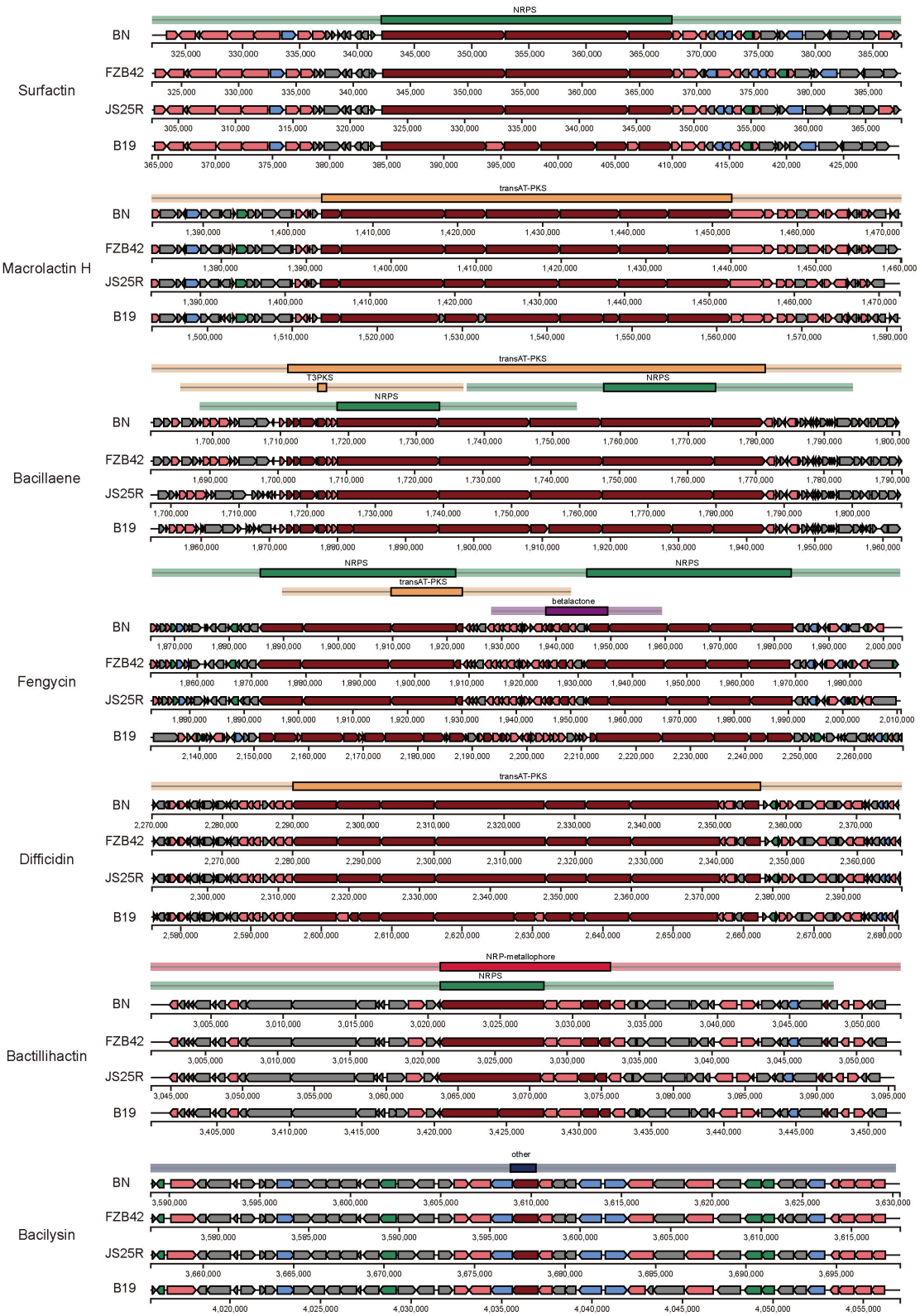

FIGURE 5
Comparison of the secondary metabolite biosynthetic gene clusters among *B. velezensis* BN and three other *B. velezensis* strains. BN, *B. velezensis* BN. FZB42, *B. velezensis* FZB42. JS25R, *B. velezensis* JS25R. B19, *B. velezensis* B19.

Macrolactin, a member of 24-membered macrolides (Supplementary Figure S6C), is renowned for the robust antibacterial potency. Studies have demonstrated its efficacy in neutralizing plant pathogens such as *Alternaria spp.* and *Pyricularia oryzae*, highlighting its significant potential in agricultural disease and pest management (Wu et al., 2021; Xue et al., 2008). Bacillibactin, a siderophore (Supplementary Figure S6D), plays a pivotal role in iron acquisition, especially under iron-deficient conditions. Notably, Chakraborty et al. (2022) has indicated bacillibactin as a promising antimicrobial agent. Difficidin, a highly unsaturated 22-membered macrolide phosphate, and bacilysin, a dipeptide antibiotic with an L-alanine residue at the N-terminal and the non-protein amino acid L-anticapsin at the C-terminal (Andrić et al., 2023; Özcengiz and Ögülür, 2015) (Supplementary Figures S6E, F), have been established in previous research to possess potent antibiotic properties, particularly against the human pathogen *Candida albicans* (Özcengiz and Ögülür, 2015). Recent studies have further revealed that they can modulate the expression of genes associated with virulence, cell division, and the synthesis of proteins and cell walls in *Xanthomonas*, pathogens responsible for rice white leaf blight and bacterial stripe disease (Chen et al., 2019). Bacillaenes, highly conjugated linear polyene with several cis-double bonds (Supplementary Figure S6G), exhibit broad antibacterial activity and are crucial for the strains survival, competition with other microorganisms, and biofilm formation (Miao et al., 2023). Bacillaene has been shown to assist *B. velezensis* FZB 42 in effectively inhibiting *E. amylovora*, the pathogen causing severe fire blight in apples and pears (Chen et al., 2009).

Although PGPR hold substantial potential as alternatives to chemical pesticides, their successful commercial applications face challenges due to species exclusion and the complexities of adapting to diverse ecological niches (Shade et al., 2012). Consequently, developing eco-friendly biopesticides requires both identifying novel, broad-spectrum antimicrobial strains and genetically modifying these strains to enhance their adaptability to fluctuating ecological conditions. Synthetic biology, a burgeoning field, employs engineering principles to redesign biological systems, thereby enabling the endowment functionalities in organisms through gene editing, gene synthesis, genetic circuits construction, and metabolic engineering (Khalil and Collins, 2010). The field is increasingly being harnessed in the development of novel biopesticides, as evidenced by the microbial synthesis of plant-derived compounds such as emodin and celangulin (Ke et al., 2021; Zhao et al., 2022). Ginkgo Bioworks has capitalized on synthetic biology to engineer efficient plant protectants by optimizing microbial production of potent insecticidal compounds for large-scale application.

Furthermore, the NRPS engineering has been a prominent area of research in recent years. By rearranging NRPS modules with various combinations, it is anticipated that new non-ribosomal peptides can be synthesized, thereby expanding the repertoire of bioactive molecules found in nature. A range of strategies for NRPS reconstruction has been developed, including the specific adjustments of adenylation domain (Stachelhaus et al., 1995), subdomain swaps, docking domain engineering (Mootz et al., 2002), and the insertion or deletion of modules/domains (Butz et al., 2008; Mootz et al., 2002). By deleting and replacing docking domains, mutating key amino acids, and using the same docking domain for multiple NRPS subdomain, the biosynthetic pathways for surfactin and fengycin have been successfully engineered, leading to the detection of products with altered chain lengths in the host cells (Liu et al., 2016; Mootz et al., 2002). The XUT method facilitates the efficient recombination of thioesterase domains from different species, enabling the targeted design and synthesis of peptides with specific bioactivities (Bozhüyük et al., 2024). Präve et al. (2024) successfully developed a novel syrbactin derivative that selectively inhibits the activity of the immunoproteasome by the XUT method.

In this study, we have successfully isolated and sequenced the *B. velezensis* BN strain, which provides potential for genetic manipulation to increase the yield of compounds antagonistic to plant pathogens. Additionally, we introduce the feasibility of utilizing synthetic biology techniques to construct and reengineer efficient antimicrobial agents within the chassis cells, such as non-ribosomal peptides. This study lays a foundation for the development of novel microbial pesticides, which are crucial for the sustainable enhancement of plant growth, nutrition, health, disease control, and overall productivity in fluctuating and challenging environmental contexts.

5 Conclusion

This study has achieved the isolation a PGPR strain from the lily rhizosphere, which was identified as *B. velezensis*. The complete genome of *B. velezensis* BN consists of a circular chromosome with a length of 3,929,791 bp and a G+C content of 46.5%. Our findings revealed that *B. velezensis* BN exhibits strong antagonism against a range of fungal plant pathogens, thereby positioning it as a PGPR with broad-spectrum antimicrobial activity. Genomic analysis showed that the genome of *B. velezensis* BN is abundant in CAZy genes, conferring a significant competitive advantage in diverse ecological niche. Moreover, genes directly involved in promoting plant growth accounted for 29% of the total gene count, providing a robust basis for plant growth enhancement. Additionally, the genome of *B. velezensis* BN encompasses genes encoding secondary metabolites with molecular weight <2.5 kDa, such as fengycin and surfactin, which account for 19.2% of the total genome and may play a pivotal role in the broad-spectrum antimicrobial activity. This study not only expands our understanding of the PGPR strain *B. velezensis* BN but also offers a scientific foundation and potential application for the development of efficient functional microbial agents and the engineering of artificially controllable biopesticide cell factories.

Data availability statement

The original contributions presented in the study are publicly available. This data can be found here: PRJNA1184975.

Author contributions

YZ: Data curation, Funding acquisition, Methodology, Writing – original draft, Writing – review & editing. TL:

Methodology, Writing – original draft. ZW: Methodology, Writing – original draft. XW: Methodology, Writing – original draft. HW: Methodology, Writing – original draft. YLi: Data curation, Funding acquisition, Writing – original draft. WZ: Data curation, Writing – original draft. SW: Data curation, Writing – original draft. YLe: Data curation, Writing – original draft. JL: Data curation, Funding acquisition, Writing – original draft. YY: Funding acquisition, Methodology, Writing – original draft. YLiu: Data curation, Writing – original draft. ZL: Data curation, Writing – original draft. QW: Writing – review & editing. YT: Data curation, Funding acquisition, Writing – review & editing.

Funding

The author(s) declare financial support was received for the research, authorship, and/or publication of this article. This work was supported jointly by the Gansu Provincial Education Department Young Ph.D. Support Program (2024QB-042), the Henan Province Science and Technology Tackling Project (232102311145), the National Natural Science Foundation of China (32460091 and 32460620), Qinghai Provincial Central Government Guide Local Science and Technology Development Project (2024ZY033), Gansu Provincial Education Department Innovation Fund Project (2024A-042), and Natural Science Foundation for Young Scholars of Gansu Province (23JRRA1702).

Conflict of interest

The authors declare that the research was conducted in the absence of any commercial or financial relationships that could be construed as a potential conflict of interest.

The author(s) declared that they were an editorial board member of Frontiers, at the time of submission. This had no impact on the peer review process and the final decision.

Publisher's note

Supplementary material

The Supplementary Material for this article can be found online at: https://www.frontiersin.org/articles/10.3389/fmicb.2024.1498653/full#supplementary-material

References

Andrić, S., Rigolet, A., Argüelles Arias, A., Steels, S., Hoff, G., Balleux, G., et al. (2023). Plant-associated *Bacillus* mobilizes its secondary metabolites upon perception of the siderophore pyochelin produced by a *Pseudomonas* competitor. *ISME J.* 17, 263–275. doi: 10.1038/s41396-022-01337-1

Bai, Y., Zhou, Y., Yue, T., Huang, Y., He, C., Jiang, W., et al. (2023). Plant growth-promoting rhizobacteria *Bacillus velezensis* JB0319 promotes lettuce growth under salt stress by modulating plant physiology and changing the rhizosphere bacterial community. *Environ. Exp. Bot.* 213:105451. doi: 10.1016/j.envexpbot.2023.105451

Berrocal-Lobo, M., and Molina, A. (2008). Arabidopsis defense response against *Fusarium oxysporum*. *Trends Plant Sci.* 13, 145–150. doi: 10.1016/j.tplants.2007.12.004

Blin, K., Shaw, S., Augustijn, H. E., Reitz, Z. L., Biermann, F., Alanjary, M., et al. (2023). antiSMASH 7.0: new and improved predictions for detection, regulation, chemical structures and visualisation. *Nucleic Acids Res.* 51, W46–W50. doi: 10.1093/nar/gkad344

Bozhüyük, K. A. J., Präve, L., Kegler, C., Schenk, L., Kaiser, S., Schelhas, C., et al. (2024). Evolution-inspired engineering of nonribosomal peptide synthetases. *Science* 383:eadg4320. doi: 10.1126/science.adg4320

Bu, Z., Li, W., Liu, X., Liu, Y., Gao, Y., Pei, G., et al. (2023). The rice endophyte-derived α-mannosidase ShAM1 degrades host cell walls to activate DAMP-triggered immunity against disease. *Microbiol. Spectrum* 11:e0482422. doi: 10.1128/spectrum.04824-22

Butz, D., Schmiederer, T., Hadatsch, B., Wohlleben, W., Weber, T., Süssmuth, R. D., et al. (2008). Module extension of a non-ribosomal peptide synthetase of the glycopeptide antibiotic balhimycin produced by *Amycolatopsis balhimycina*. *Chembiochem* 9, 1195–1200. doi: 10.1002/cbic.200800068

Chaabouni, I., Guesmi, A., and Cherif, A. (2012). "Secondary metabolites of bacillus: potentials in biotechnology," in *Bacillus thuringiensis Biotechnology*, ed. E. Sansinenea (Dordrecht: Springer Netherlands), 347–366. doi: 10.1007/978-94-007-3021-2_18

Chakraborty, K., Kizhakkekalam, V. K., Joy, M., and Chakraborty, R. D. (2022). Bacillibactin class of siderophore antibiotics from a marine symbiotic *Bacillus* as promising antibacterial agents. *Appl. Microbiol. Biotechnol.* 106, 329–340. doi: 10.1007/s00253-021-11632-0

Chen, J., Liu, T., Wei, M., Zhu, Z., Liu, W., Zhang, Z., et al. (2019). Macrolactin a is the key antibacterial substance of *Bacillus amyloliquefaciens* D2WM against the pathogen *Dickeya chrysanthemi*. *Eur. J. Plant Pathol.* 155, 393–404. doi: 10.1007/s10658-019-01774-3

Chen, X. H., Scholz, R., Borriss, M., Junge, H., Mögel, G., Kunz, S., et al. (2009). Difficidin and bacilysin produced by plant-associated *Bacillus amyloliquefaciens* are efficient in controlling fire blight disease. *J. Biotechnol.* 140, 38–44. doi: 10.1016/j.jbiotec.2008.10.015

Dash, S., Van Hemert, J., Hong, L., Wise, R. P., and Dickerson, J. A. (2012). PLEXdb: gene expression resources for plants and plant pathogens. *Nucleic Acids Res.* 40, D1194–D1201. doi: 10.1093/nar/gkr938

Dean, R., Van Kan, J. A., Pretorius, Z. A., Hammond-Kosack, K. E., Di Pietro, A., Spanu, J., et al. (2012). The Top 10 fungal pathogens in molecular plant pathology. *Mol. Plant Pathol.* 13, 414–430. doi: 10.1111/j.1364-3703.2011.00783.x

Dunlap, C. A., Kim, S. J., Kwon, S. W., and Rooney, A. P. (2016). *Bacillus velezensis* is not a later heterotypic synonym of *Bacillus amyloliquefaciens*; Bacillus methylotrophicus, *Bacillus amyloliquefaciens* subsp. plantarum and '*Bacillus oryzicola*' are later heterotypic synonyms of *Bacillus velezensis* based on phylogenomics. *Int. J. Syst. Evol. Microbiol.* 66, 1212–1217. doi: 10.1099/ijsem.0.000858

Edel-Hermann, V., and Lecomte, C. (2019). Current status of *Fusarium oxysporum* formae speciales and races. *Phytopathology* 109, 512–530. doi: 10.1094/PHYTO-08-18-0320-RVW

Fan, B., Wang, C., Song, X., Ding, X., Wu, L., Wu, H., et al. (2018). *Bacillus velezensis* FZB42 in 2018: the gram-positive model strain for plant growth promotion and biocontrol. *Front. Microbiol.* 9:2491. doi: 10.3389/fmicb.2018.02491

Fedorec, A. J. H., Karkaria, B. D., Sulu, M., and Barnes, C. P. (2021). Single strain control of microbial consortia. *Nat. Commun.* 12:1977. doi: 10.1038/s41467-021-22240-x

Fira, D., Dimkić, I., Berić, T., Lozo, J., and Stanković, S. (2018). Biological control of plant pathogens by *Bacillus* species. *J. Biotechnol.* 285, 44–55. doi: 10.1016/j.jbiotec.2018.07.044

Grady, E. N., MacDonald, J., Liu, L., Richman, A., and Yuan, Z. C. (2016). Current knowledge and perspectives of *Paenibacillus*: a review. *Microb. Cell Fact.* 15:203. doi: 10.1186/s12934-016-0603-7

Grant, J. R., and Stothard, P. (2008). The CGView server: a comparative genomics tool for circular genomes. *Nucleic Acids Res.* 36, W181–W184. doi: 10.1093/nar/gkn179

Gu, Z., Yan, H., Zhang, Q., Wang, Y., Liu, C., Cui, X., et al. (2024). Elimination of copper obstacle factor in anaerobic digestion effluent for value-added utilization: performance and resistance mechanisms of indigenous bacterial consortium. *Water Res.* 252:121217. doi: 10.1016/j.watres.2024.121217

Guo, J., Lu, L., Li, J., Kang, S., Li, G., Li, S., et al. (2024). Extraction, structure, pharmacological activity, and structural modification of Lilium polysaccharides. *Fitoterapia* 172:105760. doi: 10.1016/j.fitote.2023.105760

Hèlène, C., Wagner, B., Patrick, F., and Marc, O. (2011). "*Bacillus*-based biological control of plant diseases," in *Pesticides in the Modern World*, ed. S. Margarita (Rijeka: IntechOpen), 13.

Jayakumar, P., Rahul, G. R., Kennedy, R., Subashri, R., and Sakthivel, N. (2011). Secondary metabolite production by bacterial antagonists. *J. Biol. Control* 25, 165–181. doi: 10.18641/JBC/25/3/39985

Jia, A., Zheng, Y., Chen, H., and Wang, Q. (2021). Regulation and functional complexity of the chlorophyll-binding protein IsiA. *Front. Microbiol.* 12:774107. doi: 10.3389/fmicb.2021.774107

Ke, J., Wang, B., and Yoshikuni, Y. (2021). Microbiome engineering: synthetic biology of plant-associated microbiomes in sustainable agriculture. *Trends Biotechnol.* 39, 244–261. doi: 10.1016/j.tibtech.2020.07.008

Khalil, A. S., and Collins, J. J. (2010). Synthetic biology: applications come of age. *Nat. Rev. Genet.* 11, 367–379. doi: 10.1038/nrg2775

La, S., Li, J., Ma, S., Liu, X., Gao, L., Tian, Y., et al. (2024). Protective role of native root-associated bacterial consortium against root-knot nematode infection in susceptible plants. *Nat. Commun.* 15:6723. doi: 10.1038/s41467-024-51073-7

Le Han, H., Jiang, L., Thu Tran, T. N., Muhammad, N., Kim, S. G., Tran Pham, V. P., et al. (2022). Whole-genome analysis and secondary metabolites production of a new strain *Brevibacillus halotolerans* 7WMA2: a potential biocontrol agent against fungal pathogens. *Chemosphere* 307:136004. doi: 10.1016/j.chemosphere.2022.136004

Li, Y. Y., Wang, Y. J., Xie, Z. K., Wang, R. Y., Qiu, Y., Pan, H. Q., et al. (2013). First report of lily blight and wilt caused by *Fusarium tricinctum* in China. *Plant Dis.* 97:993. doi: 10.1094/PDIS-11-12-1010-PDN

Ling, N., Wang, T., and Kuzyakov, Y. (2022). Rhizosphere bacteriome structure and functions. *Nat. Commun.* 13:836. doi: 10.1038/s41467-022-28448-9

Liu, H., Brettell, L. E., Qiu, Z., and Singh, B. K. (2020). Microbiome-mediated stress resistance in plants. *Trends Plant Sci.* 25, 733–743. doi: 10.1016/j.tplants.2020.03.014

Liu, H., Gao, L., Han, J., Ma, Z., Lu, Z., Dai, C., et al. (2016). Biocombinatorial synthesis of novel lipopeptides by COM domain-mediated reprogramming of the plipastatin NRPS complex. *Front. Microbiol.* 7:1801. doi: 10.3389/fmicb.2016.01801

Liu, Y., Stefanic, P., Miao, Y., Xue, Y., Xun, W., Shen, Q., et al. (2022). Housekeeping gene gyrA, a potential molecular marker for *Bacillus* ecology study. *AMB Express* 12:133. doi: 10.1186/s13568-022-01477-9

Liu, Y., Zhang, W., Zhang, Z., Kou, Z., Wang, X., Wang, Y., et al. (2024). Biocontrol effects of three antagonistic bacteria strains against *Codonopsis pilosula* wilt disease caused by *Fusarium oxysporum*. *Biol. Control* 190:105446. doi: 10.1016/j.biocontrol.2024.105446

Lu, P., Chen, D., Qi, Z., Wang, H., Chen, Y., Wang, Q., et al. (2022). Landscape and regulation of alternative splicing and alternative polyadenylation in a plant pathogenic fungus. *New Phytol.* 235, 674–689. doi: 10.1111/nph.18164

Ma, F., Zhang, X., Zhu, X., Li, T., Zhan, J., Chen, H., et al. (2017). Dynamic changes of IsiA-containing complexes during long-term iron deficiency in *Synechocystis* sp. PCC 6803. *Mol. Plant* 10, 143–154. doi: 10.1016/j.molp.2016.10.009

Meier-Kolthoff, J. P., Auch, A. F., Klenk, H. P., and Göker, M. (2013). Genome sequence-based species delimitation with confidence intervals and improved distance functions. *BMC Bioinformatics* 14:60. doi: 10.1186/1471-2105-14-60

Meier-Kolthoff, J. P., and Göker, M. (2019). TYGS is an automated high-throughput platform for state-of-the-art genome-based taxonomy. *Nat. Commun.* 10:2182. doi: 10.1038/s41467-019-10210-3

Meng, Q., Jiang, H., and Hao, J. J. (2016). Effects of *Bacillus velezensis* strain BAC03 in promoting plant growth. *Biol. Control* 98, 18–26. doi: 10.1016/j.biocontrol.2016.03.010

Miao, S., Liang, J., Xu, Y., Yu, G., and Shao, M. (2023). Bacillaene, sharp objects consist in the arsenal of antibiotics produced by *Bacillus*. *J. Cell. Physiol.* 239:e30974. doi: 10.1002/jcp.30974

Mootz, H. D., Kessler, N., Linne, U., Eppelmann, K., Schwarzer, D., Marahiel, M. A., et al. (2002). Decreasing the ring size of a cyclic nonribosomal peptide antibiotic by in-frame module deletion in the biosynthetic genes. *J. Am. Chem. Soc.* 124, 10980–10981. doi: 10.1021/ja027276m

Nowicki, M., Foolad, M. R., Nowakowska, M., and Kozik, E. U. (2012). Potato and tomato late blight caused by phytophthora infestans: an overview of pathology and resistance breeding. *Plant Dis.* 96, 4–17. doi: 10.1094/PDIS-05-11-0458

Ongena, M., and Jacques, P. (2008). *Bacillus* lipopeptides: versatile weapons for plant disease biocontrol. *Trends Microbiol.* 16, 115–125. doi: 10.1016/j.tim.2007.12.009

Özcengiz, G., and Ögülür, I. (2015). Biochemistry, genetics and regulation of bacilysin biosynthesis and its significance more than an antibiotic. *N. Biotechnol.* 32, 612–619. doi: 10.1016/j.nbt.2015.01.006

Patz, S., Gautam, A., Becker, M., Ruppel, S., Rodríguez-Palenzuela, P., Huson, D., et al. (2021). PLaBAse: A comprehensive web resource for analyzing the plant growth-promoting potential of plant-associated bacteria. *bioRXiv* 2021. doi: 10.1101/2021.12.13.472471

Paula, A. J., Hwang, G., and Koo, H. (2020). Dynamics of bacterial population growth in biofilms resemble spatial and structural aspects of urbanization. *Nat. Commun.* 11:1354. doi: 10.1038/s41467-020-15165-4

Pérez-García, A., Romero, D., and de Vicente, A. (2011). Plant protection and growth stimulation by microorganisms: biotechnological applications of *Bacilli* in agriculture. *Curr. Opin. Biotechnol.* 22, 187–193. doi: 10.1016/j.copbio.2010.12.003

Präve, L., Kuttenlochner, W., Tabak, W. W. A., Langer, C., Kaiser, M., Groll, M., et al. (2024). Bioengineering of syrbactin megasynthetases for immunoproteasome inhibitor production. *Chem* 10, 3212–3223. doi: 10.1016/j.chempr.2024.07.013

Qiao, Y., Wang, Z., Sun, H., Guo, H., Song, Y., Zhang, H., et al. (2024). Synthetic community derived from grafted watermelon rhizosphere provides protection for ungrafted watermelon against *Fusarium oxysporum* via microbial synergistic effects. *Microbiome* 12:101. doi: 10.1186/s40168-024-01814-z

Rabbee, M. F., Ali, M. S., Choi, J., Hwang, B. S., Jeong, S. C., Baek, K. H., et al. (2019). *Bacillus velezensis*: a valuable member of bioactive molecules within plant microbiomes. *Molecules* 24:1046. doi: 10.3390/molecules24061046

Richter, M., Rosselló-Móra, R., Oliver Glöckner, F., and Peplies, J. (2016). JSpeciesWS: a web server for prokaryotic species circumscription based on pairwise genome comparison. *Bioinformatics* 32, 929–931. doi: 10.1093/bioinformatics/btv681

Ruiz-García, C., Béjar, V., Martínez-Checa, F., Llamas, I., and Quesada, E. (2005). *Bacillus velezensis* sp. nov., a surfactant-producing bacterium isolated from the river Vélez in Málaga, southern Spain. *Int. J. Syst. Evol. Microbiol.* 55, 191–195. doi: 10.1099/ijs.0.63310-0

Ruparelia, J., Rabari, A., Mitra, D., Panneerselvam, P., Das Mohapatra, P., Jha, D. C., et al. (2022). Efficient applications of bacterial secondary metabolites for management of biotic stress in plants. *Plant Stress* 6:100125. doi: 10.1016/j.stress.2022.100125

Savary, S., Willocquet, L., Pethybridge, S. J., Esker, P., McRoberts, N., Nelson, A., et al. (2019). The global burden of pathogens and pests on major food crops. *Nat. Ecol. Evol.* 3, 430–439. doi: 10.1038/s41559-018-0793-y

Shade, A., Peter, H., Allison, S. D., Baho, D. L., Berga, M., Bürgmann, H., et al. (2012). Fundamentals of microbial community resistance and resilience. *Front. Microbiol.* 3:417. doi: 10.3389/fmicb.2012.00417

Singh, A., Chandra, P., Bahadur, A., Debnath, P., Krishnan, S., Ellur, R., et al. B. (2023). Assessment of morpho-cultural, genetic and pathological diversity of *Rhizoctonia solani* isolates obtained from different host plants. *J. Plant Pathol.* 106, 67–82. doi: 10.1007/s42161-023-01515-w

Singh, B. K., Delgado-Baquerizo, M., Egidi, E., Guirado, E., Leach, J. E., Liu, H., et al. (2023). Climate change impacts on plant pathogens, food security and paths forward. *Nat. Rev. Microbiol.* 21, 640–656. doi: 10.1038/s41579-023-00900-7

Stachelhaus, T., Schneider, A., and Marahiel, M. A. (1995). Rational design of peptide antibiotics by targeted replacement of bacterial and fungal domains. *Science* 269, 69–72. doi: 10.1126/science.7604280

Sun, X., Xu, Z., Xie, J., Hesselberg-Thomsen, V., Tan, T., Zheng, D., et al. (2022). *Bacillus velezensis* stimulates resident rhizosphere *Pseudomonas stutzeri* for plant health through metabolic interactions. *ISME J.* 16, 774–787. doi: 10.1038/s41396-021-01125-3

Tang, F. H. M., Lenzen, M., McBratney, A., and Maggi, F. (2021). Risk of pesticide pollution at the global scale. *Nat. Geosci.* 14, 206–210. doi: 10.1038/s41561-021-00712-5

Wang, H., Zhang, F., Zhang, Y., Wang, M., Zhang, Y., Zhang, J., et al. (2024). Enrichment of novel entomopathogenic *Pseudomonas* species enhances willow resistance to leaf beetles. *Microbiome* 12:169. doi: 10.1186/s40168-024-01884-z

Wang, L., Zhang, X., Tang, C., Li, P., Zhu, R., Sun, J., et al. (2022). Engineering consortia by polymeric microbial swarmbots. *Nat. Commun.* 13:3879. doi: 10.1038/s41467-022-31467-1

Wang, L. T., Lee, F. L., Tai, C. J., and Kuo, H. P. (2008). *Bacillus velezensis* is a later heterotypic synonym of *Bacillus amyloliquefaciens*. *Int. J. Syst. Evol. Microbiol.* 58, 671–675. doi: 10.1099/ijs.0.65191-0

Wang, Y., Wang, R., and Sha, Y. (2022). Distribution, pathogenicity and disease control of *Fusarium tricinctum*. *Front. Microbiol.* 13:939927. doi: 10.3389/fmicb.2022.939927

Wardman, J. F., Bains, R. K., Rahfeld, P., and Withers, S. G. (2022). Carbohydrate-active enzymes (CAZymes) in the gut microbiome. *Nat. Rev. Microbiol.* 20, 542–556. doi: 10.1038/s41579-022-00712-1

Wu, T., Xiao, F., and Li, W. (2021). Macrolactins: biological activity and biosynthesis. *Mar. Life Sci. Technol.* 3, 62–68. doi: 10.1007/s42995-020-00068-6

Xue, C., Tian, L., Xu, M., Deng, Z., and Lin, W. (2008). A new 24-membered lactone and a new polyene delta-lactone from the marine bacterium *Bacillus marinus*. *J. Antibiot.* 61, 668–674. doi: 10.1038/ja.2008.94

Yan, H., Gu, Z., Zhang, Q., Wang, Y., Cui, X., Liu, Y., et al. (2024). Detoxification of copper and zinc from anaerobic digestate effluent by indigenous bacteria: Mechanisms, pathways and metagenomic analysis. *J. Hazard. Mater.* 469:133993. doi: 10.1016/j.jhazmat.2024.133993

Zhang, Y., Fan, Q., and Loria, R. (2016). A re-evaluation of the taxonomy of phytopathogenic genera Dickeya and Pectobacterium using whole-genome sequencing data. *Syst. Appl. Microbiol.* 39, 252–259. doi: 10.1016/j.syapm.2016.04.001

Zhao, J., Liang, D., Li, W., Yan, X., Qiao, J., Caiyin, Q., et al. (2022). Research progress on the synthetic biology of botanical biopesticides. *Bioengineering* 9:207. doi: 10.3390/bioengineering9050207

Zhao, X., Begyn, K., Delongie, Y., Rajkovic, A., and Uyttendaele, M. (2023). UV-C and wet heat resistance of *Bacillus thuringiensis* biopesticide endospores compared to foodborne *Bacillus cereus* endospores. *Food Microbiol.* 115:104325. doi: 10.1016/j.fm.2023.104325

frontiers | Frontiers in Microbiology

TYPE Original Research
PUBLISHED 19 March 2025
DOI 10.3389/fmicb.2025.1555989

OPEN ACCESS

EDITED BY
Pengfei Cheng,
Ningbo University, China

REVIEWED BY
Leonel Pereira,
University of Coimbra, Portugal
T. Mathimani,
National Institute of Technology, Tiruchirappalli, India

*CORRESPONDENCE
Yang Lu
✉ biglvyuang@jnu.edu.cn
Adili Alimujiang
✉ alimujiangadili0712@jnu.edu.cn

†These authors have contributed equally to this work

RECEIVED 06 January 2025
ACCEPTED 28 February 2025
PUBLISHED 19 March 2025

CITATION
Hao T-B, Lai P-Y, Shu Z, Liang R, Chen Z-Y, Huang R-L, Lu Y and Alimujiang A (2025) Physiological and metabolic fluctuations of the diatom *Phaeodactylum tricornutum* under water scarcity.
Front. Microbiol. 16:1555989.
doi: 10.3389/fmicb.2025.1555989

Physiological and metabolic fluctuations of the diatom *Phaeodactylum tricornutum* under water scarcity

Ting-Bin Hao[1,2†], Peng-Yu Lai[1†], Zhan Shu[1†], Ran Liang[1], Zhi-Yun Chen[3], Ren-Long Huang[1], Yang Lu[1*] and Adili Alimujiang[1*]

[1]School of Stomatology, College of Life Science and Technology, Jinan University, Guangzhou, China, [2]College of Synthetic Biology, Shanxi University, Taiyuan, China, [3]Guangzhou Zhixin High School, Ersha Campus, Guangzhou, China

Water scarcity is an escalating environmental concern. The model diatom, *Phaeodactylum tricornutum*, holds promise as a potential cell factory for the production of high-value natural compounds. However, its dependence on saline water cultivation restricts its use in areas facing water shortages. Although numerous studies have delved into the metabolic mechanisms of plants under water stress, there is a limited understanding when it comes to microalgae. In our study, we employed polyethylene glycol (PEG) to simulate water scarcity conditions, and assessed a range of parameters to elucidate the metabolic responses of *P. tricornutum*. Water stress induced the generation of reactive oxygen species (ROS), curtailed the photosynthetic growth rate, and amplified lipid content. Our insights shed light on the physiology of *P. tricornutum* when subjected to water stress, setting the stage for potential applications of microalgae biotechnology in regions grappling with water scarcity.

KEYWORDS

polyethylene glycol, water stress, lipid, *Phaeodactylum tricornutum*, diatom

Highlights

- Water scarcity stress inhibited the photosynthetic growth of microalgae.
- Water stress prompted microalgae to release excessive ROS.
- Under water stress, there was a significant accumulation of TAG.
- Fatty acids underwent *de novo* synthesis under water stress.

1 Introduction

Marine diatoms have garnered substantial attention due to their capability to produce a range of commercially valuable products such as polyunsaturated fatty acids, carotenoids, polysaccharides, and proteins. They are viewed as promising candidates for large-scale cultivation (Yang et al., 2020). However, to unlock this potential, it's imperative to make their mass cultivation economically sustainable by considerably reducing water costs (Gouveia et al., 2016). Water is pivotal for nutrient absorption, determining cell morphology, and facilitating the photosynthetic growth of microalgae (Curien et al., 2016; Yang et al., 2011). Consequently, inland regions distant from the ocean face challenges in large-scale diatom cultivation due to

limited water availability, which significantly curtails the commercial prospects of marine diatoms.

Water stress, stemming from water scarcity, increasingly constrains socio-economic development and endangers livelihoods worldwide. The rapidly growing population, economic expansion, and shifting consumption habits has led to severe worldwide water shortages and pollution (Wang et al., 2021). These issues pose significant threats to human health, the environment, and sustainable development (Chowdhary et al., 2020). Projections indicate that by 2050, more than half of the world's population will live in regions experiencing water stress (Lee et al., 2016). Addressing this scarcity poses a formidable challenge for future endeavors. Water stress acts as a prominent environmental stressor, inducing biochemical, molecular, and physiological alterations that detrimentally affect plant growth and development (Farooq et al., 2012; Rosa et al., 2020). In defense against water stress, plants exhibit a myriad of adaptive strategies, encompassing gene up- or down-regulation, transient spikes in abscisic acid, accumulation of compatible solutes and protective enzymes, enhanced antioxidant concentrations, and the modulation of energy-intensive pathways (Farooq et al., 2012; Basu et al., 2016). However, limited research has been directed toward understanding the physiology and metabolism of diatoms under water stress conditions.

As one of the most extensively studied diatoms, *Phaeodactylum tricornutum* exhibits superior characteristics in comparison to its counterparts. Its adaptability as a potential chassis is underscored by its ability to thrive across diverse culture media and its resilience to pronounced fluctuations in light intensity and pH levels (Butler et al., 2020). Furthermore, advancements in the genetic understanding of *P. tricornutum* have catalyzed its use as a chassis for identifying novel genes and producing high-value components (Daboussi et al., 2014; De Riso et al., 2009). Given its rich biochemical profile, environmental adaptability, meticulously characterized genome, and available engineering tools, *P. tricornutum* emerges as a prospective diatom cell factory for future applications. Beyond serving as a microalgal cell factory for high-value product synthesis, *P. tricornutum* has also been established as a model organism to investigate diatom physiology in various unique environments (Jallet et al., 2016; Levitan et al., 2015; Kuczynska et al., 2020). Therefore, understanding the mechanisms of *P. tricornutum*'s response to water stress is imperative for its potential deployment in water-scarce regions.

Polyethylene glycol (PEG) compounds are utilized to induce water stress in petri dishes (*in vitro*) for plants, ensuring a consistent water potential throughout the experimental period (Sharma et al., 2022; Mahpara et al., 2022). PEG has been widely employed as an abiotic stress inducer in numerous studies aimed at screening water-stress germplasm (Peršić et al., 2022; Reyes et al., 2023). As a polymer, PEG is regarded as a superior chemical for artificially inducing water stress compared to other alternatives. The application of PEG-induced water stress effectively reduces cellular water potential (Qi et al., 2023; Reza Yousefi et al., 2020). To address this challenge, our study employed PEG as a water stress inducer to investigate the response of marine diatoms to water stress. Additionally, we elucidated the potential mechanistic relationships between the stress response and metabolic reconfiguration. These insights pave the way for leveraging marine diatom biotechnology to enhance valuable product accumulation in regions with water scarcity.

2 Materials and methods

2.1 Strain and preculture conditions

The strain *P. tricornutum* Bohlin CCMP 2561 was acquired from the Provasoli-Guillard National Center for Marine Algae and Microbiota in the United States. Cells were grown in f/2 medium, which occupies 1/3 of a 250 mL conical flask. Cultivation was maintained at 20 ± 1°C with a 12/12 h circadian rhythm and 200 μmol/m^2/s light intensity. The cells were periodically cultured with an initial number of 10^4 cells/mL.

2.2 Water stress treatments

PEG 6000 was purchased from Aladdin (Aladdin, China) as the water stress inducer. In order to explore *P. tricornutum* under water stress, various concentrations of PEG 6000 (0, 1, 3, 5, 7%, *w*/*v*) were added to the f/2 medium refer to the process in plants. Cells were harvested at specific time points for further analysis.

2.3 Photosynthetic parameter determination

In order to detect the activation of the photosystem, parameters such as the maximum quantum efficiency of photosystem II (Fv/Fm), non-photochemical quenching (NPQ) and chlorophyll *a* (Chl *a*), during treatments supplemented with or without PEG 6000 were determined by a commercial phytoplankton photosynthesis analyzer PhytoPAM (Walz, Germany) following the protocols retrieved from the manufacturers.

2.4 Primary metabolites analysis

The primary metabolites of *P. tricornutum* under water stress were determined after 3 days of exposure to PEG6000 according to a previous study (Hao et al., 2022). In brief, the total lipid content was extracted by the methanol-chloroform protocol and determined gravimetrically. The total carbohydrate was isolated by the classical phenol-sulfuric acid method and then determined by spectrophotometry at OD_{562nm}. The total protein was isolated by RIPA lysis buffer (Beyotime, China) and quantified by the BCA protein assay kit (Beyotime, China).

2.5 Oxidant stress analysis

The ROS level of *P. tricornutum* under water stress was determined by the fluorescence probe DCFH-DA (Solarbio,

China). Cells were stained with 10 μM DCFH-DA and darkly incubated at 37°C for 30 min. Then, cells were washed three times with fresh f/2 medium and the fluorescence was measured by a microplate reader (Bio-Tec, Vermont, American) with an excitation wavelength of 488 nm and an emission wavelength of 528 nm.

2.6 Fluorometric and fatty acid component analysis of total lipid

The content of the major lipid, neutral lipid, in *P. tricornutum* was determined every day by using Nile Red (Aladdin, China) according to a previous study (Hao et al., 2024). Fatty acid composition of total lipid was analyzed as fatty acid methyl esters (FAMEs) by using gas chromatography–mass spectrometry (GC–MS, Agilent7890B-7000C). In summary, 500 μL of toluene was introduced to 5 mg wet algae pellet and transferred into a new tube. Subsequently, 1 mL of freshly prepared 0.5 N NaOH/MeOH was added. The mixture was thoroughly vortexed and then incubated at 80°C for 20 min. Following a 5-min cooling period at room temperature, 1 mL of freshly prepared AcCl/MeOH (1:10, v/v) was gradually added, and the mixture was incubated for an additional 20 min. Next, 1 mL of 6% K_2CO_3, 500 μL of hexane, and 10 μL of methyl nonadecylate (Aladdin, China) were incorporated, and the mixture was vortexed for 1 min. The upper phase was subsequently collected for GC–MS analysis. A DB-5 quartz capillary column measuring 30 m × 0.25 mm × 0.25 μm was employed for chromatographic separation. The column temperature program began with an initial hold at 60°C for 1 min, followed by a ramp at 10°C per minute to 160°C, and then a gradual increase at 2.5°C per minute to a final temperature of 250°C. The injector was maintained at 280°C, and 1 μL of sample was injected in splitless mode. The mass spectrometer's transfer line was set to 200°C. Fatty acids were identified using the NBS spectral library integrated into the system, and quantification was performed by analyzing the integrated peak areas.

2.7 Statistical analysis

All experiments were performed in at least biological triplicates to ensure reproducibility. GraphPad Prism 8.0 software was employed to analyze the data, which were expressed as mean ± standard deviation (SD) ($n = 3$).

3 Results

3.1 Effects of water stress on growth of *Phaeodactylum tricornutum*

As shown in Figure 1A, the lower concentration of PEG of 1% had no significant effect on growth rate of *P. tricornutum* during the cultivation period. At a PEG concentration of 3%, the growth rate of cells was significantly repressed compared to that in the control group. The cell density declined after 1 day with the addition of 3% PEG. While the concentration of PEG was increased to 5%, the growth rate decreased more than 3%, even more than the initial cell density. The inhibitory effect of 7% PEG was similar to that of 5% and the growth rate had no further decrease. Corresponding to the growth rate, the Fv/Fm values were lower for *P. tricornutum* above 3% PEG compared to the control. As shown in Figure 1B, there was a trend toward lower Fv/Fm of 5 and 7% PEG at day 1, and this trend was continued during the cultivation period. Furthermore, the NPQ value, which indicated the dissipation capacity of excessive light energy, was also repressed above 3% PEG (Figure 1C). The content of chlorophyll a directly represents the light-harvested photosynthesis of diatoms. The biosynthesis of chlorophyll a was significantly blocked under all treatments of PEG (Figure 1D). These analyses showed that water stress induced by PEG impairs the growth and photosynthetic activity of *P. tricornutum*.

3.2 Antioxidant analysis of *Phaeodactylum tricornutum*

We tracked and monitored the ROS level of *P. tricornutum* treated with PEG to evaluate the tolerance under water stress. As shown in Figure 2A, the water stress treatment with highly concentrated PEG significantly induced the release of ROS in *P. tricornutum*. With the monitoring of DCFH-DA, the fluctuating of ROS fluorescence had not been observed under the action of 1 and 3% PEG, however, the ROS levels per cell under 5 and 7% PEG were similar and significantly higher than those in the control group from the 1st to the 5th day. Along with the prolongation of the culture time, the ROS fluorescence strength of all processing groups had been consistent after 5th day. Our results showed that 5 and 7% PEG triggered a significant accumulation of ROS in *P. tricornutum*. Superoxide dismutase (SOD) is directly involved in the formation of ROS, whose activity is considered a critical indicator of oxidative stress. In order to further investigate the reasons for the significant increase in ROS content on days 1 and 3, we measured the SOD enzyme activity of *P. tricornutum*. As shown in Figure 2B, the SOD activity had no significant effect at the earlier stage of PEG cultivation, but followed a remarkable increase at day 3, showing a hysteretic reaction after the release of ROS. Our results presented the water stress, induced oxidative stress of *P. tricornutum*.

3.3 Determination of TAG content

As the iconic lipid in *P. tricornutum*, triacylglycerol (TAG) could be accumulated when cells were immersed in abiotic stresses. We employed the fluorescence intensity of Nile Red to monitor the accumulation of TAG. The quantitative fluorescence of Nile Red combined with TAG is shown in Figure 3A. Compared with the control group, 1% PEG had no significant effect on the TAG content of *P. tricornutum*. Significant accumulation of TAG was presented when the PEG concentration reached 3% and was further induced under 5 and 7% PEG. The total content of TAG in the equal volume of medium was richest under 7% PEG concentration on the 9th day. Considering the opposite effects of increased total fluorescence and declining cell numbers, the content of TAG per cell was further

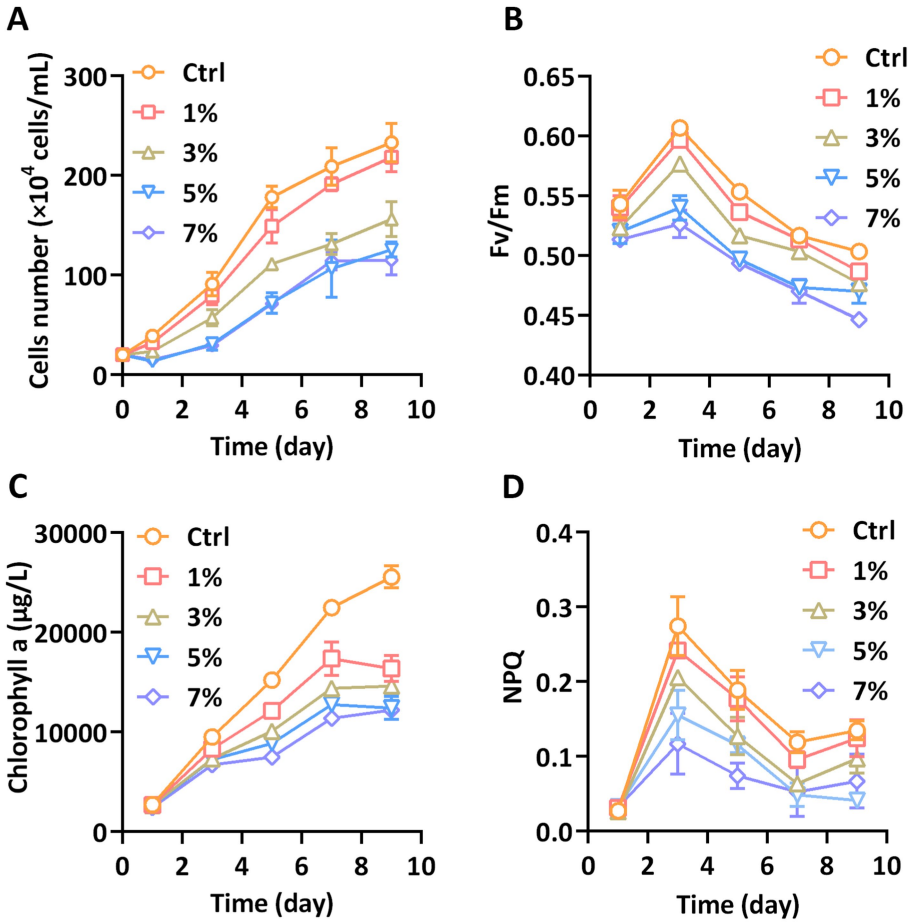

FIGURE 1
Growth and photosynthesis parameters **(A)** Cells number, **(B)** Fv/Fm, **(C)** Chlorophyll a, and **(D)** NPQ.

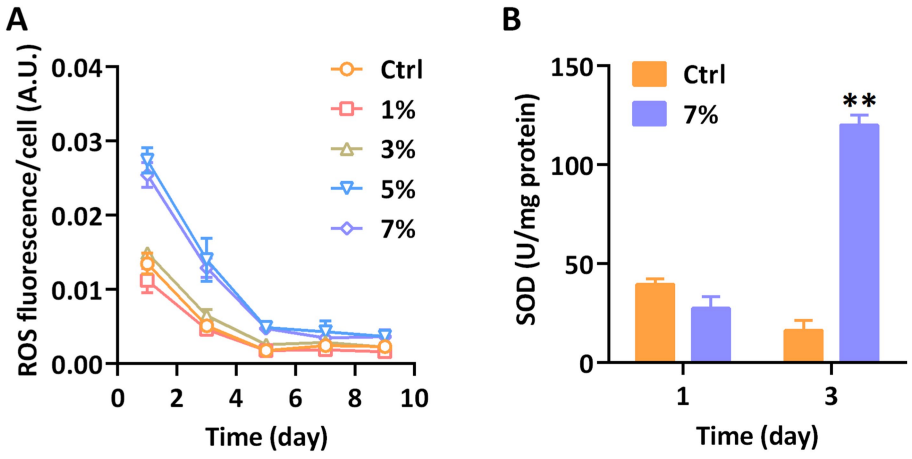

FIGURE 2
The antioxidant capacity of *P. tricornutum* exposed to water stress. **(A)** ROS fluorescence and **(B)** SOD activity. Significant difference is indicated at $p < 0.05$ (*) or $p < 0.01$ (**) level. Each value represents mean ± SD ($n = 3$).

detected. As shown in Figure 3B, the content of TAG was still significantly increased under 7% PEG; however, it declined after day 3 due to the prolonged cultivation. Our results implied that water stress could induce a significant accumulation of TAG in *P. tricornutum*.

3.4 Determination of primary metabolites and fatty acids

Water stresses are known to influence the redistribution of primary metabolites in various systems. As the major primary component in

P. tricornutum, the variation in total lipid content indicated the redistribution of primary metabolites. Hence, we determined the primary metabolites of *P. tricornutum* under 7% PEG treatment by biochemistry and gravimetric analysis. As shown in Figure 4A, the gravimetric analysis revealed that the total biomass of microalgae was significantly decreased under water stress, which was coincided with the decrease in cell number.

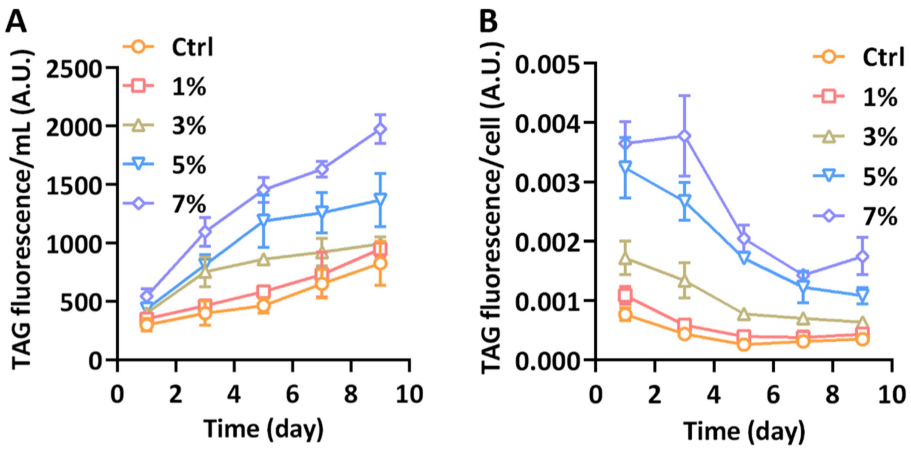

FIGURE 3
TAG content measured with Nile Red fluorometric analysis. **(A)** The total TAG fluorescence per milliliter; **(B)** The TAG fluorescence per cell.

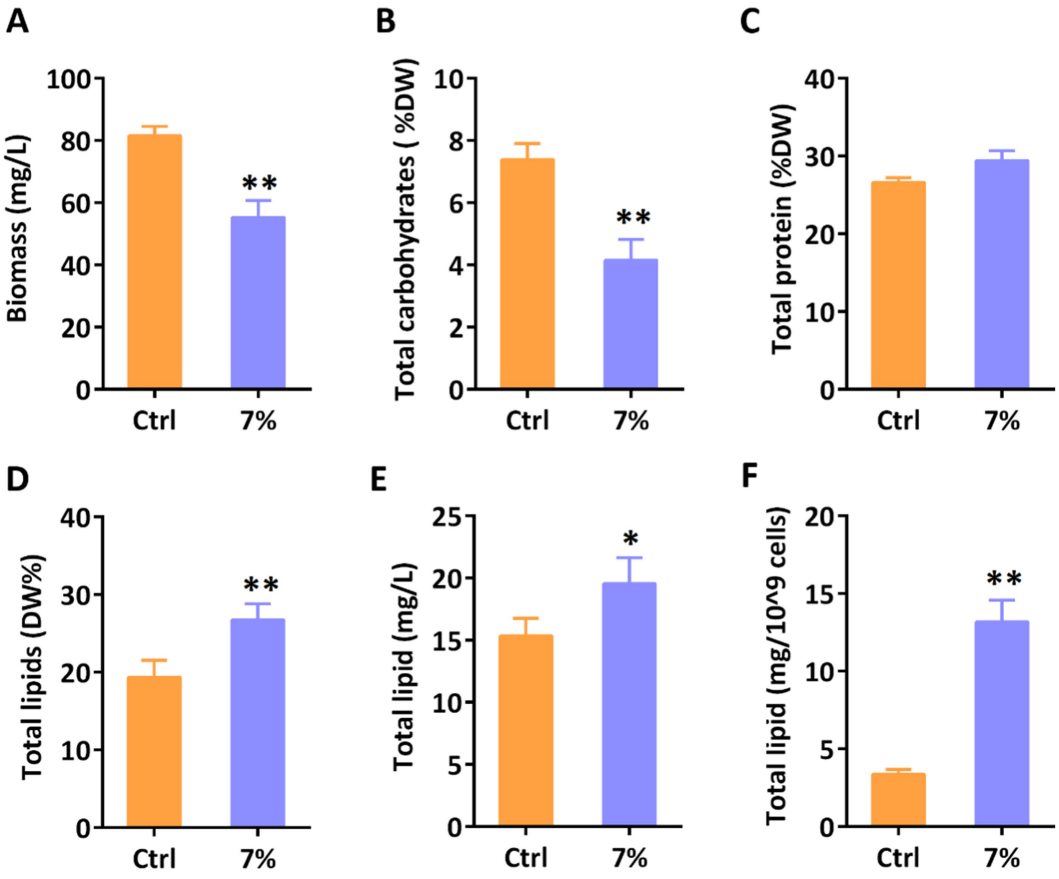

FIGURE 4
Determination of primary metabolites under water stress on day 3. **(A)** Total biomass; **(B)** Total carbohydrates content; **(C)** Total protein content; **(D)** Total lipids content; **(E)** Total lipids content per liter; **(F)** Total lipids content per 10^9 cells. Significant difference is indicated at $p < 0.05$ (*) or $p < 0.01$ (**) level. Each value represents mean ± SD ($n = 3$).

Furthermore, we determined the three major primary metabolites in *P. tricornutum* to explore the distribution of energy. Biochemistry analysis revealed that the content of total proteins was kept in balance with the control group, however, the total lipid content was elevated along with the reduced carbohydrates (Figures 4B–D). In industrial application scenarios, the total production of metabolites and their proportion to cell dry weight often exhibit different trends. Then, we determined the total lipid content on a large scale (Figures 4E, F). Conventional gravimetric analysis revealed that the total lipid content was found to increase remarkably when 10^9 cells and 1 L of algae were used as units of measurement, respectively. Our results indicated that water stress stimulates metabolic flow toward lipid synthesis.

Furthermore, we analyzed the relative fatty acid composition of total lipid at day 3 under 7% PEG. As shown in Figure 5, the content of monounsaturated fatty acids (MUFA) in total fatty acids increased while the content of saturated fatty acids (SFA) decreased. Among them, the proportions of C14:0, C16:1 and C18:1 were increased, while C16:0 and C18:0 were decreased under water stress compared to the control group, respectively. However, the accumulation of one of the most valuable polyunsaturated fatty acids (PUFA), eicosapentaenoic acid (EPA, C20:5), in *P. tricornutum* was not disturbed under water stress. These results demonstrated that water stress is involved in the *de novo* synthesis of fatty acids in *P. tricornutum*, especially regulating MUFA and SFA.

4 Discussion

Bio-products derived from diatoms are increasingly viewed as sustainable alternatives to traditional chemical products in both

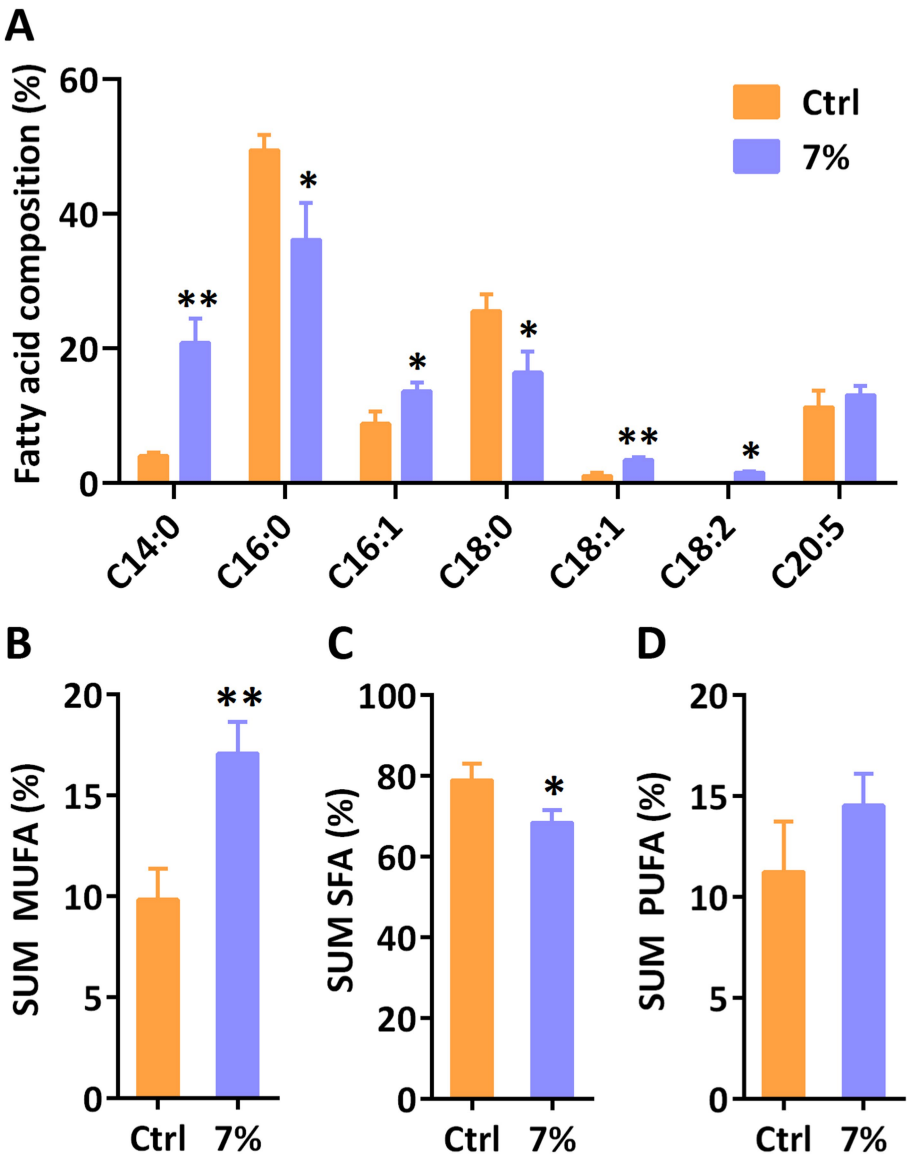

FIGURE 5
The relative fatty acid content **(A)** and sum monounsaturated fatty acids (MUFA) **(B)**, saturated fatty acids (SFA) and polyunsaturated fatty acids (PUFA) in *P. tricornutum* under water stress induced by 7% PEG. Significant differences are indicated at $p < 0.05$ (*) or $p < 0.01$ (**) level. Each value represents mean ± SD ($n = 3$).

the fuel and pharmaceutical sectors (Wang and Seibert, 2017). However, the large-scale cultivation of diatoms presents significant economic and water resource challenges, which hinder the exploitation of microalgae resources in regions with limited water availability (Piano et al., 2017; Jager et al., 2019; Arenas-Sánchez et al., 2016). While numerous studies have examined the mechanisms of water stress in higher plants and proposed strategies to address water scarcity (Farooq et al., 2012; Basu et al., 2016; Fathi and Tari, 2016), there remains a dearth of research on the mechanisms diatoms employ under water stress. This underscores the imperative to investigate the physiology and metabolism of diatoms in such conditions.

In this study, PEG 6000 was utilized to simulate water stress in the cultivation of *P. tricornutum* CCMP2561, as a model organism for studying the physiological response of diatoms under various abiotic stressors. Our results highlighted the pronounced impact of water stress on photosynthetic growth and metabolism of *P. tricornutum*, which will expand the physiological mechanism of water stress on other diatoms and microalgae. Previous studies have documented the disruptive effects of water stress on photosynthetic systems (Reddy et al., 2004; Wang et al., 2018). The reducing Fv/Fm and NPQ implied the damages in photosynthetic organs under water stress. Abiotic stress can lead to a weakness in photosynthetic capacity of chloroplast, which release signal to change the energy balance for adapting stress (Woodson, 2022; Li and Kim, 2022). Our data indicate that when exposed to levels above 3% PEG, *P. tricornutum* exhibited reductions in growth rate, photosynthetic efficiency, and chlorophyll a content. These findings align with prior observations in terrestrial plants, suggesting analogous photosynthetic responses to water stress in both microalgae and plants. Evolutionary biology establishes that plant chloroplasts share homology with microalgae (McFadden, 2001), further pointing to a shared vulnerability in chloroplasts to water stress-induced damage affecting light harvesting and cell division.

Water stress is known to induce oxidative stress, adversely affecting the physiology and metabolism of higher plants (Impa et al., 2012; Kaur and Asthir, 2017). In our study, we noted a significant release of ROS in *P. tricornutum* under water stress, aligning with prior observations in plants. This suggests a consistent oxidative stress response in both diatoms and higher plants when exposed to water stress. Interestingly, we observed that ROS content in microalgae peaked on the first day of PEG treatment, regardless of the hydration status of the microalgae, and subsequently decreased over the course of cultivation. A comparable trend was identified in *Auxenochlorella pyrenoidosa* during its bioremediation of hazardous wastewater (Wang et al., 2022). Such findings hint at a potential adaptive mechanism in microalgal cells to navigate novel environments. However, the SOD enzyme activity, crucial in neutralizing free radicals and thus alleviating stress in microalgae (Aderemi et al., 2018; Gauthier et al., 2020), did not display an immediate surge alongside the ROS increase on the first day. This lag in SOD activity elevation post-excessive ROS release might be attributed to the temporal disconnect between signal transduction and enzyme expression.

Metabolic redistribution under abiotic stress significantly influences the lipogenesis in diatoms. While numerous studies have highlighted the augmented accumulation of lipids in diatoms due to various abiotic stressors, such as excess light or nutrient deprivation (e.g., nitrogen or phosphorus starvation) (Levitan et al., 2015; Yang et al., 2014; Huete-Ortega et al., 2018), lipogenesis metabolism under water stress remains unexplored. Notably, diatoms often adapt by curtailing their growth rate and redirecting metabolic pathways toward lipogenesis during abiotic stress, ensuring cellular viability. Our study revealed the plasticity of diatoms in accumulating triglycerides under water stress. However, the weakened photosynthetic autotrophic ability hinders the accumulation of biomass under diatom water stress. The mixotrophic cultivation based on adding external organic sources can compensate for the lack of diatom biomass (Hao et al., 2020). Our study used PEG as an inducer to investigate the response of diatoms to water stress. However, PEG cannot reveal the real water stress conditions for maintaining the suspension ability of diatom cells in liquid environment. In the future, we will build a more reasonable water stress model and explore in depth the stress response mechanism of diatoms based on the results of this study. In addition, further exploration of the molecular mechanisms of diatom under water stress will be beneficial for screening water stress resistant genes to construct stress resistant algal strains using synthetic biology. Consistent with this, our findings indicate an increased lipid content under water stress, underscoring the parallels in physiological responses of diatoms and higher plants to water stress.

5 Conclusion

This study investigated the physiological and metabolic responses of *P. tricornutum* to water stress. We observed a significant induction of ROS release, inhibiting photosynthetic growth. Furthermore, water stress led to a notable increase in total lipid content and altered the fatty acid composition. Together, these findings offer insights into the potential utilization of diatoms in areas with water scarcity.

Data availability statement

The raw data supporting the conclusions of this article will be made available by the authors, without undue reservation.

Author contributions

T-BH: Writing – review & editing, Writing – original draft, Methodology, Validation. P-YL: Writing – original draft, Data curation, Investigation. ZS: Conceptualization, Software, Writing – review & editing. RL: Writing – review & editing, Formal analysis, Resources. Z-YC: Writing – review & editing, Investigation, Software. R-LH: Writing – review & editing, Software, Investigation, Supervision. YL: Writing – review & editing, Conceptualization, Resources, Validation, Visualization. AA: Conceptualization, Writing – review & editing, Formal analysis, Supervision, Writing – original draft.

Funding

The author(s) declare that financial support was received for the research and/or publication of this article. This work was supported by the Natural Science Foundation of China (42206080).

Conflict of interest

The authors declare that the research was conducted in the absence of any commercial or financial relationships that could be construed as a potential conflict of interest.

Generative AI statement

The authors declare that no Gen AI was used in the creation of this manuscript.

Publisher's note

References

Aderemi, A. O., Novais, S. C., Lemos, M. F., Alves, L. M., Hunter, C., and Pahl, O. (2018). Oxidative stress responses and cellular energy allocation changes in microalgae following exposure to widely used human antibiotics. *Aquat. Toxicol.* 203, 130–139. doi: 10.1016/j.aquatox.2018.08.008

Arenas-Sánchez, A., Rico, A., and Vighi, M. (2016). Effects of water scarcity and chemical pollution in aquatic ecosystems: state of the art. *Sci. Total Environ.* 572, 390–403. doi: 10.1016/j.scitotenv.2016.07.211

Basu, S., Ramegowda, V., Kumar, A., and Pereira, A. (2016). Plant adaptation to drought stress. *F1000Res* 5:F1000 Faculty Rev-1554. doi: 10.12688/f1000research.7678.1s

Butler, T., Kapoore, R. V., and Vaidyanathan, S. (2020). *Phaeodactylum tricornutum*: a diatom cell factory. *Trends Biotechnol.* 38, 606–622. doi: 10.1016/j.tibtech.2019.12.023

Chowdhary, P., Bharagava, R. N., Mishra, S., and Khan, N. (2020). "Role of industries in water scarcity and its adverse effects on environment and human health" in Environmental Concerns and Sustainable Development, 235–256.

Curien, G., Flori, S., Villanova, V., Magneschi, L., Giustini, C., Forti, G., et al. (2016). The water to water cycles in microalgae. *Plant Cell Physiol.* 57, pcw048–pcw1363. doi: 10.1093/pcp/pcw048

Daboussi, F., Leduc, S., Maréchal, A., Dubois, G., Guyot, V., Perez-Michaut, C., et al. (2014). Genome engineering empowers the diatom *Phaeodactylum tricornutum* for biotechnology. *Nat. Commun.* 5:3831. doi: 10.1038/ncomms4831

De Riso, V., Raniello, R., Maumus, F., Rogato, A., Bowler, C., and Falciatore, A. (2009). Gene silencing in the marine diatom *Phaeodactylum tricornutum*. *Nucleic Acids Res.* 37:e96. doi: 10.1093/nar/gkp448

Farooq, M., Hussain, M., Wahid, A., and Siddique, K. (2012). "Drought stress in plants: an overview" in Plant responses to drought stress: from morphological to molecular features, 1–33.

Fathi, A., and Tari, D. B. (2016). Effect of drought stress and its mechanism in plants. *Int. J. Life Sci.* 10, 1–6. doi: 10.3126/ijls.v10i1.14509

Gauthier, M., Senhorinho, G., and Scott, J. (2020). Microalgae under environmental stress as a source of antioxidants. *Algal Res.* 52:102104. doi: 10.1016/j.algal.2020.102104

Gouveia, L., Graça, S., Sousa, C., Ambrosano, L., Ribeiro, B., Botrel, E. P., et al. (2016). Microalgae biomass production using wastewater: treatment and costs: scale-up considerations. *Algal Res.* 16, 167–176. doi: 10.1016/j.algal.2016.03.010

Hao, T.-B., Balamurugan, S., Zhang, Z.-H., Liu, S.-F., Wang, X., Li, D.-W., et al. (2022). Effective bioremediation of tobacco wastewater by microalgae at acidic pH for synergistic biomass and lipid accumulation. *J. Hazard. Mater.* 426:127820. doi: 10.1016/j.jhazmat.2021.127820

Hao, T.-B., Yang, Y.-F., Balamurugan, S., Li, D.-W., Yang, W.-D., and Li, H.-Y. (2020). Enrichment of f/2 medium hyperaccumulates biomass and bioactive compounds in the diatom *Phaeodactylum tricornutum*. *Algal Res.* 47:101872. doi: 10.1016/j.algal.2020.101872

Hao, T.-B., Zhang, Z.-H., Yang, W.-D., Li, H.-Y., and Wang, X. (2024). Enhanced lipid production of Auxenochlorella pyrenoidosa using biochar-pretreated tobacco industry wastewater. *Chem. Eng. J.* 499:156007. doi: 10.1016/j.cej.2024.156007

Huete-Ortega, M., Okurowska, K., Kapoore, R. V., Johnson, M. P., Gilmour, D. J., and Vaidyanathan, S. (2018). Effect of ammonium and high light intensity on the accumulation of lipids in Nannochloropsis oceanica (CCAP 849/10) and *Phaeodactylum tricornutum* (CCAP 1055/1). *Biotechnol. Biofuels* 11, 60–15. doi: 10.1186/s13068-018-1061-8

Impa, S., Nadaradjan, S., and Jagadish, S. (2012). "Drought stress induced reactive oxygen species and anti-oxidants in plants" in Abiotic stress responses in plants: metabolism, productivity and sustainability, 131–147.

Jager, H. I., Efroymson, R. A., and Baskaran, L. M. (2019). Avoiding conflicts between future freshwater algae production and water scarcity in the United States at the energy-water nexus. *Water* 11:836. doi: 10.3390/w11040836

Jallet, D., Caballero, M. A., Gallina, A. A., Youngblood, M., and Peers, G. (2016). Photosynthetic physiology and biomass partitioning in the model diatom *Phaeodactylum tricornutum* grown in a sinusoidal light regime. *Algal Res.* 18, 51–60. doi: 10.1016/j.algal.2016.05.014

Kaur, G., and Asthir, B. (2017). Molecular responses to drought stress in plants. *Biol. Plant.* 61, 201–209. doi: 10.1007/s10535-016-0700-9

Kuczynska, P., Jemiola-Rzeminska, M., Nowicka, B., Jakubowska, A., Strzalka, W., Burda, K., et al. (2020). The xanthophyll cycle in diatom *Phaeodactylum tricornutum* in response to light stress. *Plant Physiol. Biochem.* 152, 125–137. doi: 10.1016/j.plaphy.2020.04.043

Lee, B. X., Kjaerulf, F., Turner, S., Cohen, L., Donnelly, P. D., Muggah, R., et al. (2016). Transforming our world: implementing the 2030 agenda through sustainable development goal indicators. *J. Public Health Policy* 37, 13–31. doi: 10.1057/s41271-016-0002-7

Levitan, O., Dinamarca, J., Zelzion, E., Lun, D. S., Guerra, L. T., Kim, M. K., et al. (2015). Remodeling of intermediate metabolism in the diatom *Phaeodactylum tricornutum* under nitrogen stress. *Proc. Natl. Acad. Sci.* 112, 412–417. doi: 10.1073/pnas.1419818112

Li, M., and Kim, C. (2022). Chloroplast ROS and stress signaling. *Plant Commun.* 3:100264. doi: 10.1016/j.xplc.2021.100264

Mahpara, S., Zainab, A., Ullah, R., Kausar, S., Bilal, M., Latif, M. I., et al. (2022). The impact of PEG-induced drought stress on seed germination and seedling growth of different bread wheat (*Triticum aestivum* L.) genotypes. *PLoS One* 17:e0262937. doi: 10.1371/journal.pone.0262937

McFadden, G. I. (2001). Primary and secondary endosymbiosis and the origin of plastids. *J. Phycol.* 37, 951–959. doi: 10.1046/j.1529-8817.2001.01126.x

Peršić, V., Ament, A., Antunović Dunić, J., Drezner, G., and Cesar, V. (2022). PEG-induced physiological drought for screening winter wheat genotypes sensitivity–integrated biochemical and chlorophyll a fluorescence analysis. *Front. Plant Sci.* 13:987702. doi: 10.3389/fpls.2022.987702

Piano, E., Falasco, E., and Bona, F. (2017). Mediterranean rivers: consequences of water scarcity on benthic algal chlorophyll a content. *J. Limnol.* 76, 39–48. doi: 10.4081/jlimnol.2016.1503

Qi, Y., Ma, L., Ghani, M. I., Peng, Q., Fan, R., Hu, X., et al. (2023). Effects of drought stress induced by hypertonic polyethylene glycol (PEG-6000) on *Passiflora edulis* Sims physiological properties. *Plan. Theory* 12:2296. doi: 10.3390/plants12122296

Reddy, A. R., Chaitanya, K. V., and Vivekanandan, M. (2004). Drought-induced responses of photosynthesis and antioxidant metabolism in higher plants. *J. Plant Physiol.* 161, 1189–1202. doi: 10.1016/j.jplph.2004.01.013

Reyes, J. A. O., Casas, D. E., Gandia, J. L., Parducho, M. J. L., Renovalles, E. M., Quilloy, E. P., et al. (2023). Polyethylene glycol-induced drought stress screening of selected Philippine high-yielding sugarcane varieties. *J. Agricult. Food Res.* 14:100676. doi: 10.1016/j.jafr.2023.100676

Reza Yousefi, A., Rashidi, S., Moradi, P., and Mastinu, A. (2020). Germination and seedling growth responses of *Zygophyllum fabago*, *Salsola kali* L. and *Atriplex canescens* to PEG-induced drought stress. *Environments* 7:107. doi: 10.3390/environments7120107

Rosa, L., Chiarelli, D. D., Rulli, M. C., Dell'Angelo, J., and D'Odorico, P. (2020). Global agricultural economic water scarcity. *Sci. Adv.* 6:eaaz6031. doi: 10.1126/sciadv.aaz6031

Sharma, V., Kumar, A., Chaudhary, A., Mishra, A., Rawat, S., Shami, V., et al. (2022). Response of wheat genotypes to drought stress stimulated by PEG. *Stress* 2, 26–51. doi: 10.3390/stresses2010003

Wang, D., Hubacek, K., Shan, Y., Gerbens-Leenes, W., and Liu, J. (2021). A review of water stress and water footprint accounting. *Water* 13:201. doi: 10.3390/w13020201

Wang, X., Mou, J.-H., Qin, Z.-H., Hao, T.-B., Zheng, L., Buhagiar, J., et al. (2022). Supplementation with rac-GR24 facilitates the accumulation of biomass and astaxanthin

in two successive stages of *Haematococcus pluvialis* cultivation. *J. Agric. Food Chem.* 70, 4677–4689. doi: 10.1021/acs.jafc.2c00479

Wang, J.-K., and Seibert, M. (2017). Prospects for commercial production of diatoms. *Biotechnol. Biofuels* 10, 1–13. doi: 10.1186/s13068-017-0699-y

Wang, W., Wang, C., Pan, D., Zhang, Y., Luo, B., and Ji, J. (2018). Effects of drought stress on photosynthesis and chlorophyll fluorescence images of soybean (*Glycine max*) seedlings. *Int. J. Agricult. Biol. Eng.* 11, 196–201. doi: 10.25165/j.ijabe.20181102.3390

Woodson, J. D. (2022). Control of chloroplast degradation and cell death in response to stress. *Trends Biochem. Sci.* 47, 851–864. doi: 10.1016/j.tibs.2022.03.010

Yang, R., Wei, D., and Xie, J. (2020). Diatoms as cell factories for high-value products: chrysolaminarin, eicosapentaenoic acid, and fucoxanthin. *Crit. Rev. Biotechnol.* 40, 993–1009. doi: 10.1080/07388551.2020.1805402

Yang, J., Xu, M., Zhang, X., Hu, Q., Sommerfeld, M., and Chen, Y. (2011). Life-cycle analysis on biodiesel production from microalgae: water footprint and nutrients balance. *Bioresour. Technol.* 102, 159–165. doi: 10.1016/j.biortech.2010.07.017

Yang, Z. K., Zheng, J. W., Niu, Y. F., Yang, W. D., Liu, J. S., and Li, H. Y. (2014). Systems-level analysis of the metabolic responses of the diatom P haeodactylum tricornutum to phosphorus stress. *Environ. Microbiol.* 16, 1793–1807. doi: 10.1111/1462-2920.12411

frontiers | Frontiers in Microbiology

TYPE Original Research
PUBLISHED 28 April 2025
DOI 10.3389/fmicb.2025.1591974

OPEN ACCESS

EDITED BY
Qi Zhang,
Nanchang University, China

REVIEWED BY
Zaidun Naji Abudi,
Mustansiriyah University, Iraq
Yanshen Li,
Yantai University, China
Wei Li,
Arizona State University, United States

*CORRESPONDENCE
Zhiyan Pan
panzhiyan@zjut.edu.cn
George Nakhla
gnakhla@uwo.ca

RECEIVED 11 March 2025
ACCEPTED 02 April 2025
PUBLISHED 28 April 2025

CITATION
Zheng X, Liu R, Li K, Sun J, Wang K, Shao Y, Hu Z, Zhu J, Pan Z and Nakhla G (2025) Microalgae-bacteria symbiosis enhanced nitrogen removal from wastewater in an inversed fluidized bed bioreactor: performance and microflora. *Front. Microbiol.* 16:1591974. doi: 10.3389/fmicb.2025.1591974

Microalgae-bacteria symbiosis enhanced nitrogen removal from wastewater in an inversed fluidized bed bioreactor: performance and microflora

Xin Zheng[1,2], Ruoting Liu[2], Kai Li[3], Junhao Sun[2], Kanming Wang[1], Yuanyuan Shao[4], Zhongce Hu[5], Jesse Zhu[2], Zhiyan Pan[1]* and George Nakhla[2]*

[1]College of Environment, Zhejiang University of Technology, Hangzhou, China, [2]Department of Chemical and Biochemical Engineering, The University of Western Ontario, London, ON, Canada, [3]Wenzhou Ecological and Environmental Monitoring Center of Zhejiang Province, Wenzhou, China, [4]Nottingham Ningbo China Beacons of Excellence Research and Innovation Institute, The University of Nottingham Ningbo China, Ningbo, China, [5]College of Biotechnology and Bioengineering, Zhejiang University of Technology, Hangzhou, China

Conventional wastewater biological nitrogen removal (BNR) processes require a large amount of air and external organic carbon, causing a significant increase in operating costs and potential secondary pollution. Herein, this study investigated the nitrogen removal performance and the underlying mechanisms of a novel simultaneous nitrification and denitrification (SND) coupled with photoautotrophic assimilation system in an inversed fluidized bed bioreactor (IFBBR). Nitrogen removal was achieved through the synergistic interaction of microalgae and bacteria, with microalgae providing O_2 for nitrification and microbial biomass decay supplying organic carbon for denitrification. The IFBBR was continuously operated for more than 240 days without aeration and external organic carbon, the total nitrogen (TN) removal efficiency reached over 95%. A novel C-N-O dynamic balance model was constructed, revealing that nitrification and denitrification were the primary pathways for nitrogen removal. The model further quantified the microbial contributions, showing that microalgae generated O_2 at a rate of 81.82 mg/L·d, while microbial biomass decay released organic carbon at a rate of 148.66 mg/L·d. Microbial diversity analysis confirmed the majority presence of microalgae (*Trebouxiophyceae*), nitrifying bacteria (*Gordonia* and *Nitrosomonas*) and denitrifying bacteria (*Ignavibacterium* and *Limnobacter*). This study successfully achieved enhanced nitrogen removal without the need for aeration or external organic carbon. These advancements provide valuable insights into efficient wastewater nitrogen removal, offering significant benefits in terms of reduced energy consumption, lower operational costs, and decreased CO_2 emissions.

KEYWORDS

microalgal-bacterial symbiosis system, biological nitrogen removal, mass balance, simultaneous nitrification and denitrification, syntrophic microbial communities

1 Introduction

Nitrogen is one of the essential nutrients for the growth of organisms in the water. However, excess nitrogenous compounds discharged into natural water can result in water quality deterioration and eutrophication (Gu et al., 2024). Biological nitrogen removal (BNR) process has been widely used for removing the nitrogen compounds from municipal wastewater (Maheepala et al., 2023; Wang et al., 2022). However, conventional BNR processes separate the nitrification and denitrification processes due to their different redox condition requirements (Alzate Marin et al., 2016; Ye et al., 2021), leading to large footprints (Manser et al., 2016), potential emission of greenhouse gases like N_2O (Tariq et al., 2025), high aeration (Yan et al., 2024), and external organic matter (Peng et al., 2020).

Recently, many researchers have focused on novel BNR technologies to enhance the nutrient removal efficiency (Wang et al., 2020; Zheng et al., 2024). Fluidized bed bioreactor (FBBR) has the merits of better mixing, enhanced mass transfer (Chowdhury and Nakhla, 2022; Nelson et al., 2017), higher microbial concentrations and activity, greater resistance to impact loads, and less residual biosolids produced (Wang et al., 2020). However, the high flow rate required by the FBBR to achieve fluidization causes high energy consumption, and high shear forces which lead to biofilm detachment (Andalib et al., 2012). The inverse fluidized bed bioreactor (IFBBR), designed with carrier particles slightly less dense than water, requires significantly less fluidization energy and minimizes shear forces. This system has been successfully used to cultivate nitrifying and denitrifying biofilms with synthetic wastewater (Wang et al., 2020; Zhang et al., 2020). With the formation and thickening of biofilm in the IFBBR, the outer and inner layers of biofilm can achieve aerobic conditions and anaerobic/anoxic conditions, respectively, thus facilitating the occurrence of simultaneous nitrification and denitrification (SND). As a novel BNR process, SND incorporates diverse metabolic pathways that could combine aerobic nitrification and anaerobic/anoxic/aerobic denitrification in one reactor (Luan et al., 2023), relying on the cooperation of nitrifiers and denitrifiers (Jin et al., 2023). However, the SND process still requires high aeration for nitrification and external organic carbon for denitrification, which significantly increases energy consumption and operational costs. Moreover, maintaining stable and harmonious cooperation between nitrification and denitrification remains a challenge, limiting its practical potential (Zhang F. et al., 2021). Therefore, if an endogenous supply of oxygen and organic carbon can be established within the SND process, enabling nitrification without aeration and denitrification without external organic carbon, as well as maintaining high nitrogen removal efficiency. Such a BNR process would offer significant potential for further research and practical applications.

Microalgal-bacterial symbiosis systems for municipal wastewater treatment, especially for nitrogen removal, have recently gained great attention, as they can greatly reduce energy, chemicals consumption and carbon dioxide release (Li et al., 2023; Lu et al., 2022). In the microalgal-bacterial symbiosis system, microalgae capture carbon dioxide released by bacteria or dissolved in water and then produce oxygen for bacterial metabolism and growth through photosynthesis (Abouhend et al., 2018; Aparicio et al., 2024), which can save 40–60% of the total energy demand in wastewater treatment (Gu et al., 2021; Huang et al., 2022). Meanwhile, organic carbon synthesized through photosynthesis could be an electron donor demand for denitrifiers (Wang et al., 2015). Tang et al. (2018) suggested that microalgae positively affected nitrogen removal in BNR process in two ways: preferential uptake of ammonia for biomass synthesis (direct effect) and increasing the activity of bacteria by synergism (indirect effect). Moreover, studies have indicated that microalgae may affect the composition and characteristics of extracellular polymeric substances (EPS) and increase floc size, facilitating the formation of anoxic/aerobic microenvironments in one system (Jin et al., 2023).

However, the effects of microalgae on the SND process, and the interactions between microalgae and bacteria, which combine diverse nitrogen removal pathways for collaboration, have yet to be thoroughly elucidated. Once the interaction mechanisms between microalgae and various functional bacteria in the SND denitrification system are clarified, efforts can focus on achieving a low-energy, low-cost, and efficient BNR process without the need for aeration or external organic carbon. This goal requires a comprehensive understanding of the microbial community structure, the migration and transformation pathways of elements, and the specific contributions of functional microbial communities at each stage. Dynamic analysis of C-N-O elements is particularly critical, as the complexity of the process makes it impossible to directly track each element. Researchers are exploring simulation models to address this challenge. However, existing models are typically designed for systems with simple elements or microbial compositions and hard to perform adequately in complex BNR systems.

This study aimed to enhance nitrogen removal by coupling SND with photoautotrophic assimilation in the IFBBR, which was fed with synthetic wastewater, started up and operated for 240 days. In this system, oxygen and organic carbon required for SND can be generated *in situ* by microalgae, eliminating the need for aeration or external organic carbon. Different nitrogen loading rates (NLR) were tested. Microbial community analysis was further conducted to detect the presence and abundance of microalgae and bacteria within the system. In addition, changes in alkalinity, which often accompany migration and transformation of nitrogen but are overlooked, were utilized to construct a novel C-N-O dynamic balance model. This model was used to identify the primary mechanisms for nitrogen removal in the IFBBR. In summary, this study successfully realized the enhanced nitrogen removal from wastewater by coupling SND with photoautotrophic assimilation in an IFBBR and successfully eliminated aeration and organic carbon needs, while the construction and application of a C-N-O dynamic balance model provided valuable insights for nitrogen removal mechanisms, offering an efficient solution for BNR process with reduced energy consumption, chemical usage, and carbon emissions.

2 Materials and methods

2.1 Inoculum and synthetic wastewater composition

Thickened waste activated sludge (TWAS) was initially collected from wastewater treatment plants and continuously operated in a laboratory-scale Anammox sequencing batch reactor (SBR) for over 300 days, demonstrating a stable nitrogen removal performance in the SBR without aeration and external organic carbon. However, the nitrogen removal rate (NRR) was only 0.02 kg N/m^3·d with the NLR

of 0.26 kg N/m^3·d. To enhance the nitrogen removal performance, 150 mL of SBR biosolids (mixed liquor volatile suspended solids concentration (MLVSS) of 920 mg/L) was inoculated into the IFBBR.

The composition of synthetic wastewater fed into the IFBBR was kept consistent with that of the Anammox SBR, primarily consisting of sodium nitrite and ammonium sulfate, as shown in Table 1, with $KHCO_3$ as the alkalinity source (500 mg/L). The influent ammonia nitrogen concentrations were kept at roughly 58–66 mg/L, roughly double the typical concentrations in municipal wastewater, while the influent nitrite nitrogen varied from 77 to 90 mg/L (Table 1) and some nitrite nitrogen was oxidated into nitrate nitrogen during dissolution. The other constituents of the synthetic medium are listed in Supplementary Table 1 of the Supplementary material. The initial pH was adjusted to about 7.8 using either 0.1 M HCl or 0.1 M NaOH. To avoid interference from external oxygen on the system, synthetic wastewater was first purged with nitrogen gas (>99%) for 30 min and then sealed by a nitrogen gas balloon before being fed into the IFBBR.

2.2 Experimental setup and operating conditions

An IFBBR was developed in this study to enhance the nitrogen removal performance (Figure 1). The working volume of the polymethyl methacrylate (PMMA) bioreactor was approximately 500 mL with an inner diameter of 3 cm and a height of 100 cm. A heat belt (HTWC 101–010, Omegalux, USA) and heat shield were mounted on the outer layer to keep the temperature at approximately 38°C, which was identical to the temperature in the Anammox SBR. An observation window with an area of 15 square centimeters was set to observe whether the carrier particles were blocked at the bottom. Polyethylene coated carbon (PEC) particles (diameter of 2.0 mm, density of 950 kg/m^3, roundness of 0.97, nonporous with specific surface area of approximately 14.94 cm^2/g) were used as carrier particles in the IFBBR with a packing ratio of 30%. After being ultrasonically cleaned three times, there was no detectable total organic carbon in the cleaning water, confirming that the PEC particles could not provide organic carbon to the system. Unlike conventional FBBRs, the PEC particles in this IFBBR have a slightly lower density than water, allowing them to float easily and achieve fluidization with significantly lower water flow. This design reduces the reactor's energy consumption for fluidization while minimizing shear forces, creating an optimal environment for biofilm growth.

The reactor was operated in 4 h cycles with each cycle including filling & discharging (10 min) and reaction (230 min). The reactor was manually purged with nitrogen gas once daily to reduce the dissolved oxygen concentration (DO) to avoid interference from external oxygen. The pH value of the IFBBR was manually detected at regular intervals. The light intensity in the laboratory is 2,500 lx, and the lights were turned on for approximately 12 h every day.

The particle fluidization was realized by circulating water from the bottom to the top using peristaltic pump (07528–10, Masterflex, USA) at a reflux ratio of 125: 1 based on the influent flow rate. Synthetic wastewater was pumped into the top and discharged from the bottom

TABLE 1 Operating conditions of each phase.

Phase	pH	HRT	Inf. NH_4^+-N	Inf. NO_2^--N	Inf. NO_3^--N	NLR
Phase I	7.8–8.0	48 h	58 ± 3 mg/L	77 ± 4 mg/L	10 ± 3 mg/L	0.07 kg N/m^3·d
Phase II	7.8–8.0	48 h	58 ± 3 mg/L	77 ± 4 mg/L	10 ± 3 mg/L	0.07 kg N/m^3·d
Phase III	7.8–8.2	48 h	66 ± 6 mg/L	90 ± 5 mg/L	22 ± 4 mg/L	0.09 kg N/m^3·d

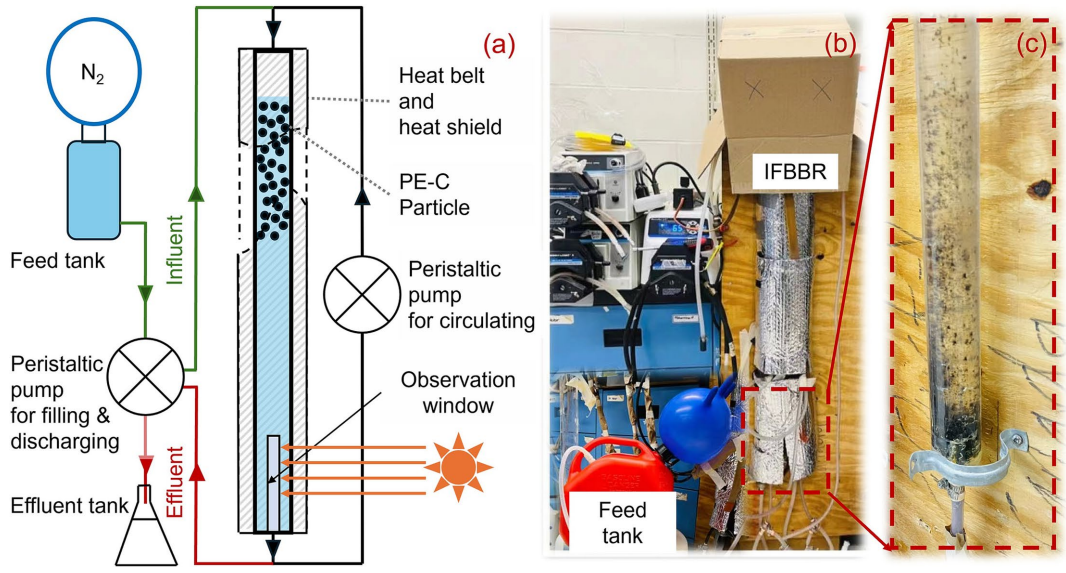

FIGURE 1
Schematic diagram **(a)**, actual **(b)** of IFBBR and biofilm at the bottom wall of IFBBR after operation of 190 days **(c)**.

of the IFBBR through another peristaltic pump (77521–50, Masterflex, USA).

The whole experiment lasted 240 days and was divided into three phases (Table 1): phase I (day 1–28) was the start-up period, Phase II (day 29–87) was the lower nitrogen loading rate (NLR, 0.07 kg N/m^3·d) period, and phase III (day 88–240) was the higher NLR period, with the NLR increased to 0.09 kg N/m^3·d.

2.3 Batch tests

In order to test the activity of nitritation (AOB), nitratation (NOB) and denitrification (denitrifier), in-situ batch tests were carried out at the end of phase III when total nitrogen (TN) removal efficiency was over 90% and the temperature of 38°C. The composition and concentration of initial solutions were the same as the daily feeding except for the nitrogen compounds (NH_4^+-N, NO_3^--N, NO_2^--N). In the three batch tests, $(NH_4)_2SO_4$, $NaNO_2$ and $NaNO_3$ were used as the only nitrogen compounds at N concentrations of 35 mg/L, 90 mg/L, and 60 mg/L, respectively. The microbial activity of nitrifiers and denitrifiers in the IFBBR was determined by the specific nitrogen removal rate (SNRR), which was calculated by the slope of the trend of ammonia, nitrite and nitrate concentration with time, respectively. Before each stage, liquid in the IFBBR was drained into a 500 mL Erlenmeyer flask. Subsequently, the initial solutions were slowly added to the IFBBR. The recirculation pump was turned on until the carrier particles floated naturally. Samples were collected at regular time intervals. After each sample collection, the system was purged with nitrogen gas for 15 min to avoid interference from external oxygen. The IFBBR ran normally for 1 to 2 days between each batch test to ensure that its performance was not affected.

2.4 Analytical methods

Liquid samples were collected at regular intervals to measure total COD (tCOD), total suspended solids (TSS) and volatile suspended solids (VSS). Soluble samples were passed through 0.45 μm filter membranes (VWR 28333–1390, China) for measuring NH_4^+-N, NO_2^--N, NO_3^--N, TN and soluble COD (sCOD) concentrations using an ultraviolet–visible spectrophotometer (DR 3900, Hach Company, USA) according to standard methods (APHA, 2012). An alkalinity auto-titrator was used for the measurement of pH and alkalinity (Alk.) (285212831, Schott, Germany), and Δalkalinity (ΔAlk.) was calculated as the effluent Alk. minus the influent Alk.

2.5 Microbial community analysis

On day 190 when TN removal efficiency was over 90%, samples were collected for the microbial community analysis. As the biofilm grew on both the surface and the bottom wall of the IFBBR, the microbial community of biofilm on the carrier and the IFBBR wall was analyzed by IRDA lab (Quebec, QC, Canada). Illumina MiSeq 2 × 300 bp sequencing was performed by the Genomic Analysis Platform of the Institute for Integrative Biology and Systems (IBIS) at Laval University (Quebec, QC, Canada). Sample preparation and DNA extraction were conducted by collecting 2.0 mL homogeneous volume of each sample using the FastDNA Spin Kit for Soil Extraction Kit (MP Biomedicals, Solon, OH, USA) (Gu et al., 2024). The quality and quantity of the extracted genomic DNA samples were determined spectrophotometrically with absorbance measurements at 260 and 280 nm using an A260/A280 ratio. Amplification of the V4 and V6 regions of archaea, bacteria 16S rRNA and eukaryote 18S rRNA were performed using the primer sequences of the specific regions (Apprill et al., 2015). A two-step dual-indexed PCR approach specifically designed for the Illumina MiSeq sequencing platform was performed. The amplicon libraries were sequenced in the paired-end format with a reading of 300 bases, 2 × 300 base pairs on each side of the DNA strand on Illumina MiSeq at the genomic analysis platform, IBIS of University Laval (Quebec, Canada). Bacteria and microalgae with the relative abundance of over 0.7% were analyzed.

2.6 C-N-O dynamic balance models

Based on the microbial community analysis and the nitrogen removal theory of microalgae and bacteria, a C-N-O dynamic balance model was developed to further ensure the nitrogen removal mechanisms.

In this microalgal-bacterial symbiosis system, NH_4^+-N was removed through two primary pathways: nitrification and microalgae assimilation (Zhang H. et al., 2021). NO_2^--N was generated via nitritation (AOB) and denitratation (DN_3), while it was removed by nitratation (NOB) and denitritation (DN_2). NO_3^--N was generated by nitratation (NOB) and removed by denitratation (DN_3). Organic carbon was generated from biomass decay and then consumed by denitrification. Oxygen, produced by microalgae, was primary utilized by nitrifying bacteria. Combined with the dynamic changes in alkalinity observed during the nitrogen removal in the IFBBR, the C-N-O dynamic balance model was constructed. Detailed derivation of the model is provided in Supplementary Text 1, with the results of C-N-O mass balance presented in section 3.4.

3 Results and discussion

3.1 Nitrogen removal performance of the IFBBR

The temporal variations of NH_4^+-N, NO_2^--N, NO_3^--N concentrations in the IFBBR during the experiment are shown in Figure 2a. In phase I, it is obvious that the concentrations of NH_4^+-N, NO_2^--N, NO_3^--N in the effluent showed a sharp decrease, then increased and remained stable after day 11. The sharp decrease can be due to the microorganisms consuming nitrogen compounds during the initial period of internal circulation without feeding. Additionally, the concentration of nitrogen compounds in effluent remained stable in the subsequent period indicating the successful start-up of the IFBBR. Figure 2b shows the TN removal performance in the IFBBR, in which the TN removal efficiency remained stable at 72 ± 2% during the remaining time of Phase I (day 1–28), which also indicates the successful start-up of the IFBBR. Interestingly, the seed biosolids was collected from the previous SBR, which had been continuously worked for more than 300 days with the TN removal efficiency

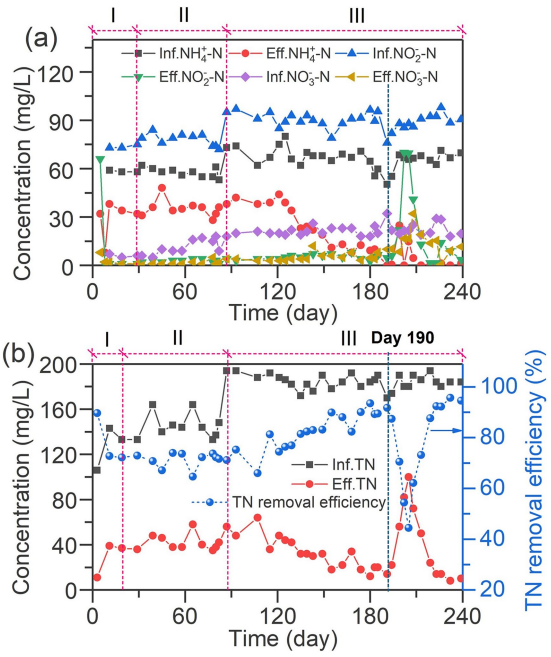

FIGURE 2
Nitrogen removal performance of the Inversed Fluidized Bed Bioreactor (IFBBR). **(a)** Temporal variations of inorganic nitrogen (NH_4^+-N, NO_2^--N, NO_3^--N); **(b)** Temporal variations of total nitrogen removal efficiency.

between 10 and 20%, NLR of 0.26 kg N/m³·d and nitrogen removal rate (NRR) of 0.02 kg N/m³·d. However, once the seed biosolids were inoculated into the IFBBR, the biofilm in the IFBBR had a stable and high nitrogen removal performance rapidly. This could be due to the low shear force of the IFBBR and the rough surface and large specific surface area of PEC particles, resulting in suitable conditions for the biofilm formation and the rapid start-up of the BNR process.

During phases I and II (days 29–87) with a low NLR of 0.07 kg N/m³·d, the effluent NH_4^+-N concentration remained stable at 35 mg/L, while NO_2^--N remained below 10 mg/L. This result indicated that stable nitrogen removal in the IFBBR was achieved. In phase III (day 88–240), NLR was increased to 0.09 kg N/m³·d to promote the growth and activity of the biofilm, leading to about a month of water quality fluctuations. It is interesting to point out that the effluent NH_4^+ -N concentration showed a significant decreasing trend after 121 days operation and was undetected (less than 1 mg/L) after 190 days operation. It has been widely reported that ammonia nitrogen was usually consumed by nitrification (Svehla et al., 2023), while microalgae also had the capability of ammonia assimilation (Yan et al., 2022), indicating a significant growth of nitrifiers or microalgae in the IFBBR during this period. Meanwhile, the effluent nitrite and nitrate nitrogen concentrations remained below 10 mg/L, which were much lower than the consumption of ammonia, with the TN removal efficiency increasing and reaching over 90% and the NRR of 0.08 kg N/m³·d, indicating that the denitrification process occurred simultaneously with the nitrification in the IFBBR. Between day 190 and day 205, due to the collection of biological samples for microbial community analysis, the TN removal efficiency significantly decreased and dropped to 44%. Surprisingly, in the following 15 days, the TN removal efficiency quickly recovered and reached over 95%, further demonstrating the stability of the nitrogen removal performance of the IFBBR.

Nitrifiers require a significant amount of oxygen for their growth and metabolism. However, the feed tank and the IFBBR were purged daily with nitrogen gas and sealed with parafilm. Additionally, the growth and metabolism of denitrifiers require organic carbon, but the only carbon source in the nutrient solution was HCO_3^-. These may be due to the presence of microalgae, which produces oxygen and organic carbon for SND. The seed sludge used in the previous SBR was the TWAS collected at the Greenway wastewater treatment plant in London, Canada, which could contain indigenous microalgae (Huang et al., 2022). In the long-term operation of the IFBBR, weak light entered through the observation window, leading to microalgae growing and accumulating at the bottom of the IFBBR. As shown in Figure 1 (day 190), there is indeed a biofilm-like microalgae growing on the wall, microbial community analysis in section 3.3 further proves the presence of microalgae in the IFBBR. In summary, SND and microalgal photoautotrophic assimilation were coupled in the IFBBR. Microalgae provide the necessary oxygen and organic carbon source for SND, while bacteria supply CO_2 to microalgae. It is precisely due to the presence of microalgae that enhanced the nitrogen removal performance, especially the ammonia removal efficiency, significantly improved after day 121.

In conventional microalgal-bacterial symbiosis systems, it is difficult for microalgae to supply sufficient oxygen and organic carbon to support bacterial growth and metabolism. As a result, additional conditions such as strong light sources, aeration, and external organic carbon supplementation are often required to sustain bacterial activity and ensure the system's stable operation. Jin et al. (2023) integrated microalgae with simultaneous nitrification and denitrification in microalgal-bacterial sequencing batch reactors (MB-SBR) illuminated by a sunlight-simulating light source. With aeration and the addition of organic carbon sources (starch and glucose), the MB-SBR achieved a TN removal efficiency of 66.74%. Bucci et al. (2024) developed an algal-bacterial granular system in an SBR for the aerobic treatment of cheese whey wastewaters. The system was continuously illuminated using light-emitting diodes (LED) and exhibited COD, ammonia and inorganic nitrogen removal rates of 100, 94, and 30%, respectively, without aeration. Li et al. (2023) investigated nitrogen removal in six enclosed, open and aerated reactors. Under oxygen-limited and glucose-sufficient conditions, with a 12-h light phase (5,000 ± 500 lux) followed by a 12-h dark phase, the algal-bacterial consortium achieved enhanced TN removal of 74.6%. However, in this study, without aeration and external organic carbon, TN removal efficiency of 95% was achieved in the IFBBR with the illumination of weak light.

In order to explore the interactions between microalgae, nitrifiers and denitrifiers during 240 days of operation, alkalinity and sCOD were monitored. The temporal variations of ΔAlk. value, shown in Figure 3a, were used to evaluate the activity of nitrification, denitrification and microalgal ammonia assimilation in this work. Theoretically, nitrification consumes 7.14 g $CaCO_3$/g NH_4^+-$N_{oxidized}$ while denitrification generates 3.57 g $CaCO_3$/g $N_{reduced}$ (Tchobanoglous et al., 2014). In addition, microalgal ammonia assimilation consumes 3.57 $CaCO_3$/g NH_4^+-$N_{assimilated}$. During Phases I and II, the ΔAlk. remained above 200 mg $CaCO_3$/L, suggesting that denitrification was the dominant nitrogen removal pathway. However, with the TN removal at approximately 100 mg/L in Phases I and II, the Alk. generated by denitrifiers should be around 357 mg $CaCO_3$/L, greater

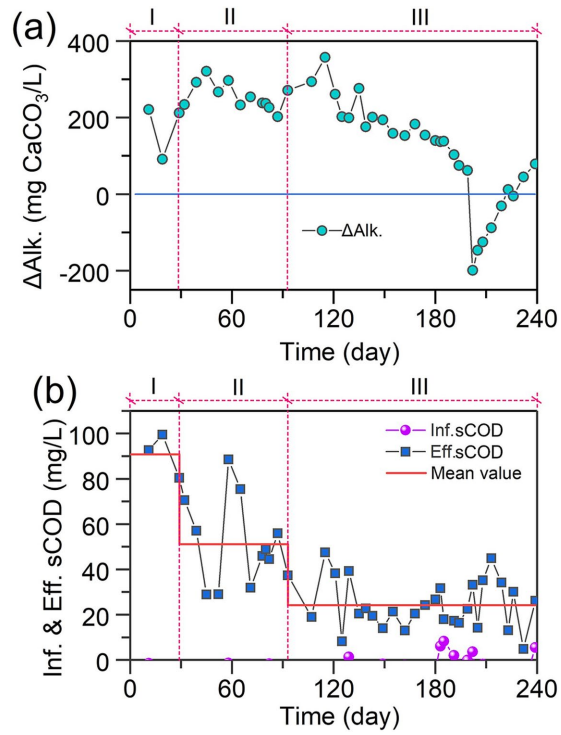

FIGURE 3
Temporal variations of **(a)** ΔAlk and **(b)** sCOD in IFBBR.

than the real ΔAlk. value (approximately 260 mg $CaCO_3$/L), this can be due to the presence of nitrifiers and microalgae which consumed the Alk. from day 121 to day 190, there was a sustained decline of ΔAlk., indicating that the increase of NLR led to a significant growth of nitrifiers and microalgae. Interestingly, as shown in Figure 2b, after day 121, TN removal efficiency kept increasing, suggesting the growth of denitrifiers. Results further indicated that with the growth of nitrifiers and microalgae, denitrifiers grew simultaneously.

Figure 3b shows the temporal variations of sCOD in influent and effluent during 240 days of operation. Except for a few instances (day 129, 183,185,191, 202) in which microalgae grew in the feed tank, the sCOD in influent remained at 0 throughout the rest of the time. Previous study found that the sCOD could be contributed by ammonia nitrogen (0.45 mg COD/ mg NH_4^+-N), and nitrite nitrogen (1.24 mg COD/mg NO_2^--N), as shown in Supplementary Figure 1. However, even after subtracting the sCOD contributions from ammonia and nitrite nitrogen, the effluent still exhibited a relatively high sCOD level. Results indicate that organic carbon was generated inside the IFBBR, while some microorganisms such as microalgae could convert the inorganic carbon into organic carbon. Additionally, the effluent sCOD values in Phase III were lower than those in Phase II (26 ± 12 mg/L vs. 52 ± 21 mg/L), potentially due to the enhancement of denitrification as reflected by the aforementioned increase in TN removal efficiency.

The results above indicate that during the 240 days of operation, nitrification and denitrification occurred simultaneously due to the growth and accumulation of microalgae at the bottom wall of the IFBBR. Especially from day 121 to day 190, the notable improvement in ammonia nitrogen and TN removal performance revealed the enhancement of nitrification and denitrification. Generally, microalgae contribute to nitrogen removal in two ways: directly assimilating ammonia nitrogen (Gu et al., 2021; Lu et al., 2022) and synergistically increasing the activity of bacteria.

Microalgae provided the necessary O_2 and organic carbon for nitrification and denitrification, while bacteria supplied CO_2 to microalgae (Yan et al., 2022). In addition, microalgae can influence the composition and characteristics of EPS, with weak light entering through the observation window, both microalgae and bacteria grew on the smooth wall at the bottom of the IFBBR. In summary, enhanced nitrogen removal was first achieved in the IFBBR without external air and organic carbon source by coupling the SND with microalgal photoautotrophic assimilation.

3.2 Microbial activities in the IFBBR

The results of in-situ batch tests for nitrogen removal performance, shown in Figure 4, indicate the simultaneous presence of nitrifiers, denitrifiers and microalgae. Interestingly, the concentrations of ammonia, nitrite, and nitrate nitrogen showed a significant and sustained decline even when the IFBBR was purged by nitrogen gas and sealed after each sample collection. In addition, the only carbon-containing substance in the initial solutions was HCO_3^-. The O_2 required for nitrification and the organic carbon required for denitrification were generated within the IFBBR, possibly due to the presence of microalgae. Moreover, as apparent from Figure 4, the SNRR of NH_4^+ -N, NO_2^- -N, NO_3^- -N, calculated from the slope of nitrogen concentration over time were 3.17, 3.31, and 1.17 mg/L·h, respectively. In addition, the SNRR of TN in the three batch tests were 2.03, 1.85, and 0.6 mg/L·h, respectively, indicating the nitrogen can be removal within the HRT of 48 h. In the third batch test, which focused on nitrate nitrogen removal, the NO_3^- -N removal rate was significantly slower and most parameters remained stable in the final hours. This could be attributed to the DO accumulation in the absence of nitrification and the slow decay of microalgae and nitrifiers. The in-situ batch tests further confirmed the simultaneous occurrence of nitrification and denitrification within the IFBBR, in which SND was coupled with microalgal photoautotrophic assimilation. Microalgae generated the necessary O_2 and organic carbon for nitrification and denitrification.

3.3 Microbial community analysis

3.3.1 Distribution of eukaryotic community

The analysis of the eukaryotic community (Figure 5b) indicated that *Trebouxiophyceae* was the dominant genus accounting for 99.04% of the total eukaryotic community in S_p and 99.26% in S_w. *Trebouxiophyceae* is green microalgae that has high ammonium tolerance (Díaz et al., 2024). The remaining eukaryote belongs to the genus of *Chlorophyceae*. Both *Trebouxiophyceae* and *Chlorophyceae* belong to the phylum *Chlorophyta* (Figure 5a), which has the capability of autotrophic photosynthetic growth with inorganic substrates or heterotrophic growth by organic substrates assimilation (Jin et al., 2023).

The seed sludge used in the previous SBR was the TWAS, which was environmental sample that could contain bacteria and microalgae.

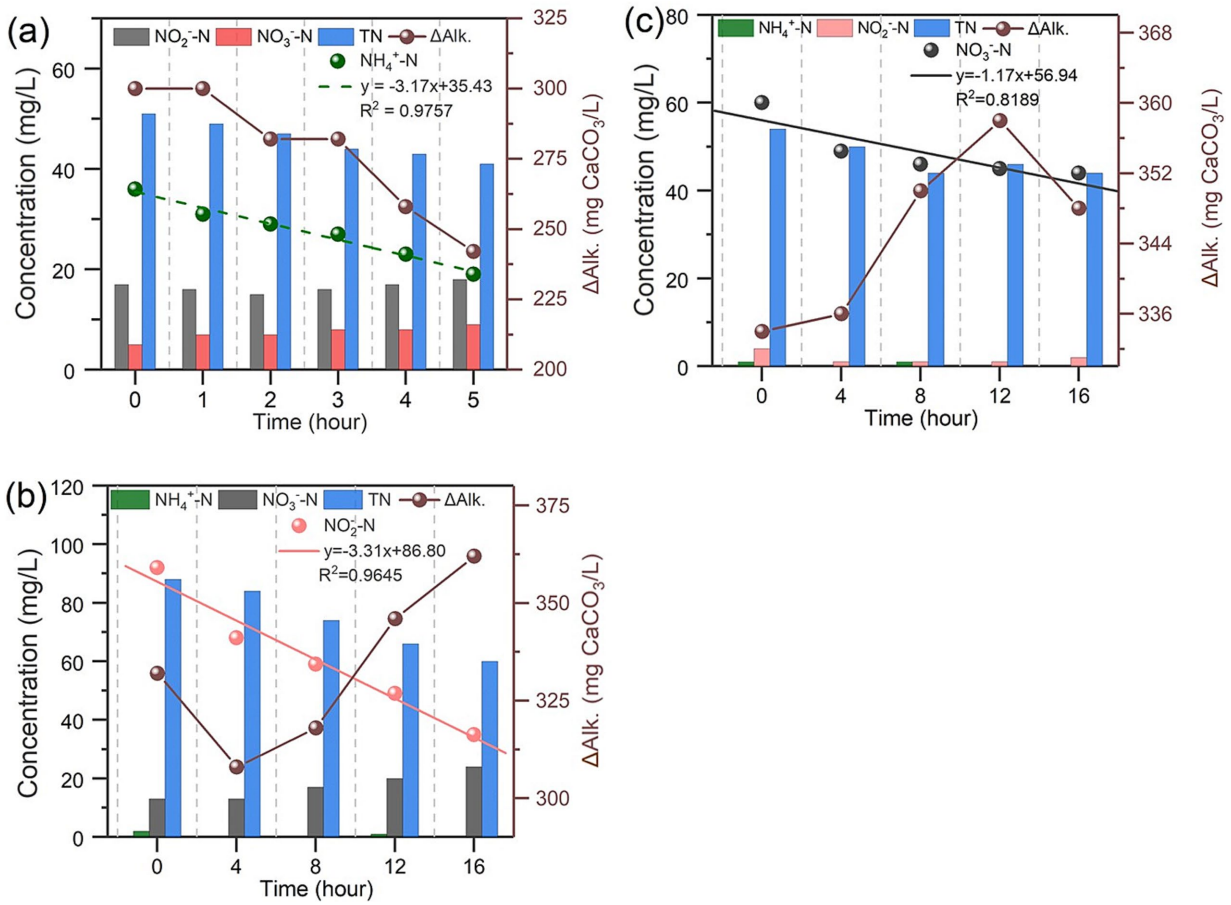

FIGURE 4
Nitrogen removal performance of IFBBR in Microbial Activities batch tests **(a)** First batch test (Ammonia); **(b)** Second batch test (Nitrite); **(c)** Third batch test (Nitrate).

During the 240 days of operation in the IFBBR, microalgae grew and accumulated in the IFBBR. Microalgae can influence the composition and characteristics of EPS (Jin et al., 2023), allowing biofilm to accumulate on the smooth surface of the wall. In the microalgal-bacterial symbiosis system, microalgae can capture CO_2 dissolved in water or released by bacteria and then produce O_2 for bacterial growth (Lu et al., 2022). Meanwhile, organic carbon synthesized by microalgae could serve as the electron donor for bacteria (Wang et al., 2015). Microalgae can also absorb growth-promoting substances by bacteria (Huang et al., 2022) and affect bacterial metabolism through signaling communication (Wu et al., 2024), which promotes the growth of both microalgae and bacteria.

3.3.2 Distribution of prokaryotic communities

Figure 5c illustrates the prokaryotic community in two different areas (particle and wall) in the IFBBR at the phylum, the top three dominant phyla in S_p and S_w were identical, namely *Bacteroidota*, *Proteobacteria* and *Chloroflexi*. The relative abundance of *Bacteroidota* was 41% in S_p and 10% in S_w, which is commonly found in WWTPs (Zhang H. et al., 2021). *Proteobacteria* had a high relative abundance in both S_p and S_w, 35 and 33%, respectively. Many kinds of microorganisms belonging to *Proteobacteria* and *Bacteroidota* are related to the removal of nitrogenous compounds by denitrification (Yang et al., 2024; Zhang G. et al., 2024).

The relative abundance of *Chloroflexi* in S_w was higher than that in S_p (41% vs. 10%). *Chloroflexi* is typically a filamentous bacterium with extremely diverse nutritional methods including photoautotrophy, chemoautotrophy, photoheterotrophy, and chemoheterotrophy (Davis et al., 2011; Thiel et al., 2019). *Chloroflexi* is well-adapted to anaerobic environments and exhibits light orientation, serving as a bridge for sludge flocs and facilitating the formation of microalgal-bacterial symbiosis systems (Johnston et al., 2019). This may be the reason that the *Chloroflexi* abundance on the wall was more than that on the particle, and it could also confirm that an anoxic microenvironment existed in the IFBBR.

In addition, *Chloroflexi* is commonly found in BNR processes. Members of this phylum are also capable of inorganic CO_2 fixation, aerobic nitrite oxidation, and nitrate reduction (Narsing Rao et al., 2022). Several publications have highlighted the significant role of *Chloroflexi* in autotrophic systems (Chu et al., 2015), in which they degrade complex compounds such as polysaccharides and proteins, and even utilize the decaying bacteria cell materials to generate energy through chlorophyll-mediated photosynthesis (Zhu et al., 2024).

Figure 5d presents the bacterial community diversity and richness at the genus level. The abundances of *Ignavibacterium* (40% vs. 1%), *Lautropia* (17% vs. 2%), *Dechloromonas* (4% vs. 0%) in S_p are much greater than those in S_w. While the abundances of *Limnobacter* (6% vs. 17%), *Arenimonas* (1% vs. 6%), *Truepera* (3% vs. 0.2%) in S_p are much

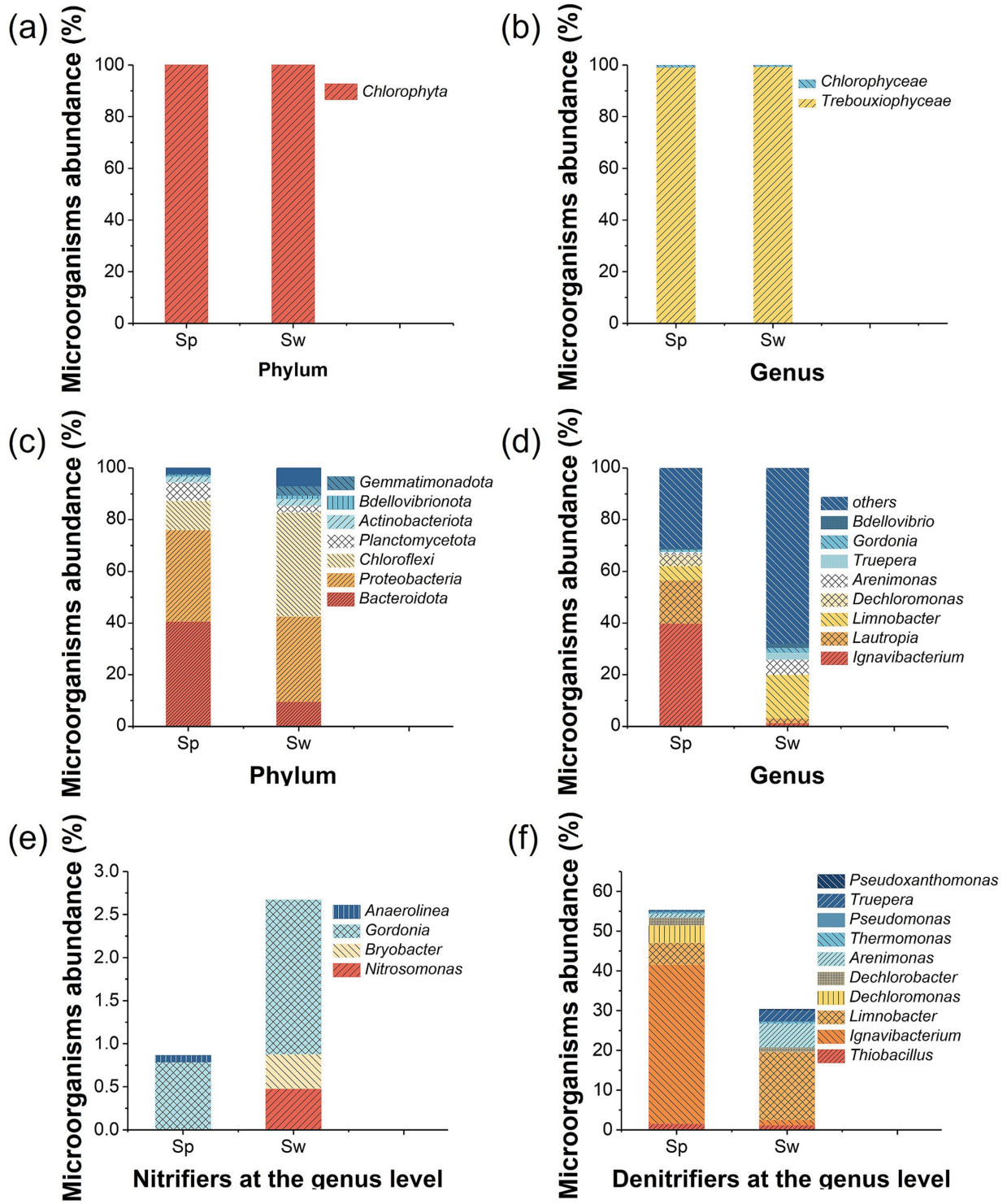

FIGURE 5
Relative abundance of microalgae and bacteria on particles (Sp) and the wall (Sw) in the IFBBR. **(a)** Eukaryotic community at phylum level; **(b)** Eukaryotic community at genus level; **(c)** Prokaryotic community at phylum level; **(d)** Prokaryotic community at genus level; **(e)** Nitrifiers at genus level; **(f)** Denitrifiers at genus level.

lower than those in S_w. As can be seen in Figure 5e, even if the relative abundance of nitrifiers in S_p and S_w was low, AOB and NOB were present in both two areas. *Gordonia* (0.8% in S_p vs. 1.8% in S_w) belongs to NOB (Zhang et al., 2023). Interestingly, some species of *Gordonia*, such as *polyisoprenivorans*, are capable of degrading organic pollutants (Wang et al., 2023). *Bryobacter* (0.0% in S_p vs. 0.4% in S_w) and *Nitrosomonas* (0.0% in S_p vs. 0.5% in S_w) which are AOB (Liu et al., 2024), were only present on the wall of the IFBBR. Moreover, another research indicated that *Anaerolinea* (0.1% in S_p vs. 0.0% in S_w) was the primary AOB in the microbial electrolysis cells, used for wastewater

nitrification (Yang et al., 2024). Overall, the relative abundance of AOB and NOB in S_w was higher than that in S_p, which may be due to the microalgae on the wall generating O_2 and nutrients, creating the necessary microaerobic environment and further promoting the growth of nitrifiers, as evidenced by the results in Section 3.1.

Figure 5f presents the relative abundance of denitrifiers at the genus level. *Ignavibacterium* (40.0%), *Limnobacter* (5.5%) and *Dechloromonas* (4.4%) were dominant in S_p, while *Limnobacter* (17.1%), *Arenimonas* (6.0%) and *Truepera* (2.8%) were dominant in S_w. *Ignavibacterium* and *Truepera* are common heterotrophic denitrifiers (Chen et al., 2024; Li et al., 2022). *Arenimonas* belongs to denitrifiers and Egbadon et al. (2024) suggested it was active in a microaerobic bioreactor. In addition, as shown in Figure 5d, *Lautropia*, a heterotrophic denitrifier (Sun et al., 2018; Zhuang et al., 2024), had a higher abundance in S_p than in S_w (16.9% vs. 1.9%). The different distribution of these bacteria may be due to varying microenvironments. Microalgae on the wall generated O_2 which could inhibit the activity of a significant proportion of denitrifying bacteria. *Limnobacter* is a denitrifier with the capability of SO_4^{2-} reduction (Wang et al., 2024). *Thiobacillus* (1.6% in S_p and 1.24% in S_w) is known as a sulfur-based autotrophic denitrifying bacterium (Peng et al., 2021). By reducing SO_4^{2-} in the nutrient solution, *Limnobacter* could supply reduced sulfur to *Thiobacillus*, facilitating sulfur-based autotrophic denitrification in the IFBBR.

Microbial community analysis further confirmed the existence of microalgae, nitrifiers and denitrifiers. Autotrophic nitrifiers and heterotrophic denitrifiers were the major nitrogen removal bacteria. O_2 required for nitrification and organic carbon required for denitrification could be generated by microalgae. Meanwhile, anoxic/aerobic microenvironments were created, leading to the different distribution of nitrifiers and denitrifiers. In summary, microalgae played an important role in the IFBBR: preferentially assimilating ammonia nitrogen and promoting SND. Due to the coupling of SND with microalgal photoautotrophic assimilation, a novel microalgal-bacterial symbiosis system was first realized in the IFBBR without aeration and external organic carbon. This study might provide a new solution to achieve efficient nitrogen removal while reducing energy usage, operating cost, and CO_2 release for WWTPs.

3.4 Results of C-N-O dynamic balance model

To elucidate the nitrogen removal pathway and the mechanisms of O_2 and organic carbon generation, a C-N-O dynamic balance model was developed based on the reaction chemical formulae and theoretical parameters of microalgae and bacteria. In combination with the experimental water quality data (Supplementary Table 2), when the TN removal efficiency stabilized above 90%, the results of the C-N-O dynamic balance model were established, as shown in Figure 6. These results illustrate the mass balances of NH_4^+-N, NO_2^--N, NO_3^--N, O_2 and organic carbon (OC).

As mentioned in Section 3.1 and further confirmed in Section 3.3, microalgae were present in the IFBBR. Figures 6a–c illustrate the mass balances of NH_4^+-N, NO_2^--N, NO_3^--N, respectively. In the IFBBR, there were two possible mechanisms for NH_4^+-N removal: nitritation (AOB, 47.58 mg N/L) and microalgae assimilation (9.42 mg N/L) (Zhang H. et al., 2021). Nitrite nitrogen could be generated by nitritation (AOB) and denitratation (DN_3), while consumed by nitratation (NOB, 0.82 mg N/L) and denitritation (DN_2, 150.58 mg N/L). Nitrate nitrogen could be generated by nitratation (NOB) and consumed by denitratation (DN_3, 16.82 mg N/L). Figures 6d,e illustrate the mass balances of O_2 and

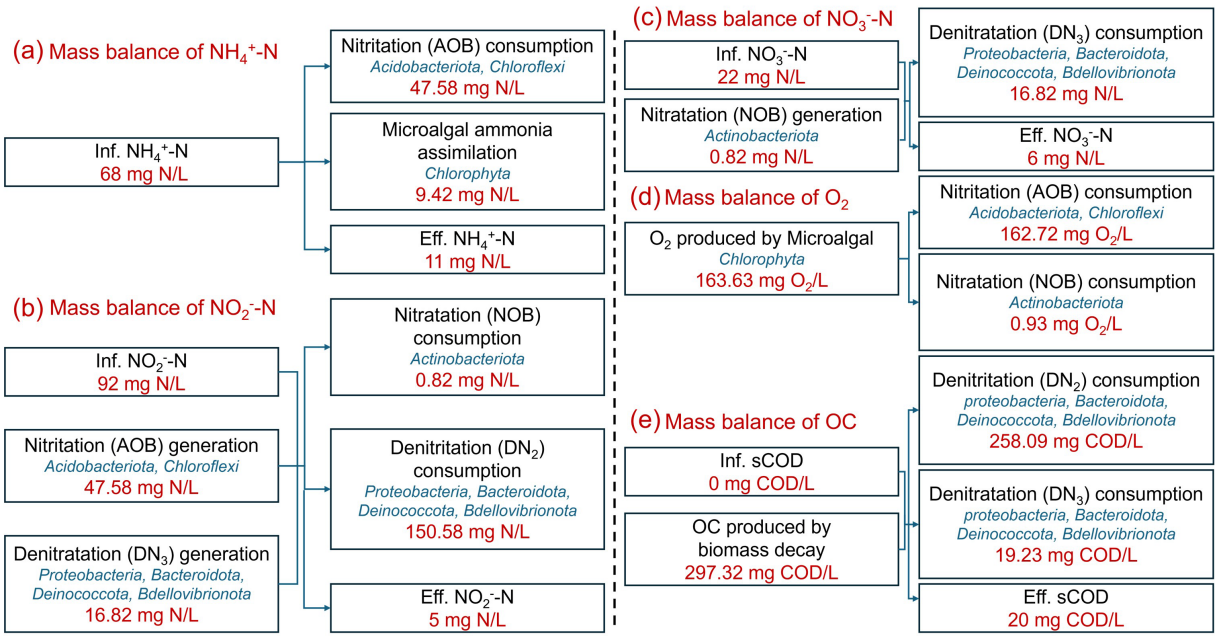

FIGURE 6
Mass balances of NH_4^+-N **(a)**, NO_2^--N **(b)**, NO_3^--N **(c)**, O_2 **(d)**, and organic carbon (OC) **(e)** in IFBBR.

COD, respectively. O_2 (163.63 mg/L) was generated by microalgae (Yan et al., 2022) and consumed by AOB (162.72 mg/L) and NOB (0.93 mg/L). COD was produced by microbial biomass decay (297.32 mg/L) and consumed by DN_2 (258.09 mg COD/L) and DN_3 (19.23 mg COD/L).

The C-N-O dynamic balance model further explained the interactions between microalgae, nitrification and denitrification in the IFBBR. The calculations and coefficients in the model were derived from alkalinity variation, reaction stoichiometry and theoretical parameters of microalgae nitrogen assimilation, nitrification and denitrification. Consequently, this model can be widely applied to various nitrification and denitrification reactors with or without the microalgae. However, for large-scale implementation and practical applications, the model parameters should be appropriately adjusted t depending on specific operational conditions.

4 Conclusion

To address the challenges of aeration and external organic carbon requirements in BNR process, this study successfully achieved enhanced nitrogen removal without aeration or external organic carbon. The innovative integrated IFBBR system, combining SND with photoautotrophic assimilation, was rapidly started up in 11 days and maintained stable operation for 240 days with weak light. During the stable period following the rapid startup, the TN removal efficiency of the IFBBR stabilized at 72 ± 2%. After the influent NLR increased from 0.07 to 0.09 kg N/m^3·d on day 88, nitrogen removal performance was further enhanced since day 121, the ammonia nitrogen removal rate showed a continuous upward trend. On day 190, with an HRT of 48 h, the ammonia nitrogen removal rate approached 100%, achieving a TN removal rate as high as 95%. Microbial community analysis confirmed the presence of microalgae and identified autotrophic nitrifiers and heterotrophic denitrifiers as the primary bacteria groups responsible for nitrogen removal. Furthermore, a C-N-O dynamic balance model was developed to provide a quantitative understanding of the interactions between microalgae and bacteria. O_2 required for nitrification was generated by microalgae at a rate of 81.82 mg/L·d, while organic carbon required for denitrification originated from microbial biomass decay at a rate of 148.66 mg/L·d. This study provides a novel efficient nitrogen removal technology to minimize energy consumption, operating cost and CO_2 emissions in BNR processes. Future research should focus on the performance of nitrogen removal with photoautotrophic assimilation in a scale-up IFBBR for the real WWTPs.

Data availability statement

The original contributions presented in the study are included in the article/Supplementary material, further inquiries can be directed to the corresponding authors.

Author contributions

XZ: Conceptualization, Data curation, Formal analysis, Investigation, Methodology, Validation, Visualization, Writing – original draft. RL: Formal analysis, Investigation, Methodology, Writing – review & editing. KL: Data curation, Resources, Visualization, Writing – review & editing. JS: Data curation, Methodology, Writing – review & editing. KW: Resources, Visualization, Writing – review & editing. YS: Methodology, Resources, Writing – review & editing. ZH: Methodology, Resources, Writing – review & editing. JZ: Conceptualization, Project administration, Resources, Supervision, Writing – review & editing. ZP: Conceptualization, Funding acquisition, Project administration, Supervision, Writing – review & editing. GN: Conceptualization, Funding acquisition, Project administration, Supervision, Writing – review & editing.

Funding

The author(s) declare that financial support was received for the research and/or publication of this article. This work was supported by the National Key Research and Development Program of China (2019YFE0117200) and Program of the China Scholarship Council (Grant No. 202108330355).

Conflict of interest

The authors declare that the research was conducted in the absence of any commercial or financial relationships that could be construed as a potential conflict of interest.

Generative AI statement

The authors declare that no Gen AI was used in the creation of this manuscript.

Publisher's note

Supplementary material

The Supplementary material for this article can be found online at: https://www.frontiersin.org/articles/10.3389/fmicb.2025.1591974/full#supplementary-material

References

Abouhend, A. S., McNair, A., Kuo-Dahab, W. C., Watt, C., Butler, C. S., Milferstedt, K., et al. (2018). The oxygenic photogranule process for aeration-free wastewater treatment. *Environ. Sci. Technol.* 52, 3503–3511. doi: 10.1021/acs.est.8b00403

Alzate Marin, J. C., Caravelli, A. H., and Zaritzky, N. E. (2016). Nitrification and aerobic denitrification in anoxic-aerobic sequencing batch reactor. *Bioresour. Technol.* 200, 380–387. doi: 10.1016/j.biortech.2015.10.024

Andalib, M., Nakhla, G., and Zhu, J. (2012). High rate biological nutrient removal from high strength wastewater using anaerobic-circulating fluidized bed bioreactor (A-CFBBR). *Bioresour. Technol.* 118, 526–535. doi: 10.1016/j.biortech.2012.05.068

Aparicio, S., Borras Falomir, L., Jimenez Benítez, A., Seco, A., and Robles, A. (2024). Urban wastewater treatment at ambient conditions using microalgae-bacteria consortia in a membrane high-rate algal pond (MHRAP): the effect of hydraulic retention time and influent strength. *Environ. Technol. Innov.* 36:103846. doi: 10.1016/j.eti.2024.103846

Apprill, A., McNally, S., Parsons, R., and Weber, L. (2015). Minor revision to V4 region SSU rRNA 806R gene primer greatly increases detection of SAR11 bacterioplankton. *Aquat. Microb. Ecol.* 75, 129–137. doi: 10.3354/ame01753

APHA (2012). Standard methods for the examination of water and wastewater. American Public Health Association (APHA), Washington, DC, USA.

Bucci, P., Montero, E. J. M., García Depraect, O., Zaritzky, N., Caravelli, A., and Munoz, R. (2024). Assessment of the performance of a symbiotic microalgal-bacterial granular sludge reactor for the removal of nitrogen and organic carbon from dairy wastewater. *Chemosphere* 351:141250. doi: 10.1016/j.chemosphere.2024.141250

Chen, W., Qin, S., Yang, C., Long, K., Liang, S., Liu, H., et al. (2024). Bioaugmentation using salt-tolerant bacteria in a dual-stage process for high-salinity wastewater treatment: performance, microbial community, and salt-tolerance mechanism. *J. Water Process. Eng.* 57:104620. doi: 10.1016/j.jwpe.2023.104620

Chowdhury, M. M. I., and Nakhla, G. (2022). Enhanced mainstream nitrogen removal from synthetic wastewater using gel-immobilized anammox in fluidized bed bioreactors: process performance and disintegration mechanisms. *Sci. Total Environ.* 811:151373. doi: 10.1016/j.scitotenv.2021.151373

Chu, Z., Wang, K., Li, X., Zhu, M., Yang, L., and Zhang, J. (2015). Microbial characterization of aggregates within a one-stage nitritation-anammox system using high-throughput amplicon sequencing. *Chem. Eng. J.* 262, 41–48. doi: 10.1016/j.cej.2014.09.067

Davis, K. E. R., Sangwan, P., and Janssen, P. H. (2011). *Acidobacteria*, *Rubrobacteridae* and *Chloroflexi* are abundant among very slow-growing and mini-colony-forming soil bacteria. *Environ. Microbiol.* 13, 798–805. doi: 10.1111/j.1462-2920.2010.02384.x

Díaz, V., Maza Márquez, P., Antiñolo, L., Poyatos, J. M., Martín Pascual, J., and Muñío, M. D. M. (2024). Effect of urban wastewater ratio in the influent of a membrane photobioreactor for microalgae cultivation and nutrient removal. *J. Environ. Chem. Eng.* 12:112527. doi: 10.1016/j.jece.2024.112527

Egbadon, E. O., Wigley, K., Nwoba, S. T., Carere, C. R., Weaver, L., Baronian, K., et al. (2024). Microaerobic methane-driven denitrification in a biotrickle bed-investigating the active microbial biofilm community composition using RNA-stable isotope probing. *Chemosphere* 346:140528. doi: 10.1016/j.chemosphere.2023.140528

Gu, Z., Liu, Y., Zou, G., Zhang, Q., Lu, R., Yan, H., et al. (2021). Enhancement of nutrients removal and biomass accumulation of *Chlorella vulgaris* in pig manure anaerobic digestate effluent by the pretreatment of indigenous bacteria. *Bioresour. Technol.* 328:124846. doi: 10.1016/j.biortech.2021.124846

Gu, Z., Yan, H., Zhang, Q., Wang, Y., Liu, C., Cui, X., et al. (2024). Elimination of copper obstacle factor in anaerobic digestion effluent for value-added utilization: performance and resistance mechanisms of indigenous bacterial consortium. *Water Res.* 252:121217. doi: 10.1016/j.watres.2024.121217

Huang, Q., Yan, H., Liu, Y., Cui, X., Wang, Y., Yu, Z., et al. (2022). Effects of microalgae-bacteria inoculation ratio on biogas slurry treatment and microorganism interactions in the symbiosis system. *J. Clean. Prod.* 362:132271. doi: 10.1016/j.jclepro.2022.132271

Jin, Y., Zhan, W., Wu, R., Han, Y., Yang, S., Ding, J., et al. (2023). Insight into the roles of microalgae on simultaneous nitrification and denitrification in microalgal-bacterial sequencing batch reactors: nitrogen removal, extracellular polymeric substances, and microbial communities. *Bioresour. Technol.* 379:129038. doi: 10.1016/j.biortech.2023.129038

Johnston, J., LaPara, T., and Behrens, S. (2019). Composition and dynamics of the activated sludge microbiome during seasonal nitrification failure. *Sci. Rep.* 9:4565. doi: 10.1038/s41598-019-40872-4

Li, J., Li, Y., Chen, P., Sathishkumar, K., Lu, Y., Naraginti, S., et al. (2022). Biological mediated synthesis of reduced graphene oxide (rGO) as a potential electron shuttle for facilitated biological denitrification: insight into the electron transfer process. *J. Environ. Chem. Eng.* 10:108225. doi: 10.1016/j.jece.2022.108225

Li, Q., Xu, Y., Liang, C., Peng, L., and Zhou, Y. (2023). Nitrogen removal by algal-bacterial consortium during mainstream wastewater treatment: transformation mechanisms and potential N_2O mitigation. *Water Res.* 235:119890. doi: 10.1016/j.watres.2023.119890

Liu, F., Xu, H., Shen, Y., Li, F., and Yang, B. (2024). Rapid start-up strategy and microbial population evolution of anaerobic ammonia oxidation biofilm process for low-strength wastewater treatment. *Bioresour. Technol.* 394:130201. doi: 10.1016/j.biortech.2023.130201

Lu, R., Yan, H., Liu, Y., Wang, Y., Cui, X., Wu, X., et al. (2022). Enhancement of nutrients recovery and cell metabolism in piggery anaerobic digestate by the co-cultivation of indigenous microalgae and bacteria. *J. Clean. Prod.* 375:134193. doi: 10.1016/j.jclepro.2022.134193

Luan, Y. N., Yin, Y., Xu, Y., Zhang, F., Wang, X., Zhao, F., et al. (2023). Simultaneous nitrification and denitrification in a novel rotating self-aerated biofilm reactor for decentralized wastewater treatment. *Bioresour. Technol.* 369:128513. doi: 10.1016/j.biortech.2022.128513

Maheepala, S. S., Hatamoto, M., Mitsuishi, Y., Watari, T., and Yamaguchi, T. (2023). A syphon-downflow hanging sponge (DHS) reactor for improving the denitrification efficiency of sewage water treatment. *Environ. Technol. Innov.* 31:103205. doi: 10.1016/j.eti.2023.103205

Manser, N. D., Wang, M., Ergas, S. J., Mihelcic, J. R., Mulder, A., Van De Vossenberg, J., et al. (2016). Biological nitrogen removal in a photosequencing batch reactor with an algal-nitrifying bacterial consortium and anammox granules. *Environ. Sci. Tech. Let.* 3, 175–179. doi: 10.1021/acs.estlett.6b00034

Narsing Rao, M. P., Luo, Z. H., Dong, Z. Y., Li, Q., Liu, B. B., Guo, S. X., et al. (2022). Metagenomic analysis further extends the role of *Chloroflexi* in fundamental biogeochemical cycles. *Environ. Res.* 209:112888. doi: 10.1016/j.envres.2022.112888

Nelson, M. J., Nakhla, G., and Zhu, J. (2017). Fluidized-bed bioreactor applications for biological wastewater treatment: a review of research and developments. *Engineering* 3, 330–342. doi: 10.1016/J.ENG.2017.03.021

Peng, C., Fan, X., Xu, Y., Ren, H., and Huang, H. (2021). Microscopic analysis towards rhamnolipid-mediated adhesion of *Thiobacillus denitrificans*: a QCM-D study. *Chemosphere* 271:129539. doi: 10.1016/j.chemosphere.2021.129539

Peng, S., Kong, Q., Deng, S., Xie, B., Yang, X., Li, D., et al. (2020). Application potential of simultaneous nitrification/Fe^0-supported autotrophic denitrification (SNAD) based on iron-scraps and micro-electrolysis. *Sci. Total Environ.* 711:135087. doi: 10.1016/j.scitotenv.2019.135087

Sun, Y., Guan, Y., Zeng, D., He, K., and Wu, G. (2018). Metagenomics-based interpretation of AHLs-mediated quorum sensing in Anammox biofilm reactors for low-strength wastewater treatment. *Chem. Eng. J.* 344, 42–52. doi: 10.1016/j.cej.2018.03.047

Svehla, P., Michal, P., Benakova, A., Hanc, A., and Tlustos, P. (2023). Nitrification of the liquid phase of digestate: the transfer of the process from laboratory to pilot plant and full scale conditions. *Environ. Technol. Innov.* 30:103084. doi: 10.1016/j.eti.2023.103084

Tang, C. C., Tian, Y., He, Z. W., Zuo, W., and Zhang, J. (2018). Performance and mechanism of a novel algal-bacterial symbiosis system based on sequencing batch suspended biofilm reactor treating domestic wastewater. *Bioresour. Technol.* 265, 422–431. doi: 10.1016/j.biortech.2018.06.033

Tariq, A., Hansen, L. V., Brændholt, A., Jensen, L. S., and Bruun, S. (2025). Assessing nitrous oxide mitigation efficiency of three nitrification inhibitors with synthetic and organic fertilisers in eastern Denmark. *Environ. Technol. Innov.* 37:103952. doi: 10.1016/j.eti.2024.103952

Tchobanoglous, G., Stensel, H. D., Tsuchihashi, R., and Burton, F. (2014). Wastewater engineering: Treatment and resource recovery. New York: McGraw-Hill Education.

Thiel, V., Fukushima, S. I., Kanno, N., and Hanada, S. (2019). "Chloroflexi". in Encyclopedia of Microbiology (Fourth Edition), ed. T. M. Schmidt (New York, FL: Academic Press), 651–662.

Wang, H., Guan, F., Zhu, Y., Pan, Y., Liu, Q., Liu, Q., et al. (2023). Biofilm formation promoted biodegradation of polyethylene in *Gordonia polyisoprenivorans* B251 isolated from bacterial enrichment acclimated by hexadecane for two years. *Chemosphere* 344:140383. doi: 10.1016/j.chemosphere.2023.140383

Wang, H., He, X., Nakhla, G., Zhu, J., and Su, Y. K. (2020). Performance and bacterial community structure of a novel inverse fluidized bed bioreactor (IFBBR) treating synthetic municipal wastewater. *Sci. Total Environ.* 718:137288. doi: 10.1016/j.scitotenv.2020.137288

Wang, L., Hu, Z., Hu, M., Zhao, J., Zhou, P., Zhang, Y., et al. (2022). Cometabolic biodegradation system employed subculturing photosynthetic bacteria: a new degradation pathway of 4-chlorophenol in hypersaline wastewater. *Bioresour. Technol.* 361:127670. doi: 10.1016/j.biortech.2022.127670

Wang, J., Song, C., Huo, L., Wang, X., Liu, H., and Zhang, X. (2024). Nitrogen removal performance and thermodynamic mechanisms of Feammox mediated by ferric pyrophosphate at various pHs. *J. Water Process Eng.* 58:104864. doi: 10.1016/j.jwpe.2024.104864

Wang, M., Yang, H., Ergas, S. J., and Van Der Steen, P. (2015). A novel shortcut nitrogen removal process using an algal-bacterial consortium in a photo-sequencing batch reactor (PSBR). *Water Res.* 87, 38–48. doi: 10.1016/j.watres.2015.09.016

Wu, X., Kong, L., Feng, Y., Zheng, R., Zhou, J., Sun, J., et al. (2024). Communication mediated interaction between bacteria and microalgae advances photogranulation. *Sci. Total Environ.* 914:169975. doi: 10.1016/j.scitotenv.2024.169975

Yan, H., Gu, Z., Zhang, Q., Wang, Y., Cui, X., Liu, Y., et al. (2024). Detoxification of copper and zinc from anaerobic digestate effluent by indigenous bacteria: mechanisms, pathways and metagenomic analysis. *J. Hazard. Mater.* 469:133993. doi: 10.1016/j.jhazmat.2024.133993

Yan, H., Lu, R., Liu, Y., Cui, X., Wang, Y., Yu, Z., et al. (2022). Development of microalgae-bacteria symbiosis system for enhanced treatment of biogas slurry. *Bioresour. Technol.* 354:127187. doi: 10.1016/j.biortech.2022.127187

Yang, X., Liao, Y., Zeng, M., and Qin, Y. (2024). Nitrite accumulation performance and microbial community of algal-bacterial symbiotic system constructed by *Chlorella* sp. and *Navicula* sp. *Bioresour. Technol.* 399:130638. doi: 10.1016/j.biortech.2024.130638

Ye, F., Yan, J., and Li, T. (2021). Analysis of municipal sewage pollution and denitrification treatment under low oxygen conditions. *Environ. Technol. Innov.* 21:101188. doi: 10.1016/j.eti.2020.101188

Zhang, H., Gong, W., Zeng, W., Chen, R., Lin, D., Li, G., et al. (2021). Bacterial-algae biofilm enhance MABR adapting a wider COD/N ratios wastewater: performance and mechanism. *Sci. Total Environ.* 781:146663. doi: 10.1016/j.scitotenv.2021.146663

Zhang, W., Guan, A., Peng, Q., Qi, W., and Qu, J. (2023). Microbe-mediated simultaneous nitrogen reduction and sulfamethoxazole/N-acetylsulfamethoxazole removal in lab-scale constructed wetlands. *Water Res.* 242:120233. doi: 10.1016/j.watres.2023.120233

Zhang, H., Li, G., Li, W., Li, Y., Zhang, S., and Nie, Y. (2024). Biochemical properties of sludge derived hydrothermal liquid products and microbial response of wastewater treatment. *Process Biochem.* 144, 294–305. doi: 10.1016/j.procbio.2024.06.007

Zhang, G., Li, W., Li, D., Wang, S., and Lv, L. (2024). Integration of ammonium assimilation with denitrifying phosphorus removal for efficient nutrient management in wastewater treatment. *J. Environ. Manag.* 353:120116. doi: 10.1016/j.jenvman.2024.120116

Zhang, F., Peng, Y., Wang, Z., Jiang, H., Ren, S., and Qiu, J. (2021). Achieving synergetic treatment of sludge supernatant, waste activated sludge and secondary effluent for wastewater treatment plants (WWTPs) sustainable development. *Bioresour. Technol.* 337:125416. doi: 10.1016/j.biortech.2021.125416

Zhang, Q., Yu, Z., Jin, S., Liu, C., Li, Y., Guo, D., et al. (2020). Role of surface roughness in the algal short-term cell adhesion and long-term biofilm cultivation under dynamic flow condition. *Algal Res.* 46:101787. doi: 10.1016/j.algal.2019.101787

Zheng, X., Zuo, J., Xu, S., Wang, J., Sun, F., Xie, Y., et al. (2024). Efficient partial denitrification-anammox process enabled by a novel denitrifier with truncated nitrite reduction pathway. *Environ. Technol. Innov.* 36:103830. doi: 10.1016/j.eti.2024.103830

Zhu, H., Liu, Y., Peng, Z., Liu, Q., Pan, X., and Yang, B. (2024). Enhanced nitrogen removal by an isolated aerobic denitrifying strain in a vertical-flow constructed wetland. *Chemosphere* 359:142131. doi: 10.1016/j.chemosphere.2024.142131

Zhuang, W., Tan, Z., Guo, Z., Liu, Q., Han, F., Xie, J., et al. (2024). Nitrogen metabolism network in the biotreatment combination of coking wastewater: Take the OHO process as a case. *Chemosphere.* 364:143025. doi: 10.1016/j.chemosphere.2024.143025

frontiers | Frontiers in Microbiology

TYPE Original Research
PUBLISHED 01 May 2025
DOI 10.3389/fmicb.2024.1437056

OPEN ACCESS

EDITED BY
Shuhao Huo,
Jiangsu University, China

REVIEWED BY
Chong Chen,
Yangzhou University, China
Dechun Chen,
Southwest Minzu University, China

*CORRESPONDENCE
Guo Aizhen
aizhen@mail.hzau.edu.cn

RECEIVED 23 May 2024
ACCEPTED 06 December 2024
PUBLISHED 01 May 2025

CITATION
Mingcheng W, Daoqi L, Huili X, Gailing W, Chaoying L, Yanan G and Aizhen G (2025) Multiomics-based analysis of the mechanism of ammonia reduction in *Sphingomonas*. *Front. Microbiol.* 15:1437056. doi: 10.3389/fmicb.2024.1437056

Multiomics-based analysis of the mechanism of ammonia reduction in *Sphingomonas*

Wang Mingcheng[1,2,3,4], Liu Daoqi[4], Xia Huili[4], Wang Gailing[4], Liu Chaoying[4], Guo Yanan[5] and Guo Aizhen[1,2,3]*

[1]Country National Laboratory of Agricultural Microbiology, Wuhan, Hubei, China, [2]Country College of Veterinary Medicine, Wuhan, Hubei, China, [3]Hubei Hongshan Laboratory, Huazhong Agricultural University, Wuhan, Hubei, China, [4]College of Biological and Food Engineering, Huanghuai University, Zhumadian, Henan, China, [5]Institute of Animal Science, Ningxia Academy of Agriculture and Forestry Sciences, Yinchuan, Ningxia, China

Ammonia is the primary component of malodorous substances in chicken farms. Currently, the microbial ammonia reduction is considered a potential method due to its low cost, high safety, and environmental friendliness. *Sphingomonas* sp. Z392 can significantly reduce the ammonia level in broiler coops. However, the mechanisms of ammonia nitrogen reduction by *Sphingomonas* sp. Z392 remain unclear. To explore the mechanisms of ammonia reduction by *Sphingomonas* sp. Z392, the transcriptome and metabolome analysis of *Sphingomonas* sp. Z392 under high ammonium sulfate level were conducted. It was found that the transcription levels of genes related to purine metabolism (*RS01720*, *RS07605*, *purM*, *purC*, *purO*) and arginine metabolism (*glsA*, *argB*, *argD*, *aguA*, *aguB*) were decreased under high ammonium sulfate environment, and the levels of intermediate products such as ornithine, arginine, IMP, and GMP also were also decreased. In addition, the *ncd2* gene in nitrogen metabolism was upregulated, and intracellular nitrite content increased by 2.27 times than that without ammonium sulfate. These results suggested that under high ammonium sulfate level, the flux of purine and arginine metabolism pathways in *Sphingomonas* sp. Z392 might decrease, while the flux of nitrogen metabolism pathway might increase, resulting in increased nitrite content and NH_3 release. To further verify the effect of the *ncd2* gene on ammonia removal, *ncd2* was successfully overexpressed and knocked out in *Sphingomonas* sp. Z392. *ncd2* Overexpression exhibited the most ammonia reduction capability, the ammonia concentration of *ncd2* overexpression group decreased by 43.33% than that of without *Sphingomonas* sp. group, and decreased by 14.17% than that of *Sphingomonas* sp. Z392 group. In conclusion, *Sphingomonas* sp. Z392 might reduce the release of NH_3 by reducing the flux of purine and arginine metabolisms, while enhancing ammonia assimilation to form nitrite. In this context, *ncd2* might be one of the key genes to reduce ammonia.

KEYWORDS

ammonia reduction, ncd2 gene, transcriptomics, metabolomics, *Sphingomonas* ammonia reduction by Sphingomonas

1 Introduction

The current environmental pollution in the livestock industry mainly comes from to feces, urine, sewage, noxious gases, noise, smoke, and dust (Ji et al., 2022), among them, the emission of malodor from livestock farms is also a major component of pollution in the animal husbandry industry. Studies have shown that large amounts of malodorous substances are generated during livestock farming and manure storage, posing a serious threat to both human and livestock health. These substances primarily include organic compounds, in addition to inorganic compounds, such as ammonia (NH_3) and hydrogen sulfide (H_2S), of which NH_3 is particularly common and directly harmful. High ammonia concentrations in chicken coops jeopardize both human and animal health.

Currently, ammonia removal measures in chicken coops mainly include physical, chemical, feed regulation, and biological methods (Zhou and Wang, 2023). Physical methods include enhanced mechanical ventilation in the coop and the addition of physical deodorisers to the diet, which are often costly (Lubensky et al., 2019). Chemical methods include the use of inorganic metal ions, compounds, and acidifying agents, which tend to generate secondary pollution (Haq et al., 2021; Nancharaiah et al., 2016). The use of probiotics in poultry farming offers a promising approach to reducing ammonia emissions, improving animal health, and potentially promoting more sustainable and environmentally friendly agricultural practices (Chen and Ni, 2012). Microbial treatment techniques are not only characterized by strong selectivity, low cost, simple operation, high safety, non-toxic by-products, and lack of secondary pollution but can also lead to reductions in various environmental pollutants, thus positioning them as the optimal choice for bioremediation (Pang and Wang, 2021; Zhou and Wang, 2023). Different microorganisms have been reported to improve feed conversion efficiency, reduce fecal nitrogen levels in animals, and contribute to ammonia emission reduction, such as *Bacillus subtilis*, *Clostridium butyricum*, *Acinetobacter* (Huang et al., 2013), *Pseudomonas* (Jin et al., 2015), and *Agrobacterium* (Chen and Ni, 2012). However, few studies characterizing ammonia nitrogen-removing bacterial strains and their mechanisms have been conducted. In addition, previous studies have shown that adding *Sphingomonas* to broiler chicken feed significantly reduces ammonia concentrations in chicken coops during breeding (Wang et al., 2021). However, the mechanism of ammonia nitrogen reduction by *Sphingomonas* remains unclear. Therefore, to investigate the mechanism of ammonia removal in *Sphingomonas*, the transcriptome and metabolome of *Sphingomonas* were analyzed under different ammonium sulfate conditions, and the key genes in *Sphingomonas* associated with the reduction of ammonia release were screened. Subsequently, the effect of these key genes on the ability of *Sphingomonas* to reduce ammonia release was further investigated.

2 Materials and methods

2.1 Strains, media, and culture conditions

Sphingomonas sp. Z392 (GenBank accession no: MN108136) were isolated and stored at the Institute of Biology and Food Engineering of Huanghuai University. *Escherichia coli* β2155 was used for plasmid amplification.

Sphingomonas sp. Z392 and *E. coli* β2155 were cultured in Luriae–Bertani (LB) medium at 37°C. The heterotrophic nitrification medium (medium B) contained 0.5 g $(NH_4)_2SO_4$, 5.62 g sodium succinate, and 50 mL Vicker's salt solution (5 g K_2HPO_4, 2.5 g $MgSO_4{\cdot}7H_2O$, 2.5 g NaCl, 0.05 g $FeSO_4{\cdot}7H_2O$, 0.05 g $MnSO_4{\cdot}4H_2O$, and 1 L distilled), distilled water 1.0 L. Moreover, media C and D were prepared by increasing the concentration of $(NH_4)_2SO_4$ in medium B to 0.66 g/L and 1.06 g/L, respectively.

2.2 Transcriptome and metabolomics analysis

Sphingomonas sp. Z392 was cultured in LB medium at 37°C for 24 h. The cells were harvested by centrifugation (3,000 × *g*, 10 min) and washed with sterile saline, and the cell pellet was inoculated into medium B, incubated at 37°C. Then, the cells collected from medium B were added to medium C, incubated at 37°C. Finally, the cells from medium C were collected, transferred to medium D, incubated at 37°C. The cells from medium D were used for transcriptome and metabolome analysis.

Total RNA of the cells from medium D was extracted, transcriptome sequencing was performed by Gene *DeNovo* (Guangzhou, China) (Love et al., 2014). To obtain significant differentially expressed genes (DEGs), DESeq2 software was used with FC ≥ 2 or ≤ 0.5 ($|\log2(FC)| > 1$) and $p < 0.05$ as screening conditions. Intracellular metabolites of the cells from medium D were detected by LC-MS, and metabolome were analyzed by Gene *DeNovo* (Guangzhou, China).

2.3 Strain construction

To screen antibiotics sensitive to *Sphingomonas* sp. Z392 as selection markers for genetic modification, the minimum inhibitory concentration (MIC) of gentamicin (Gm), streptomycin, and tetracycline against *Sphingomonas* sp. Z392 were determined. The experimental design for MIC using microplates were shown in Supplementary Tables 1, 2. For construction of *ncd2* gene overexpression plasmid, *ncd2* was amplified from the genomic DNA of Z392 strain. Then the PCR products were inserted into the expression plasmid p1600-gent-Flag with restriction sites *Nco*I and *Ecor*I through the Gibson assembly method, generating p1600-*ncd2*-Flag plasmid. The Z392 strain were transformed with 5 μg p1600-*ncd2*-Flag plasmid by electroporation (2.5kV/cm, 200 Ω , 5 ms).

To construct *ncd2* knockout strain, the targeting fragments (Δ*ncd2*:Gm) included the upstream and downstream homologous recombination arms of the *ncd2* gene, and were constructed by overlap PCR. Subsequently, The targeting fragment was cloned into the suicide plasmid pCVD442, resulting in the targeting plasmid pCVD442-Δ*ncd2*:Gm. The targeting vector pCVD442-Δ*ncd2*:Gm was then electrotransformed into the *E. coli* β2155 strain to generate the donor strain β2155/pCVD442-Δ*ncd2*:Gm. Finally, the *ncd2* gene knockout was achieved by conjugating the donor strain with the recipient strain (*Sphingomonas* sp. Z392), and the knockout of *ncd2* was verified by PCR.

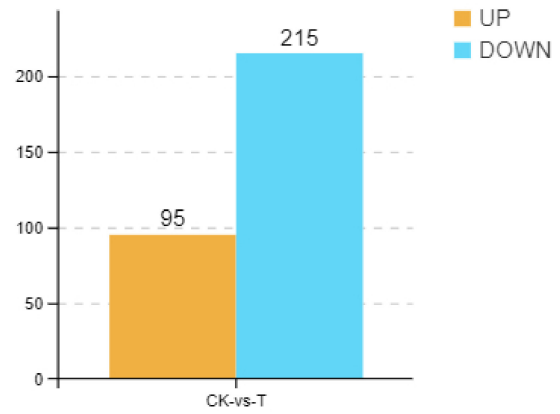

FIGURE 1
Differential expression genes of *Sphingomonas* sp. Z392 under high levels of ammonia sulfate. The *Y*-axis represents the number of up- and downregulated genes, orange represents upregulation, and blue represents downregulation.

2.4 Feeding and management of the experimental broiler chickens

A total of 1, 200 one- day-old Cobb broiler chickens with similar body weights (42 ± 2 g) were randomly divided into 4 groups: a control group (CK) without *Sphingomonas* sp. Z392, fed with *Sphingomonas* sp. Z392 group (WT), fed with Z392 OV*ncd2* group (OV), and fed with Z392 Δ*ncd2* (KO). The method refers to the research of Wang et al. (2021). At 7, 14, 21, 28, 35, and 42 days of age, fresh feces were collected from the broilers. The concentrations of total nitrogen, uric acid, ammonium nitrogen, and nitrate nitrogen in chicken manure were measured separately.

2.5 Nitrogen concentrations in chicken coops

The ammonia concentrations in the chicken coops were measured using an ammonia sensor (Bist et al., 2023). And total nitrogen, ammonia nitrogen, and nitrate nitrogen contents in chicken manure were measured (Such et al., 2023). Then, the determination of intracellular nitrite content was carried out using ion chromatography (Varão Moura et al., 2022).

2.6 Data and statistical analysis

All experiments were conducted in three biological replicates. The data were analyzed for statistical significance using SPSS 19.0 software. One-way analysis of variance (ANOVA) was used to express the significance of differences ($P \leq 0.05$) between the groups. Figures were drawn using the GraphPad Prism 8 (GraphPad Software, USA).

3 Results

3.1 Transcriptomics analysis of *Sphingomonas* sp. Z392 under high level of ammonium sulfate

Previous studies have demonstrated that *Sphingomonas* sp. Z392 can significantly reduce ammonia nitrogen level by converting ammonium nitrogen into nitrate nitrogen in chicken manure, decreasing the emission of ammonia from chicken feces. To explore the mechanisms of *Sphingomonas*

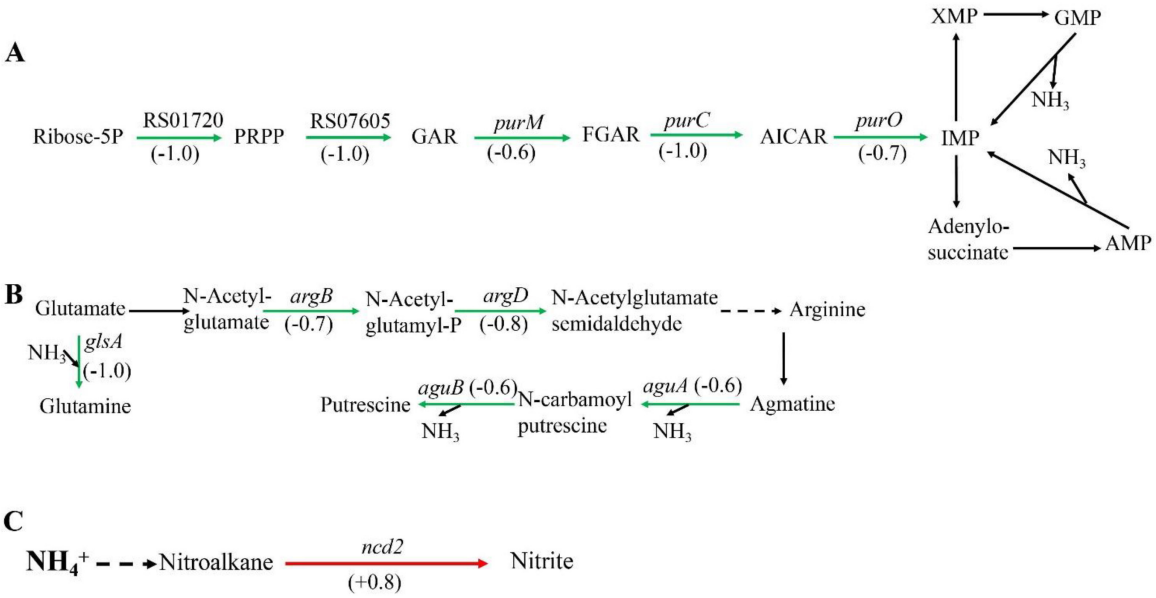

FIGURE 2
Significantly enriched metabolic pathways associated with ammonia degradation. **(A)** purine metabolism pathway. **(B)** Arginine metabolism pathway. **(C)** Nitrogen metabolism pathway. The green arrows indicate downregulation, and the red arrows indicate upregulation.

sp. Z392 in reducing ammonia release, in this paper, transcriptomics analysis of *Sphingomonas* sp. Z392 cultured under high ammonium sulfate condition was performed. As shown in Figure 1, a total of 310 differentially expressed genes (DEGs) were identified between the high ammonium sulfate group and the control group (CK_vs_T), including 95 upregulated genes and 215 downregulated genes. Subsequently, the metabolic pathways enriched by the DEGs were further analyzed. As shown in Supplementary Figure 1, the DEGs were involved in the following pathways: ribosome, photosynthesis, drug metabolism, biosynthesis of some antibiotics, purine metabolism, oxidative phosphorylation, biosynthesis of secondary metabolites, monobactam biosynthesis, VB_6 metabolism, pentose phosphate pathway, glutathione metabolism, cyanoamino acid metabolism, arginine biosynthesis, arginine and proline metabolism, amino acid biosynthesis, and nitrogen metabolism.

Among the metabolic pathways, amino acid metabolism, purine metabolism, and nitrogen metabolism are closely associated with nitrogen. Some amino acids can act as carriers of ammonia, such as arginine and glutamine. In addition, ammonia also exists in purines, which can release ammonia during purine metabolism. When *Sphingomonas* sp. Z392 was cultured under high concentration of ammonium sulfate, the purine metabolism, arginine biosynthesis, arginine and proline metabolism, and nitrogen metabolism pathways were significantly enriched. These pathways were closely associated with the reduce of ammonia (Figure 2).

In purine metabolism, ribose 5-phosphate accepts amino groups from glutamine, aspartate, and glycine to form inosine monophosphate (IMP), which serves as a carrier for the amino groups (Pedley and Benkovic, 2017). And, IMP can interconvert with adenylic acid (AMP) and guanosine monophosphate (GMP), accompanied by the release of NH_3 (Gooding et al., 2015). As shown in Figure 2A, under high concentration of ammonium sulfate, the transcription levels of *RS01720*, *RS07605*, *purM*, *purC*, and *purO* genes in the purine metabolism of *Sphingomonas* sp. Z392 were significantly downregulated. As a result, the synthesis of IMP, GMP, and AMP might be reduced, which would lead to a decrease in the production of NH_3 from the purine metabolism.

In addition, the biosynthesis and metabolism of arginine are also closely related to the intracellular ammonia concentration. Glutamate is converted to arginine via catalysis by a series of enzymes. Arginine, serving as a carrier of ammonia, undergo the arginine metabolism pathway to produce putrescine, and the ammonia is released (Landete et al., 2010). As shown in Figure 2B, under high concentration of ammonium sulfate, the transcription levels of *glsA*, *argB*, and *argD* genes of *Sphingomonas* sp. Z392 in arginine biosynthesis pathway were significantly downregulated, and the transcription levels of *aguB*, *aguA* genes in arginine metabolism pathway were also significantly downregulated.

In addition to purine and arginine metabolism, intracellular ammonia in *Sphingomonas* sp. Z392 might form nitromethane through a series of enzymes, then nitromethane is converted to nitrite via catalysis by a nitronate monooxygenase (encoded by the *ncd2* gene) (Figure 2C). When *Sphingomonas* sp. Z392 was cultured under high ammonium sulfate concentration, the transcription levels of *ncd2* in nitrogen metabolism pathway was significantly upregulated, which would facilitate the conversion of ammonia into nitrite, enhancing the elimination for intracellular ammonia.

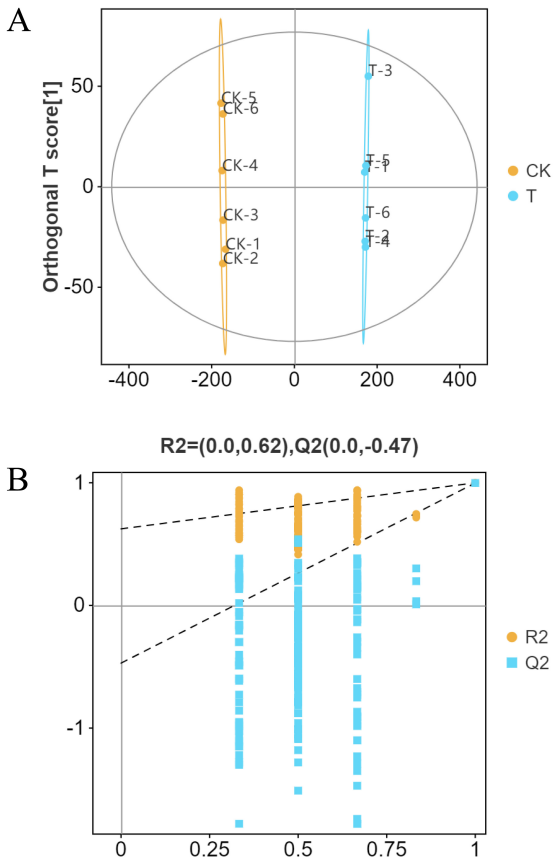

FIGURE 3
OPLS-DA score map **(A)** and displacement test **(B)** of metabolomics. OPLS-DA score plot and permutation test for the metabolome of *Sphingomonas* sp. Z392 under high levels of ammonia sulfate.

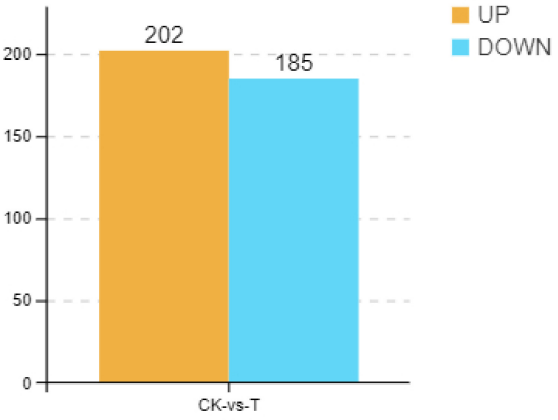

FIGURE 4
Differential expression metabolites of *Sphingomonas* sp. Z392 under high levels of ammonia sulfate., the *Y*-axis represents the number of up- and downregulated metabolites, orange represents upregulation, and blue represents downregulation.

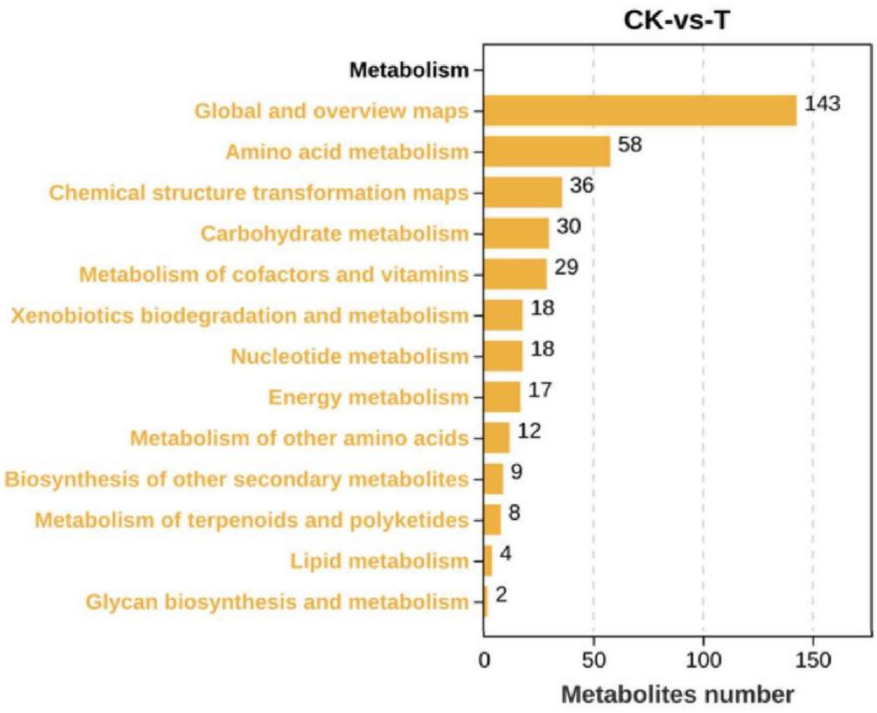

FIGURE 5
KEGG metabolic pathways enriched in differential expression metabolites.

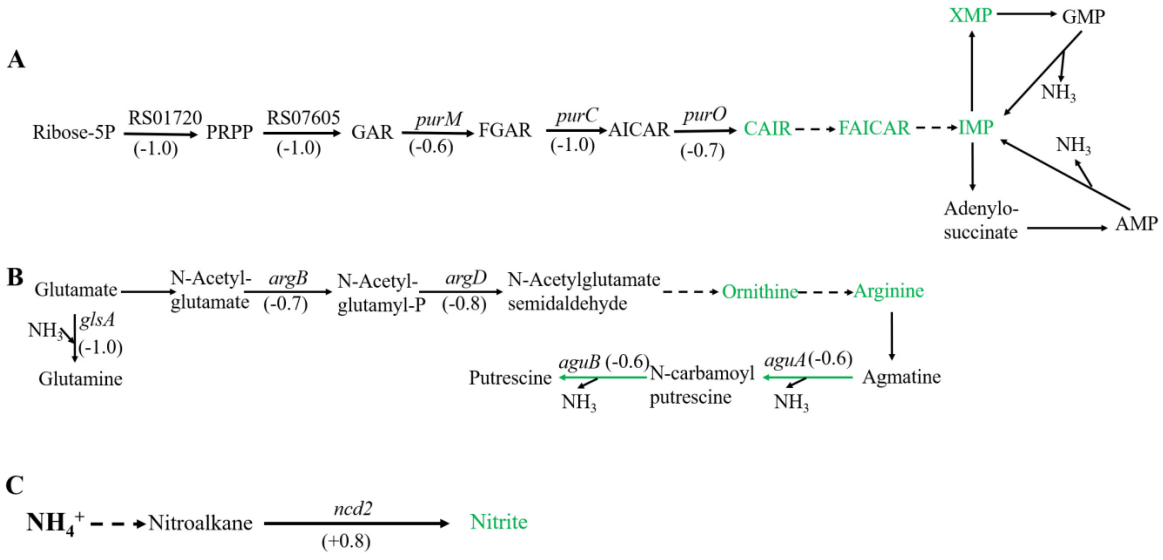

FIGURE 6
Differential expression metabolites in the purine metabolism **(A)** and arginine metabolism **(B)** pathways, and nitrogen metabolism pathway **(C)**. The green metabolites indicate downregulation, and the red metabolites indicate upregulation.

3.2 Metabolomics analysis of *Sphingomonas* sp. Z392 under high level of ammonium sulfate

The metabolites of *Sphingomonas* sp. Z392 from the high ammonium sulfate and control groups were identified by LC-MS/MS. To analyze the changes in differential metabolites of *Sphingomonas* sp. Z392 under the high ammonium sulfate, the differential expression of metabolites (DEMs) between the CK and T groups were analyzed using orthogonal partial least squares-discriminant analysis (OPLS-DA). As shown in Figure 3, the clear separation of the profiles between the T and CK groups indicated that the model had a good predictive power, suggesting the existence of DEMs between the T and CK groups.

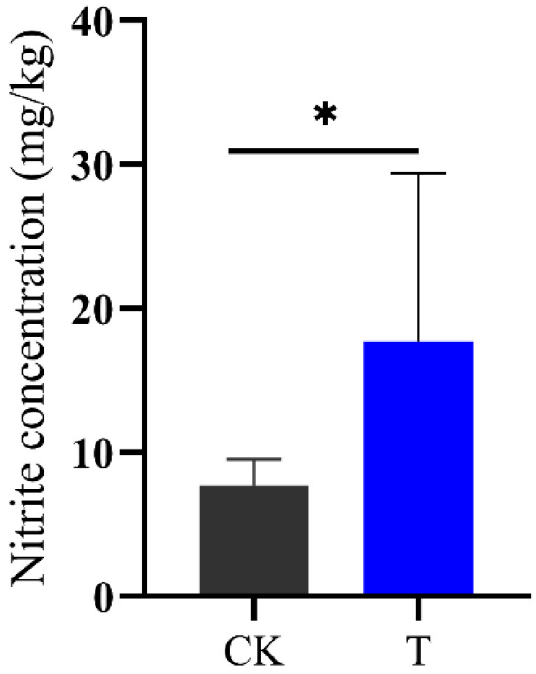

FIGURE 7
The nitrite concentrations of *Sphingomonas* sp. Z392 under conditions with (T) and without (CK) high levels of ammonia sulfate. * represents $p < 0.05$.

As shown in Figure 4, there were 442 DEMs, of which 223 were significantly upregulated, and 219 were significantly downregulated when the *Sphingomonas* sp. Z392 was cultured under the high ammonium sulfate. Then, the KEGG metabolic pathways were enriched in DEMs. As shown in Figure 5, the DEMs were involved in the following pathways: amino acid metabolism, metabolism of other amino acids, nucleotide metabolism, carbohydrate metabolism, metabolism of cofactors and vitamins, biosynthesis of secondary metabolites, lipid metabolism, energy metabolism, xenobiotics biodegradation and metabolism, and metabolism of terpenoids and polyketides. Among these pathways, amino acid and nucleotide metabolisms are closely associated with nitrogen metabolism.

As shown in Figure 6, under high ammonium sulfate condition, the levels of carboxyaminoimidazole ribonucleotide (CAIR), 5-formamidoimidazole-4-carboxamide ribotide (FAICAR), IMP, and xanthosine monophosphate (XMP) of *Sphingomonas* sp. Z392 in purine metabolism were downregulated. In addition, under high ammonium sulfate condition, the levels of ornithine and arginine in the arginine metabolism pathway were downregulated. Therefore, under high concentration of ammonium sulfate, the concentration of arginine in *Sphingomonas* sp. Z392 might decrease, potentially leading to a reduced flux of arginine deamination to produce putrescine, which in turn decreases the production of NH_3 from arginine decomposition.

Intercellular nitrite and NH_3 are closely related (Figure 2C), this study used ion chromatography to detect the intercellular nitrite content of *Sphingomonas* sp. Z392. Under high concentration of ammonium sulfate, the intercellular nitrite content of *Sphingomonas* sp. Z392 was 17.67 mg/kg, which was 2.27 times that of the *Sphingomonas* sp. Z392 without ammonium sulfate (7.77 mg/kg) (Figure 7).The above results showed that under high ammonium sulfate concentration, the transcription levels of *RS01720*, *RS07605*, *purM*, *purC*, and *purO* genes in the purine metabolism were significantly downregulated, and the corresponding levels of CAIR, FAICAR, IMP, and XMP of purine metabolism were also downregulated; In arginine biosynthesis and metabolism pathways, the transcription levels of *glsA*, *argB*, *argD*, *aguB*, and *aguA* genes were significantly downregulated, and the levels of ornithine and arginine were also downregulated. In addition, under high ammonium sulfate concentration, the transcription level of *ncd2* gene in nitrogen metabolism was significantly upregulated, and the intracellular nitrate content increased markedly.

3.3 Knockout and overexpression of the ncd2 gene in *Sphingomonas* sp. Z392

The above results demonstrated that the *ncd2* gene may contribute to ammonia reduction in *Sphingomonas* sp. Z392. To further explore the effect of the *ncd2* gene on the ammonia degradation ability of *Sphingomonas* sp. Z392, this study overexpressed and knocked out the *ncd2* gene in *Sphingomonas* sp. Z392, respectively, and named them Z392 OV*ncd2* and Z392 Δ*ncd2*. To validate the overexpression of *ncd2*, we performed quantitative RT-qPCR. As shown in Figure 8, the expression level of the *ncd2* in Z392 OV*ncd2* was significantly increased than that of the *Sphingomonas* sp. Z392. Furthermore, the genomic DNA of Z392 Δ*ncd2* was used as template, we amplified the target band with primers flanking *ncd2* and confirmed the successful knockout of the *ncd2* gene through sequencing.

3.4 Effect of *ncd2* on nitrogen content in chicken feces

To confirm the effect of *ncd2* on ammonia reduction, the broiler chickens were fed with *Sphingomonas* sp. Z392, Z392 OV*ncd2*, and Z392 Δ*ncd2* strains, respectively. Chicken manure was collected and tested for its contents of total nitrogen, ammonia nitrogen, and nitrate nitrogen (Figure 9).

When the broiler chickens were fed with *Sphingomonas* sp. Z392, Z392 OV*ncd2*, and Z392 Δ*ncd2* strains, the contents of total nitrogen and ammonium nitrogen in chicken manure were significantly decreased than that of without *Sphingomonas* sp., while nitrate nitrogen content was significantly increased than that of without *Sphingomonas* sp. Furthermore, Z392 OV*ncd2* strain exhibited the most ammonia reduction capability. The ammonia concentration of the group fed with Z392 OV*ncd2* decreased by 43.33% than that of without *Sphingomonas* sp. group, and decreased by 14.17% than that of group fed with *Sphingomonas* sp. Z392. In summary, overexpressing the *ncd2* gene in *Sphingomonas* sp. Z392 resulted in reduced ammonia emission and ammonium nitrogen content, while increasing nitrate nitrogen content in chicken coop. Overexpression of *ncd2* facilitated the conversion of ammonium nitrogen in chicken manure into nitrate nitrogen, thereby reducing ammonia emissions from chicken manure.

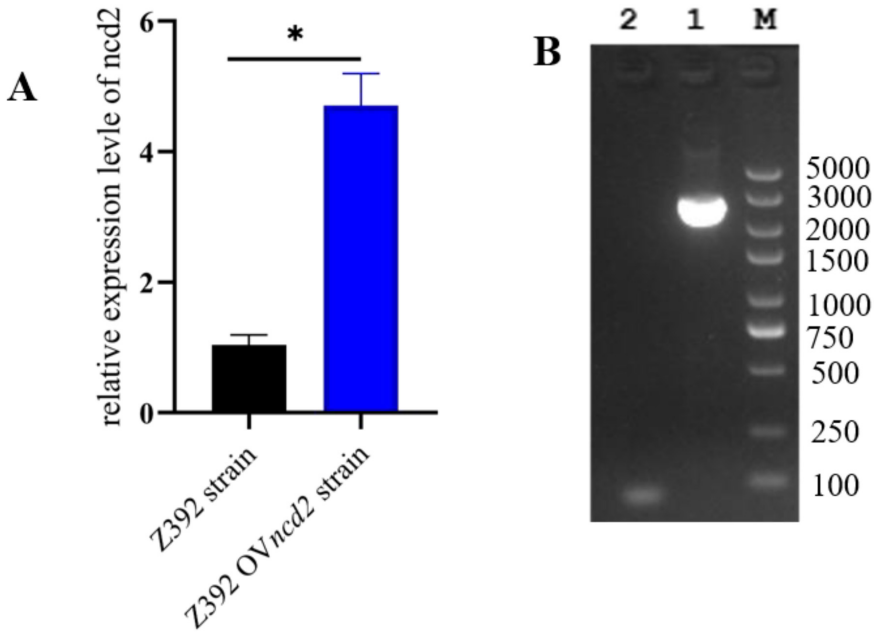

FIGURE 8
The verification of *ncd2* overexpression and knockout in *Sphingomonas* sp. Z392 by RT-qPCR **(A)** and PCR amplification **(B)**, respectively. Lane 1 represents band by the external primers, Lane 2 represents the negative band. M represents DL 5000 DNA Marker. * represents $p < 0.05$.

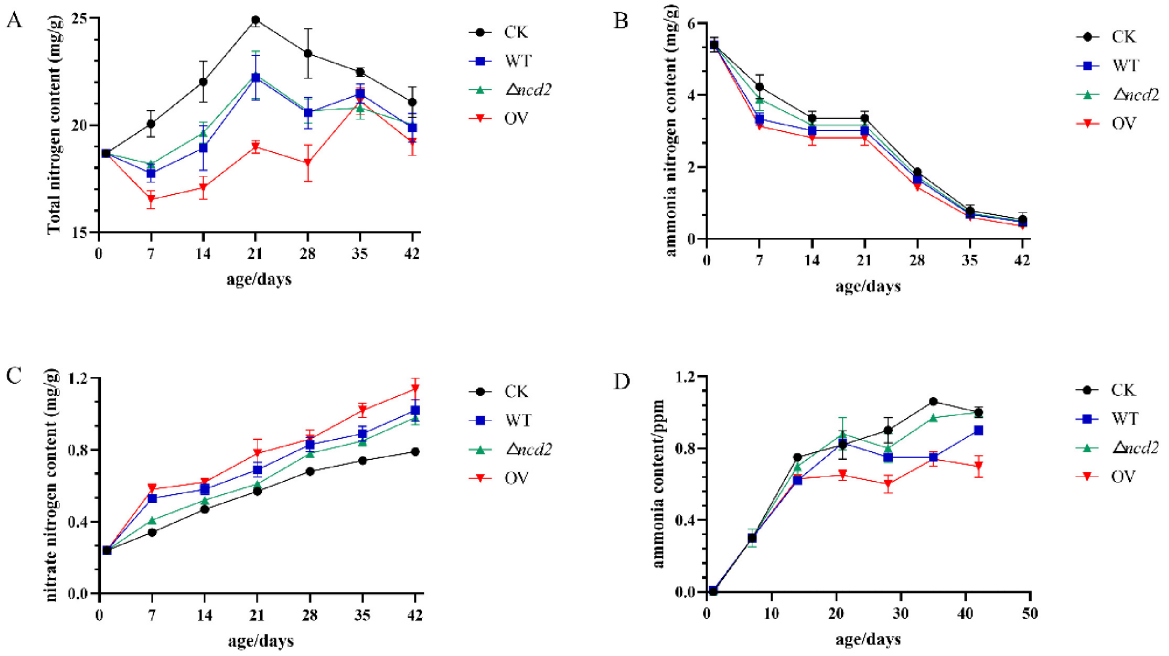

FIGURE 9
The changes of total nitrogen **(A)**, ammonium nitrogen **(B)**, nitrate nitrogen **(C)**, and ammonia **(D)** contents in chicken manure fed with *Spingomonas* sp. Z392, Z392 OV*ncd2*, Z392 Z392 Δ*ncd2*, and without *Spingomonas* sp.

4 Discussion

Currently, biodegradation has received an increasing attention due to its advantages of low cost, high efficiency, simple operation, and environmental friendliness (Mi et al., 2019). The microorganisms reported to reduce ammonia mainly include *Alcaligenes faecalis*, *Pseudomonas*, *Rhodococcus*, *Acinetobacter*, and *Bacillus methylotrophicus* (Kim et al., 2005; Mi et al., 2019; Robertson and Kuenen, 1990; Zhao et al., 2010). However, the specific degradation mechanisms of these microorganisms toward ammonia are still unclear. *Sphingomonas* exhibits potential ammonia degradation ability due to its numerous pollutant

degradation genes, but its systematic degradation pathway remains to be further studied.

In this study, *Sphingomonas* sp. Z392 was cultured under high ammonium sulfate environment, and transcriptome and metabolome analysis were performed jointly. It was found that the expression levels of genes related to purine metabolism and arginine metabolism in *Sphingomonas* sp. Z392 were decreased, and the levels of ornithine, arginine, IMP, and XMP were also downregulated. Purine metabolism and arginine metabolism are closely related to the intracellular ammonia concentration, under high ammonium sulfate environment, the flux of purine and arginine metabolisms might decrease, which might contribute to reduce NH_3 release. Under high ammonium sulfate conditions, *Sphingomonas* sp. Z392 reduced the flux of purine metabolism, which not only helps to reduce ammonia release but also saves cellular energy, enhancing its survival ability in adverse environments. However, purine metabolism is closely related to the growth and reproduction of *Sphingomonas* sp. Z392, so the reduction of this metabolic flux can only be within a certain range, as excessive reduction may have adverse effects on cell growth and reproduction (Zhao et al., 2010). Arginine metabolism is an essential biochemical process for microorganisms to maintain normal growth and metabolism. This study found that under high ammonium sulfate conditions, the transcription levels of genes in arginine metabolism of *Sphingomonas* sp. Z392 decreased, resulting in reduced the levels of arginine and ornithine. Similarly, although the decrease in arginine metabolism flux could decrease NH_3 release, this flux could only be reduced to a certain extent, otherwise it would affect the growth of *Sphingomonas* sp. Z392. Therefore, the reduction of flux in purine and arginine metabolism pathways might decrease ammonia release to some extent, but it cannot serve as the primary strategy. It is necessary to comprehensively consider the metabolic characteristics and growth requirements of *Sphingomonas* sp. to seek more effective and sustainable ammonia reduction solutions.

In addition, this study also found that under high ammonium sulfate environment, the transcriptional level of the *ncd2* in nitrogen metabolism pathway was upregulated, accompanied by a 2.27-fold increase in intracellular nitrite content. This pathway potentially converts NH_3 into nitrite through a series of complex reactions, leading to a reduction in NH_3 level. The *ncd2* encodes nitroalkane monooxygenase, which has been studied for the degradation of nitroalkanes (Gadda and Francis, 2010; Rolfes, 2006). After knocking out the *ncd2* gene, the ammonia concentrations in the chicken coop significantly increased, while the *ncd2*-overexpressing strain significantly reduced the ammonia concentration in the chicken coop, which was consistent with the previous studies (Vodovoz and Gadda, 2020; Nishino et al., 2010). Similar to the case of *Penicillium* and *Pseudomonas* aeruginosa, this enzyme is also involved in the metabolism of nitroalkanes, generating malondialdehyde, nitrite, and nitrate (Torres-Guzman et al., 2021). In this study, *Sphingomonas* sp. Z392 could increase the removal of ammonia by enhancing ammonia assimilation to form nitrite, which would become an effective pathway for ammonia degradation. Although, this study has discovered that *Sphingomonas* sp. Z392 might utilize the nitroalkane monooxygenase encoded by *ncd2* to convert nitromethane into nitrite, the specific pathway for ammonia to transform into nitromethane remains unknown. Current research suggested that completely ammonia-oxidizing bacteria have the potential for safe ammonia oxidation, which can directly oxidize ammonia to nitrate. The specific pathway for *Sphingomonas* sp. Z392 to convert ammonia into nitromethane still needs further exploration.

5 Conclusion

In this study, under high concentration of ammonium sulfate, the transcription levels of the genes related to purine metabolism and arginine metabolism pathways were significantly downregulated, and the corresponding levels of ornithine, arginine, IMP, and XMP were also downregulated in *Sphingomonas* sp. Z392. In addition, under high ammonium sulfate concentration, the transcription level of *ncd2* gene in nitrogen metabolism was significantly upregulated, and the intracellular nitrate content increased markedly. Under high concentration of ammonium sulfate, *Sphingomonas* sp. Z392 might reduce the release of NH_3 by decreasing the flux of purine metabolism and arginine metabolism pathway, and increasing the assimilation flux of ammonia. Furthermore, *ncd2* was a key gene for ammonia reduction in *Sphingomonas* sp. Z392. In a word, this study not only systematically clarifies the metabolic pathway of ammonia reduction in *Sphingomonas*, but also points out future research directions.

Data availability statement

The datasets presented in this study can be found in online repositories. The names of the repository/repositories and accession number(s) can be found below: BioProject: Processed PRJNA1112986: the transcriptome of *Sphingomonas* sp. Z392 under high ammonium sulfate.

Ethics statement

The animal studies were approved by the Ethics Committee of Experimental Animals of Huanghuai University and strictly follows the provisions of the "Ethical Review of Experimental Animals of Huanghuai University" (Acceptance Number: 202009220005). The studies were conducted in accordance with the local legislation and institutional requirements. Written informed consent was obtained from the owners for the participation of their animals in this study.

Author contributions

WM: Formal Analysis, Methodology, Writing – original draft, Writing – review and editing. LD: Investigation, Methodology, Writing – original draft. XH: Investigation, Methodology, Writing – original draft. WG: Data curation, Writing – original draft. LC: Data curation, Writing – original draft. GY: Data curation, Writing – original draft. GA: Writing – original draft, Writing – review and editing.

Funding

The authors declare that financial support was received for the research, authorship, and/or publication of this article. This work was supported by the Key R&D projects of Ningxia Hui Autonomous Region (2021BEE02032), the Science and Technology Development Plan Project of Henan province of China (172102110201 and 212102110005), and Natural Science Foundation of Henan Province (232300421270).

Conflict of interest

The authors declare that the research was conducted in the absence of any commercial or financial relationships that could be construed as a potential conflict of interest.

Publisher's note

Supplementary material

The Supplementary Material for this article can be found online at: https://www.frontiersin.org/articles/10.3389/fmicb.2024.1437056/full#supplementary-material

References

Bist, R. B., Subedi, S., Chai, L., and Yang, X. (2023). Ammonia emissions, impacts, and mitigation strategies for poultry production: a critical review. *J. Environ. Manage.* 328:116919. doi: 10.1016/j.jenvman.2022.116919

Chen, Q., and Ni, J. (2012). Ammonium removal by Agrobacterium sp. LAD9 capable of heterotrophic nitrification-aerobic denitrification. *J. Biosci. Bioeng.* 113, 619–623. doi: 10.1016/j.jbiosc.2011.12.012

Gadda, G., and Francis, K. (2010). Nitronate monooxygenase, a model for anionic flavin semiquinone intermediates in oxidative catalysis. *Arch. Biochem. Biophys.* 493, 53–61. doi: 10.1016/j.abb.2009.06.018

Gooding, J. R., Jensen, M. V., Dai, X., Wenner, B. R., Lu, D., Arumugam, R., et al. (2015). Adenylosuccinate is an insulin secretagogue derived from glucose-induced purine metabolism. *Cell Rep.* 13, 157–167. doi: 10.1016/j.celrep.2015.08.072

Haq, S. U., Aghajamali, M., and Hassanzadeh, H. (2021). Cost-effective and sensitive anthocyanin-based paper sensors for rapid ammonia detection in aqueous solutions. *RSC Adv.* 11, 24387–24397. doi: 10.1039/d1ra04069c

Huang, X., Li, W., Zhang, D., and Qin, W. (2013). Ammonium removal by a novel oligotrophic Acinetobacter sp. Y16 capable of heterotrophic nitrification-aerobic denitrification at low temperature. *Bioresour. Technol.* 146, 44–50. doi: 10.1016/j.biortech.2013.07.046

Ji, J., Zhao, Y., Wang, H., Jiang, L., Yuan, X., and Wang, H. (2022). Resource utilization of chicken manure to produce biochar for effective removal of levofloxacin hydrochloride through peroxymonosulfate activation: the synergetic function of graphitization and nitrogen functionality. *Chemosphere* 309(Pt. 1):136419. doi: 10.1016/j.chemosphere.2022.136419

Jin, R., Liu, T., Liu, G., Zhou, J., Huang, J., and Wang, A. (2015). Simultaneous heterotrophic nitrification and aerobic denitrification by the marine origin bacterium *Pseudomonas* sp. ADN-42. *Appl. Biochem. Biotechnol.* 175, 2000–2011. doi: 10.1007/s12010-014-1406-0

Kim, J. K., Park, K. J., Cho, K. S., Nam, S. W., Park, T. J., and Bajpai, R. (2005). Aerobic nitrification-denitrification by heterotrophic Bacillus strains. *Bioresour. Technol.* 96, 1897–1906. doi: 10.1016/j.biortech.2005.01.040

Landete, J. M., Arena, M. E., Pardo, I., Manca de Nadra, M. C., and Ferrer, S. (2010). The role of two families of bacterial enzymes in putrescine synthesis from agmatine via agmatine deiminase. *Int. Microbiol.* 13, 169–177. doi: 10.2436/20.1501.01.123

Love, M. I., Huber, W., and Anders, S. (2014). Moderated estimation of fold change and dispersion for RNA-seq data with DESeq2. *Genome Biol.* 15:550. doi: 10.1186/s13059-014-0550-8

Lubensky, J., Ellersdorfer, M., and Stocker, K. (2019). Ammonium recovery from model solutions and sludge liquor with a combined ion exchange and air stripping process. *J. Water Process Eng.* 32:100909.

Mi, J., Chen, X., and Liao, X. (2019). Screening of single or combined administration of 9 probiotics to reduce ammonia emissions from laying hens. *Poult. Sci.* 98, 3977–3988. doi: 10.3382/ps/pez138

Nancharaiah, Y. V., Venkata Mohan, S., and Lens, P. N. L. (2016). Recent advances in nutrient removal and recovery in biological and bioelectrochemical systems. *Bioresour. Technol.* 215, 173–185. doi: 10.1016/j.biortech.2016.03.129

Nishino, S. F., Shin, K. A., Payne, R. B., and Spain, J. C. (2010). Growth of bacteria on 3-nitropropionic acid as a sole source of carbon, nitrogen, and energy. *Appl. Environ. Microbiol.* 76, 3590–3598. doi: 10.1128/aem.00267-10

Pang, Y., and Wang, J. (2021). Various electron donors for biological nitrate removal: a review. *Sci. Total Environ.* 794:148699. doi: 10.1016/j.scitotenv.2021.148699

Pedley, A. M., and Benkovic, S. J. (2017). A new view into the regulation of purine metabolism: the purinosome. *Trends Biochem. Sci.* 42, 141–154. doi: 10.1016/j.tibs.2016.09.009

Robertson, L. A., and Kuenen, J. G. (1990). Combined heterotrophic nitrification and aerobic denitrification in Thiosphaera pantotropha and other bacteria. *Antonie Van Leeuwenhoek* 57, 139–152. doi: 10.1007/bf00403948

Rolfes, R. J. (2006). Regulation of purine nucleotide biosynthesis: in yeast and beyond. *Biochem. Soc. Trans.* 34(Pt. 5), 786–790. doi: 10.1042/bst0340786

Such, N., Mezõlaki, Á, Rawash, M. A., Tewelde, K. G., Pál, L., Wágner, L., et al. (2023). Diet composition and using probiotics or symbiotics can modify the urinary and faecal nitrogen ratio of broiler chicken's excreta and also the dynamics of *in vitro* ammonia emission. *Animals (Basel)* 13:332. doi: 10.3390/ani13030332

Torres-Guzman, J. C., Padilla-Guerrero, I. E., Cervantes-Quintero, K. Y., Martinez-Vazquez, A., Ibarra-Guzman, M., and Gonzalez-Hernandez, G. A. (2021). Peculiarities of nitronate monooxygenases and perspectives for *in vivo* and *in vitro* applications. *Appl. Microbiol. Biotechnol.* 105, 8019–8032. doi: 10.1007/s00253-021-11623-1

Varão Moura, A., Aparecido Rosini Silva, A., Domingos Santo da Silva, J., Aleixo Leal Pedroza, L., Bornhorst, J., Stiboller, M., et al. (2022). Determination of ions in Caenorhabditis elegans by ion chromatography. *J. Chromatogr. B Analyt. Technol. Biomed. Life Sci.* 1204:123312. doi: 10.1016/j.jchromb.2022.123312

Vodovoz, M., and Gadda, G. (2020). Kinetic solvent viscosity effects reveal a protein isomerization in the reductive half-reaction of Neurospora crassa class II nitronate monooxygenase. *Arch. Biochem. Biophys.* 695:108625. doi: 10.1016/j.abb.2020.108625

Wang, M. C., Wang, Y., Wang, G. L., Xu, L. L., and Li, E. Z. (2021). Isolation and identification of *Sphingomonas sp.* from chicken cecum and its ammonia-degrading activity. *J. Biotech Res.* 12, 65–73.

Zhao, B., He, Y. L., Hughes, J., and Zhang, X. F. (2010). Heterotrophic nitrogen removal by a newly isolated Acinetobacter calcoaceticus HNR. *Bioresour. Technol.* 101, 5194–5200. doi: 10.1016/j.biortech.2010.02.043

Zhou, Y., and Wang, J. (2023). Detection and removal technologies for ammonium and antibiotics in agricultural wastewater: recent advances and prospective. *Chemosphere* 334:139027. doi: 10.1016/j.chemosphere.2023.139027

frontiers | Frontiers in Microbiology

TYPE Original Research
PUBLISHED 14 May 2025
DOI 10.3389/fmicb.2025.1602768

OPEN ACCESS

EDITED BY
Qi Zhang,
Nanchang University, China

REVIEWED BY
Mahmood Laghari,
Sindh Agriculture University, Pakistan
Ting Zhou,
University of Technology Sydney, Australia

*CORRESPONDENCE
Zhiyan Pan
✉ 904703650@qq.com

RECEIVED 30 March 2025
ACCEPTED 22 April 2025
PUBLISHED 14 May 2025

CITATION
Zheng X, Zhang Y, Ye Z and Pan Z (2025) Biodegradation mechanisms of *p*-nitrophenol and microflora dynamics in fluidized bed bioreactors.
Front. Microbiol. 16:1602768.
doi: 10.3389/fmicb.2025.1602768

Biodegradation mechanisms of *p*-nitrophenol and microflora dynamics in fluidized bed bioreactors

Xin Zheng[1], Yongjie Zhang[1,2], Zhiheng Ye[1] and Zhiyan Pan[1]*

[1]College of Environment, Zhejiang University of Technology, Hangzhou, China, [2]Wenzhou Center for Integrated Material and Ecological Management, Wenzhou, China

p-Nitrophenol (PNP), a member of the nitroaromatic family, is widely used in the production of pesticides, dyes, pharmaceuticals, and petroleum products. As a toxic compound, PNP is highly resistance to degradation, posing a significant challenge in agricultural and industrial wastewater treatment. Conventional PNP wastewater treatment methods require complex operational conditions that incur high chemical and equipment costs, and potential secondary pollution. Therefore, this study developed an anoxic fluidized bed bioreactor (AFBBR) and an anaerobic-aerobic fluidized bed bioreactor (AAFBBR) to evaluate the biodegradation performance and underlying mechanisms of PNP over a period of 90 days. The effect of glucose to PNP co-substrate ratios and C/N ratios have been systemically investigated. At an influent PNP concentration of 100 mg/L, a glucose to PNP co-substrate ratio of 6:1, and a C/N ratio of 10:1, the degradation of PNP reached 88.8 $\pm$ 1.0% in the AFBBR at an HRT of 8.5 h and 95.3 $\pm$ 0.3% in the AAFBBR at an HRT of 12.7 h. Meanwhile, the mechanism of PNP biodegradation and microbial community were also studied. Results of the LC–MS/MS revealed the intermediate products and confirmed that PNP biodegradation in both reactors followed the hydroquinone as well as the hydroxyquinol pathways, with the hydroquinone pathway being dominant. Results of the 16S rRNA high throughput sequencing further revealed a predominant presence of *Proteobacteria* (34% in the AFBBR, 42 and 65% in the anaerobic as well as aerobic zones of the AAFBBR, respectively), *Firmicutes* (35, 40, and 4%), *Saccharibacteria* (14, 9, and 4%) and *Bacteroidetes* (5, 4, and 19%). In the AFBBR and the AAFBBR, the key bacterial genera responsible for PNP degradation include *Lactococcus*, *Escherichia-Shigella*, *Saccharibacteria_norank*, *Acinetobacter*, *Comamonas, Zoogloea*, and *Pseudomonas*. Notably, the hydroxyquinol pathway was observed only in the AFBBR and the aerobic zone of the AAFBBR, where *Pseudomonas* were identified as key PNP degrading bacteria. These phenomena can be attributed to the varying dissolved oxygen concentrations across different zones in the two reactors, offering valuable insights into optimizing PNP removal in pilot-scale bioreactors. This study highlights an efficient, sustainable and cost-effective approach for PNP removal from agricultural and industrial wastewater.

KEYWORDS

p-nitrophenol, fluidization, hydroquinone route, biofilm, microbial community

1 Introduction

As a crucial chemical compound in the nitroaromatic family, *p*-nitrophenol (PNP, $C_6H_5NO_3$) is characterized by its toxicity, persistence, high stability and strong solubility in water (Feng et al., 2024). Meanwhile, PNP is widely used as both a synthetic intermediate or a raw material in dyes, pharmaceuticals, petroleum and pesticides (Kitagawa et al., 2004). As a result, its presence in agricultural and industrial wastewater is widespread. However, PNP pose significant threats to both ecological systems and human health since they were listed as a priority pollutant by the Environmental Protection Agency (USEPA) (Wang et al., 2024). Therefore, it is necessary to remove PNP prior to discharge of agricultural and industrial wastewater into water bodies for environmental safety and human health (Tang et al., 2012).

Traditional physical, chemical and biological techniques have been purposed for treating PNP wastewater, including adsorption, membrane filtration, distillation, oxidation, hydrogenation reduction and ion exchange (Badamasi et al., 2025). However, most of these techniques have disadvantages of complex reaction processes, high costs of chemical and equipment, and the generation of secondary pollution (Yan et al., 2022). Biological wastewater treatment (BWT) has great research and application potential in the field of organic wastewater treatment due to its sustainability and cost-effectiveness (Yan et al., 2024). Based on different aeration conditions, BWT processes are usually divided into anaerobic, anoxic, and aerobic biological treatments. Among them, a single aerobic biological treatment has the disadvantages of unstable organic carbon and nitrogen removal, as well as poor impact load resistance. Therefore, the anaerobic/anoxic biological processes are often implemented prior to aerobic processes, a configuration that has been proven effective for wastewater treatment in practical applications (Sun et al., 2025). However, due to the stable structure and biological toxicity of PNP, previous studies have found that biodegradation process is greatly inhibited during the treatment of PNP wastewater (Xu et al., 2021).

Recently, many researchers have focused on novel BWT technologies to enhance PNP degradation efficiency. The Fluidized bed bioreactor (FBBR) has been widely used for biological treatment of organic pollutants (Mallikarjuna and Dash, 2020), with advantages such as excellent mass transfer (Chowdhury and Nakhla, 2022; Lu et al., 2025), a large specific surface area (Karadag et al., 2015), high microbial activity, strong resistance to impact loads, and minimal residual biosolids production (Wang H. et al., 2020). In the FBBR, carrier particles with attached biofilm are driven by liquid or air flow to achieve a stable fluidization. By selecting various carrier particles, adjusting flow rates, and optimizing reactor structures, multiple carrier particles and diverse reaction conditions can be integrated within a single FBBR. This integration promotes the synergistic growth of functional microorganisms, enhances microbial adaptability, and improves biodegradation efficiency for wastewater treatment. Zheng et al. (2021) employed an anoxic carbon-based fluidized bed bioreactor to treat coal pyrolysis wastewater and achieved over 90% degradation of phenolic compounds with the *Brachymonas* as critical functional genus. Kuyukina et al. (2017) applied a fluidized-bed bioreactor for oilfield wastewater treatment and achieved 70% biodegradation efficiencies for alkanes and PAHs with the inoculation of co-immobilized *Rhodococcus*. In addition, Eldyasti et al. (2010) utilized a pilot-scale liquid solid circulating fluidized bed bioreactor for landfill leachate treatment, attaining COD removal efficiencies of 85%. These findings highlight the significant potential of FBBR in treating recalcitrant organic matter and persistent organic pollutants (POPs), with PNP serving as a representative example. However, most studies have focused on PNP biodegradation at the lab-scale, while research on its treatment mechanisms and microbial community composition in pilot- or full-scale reactors remains limited.

This study aimed to enhance PNP removal using the FBBR systems, indicating its biodegradation mechanisms and microflora dynamics. Stable treatment of PNP synthetic wastewater was initially achieved in an anoxic fluidized bed bioreactor (AFBBR). Subsequently, the PNP synthetic wastewater was inoculated into a pilot-scale anaerobic-aerobic fluidized bed bioreactor (AAFBBR) to further enhance the PNP removal performance. Both reactors were successfully started up and stably operated for over 90 days. Effects of glucose to PNP co-substrate ratios and C/N ratios on PNP biodegradation efficiency were tested. Intermediate products were detected to construct the PNP biodegradation mechanisms. In addition, microbial community analysis was further conducted to identify the functional bacteria within the system. In summary, this study successfully achieved enhanced PNP removal from wastewater in both the AFBBR and AAFBBR systems, and elucidated the potential biodegradation mechanisms as well as the key functional microorganisms involved in the PNP biodegradation.

2 Materials and methods

2.1 Experimental setup and operating conditions

In this study, a lab-scale AFBBR and a pilot-scale AAFBBR were constructed (Figure 1), with their main bodies made of polymethyl methacrylate (PMMA). The main body of the AFBBR is cylindrical, with a height of 1,200 mm, a radius of 50 mm, and a working volume of 8.5 L. In the AAFBBR (600 mm (L) × 180 mm (W) × 1,700 mm (H)), the anaerobic and aerobic zones had working volumes of approximately 50 L and 133 L, respectively.

As shown in Figure 1a, the AFBBR was operated continuously with inlet and outlet, purging by air and controlled by ball valves to maintain the dissolved oxygen (DO) concentrations at 0.5 ± 0.2 mg/L. The internal circulating water was discharge from the top of the reactor and inoculated into the bottom by a circulating centrifugal pump (YY7112, Southern Pump Industry Co., Ltd., China) at the reflux ratios of 480:1, achieving the fluidization of the particle. Synthetic wastewater was pumped into the bottom of the reactor by a peristaltic pump (77521-50, Masterflex, United States) and then overflowed from the top. The influent flow rate was maintained at 16.2 mL/min, resulting in an HRT of approximately 8.5 h.

Similarly, as shown in Figure 1b, the AAFBBR was operated continuously with inlet and outlet. The DO concentration in the anaerobic zone was maintained at 0.0–0.2 mg/L, and the aerobic zone was purged by air and controlled by ball valves to maintain the DO concentrations between 2.0–3.0 mg/L. Particle fluidization was realized by internal circulating water driven by two circulating centrifugal pumps (YY7112, Southern Pump Industry Co., Ltd., China) at the reflux ratios of 33:1 and 139:1 in the anaerobic and aerobic zones, respectively, based on the influent flow rate of the

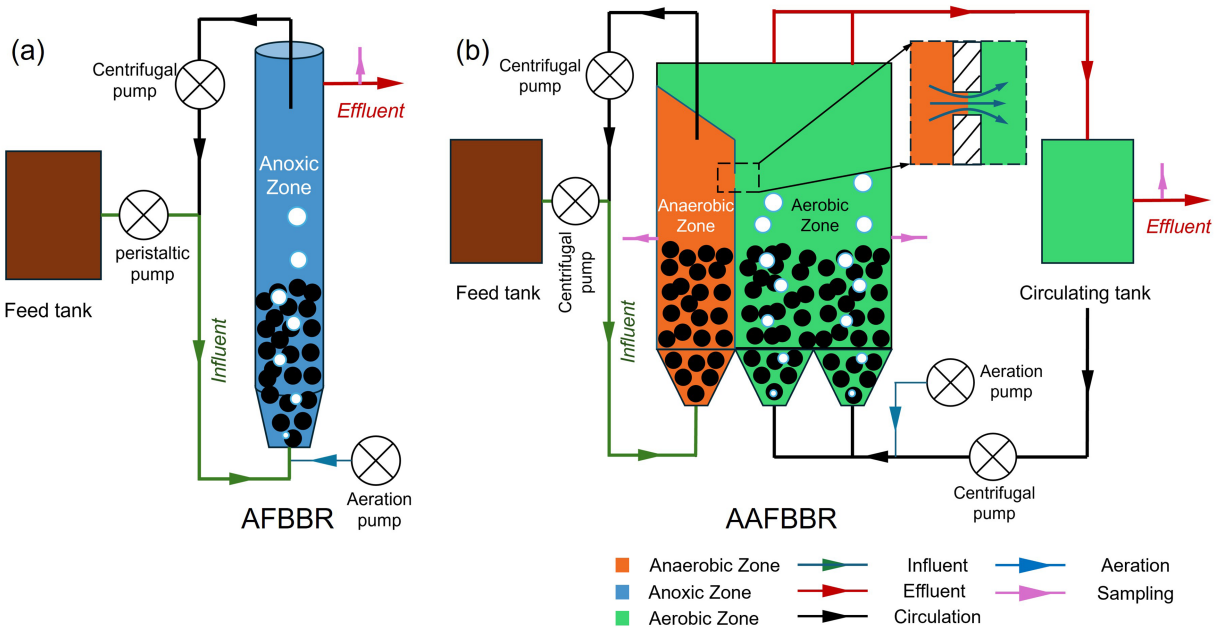

FIGURE 1
Schematic diagram of **(a)** AFBBR and **(b)** AAFBBR.

AAFBBR. The internal circulation of the anaerobic zone was discharged from the upper part and pumped back at the bottom. In the aerobic zone, the circulating water overflowed into a circulating tank and was then pumped back into the bottom of the aerobic zone. A small channel was designed at the side of the anaerobic zone, connecting it to the aerobic zone, which allowed the wastewater to flow slowly from the anaerobic zone to the aerobic zone. Synthetic wastewater was pumped into the bottom of the anaerobic zone using an inlet centrifugal pump (AKS800NHP0800, Nanjing Suchangyuan Technology Industrial Co., Ltd., China) and flowed into the aerobic zone through the channel connecting the two zones. After microbial treatment in the aerobic zone, the wastewater naturally overflowed into the circulating tank and was ultimately overflowed from the top of the circulating tank. To facilitated sample collection, two sampling ports (as shown in Figure 1) were strategically installed in both the anaerobic and aerobic zones. The influent flow rate was maintained at 240 mL/min, resulting in an HRT of approximately 3.5 h in the anaerobic zone and 9.2 h in the aerobic zone.

2.2 Inoculum and synthetic wastewater composition

The initial seed sludge, with a mixed liquor volatile suspended solids concentration (MLVSS) of 4,000 mg/L, was collected from the secondary sedimentation tank of a dye manufacturing plant's (Zhejiang Dinglong Technology Co., Ltd.) wastewater treatment facility. Having been continuously exposed to phenol-containing wastewater, its microbial community had great potential to efficiently degrade recalcitrant pollutants.

Semicokes with a particle size smaller than 3 mm are defined as waste coke particles (WCPs), accounting for approximately 15% of the total semicoke production (Hu et al., 2013). However, due to their small size, these fine semicoke particles are difficult to utilize in industries such as chemical engineering, smelting, as well as fertilizer manufacturing. and have therefore become a problematic form of solid waste (Hu et al., 2013). Nevertheless, the specific characteristics of WCPs, such as their irregular surface, large surface area, and proper density, make them highly suitable as biofilm carriers in the FBBR. Therefore, WCPs were provided by Shenmu Sanjiang Coal Chemical Co., Ltd. and utilized as carrier particles for biofilm in both reactors, with the characteristics of WCPs are listed in Supplementary Table 1.

The composition of PNP synthetic wastewater was primarily consisting of PNP, glucose, ammonium chloride and potassium dihydrogen phosphate, with $NaHCO_3$ as the alkalinity source. The other constituents of the synthetic medium including trace elements are listed in Supplementary Table 2. The initial pH was adjusted to about 7.5 using either 0.1 M HCl or 0.1 M NaOH.

To ensure the stable startup and operation, 0.75 kg of WCPs were inoculated into the AFBBR, 6.75 kg and 13.50 kg of WCPs were inoculated into the anaerobic and aerobic zones of the AAFBBR, with packing ratios of 14, 20 and 13%, respectively. Additionally, 4 g, 20 g and 40 g seed sludge were inoculated into the AFBBR, as well as the anaerobic and aerobic zones of the AAFBBR, respectively. The AFBBR and the AAFBBR were then filled with PNP synthetic wastewater and continuously operated at temperature of 22 ± 2°C.

The whole experiments lasted 90 days for the AFBBR and 90 days for the AAFBBR, which were divided into three phases, summarized in Table 1: phase I involved the start-up of the PNP removal system, during which the influent PNP concentration was gradually increased from 0 to 100 mg/L to enhance the microorganisms' tolerance capacity. In phase II, the influent glucose concentration was gradually reduced from 1,200 mg/L to 300 mg/L to achieve the different glucose to PNP co-substrate ratios, in order to investigate the effect of the glucose to PNP ratio on PNP degradation. In phase III, ammonium

TABLE 1 Operation conditions in the AFBBR and the AAFBBR.

Condition	Phase I	Phase II				Phase III			
	Start-up	Glucose to PNP co-substrate ratio				C/N ratio			
Time (d)	0–34	35–41	42–48	49–55	56–62	63–69	70–76	77–83	84–90
Initial NH_4Cl (mg/L)	0	0	0	0	0	223	93	49	27
Initial PNP (mg/L)	0–100	100	100	100	100	100	100	100	100
Initial glucose (mg/L)	–	1,200	900	600	300	600	600	600	600
Temperature (°C)	22 ± 2	22 ± 2	22 ± 2	22 ± 2	22 ± 2	22 ± 2	22 ± 2	22 ± 2	22 ± 2
DO in the AFBBR (mg/L)	0.5 ± 0.2								
DO in the anaerobic zone of AAFBBR (mg/L)	0.0–0.2								
DO in the aerobic zone of AAFBBR (mg/L)	2.0–3.0								
pH	7.5 ± 0.3								

chloride (NH_4Cl) was added at concentrations of 223 mg/L, 93 mg/L, 49 mg/L and 27 mg/L, achieving C/N ratios of 5:1, 10:1, 15:1, and 20:1, to examine the effect of the C/N ratio on PNP degradation.

2.3 Analytical methods

All samples were collected and filtered through a 0.45 μm membrane filter, concentration of chemical oxygen demand (COD) and total nitrogen (TN) were measured using Chinese standard methods: the potassium dichromate oxidation method (HJ 828-2017) for COD and the alkaline potassium persulfate digestion UV spectrophotometric method (HJ 636-2012) for TN. Measurement were performed using an UV–vis spectrophotometer (UV2600, Shimadzu, Japan). DO concentration and pH were measured using a DO meter (JPB-607, REX, Shanghai, China) and precision pH meter (PHS-3Eph, REX, shanghai, China), respectively. The concentrations of PNP and *p*-aminophenol (PAP, C_6H_7NO) were determined following the method described by Luo et al. (2021) using high performance liquid chromatography (HPLC) with a Thermo UltiMate3000 system equipped with a C18 column (5 μm, 250 × 4.6 mm) and a UV detector. The detection wavelength was set at 254 nm. A methanol–water mixture (of volumetric proportion 40:60) was used as the mobile phase at a flow rate of 1.0 mL/min. In order to ensure the accuracy of the experiment, each test was repeated three times, and the average value was taken. The removal rates of PNP, TN, and COD in the AFBBR, as well as in the anaerobic and aerobic zones of the AAFBBR, were calculated using the following equations (as shown in Equations 1–3, with PNP removal as an example):

$$\text{PNP removal rate in the AFBBR}(\%) = \frac{\text{Inf.}(\text{PNP}) - \text{Eff.}(\text{PNP})}{\text{Inf.}(\text{PNP})} \times 100\% \quad (1)$$

$$\text{PNP removal rate in the anaerobic zone of AAFBBR}(\%) = \frac{\text{Inf.}(\text{PNP}) - \text{anaerobic}(\text{PNP})}{\text{Inf.}(\text{PNP})} \times 100\% \quad (2)$$

$$\text{PNP removal rate in the aerobic zone of AAFBBR}(\%) = \frac{\text{Inf.}(\text{PNP}) - \text{aerobic}(\text{PNP})}{\text{Inf.}(\text{PNP})} \times 100\% \quad (3)$$

To analyze the degradation intermediates of PNP, liquid chromatography-mass spectrometry (LC–MS/MS) was performed on filtered (0.22 μm organic filter membrane) samples collected from the AFBBR and the AAFBBR. Chromatographic separation was achieved using a Waters C18 column (1.7 μm × 2.1 mm, 100 mm) at 40°C, with a mobile phase consisting of 0.1% formic acid (Solvent A) and acetonitrile (Solvent B). The injection volume was 0.1 μL. Mass spectrometry was conducted in positive electrospray ionization mode (ESI+), with a drying gas flow rate of 10 mL/min, heating gas flow rate of 10 mL/min, and atomizing gas flow rate of 3 mL/min. The interface voltage was set to 4.0 kV, with an interface temperature of 30°C, a desolvation temperature of 526°C, a DL temperature of 250°C, and a heating block temperature of 400°C. Additional parameters included a conversion tap voltage of 10.0 kV, detector voltage of 1.76 kV, IG vacuum of 0.002 Pa, PG vacuum degree of 130 Pa, and CID gas pressure of 270 kPa. The scan range was set of m/z 50–500.

2.4 Microbial community analysis

The total genome DNA from samples was extracted using CTAB/SDS method (MK Biotechnology Co. Ltd., Hangzhou, China). The DNA concentration and purity were examined using 2% agarose gel electrophoresis. Once the concentrations of the DNA samples were

recorded, DNA was diluted to 1 ng/μL using sterile water. The molecular marker chosen for this study was the 16S rRNA genes. The amplification of this marker was performed using specific primers with a barcode. The primers pairs used 16S V4-V5: 515F-907R. All polymerase chain reaction (PCR) reactions were carried out in 30 μL reactions with 15 μL of Phusion®High-Fidelity PCR Master Mix (New England Biolabs); 0.2 μM of forward and reverse primers, and about 10 ng template DNA. The PCR amplification conditions comprised initial denaturation at 98°C for 1 min, followed by 30 cycles of denaturation at 98°C for 10 s, annealing at 50°C for 30 s, and elongation at 72°C for 60 s. Finally, 72°C for 5 min. Sequences with ≥97% similarity was assigned to the same operational taxonomic units (OTUs).

3 Results and discussion

3.1 Reactor performance

3.1.1 Effect of initial PNP concentration on PNP degradation

The temporal variations in PNP, COD, and TN concentrations and removal efficiencies in the AFBBR and the AAFBBR are illustrated in Figures 2–4, respectively. In the phase I, the AFBBR and AAFBBR were performing stable COD removal efficiency over 90% at the beginning without the inoculated of PNP. Subsequently, the influent PNP concentration was gradually increased from 0 mg/L to 100 mg/L (day 1 to day 34) to realize the start-up of PNP removal. Concurrently, the influent COD concentration rose from 600 mg/L to 750 mg/L with glucose supplementation, and the influent TN concentration increased from 1 mg/L to 10 mg/L which was primarily contributed by PNP.

As shown in Figure 2, after the PNP synthetic wastewater inoculated into both reactors, AFBBR initially achieved the 25% of PNP removal efficiency and gradually increased to 90% within 7 days. While AAFBBR exhibited a strong PNP degradation capability at the beginning, achieving an initial removal efficiency of 87% on the day 1, which rose to over 90% from the second day. PNP was primarily degraded in the anaerobic zone and further broken down in the aerobic zone in the AAFBBR. The PNP removal rate in both reactors quickly exceeded 90%, attributing to the initial seed sludge which was collected from the actual wastewater treatment process of a chemical plant and exhibited excellent adaptability to phenolic wastewater. However, the AAFBBR demonstrated a faster start-up time than the AFBBR, as the synthetic wastewater first passed through the anaerobic zone, where microorganisms exhibited greater resilience to PNP, thereby mitigating its inhibitory effects on aerobic microorganisms.

During the start-up period, the AFBBR and the AAFBBR exhibited distinct response patterns to variations in influent PNP concentration, characterized by transient fluctuations and temporary declines in PNP removal efficiency following each concentration increase. In the AFBBR, the PNP removal rate dropped sharply to around 80% after each increase in PNP concentration, but recovered to above 95% within a few days. The AAFBBR showed similar fluctuations when the PNP concentration gradually increased from 0 to 40 mg/L. However, as the influent PNP concentration increased from 40 to 100 mg/L, the PNP removal rate in the AAFBBR remained at approximately 90%. This trend may be due to the initial inhibitory effects of elevated PNP concentration on the microbial community, followed by microbial adaptation and growth under the high PNP concentration (Mei et al., 2019), ultimately enhancing the PNP removal capacity in the system. The more stable PNP removal performance observed in the AAFBBR as the influent PNP increased from 40 to 100 mg/L indicated that the anaerobic microorganisms in its anaerobic zone exhibited stronger shock resistance and adaptability. While the AFBBR achieved a higher PNP removal rate than the AAFBBR (93.8 ± 1.4% vs. 90.4 ± 0.1%) at the end of phase I. This phenomenon could be attributed to the synergistic interactions among anaerobic, anoxic, and aerobic microorganisms, which played a crucial role in enhancing PNP removal efficiency in the AFBBR system. PAP is a primary reduction product of PNP under anoxic conditions (Sponza and Kuscu, 2011). However, as shown in Figure 2, PAP production rate in two reactors were lower than the reduction rate of PNP, indicating the further degradation of PAP. In the AAFBBR, the PAP concentration in the anaerobic zone was higher than that in the aerobic zone, suggesting that PAP was further degraded in aerobic zone.

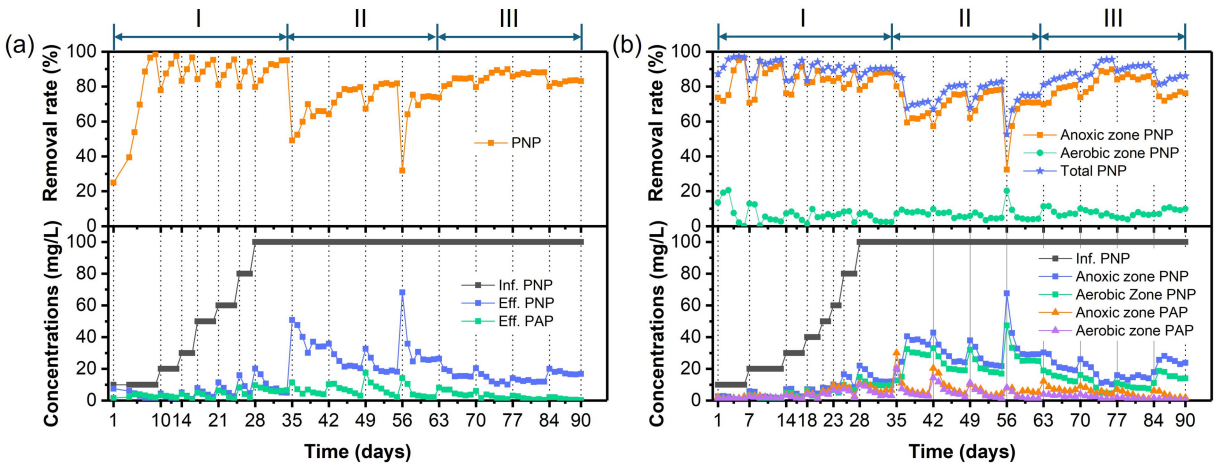

FIGURE 2
Temporal variations of PNP/PAP concentrations and removal rates in **(a)** the AFBBR and **(b)** the AAFBBRover the 90-day operation.

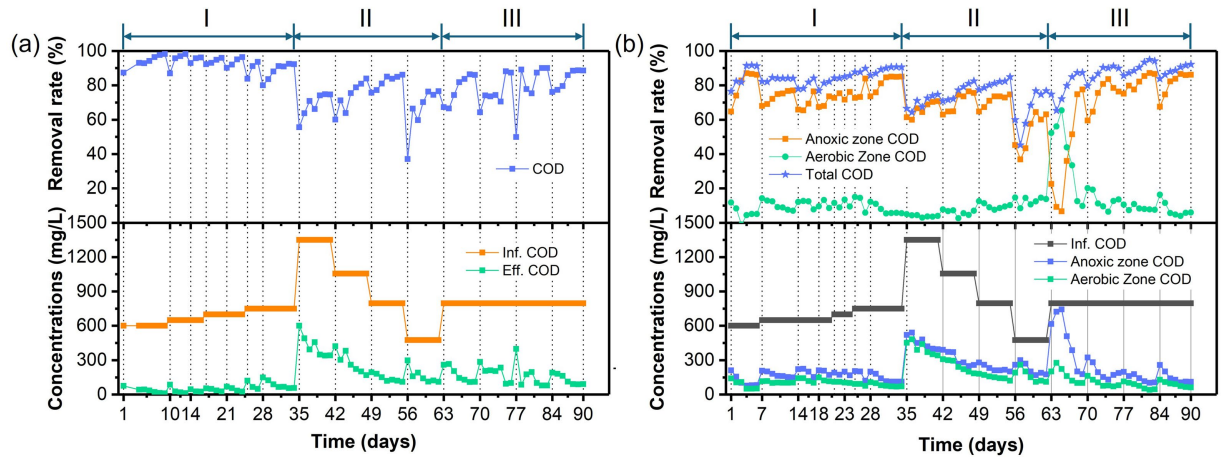

FIGURE 3
Temporal variations of COD concentrations and removal rates in **(a)** the AFBBR and **(b)** the AAFBBRover the 90-day operation.

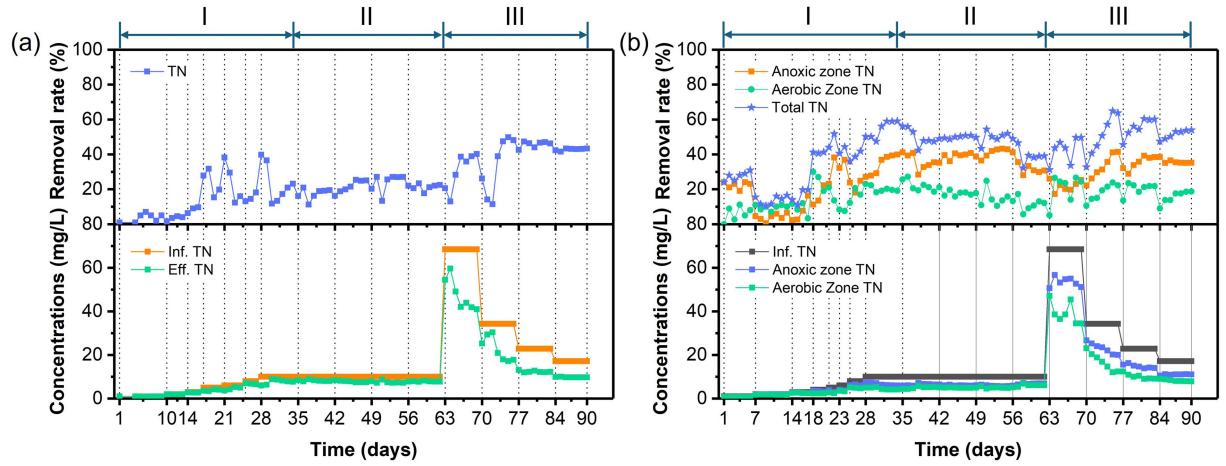

FIGURE 4
Temporal variations of TN concentrations and removal rates in **(a)** the AFBBR and **(b)** the AAFBBRover the 90-day operation.

Figures 3, 4 presents the temporal variations of COD and TN concentrations and removal efficiencies in AFBBR and AAFBBR. At the end of phase I, with the influent PNP concentration of 100 mg/L and the influent COD concentration of 750 mg/L, the COD removal efficiency in AFBBR and AAFBBR reached 91.8 ± 0.8% and 90.6 ± 0.1%, the TN removal efficiency in AFBBR and AAFBBR reached 20.5 ± 3.0% and 58.3 ± 1.4%, respectively. In the AFBBR, anaerobic, anoxic and aerobic microorganisms could simultaneously growth, resulting the COD removal efficiency of AFBBR is comparable to that of AAFBBR. However, biological nitrogen removal is highly dependent on DO conditions (Liu et al., 2020). In AAFBBR, the higher DO concentration in the aerobic zone created a more favorable environment for microbial nitrogen transformations, leading to a significant enhancement nitrogen removal compared to the AFBBR.

As the influent PNP concentration gradually increased, the PNP removal efficiency in both AFBBR and AAFBBR ultimately stabilized above 90% after fluctuation. At the end of phase I, the AFBBR and AAFBBR realized the PNP removal efficiency of 90.0 ± 0.1% and 93.8 ± 1.4% with the influent PNP concentration at 100 mg/L, indicating the successfully start-up of PNP removal in two reactors.

3.1.2 Effect of glucose to PNP co-substrate ratio on PNP degradation

Glucose can undergo bio-oxidation to generate endogenous electron donors, which facilitate the biodegradation of organic compounds (Bai et al., 2015). In the phase II, the effect of glucose to PNP co-substrate ratio on PNP degradation was investigated in both reactors. With an influent PNP concentration of 100 mg/L, the influent glucose concentration was gradually decreased from 1,200 mg/L to 300 mg/L, corresponding to glucose to PNP co-substrate ratios of 12:1, 9:1, 6:1, 3:1.

Different glucose to PNP co-substrate ratios led microbes to utilize varying electron donors when degrading PNP through co-substrate pathways. As shown in Figure 2, decreasing the glucose to PNP co-substrate ratio in the influent from 12:1 to 6:1 led to a significant increase in PNP removal efficiency—from 65.0 ± 1.7% to

81.6 ± 0.4% in the AFBBR, and from 70.8 ± 0.7% to 82.4 ± 0.5% in the AAFBBR. The similar trend was also observed in COD removal (Figure 3). The excessive glucose supplementation negatively affected PNP degradation, which can be due to that glucose as a readily biodegradable carbon source, was preferentially consumed by microorganisms instead of PNP (Vo et al., 2020). However, further reducing the glucose to PNP co-substrate ratio to 3:1 led to a significant decline in the PNP and COD removal efficiencies in both reactors. Over the following days, as microorganisms adapted and their metabolic activity improved, the PNP removal efficiencies gradually increased and stabilized (74.2 ± 0.2% in the AFBBR and 74.9 ± 0.1% in the AAFBBR). The removal rates of PNP and COD in the two reactors remained lower than those observed when the influent glucose to PNP ratio of 6:1. These results suggest that an optimal glucose addition can enhance PNP degradation through co-substrate metabolism (Wang et al., 2022). As the influent co-substrate ratios decreased from 12:1 to 6:1, the TN removal efficiencies in AFBBR and AAFBBR kept stable (Figure 4). Further reducing the influent co-substrate ratio to 3:1, the TN removal efficiency in AAFBBR showed a significant decrease, which could be due to the limited carbon source restricted nitrogen removal through denitrification (Liu et al., 2020).

At an influent glucose to PNP co-substrate ratio of 6:1, the highest removal efficiencies of PNP, COD, and TN in AFBBR were 81.6 ± 0.4%, 85.0 ± 1.0%, and 26.7 ± 0.7%, respectively. Similarly, in AAFBBR, the maximum removal efficiencies of PNP, COD, and TN at the same glucose to PNP ratio were 82.4 ± 0.5%, 83.1 ± 1.5%, and 50.5 ± 1.6%, respectively. However, the PNP removal rates in the phase II were significantly lower than those at the end of phase I for both the AFBBR and AAFBBR. This decline was attributed to changes in influent concentration and the toxic effects of PNP, which may have led to biofilm loss.

3.1.3 Effect of C/N ratio on PNP degradation

In the phase III, the effect of C/N ratio on PNP degradation in the two reactors was investigated. With the influent PNP and glucose concentration of 100 mg/L and 600 mg/L, respectively, the influent C/N ratio was systematically adjusted by supplementing nitrogen source (NH_4Cl). C/N ratio in 5:1, 10:1, 15:1, and 20:1 was controlled with the adding of NH_4Cl concentrations at 223 mg/L, 93 mg/L, 49 mg/L and 27 mg/L, respectively.

As shown in Figures 2, 3, the PNP and COD removal rates exhibited a significant increase in both reactors following the addition of the nitrogen source. As the influent C/N ratio increased from 5:1 to 15:1, the PNP removal performance exhibited a continuous upward trend in both reactors. In the AFBBR, the PNP removal rate increased from 84.7 ± 0.2% to 88.2 ± 0.1%, while in the AAFBBR, it increased from 87.1 ± 1.2% to 92.0 ± 0.3%. The highest PNP removal efficiency was observed at a C/N ratio of 10:1, reaching 88.8 ± 1.0% in the AFBBR and 95.3 ± 0.3% in the AAFBBR. However, further increasing the C/N ratio to 20:1 resulted in a significant decline in PNP and COD removal rates in both reactors. Given that denitrification requires organic carbon as an electron donor for nitrogen removal, the limitation of nitrogen source could reduce the organic carbon consumption and inhibit the microbial growth and metabolism (Yang et al., 2024). This trend may be attributed to the impact of the C/N ratio on bacterial extracellular polymeric substances (EPS) synthesis, both excessively high or low C/N ratio can disrupt the EPS secretion, leading to reduced biofilm formation and subsequently inhibiting PNP degradation (Ye et al., 2011). Nevertheless, even at a C/N ratio of 20:1, where the PNP removal rate declined to 83.3 ± 0.3% in the AFBBR and 85.3 ± 0.7% in the AAFBBR, the PNP removal performance in both reactors were still higher than that at the end of phase II. These findings suggest that the nitrogen supplementation effectively enhances PNP degradation in both AFBBR and AAFBBR.

As shown in Figure 4, TN removal rates exhibited a significant increase during phase III. At C/N ratio of 10:1, the maximum TN removal efficiency in the AFBBR reached 48.5 ± 1.2%, while the highest TN removal efficiency of 61.9 ± 4.2% was observed at a C/N ratio of 10:1 in the AAFBBR. The superior TN removal performance in the AAFBBR could be attributed to its integrated anaerobic and aerobic conditions, which create a more favorable DO environment for the growth and metabolism of nitrifying and denitrifying bacteria, thereby enhancing nitrogen removal efficiency (Liu et al., 2020).

3.2 PNP degradation mechanism in AFBBR and AAFBBR

Generally, PNP biodegradation follows two distinct pathways: the hydroquinone pathway and the hydroxyquinol pathway. In the hydroquinone pathway, PNP is sequentially transformed into benzoquinone, hydroquinone (HQ, $C_6H_6O_2$) and γ-hydroxymuconic semialdehybe before ultimately converting into maleylacetate (Badamasi et al., 2025). In the hydroxyquinol pathway, PNP is first converted into 4-nitrocatechol (NC, $C_6H_5NO_4$), which is further degraded into 2-hydroxy-1,4-benzoquinone and hydroxyquinol, eventually leading to the formation of maleylacetate (Badamasi et al., 2025).

On day 83, with an influent PNP concentration of 100 mg/L, a glucose to PNP co-substrate ratio of 6:1 and an influent C/N ratio of 10:1, the average PNP removal rates reached approximately 88.8% in the AFBBR and 95.3% in the AAFBBR. To elucidate the PNP degradation mechanism, intermediate products in the AFBBR, as well as the anaerobic and aerobic zones of AAFBBR, were analyzed using LC–MS/MS.

Supplementary Table 3 presents the primary intermediate products in the AFBBR as well as the anaerobic and aerobic zones of the AAFBBR. The primary intermedia products in AFBBR (Supplementary Figure 1) were *p*-nitrosophenol ($C_6H_5NO_2$), NC, HQ and PAP. Based on signal intensity, the relative concentrations followed the order: HQ > PAP > *p*-nitrosophenol > NC. The primary intermediate products in the anaerobic zone of the AAFBBR (Supplementary Figure 2) were PNP, *p*-hydroxyaminophenol ($C_6H_7NO_2$), PAP and HQ. Based on signal intensity, the relative concentrations followed the order: HQ > PNP > PAP > *p*-hydroxyaminophenol. The primary intermediate products in the aerobic zone of the AAFBBR (Supplementary Figure 3) were PNP, PAP, HQ and NC. Based on signal intensity, the relative concentrations followed the order: HQ > PAP > PNP > NC.

The reduction of the nitro functional group ($-NO_2$) to the amino functional group ($-NH_2$) is generally considered to follow a stepwise process. Initially, the nitro group is reduced to a nitroso group (-NO), which is subsequently converted into a hydroxylamine group (-NHOH) (Mu et al., 2004). Finally, the hydroxylamine group

undergoes further reduction to form the amino group (-NH_2) (Mu et al., 2004). The detection of intermediate products, including p-nitrosophenol and p-hydroxyaminophenol, confirmed that PNP underwent stepwise reduction to PAP in the AFBBR and the AAFBBR. As shown in Figure 5, PNP was reduced to PAP and then hydroxyl-substituted amino groups were transformed under reductive conditions (Luo et al., 2021), leading to the formation of HQ. In addition, the NC was ovserved in the AFBBR and the aerobic zone of the AAFBBR, albeit at low concentrations, suggesting that the hydroxyquinol pathway occurred with the present of aerobic bacteria. Thus, the PNP biodegradation pathway in the AFBBR was inferred to involve both the hydroquinone and the hydroxyquinol pathways, with the hydroquinone pathway being the dominant route. In the anaerobic zone of the AAFBBR, PNP degradation primarily proceeded via the hydroquinone pathway, while biodegradation mechanisms in the aerobic zone of the AAFBBR closely resembled those observed in the AFBBR.

3.3 Microbial community analysis

The biodegradation mechanism of PNP was closely linked to the microbial communities in the AFBBR and the AAFBBR. To investigate the microbial community composition, biofilm samples were collected from the AFBBR and both the anaerobic and aerobic zones of AAFBBR at two critical stages: before the inoculate of PNP (Anoxic_day 0, Anaerobic_day 0 and Aerobic_day 0) and on the day 83 when PNP removal efficiency reached the maximum (Anoxic_day 83, Anaerobic_day 83 and Aerobic_day 83). These samples were subsequently analyzed using high-throughput sequencing. The number of sequences, the species richness (OTU abundances), and the Alpha diversity indices of all samples were listed in Table 2.

The Alpha diversity analysis included Coverage, Chao, Simpson and Shannon indices. The Coverage indexes of all four samples exceeded 0.995, indicating that the sequencing results effectively reflected the true microbial composition of the samples. The Chao index was used to assess community richness, while the Shannon index measured microbial diversity and evenness. The Simpson index, on the other hand, estimated microbial dominance (Tong et al., 2022). Comparing the two operation stages, microbial diversity and richness showed clear changes with PNP exposure (Figure 4a). The Chao1 (Figure 6a) index was much higher in Anaerobic_day 0 and Aerobic_day 0 than in Anaerobic_day 83 and Aerobic_day 83, while Anoxic_day 0 had slightly higher value than Anoxic_day 83. This suggests that the increased PNP toxicity reduced microbial community richness, microorganisms unable to survive in the PNP environment were gradually removed from two reactors. In addition, the Shannon (Figure 6b) index was significantly higher in Anaerobic_day 0 and Aerobic_day 0 than that in Anaerobic_day 83 and Aerobic_day 83, while Anoxic_day 83 showed a marginal increase compared to Anoxic_ day 0. Conversely, Simpson index analysis (Figure 6c) revealed an inverse patterns: Anaerobic_day 0 and Aerobic_day 0 displayed lower values than Anaerobic_day 83 and Aerobic_day 83, whereas AFBBR maintained comparable values. These results indicate that as the PNP degradation system operated, microbial diversity decreased in both anaerobic and aerobic zones of the AAFBBR with a few PNP-tolerant and metabolizing bacteria becoming dominant. Since microbial pollutant removal is primarily driven by functional microbial groups, there was no direct correlation between PNP removal efficiency and community diversity (Tong et al., 2022). Instead, the dominance of PNP-degrading microorganisms was the key factor contributing to the enhanced PNP removal rate. However, the microbial community exhibited a slight increase in diversity while maintaining stable evenness, suggesting selective enrichment of specific functional taxa without disrupting the overall community balance. These results may be due to the anoxic environment led to the simultaneous growth of anaerobic, anoxic and aerobic microorganisms.

The Venn diagram (Figure 7c) illustrates the shared and unique OTUs (relative abundance > 1.0%) in the AFBBR and the AAFBBR when PNP removal efficiency reached the maximum, providing an intuitive representation of the similarity and overlap in OTU composition. The bacterial composition and abundance were

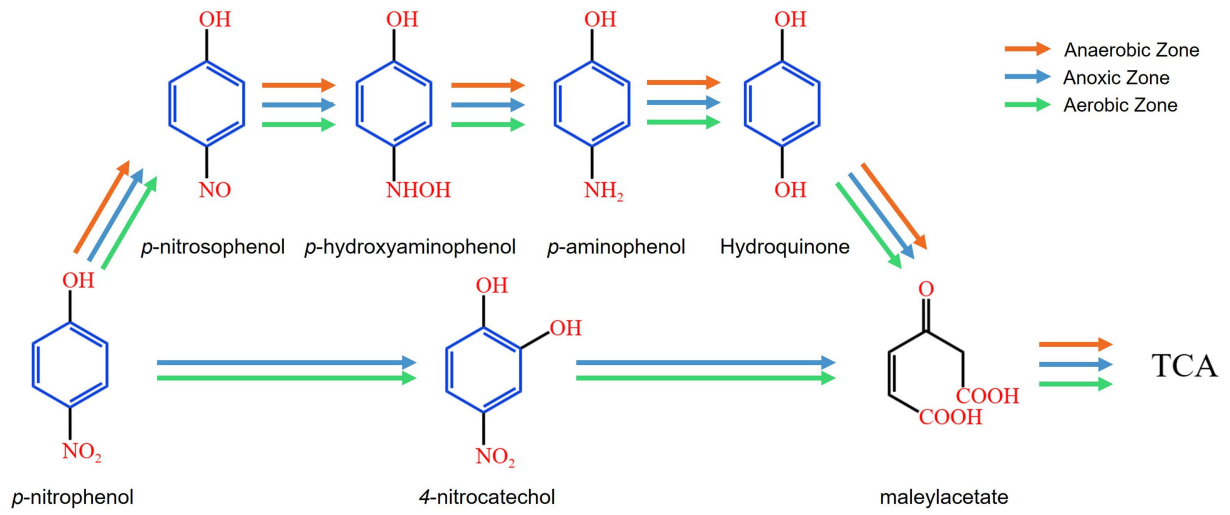

FIGURE 5
Intermediate products and proposed biodegradation pathways in the AFBBR and the AAFBBR.

10.3389/fmicb.2025.1602768

TABLE 2 Microbial richness and diversity in the AFBBR and the AAFBBR.

Samples	Number of sequences	Number of total OTUs	Alpha diversity indices			
			Coverage	Chao	Shannon	Simpson
Anoxic_day 0	32,795	371	0.996233	492.000000	3.175714	0.08016
Anoxic_day 83	50,911	343	0.996389	468.849057	3.293498	0.079518
Anaerobic_day 0	51,479	707	0.998339	847.123967	4.19701	0.046812
Anaerobic_day 83	50,077	334	0.997136	410.109091	3.130425	0.094015
Aerobic_day 0	34,049	763	0.995196	806.907563	4.478895	0.024908
Aerobic_day 83	45,783	386	0.996731	483.500000	3.525593	0.080666

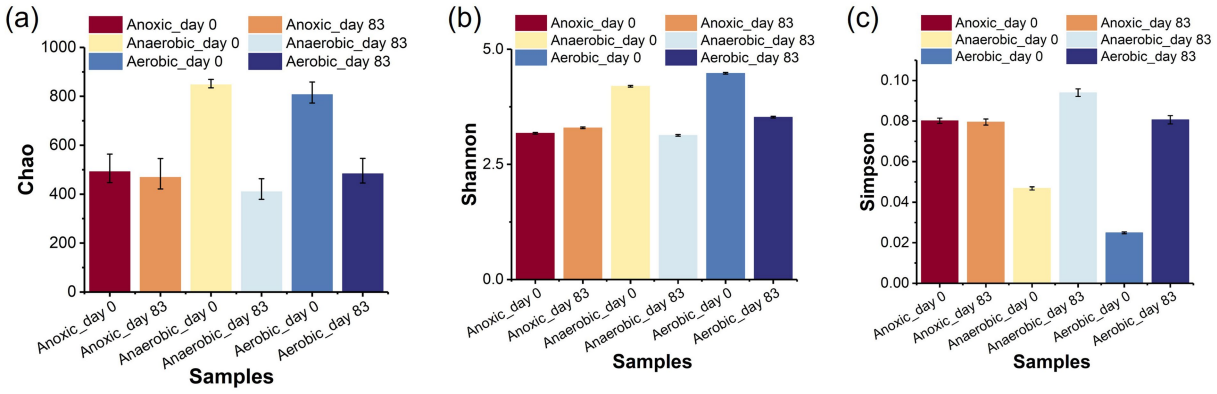

FIGURE 6
Analysis of Alpha diversity indices: **(a)** Chao, **(b)** Shannon, **(c)** Simpson.

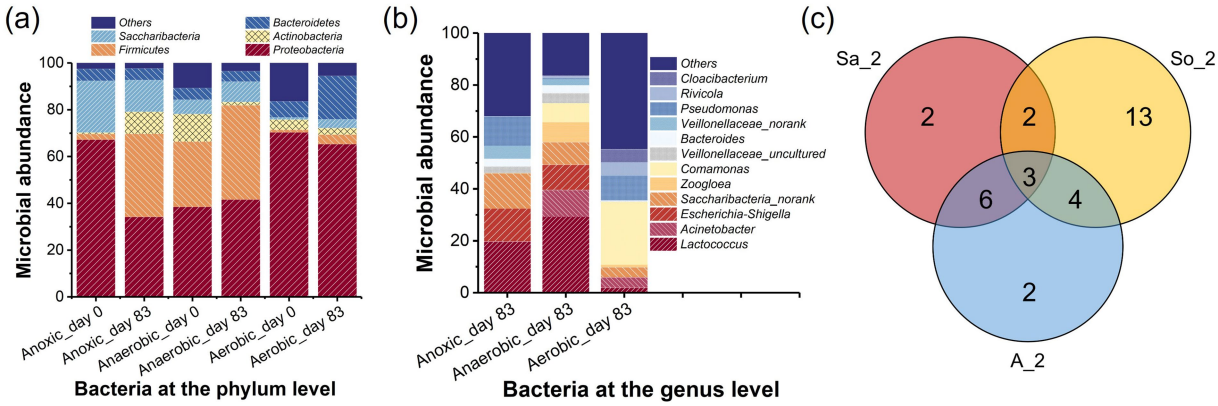

FIGURE 7
Microbial community analysis at the **(a)** phylum level, **(b)** genus level, and **(c)** Venn diagram.

primarily affected by the introduction of PNP wastewater. Some bacterial populations declined, likely due to the inhibitory effects of PNP, while others showed a significant increase, demonstrating their strong adaptability and metabolic capacity in the PNP environment. There were three overlapping OTUs (*Saccharibacteria_norank*, *Enterobacter*, and *Lactococcus*) among all three samples. Six OTUs (*Bacteroides*, *Escherichia-Shigella*, *Veillonellaceae_uncultured*, *Streptococcus*, *Veillonella* and *Veillonellaceae_norank*) were shared between Anaerobic_day 83 and Anoxic_day 83, both of which were under low DO conditions. Additionally, two OTUs (*Comamonas*, *Acinetobacter*) were common between Anaerobic_day 83 and Aerobic_day 83, as both samples were collected from the AAFBBR. These findings suggest that these microbial taxa exhibit strong adaptability and may play a crucial role in PNP metabolism. The characteristics and functional roles of these bacteria will be further explored in the following sections.

The main taxonomic analysis in this experiment assigned to phylum and genus taxa level were summarized in Figure 7. The effects

of the PNP introduction on biofilm community structure in the AFBBR and AAFBBR were compared at the phylum level, as well as the potential functional bacteria at the genus level were summarized. Within the AFBBR and the AAFBBR, distinct DO conditions were established across different areas, enabling the simultaneous coexistence and metabolic activity of anaerobic, anoxic, and aerobic microorganisms in both reactors.

The taxonomic classifications of effective bacterial sequences from biofilm samples before and after the introduction of PNP at the phylum level are summarized in Figure 7a, highlighting the effects of PNP wastewater on microbial community dynamics. Before the introduction of PNP wastewater, as shown in Figure 7a, there were mainly five phyla in the six samples, accounting for 97, 89 and 83% of the total microbial population in the Anoxic_day 0, Anaerobic_day 0 and Aerobic_day 0, respectively, including *Proteobacteria* (67% in Anoxic_day 0, 38% in Anaerobic_day 0, 70% in Aerobic_day 0), *Firmicutes* (2, 28, 1%), *Actinobacteria* (1, 12, 4%), *Saccharibacteria* (22, 6, 1%) and *Bacteroidetes* (5, 5, 7%). These phyla are commonly found in activated sludge microbial community (Liao et al., 2014), and the variations in microbial diversity and richness could be attributed to the different DO concentrations in anaerobic, anoxic and aerobic conditions. After 83 days of operations and optimizations, significant shifts in microbial richness were observed at the phylum level when the average PNP removal rate reached approximately 88.8 and 95.3% in the AFBBR and the AAFBBR, respectively. At this stage, the dominant phyla in the AFBBR (Anoxic_day 83) were *Proteobacteria* (34%), *Firmicutes* (36%), and Saccharibacteria (14%). In the AAFBBR, the dominant phyla in the anaerobic zone (Anaerobic_day 83) were *Proteobacteria* (42%), *Firmicutes* (40%), *Saccharibacteria* (9%), while *Proteobacteria* (65%), *Bacteroidetes* (19%), and *Firmicutes* (4%) were the dominant phyla in the aerobic zone (Aerobic_day 83). Among the six samples, *Proteobacteria* was the most abundant phylum before and after the introduction of PNP wastewater, indicating that *Proteobacteria* has strong adaptability to PNP wastewater. Ji et al. (2017) reported that *Proteobacteria* exhibit significant metabolic versatility in the biodegradation of phenolics, polycyclic aromatic hydrocarbons and heterocyclic, illustrating its potential metabolic capability to PNP. *Bacteroidetes* remained a high abundance in the AFBBR and AAFBBR, especially in the aerobic zone of the AFBBR, many species within this phylum are known to be responsible for denitrifying and organic pollutions degrading process (Yang et al., 2024). The high nitrogen removal efficiency observed in the AAFBBR could be attributable to the substantial abundance of *Bacteroidetes*. Additionally, with the introduce of PNP wastewater, *Firmicutes* exhibited a notable increase in anaerobic (27 to 40%) and aerobic zone (1 to 4%) of the AAFBBR and in the AFBBR (2 to 36%). This trend aligns with the ability of *Firmicutes* to form endospores, granting them high resistance to environmental stressors and enabling the efficient degradation of various recalcitrant organic compounds (Garcia et al., 2011).

Actinobacteria, which initially comprised a significant proportion in the AAFBBR (12% in the anaerobic and 4% in the aerobic zones), experienced a marked decline after 92 days (to 1 and 3%, respectively). This observation similar with the finding of Tong et al. (2022) and may attributed to the inhabitation of high influent PNP concentration. However, the abundance of *Actinobacteria* in AFBBR increased from 1 to 9%, suggesting its better adaptability in the anoxic condition. With the introduction of PNP wastewater, the relative abundance of *Saccharibacteria* increased in anaerobic zone (6 to 9%) and aerobic zone (1 to 4%) of the AAFBBR, while decreased in the AFBBR (22 to 14%). Prior studies have reported that *Saccharibacteria* possess metabolic potential for degrading complex carbon sources and play a role in biofilm formation (Li and Bae, 2024). Moreover, it was reported that *Saccharibacteria* had been identified as a key taxon in plastic degradation in polylactic acid soil environment (Ruthi et al., 2020). Under PNP-induced acclimatization, *Proteobacteria*, *Firmicutes*, *Actinobacteria*, *Saccharibacteria*, and *Bacteroidetes* exhibited strong adaptability to the high-toxicity PNP environment, sustaining growth and metabolic activity. Synergistic interactions among these diverse microbial communities played a crucial role in facilitating the efficient biodegradation of PNP under the anaerobic, anoxic, and aerobic conditions.

Figure 7b presents the taxonomic analysis at the genus level when the average PNP removal rate reached approximately 88.8 and 95.3% in the AFBBR and the AAFBBR, providing deeper insights into the potential functional bacteria present in two reactors. *Lactococcus* (20% in Anoxic_day 83 and 29% in Anaerobic_day 83), *Escherichia-Shigella* (13% in Anoxic_day 83 and 10% in Anaerobic_day 83), and *Saccharibacteria_norank* (14% in Anoxic_day 83 and 9% in Anaerobic_day 83) were the dominant genera in the AFBBR and the anaerobic zone of the AAFBBR, indicating their adaption and survival under low DO conditions with the inlet of PNP wastewater. Among these genera, *Lactococcus*, as a member of the phylum *Firmicutes*, is reported to play an important role in organic matter degradation and acidogenic fermentation (Cui et al., 2022; Wang C. et al., 2020). *Escherichia-Shigella* is reported to be associated with nitrogen removal (Sun et al., 2022) and *Saccharibacteria_norank* is associated with pyrimidine degradation (Hou et al., 2020), suggesting its potential involvement in organic compounds metabolism.

In addition, *Acinetobacter* (10% in Anaerobic_day 83 and 4% in Aerobic_day 83), *Comamonas* (7 and 24%), *Zoogloea* (8 and 1%), and *Pseudomonas* (1 and 10%) had high abundance in the AAFBBR. *Acinetobacter* has been reported to exhibit exceptional phenol degradation capability (Gallego et al., 2007), and *Comamonas* is known for its efficient metabolism of phenolic compounds (Huang et al., 2016; Tong et al., 2022). *Pseudomonas* is a typical gram-negative bacterium that is commonly enriched in the PNP wastewater treatment processes (Badamasi et al., 2025). Previous studies have demonstrated that members of the genus *Pseudomonas* could utilize PNP as their sole source of carbon, nitrogen, and energy (Chen et al., 2016), and are capable of degrading PNP via both the hydroquinone and hydroxyquinol pathways (Zhang et al., 2012). Moreover, *Zoogloea is* an important component of activated sludge and biofilms, plays a vital role in the structure and performance of sludge flocs (Gao et al., 2014). The enrichment of *Zoogloea* is beneficial for enhancing the resistance of biofilm to adverse environmental conditions.

The aerobic zone of the AAFBBR also contained unique microbial genera, such as *Cloacibacterium* (5%), *Geobacter* (1%), and *Rivicola* (5%). Although their relative abundances were low, their roles in AAFBBR could not be overlooked. Studies have reported that *Cloacibacterium* could utilize biodegradable organic matter as a carbon source to produce EPS, which protect the bacteria from the toxicity of high concentrations of recalcitrant organic pollutants (Ram et al., 2018). *Geobacter*, on the other hand, has demonstrated the capability to oxidize benzene-derived and phenolic compounds (Zhou et al., 2016), suggesting its potential role in PNP degradation. Additionally, *Rivicola* has been reported to participate in nitrogen removal (Huang et al., 2024) and its increased abundance may be attributed to nitrogen supplement in AAFBBR.

Building on the conclusions in section 3.2, the PNP biodegradation pathway was inferred to involve both the hydroquinone and the hydroxyquinol pathways, which can be attributed to the synergistic interactions among diverse microbial communities under varying DO conditions. In both the AFBBR and the AAFBBR, key bacterial genera, including *Lactococcus*, *Escherichia-Shigella*, *Saccharibacteria_norank*, *Acinetobacter*, *Comamonas*, *Zoogloea*, and *Pseudomonas*, were suggested to play crucial roles in the hydroquinone pathway. Notably, the hydroxyquinol pathway was observed only in the AFBBR and the aerobic zone of the AAFBBR, where the DO concentrations were higher. *Pseudomonas*, a key microorganism capable of degrading PNP via both the hydroquinone and hydroxyquinol pathways, exhibited significantly higher abundance in the anoxic and aerobic zones than in the anaerobic zone of the AAFBBR. This suggests that *Pseudomonas* was likely a major contributor to the hydroxyquinol degradation pathway.

4 Conclusion

This study successfully established an anoxic fluidized bed bioreactor (AFBBR) and an anaerobic-aerobic fluidized bed bioreactor (AAFBBR) for enhancing PNP biodegradation efficiency during 90-day operation. Under an influent PNP concentration of 100 mg/L, a glucose to PNP co-substrate ratio of 6:1, and a C/N ratio of 10:1, the AFBBR achieved PNP, COD, and TN removal efficiencies of 88.8 ± 1.0%, 80.9 ± 8.9%, and 47.0 ± 3.1%, respectively, while the AAFBBR reached 95.3 ± 0.3%, 90.4 ± 0.7%, and 61.9 ± 4.2%, respectively. PNP biodegradation in both reactors followed the hydroquinone and hydroxyquinol pathways, with the hydroquinone pathway being dominant. *Proteobacteria* (34% in the AFBBR, 42 and 65% in the anaerobic and aerobic zones of the AAFBBR), *Firmicutes* (35, 40, and 4%), *Saccharibacteria* (14, 9, and 4%) and *Bacteroidetes* (5, 4 and 19%) were the predominant phyla in PNP biodegradation. Key bacterial genera, including *Lactococcus*, *Escherichia-Shigella*, *Saccharibacteria_norank*, *Acinetobacter*, *Comamonas*, *Zoogloea*, and *Pseudomonas*, played crucial roles in the hydroquinone pathway, with *Pseudomonas* as the key contributor to the hydroxyquinol pathway. These findings provide a scientific foundation and theoretical support for the pilot-scale implementation and efficient biological treatment of PNP in the industrial and agricultural wastewater.

Data availability statement

The data presented in the study are deposited in the NCBI repository, accession number PRJNA1258386.

Author contributions

XZ: Conceptualization, Data curation, Formal analysis, Investigation, Methodology, Validation, Visualization, Writing – original draft. YZ: Conceptualization, Data curation, Investigation, Methodology, Writing – original draft. ZY: Resources, Visualization, Writing – review & editing. ZP: Conceptualization, Funding acquisition, Project administration, Supervision, Writing – review & editing.

Funding

The author(s) declare that financial support was received for the research and/or publication of this article. This work was supported by the National Key Research and Development Program of China (2019YFE0117200).

Conflict of interest

The authors declare that the research was conducted in the absence of any commercial or financial relationships that could be construed as a potential conflict of interest.

Generative AI statement

The authors declare that no Gen AI was used in the creation of this manuscript.

Publisher's note

Supplementary material

The Supplementary material for this article can be found online at: https://www.frontiersin.org/articles/10.3389/fmicb.2025.1602768/full#supplementary-material

References

Badamasi, H., Naeem, Z., Antoniolli, G., Kumar, A. P., Olaleye, A. A., Sadiq, I. S., et al. (2025). A review of recent advances in green and sustainable technologies for removing *4*-nitrophenol from the water and wastewater. *Sustain. Chem. Pharm.* 43:101867. doi: 10.1016/j.scp.2024.101867

Bai, Q., Yang, L., Li, R., Chen, B., Zhang, L., Zhang, Y., et al. (2015). Accelerating quinoline biodegradation and oxidation with endogenous electron donors. *Environ. Sci. Technol.* 49, 11536–11542. doi: 10.1021/acs.est.5b03293

Chen, Q., Tu, H., Luo, X., Zhang, B., Huang, F., Li, Z., et al. (2016). The regulation of *Para*-Nitrophenol degradation in *Pseudomonas putida* DLL-E4. *PLoS One* 11:18. doi: 10.1371/journal.pone.0155485

Chowdhury, M., and Nakhla, G. (2022). Enhanced mainstream nitrogen removal from synthetic wastewater using gel-immobilized anammox in fluidized bed bioreactors: process performance and disintegration mechanisms. *Sci. Total Environ.* 811:151373. doi: 10.1016/j.scitotenv.2021.151373

Cui, Y., Zhang, H., Zhang, J., Lv, B., and Xie, B. (2022). The emission of volatile organic compounds during the initial decomposition stage of food waste and its relationship with the bacterial community. *Environ. Technol. Innov.* 27:102443. doi: 10.1016/j.eti.2022.102443

Eldyasti, A., Chowdhury, N., Nakhla, G., and Zhu, J. (2010). Biological nutrient removal from leachate using a pilot liquid-solid circulating fluidized bed bioreactor (LSCFB). *J. Hazard. Mater.* 181, 289–297. doi: 10.1016/j.jhazmat.2010.05.010

Feng, A., Lin, C., Zhou, H., Jin, W., Hu, Y., Li, D., et al. (2024). Catalytic transformation of *4*-nitrophenol into *4*-aminophenol over ZnO nanowire array-decorated cu nanoparticles. *Green Chem. Eng.* 5:205212, 205–212. doi: 10.1016/j.gce.2023.03.003

Gallego, J. L. R., García-Martínez, M. J., and Llamas, J. F. (2007). Biodegradation of oil tank bottom sludge using microbial consortia. *Biodegradation* 18:269281, 269–281. doi: 10.1007/s10532-006-9061-y

Gao, C., Wang, A., Wu, W., Yin, Y., and Zhao, Y. (2014). Enrichment of anodic biofilm inoculated with anaerobic or aerobic sludge in single chambered air-cathode microbial fuel cells. *Bioresour. Technol.* 167:124132, 124–132. doi: 10.1016/j.biortech.2014.05.120

Garcia, S. L., Jangid, K., Whitman, W. B., and Das, K. C. (2011). Transition of microbial communities during the adaption to anaerobic digestion of carrot waste. *Bioresour. Technol.* 102, 7249–7256. doi: 10.1016/j.biortech.2011.04.098

Hou, H., Duan, L., Zhou, B., Tian, Y., Wei, J., and Qian, F. (2020). The performance and degradation mechanism of sulfamethazine from wastewater using IFAS-MBR. *Chinese Chem. Lett.* 31:543546, 543–546. doi: 10.1016/j.cclet.2019.08.031

Hu, F., Zhou, H., Jin, Z., Sun, Q., Pan, Z., and Zhu, J. (2013). Biodegradation of TCP in a sequencing batch-fluidized bed bioreactor with waste coke particles as the carrier. *J. Environ. Eng.* 139, 1222–1227. doi: 10.1061/(ASCE)EE.1943-7870.0000728

Huang, K., He, Y., Wang, W., Jiang, R., Zhang, Y., Li, J., et al. (2024). Temporal differentiation in the adaptation of functional bacteria to low-temperature stress in partial denitrification and anammox system. *Environ. Res.* 244:117933. doi: 10.1016/j.envres.2023.117933

Huang, Y., Hou, X., Liu, S., and Ni, J. (2016). Correspondence analysis of bio-refractory compounds degradation and microbiological community distribution in anaerobic filter for coking wastewater treatment. *Chem. Eng. J.* 304:864872, 864–872. doi: 10.1016/j.cej.2016.05.142

Ji, F., Yuan, Y., and Lai, B. (2017). Microbial community dynamics in aerated biological fluidized bed (ABFB) with continuously increased *p*-nitrophenol loads. *Process Biochem.* 63, 185–192. doi: 10.1016/j.procbio.2017.07.033

Karadag, D., Koeroglu, O. E. K., Ozkaya, B., and Cakmakci, M. (2015). A review on anaerobic biofilm reactors for the treatment of dairy industry wastewater. *Process Biochem.* 50, 262–271. doi: 10.1016/j.procbio.2014.11.005

Kitagawa, W., Kimura, N., and Kamagata, Y. (2004). A novel p-nitrophenol degradation gene cluster from a gram-positive bacterium, Rhodococcus opacus SAO101. *J. Bacteriol.* 186, 4898–4902. doi: 10.1128/JB.186.15.4894-4902.2004

Kuyukina, M. S., Ivshina, I. B., Serebrennikova, M. K., Krivoruchko, A. V., Korshunova, I. O., Peshkur, T. A., et al. (2017). Oilfield wastewater biotreatment in a fluidized-bed bioreactor using co-immobilized *Rhodococcus* cultures. *J. Environ. Chem. Eng.* 5, 1252–1260. doi: 10.1016/j.jece.2017.01.043

Li, M., and Bae, S. (2024). Exploring the effects of polyethylene and polyester microplastics on biofilm formation, membrane fouling, and microbial communities in modified ludzack-ettinger-reciprocation membrane bioreactors. *Bioresour. Technol.* 414, 0960–8524. doi: 10.1016/j.biortech.2024.131636

Liao, R., Li, Y., Yu, X., Shi, P., Wang, Z., Shen, K., et al. (2014). Performance and microbial diversity of an expanded granular sludge bed reactor for high sulfate and nitrate waste brine treatment. *J. Environ. Sci.* 26:717725, 717–725. doi: 10.1016/S1001-0742(13)60479-9

Liu, X., Kim, M., Nakhla, G., Andalib, M., and Fang, Y. (2020). Partial nitrification-reactor configurations, and operational conditions: performance analysis. *J. Environ. Chem. Eng.* 8:103984. doi: 10.1016/j.jece.2020.103984

Lu, R., Hong, B., Wang, Y., Cui, X., Liu, C., Liu, Y., et al. (2025). Microalgal biofilm cultivation on lignocellulosic based bio-carriers: effects of material physical characteristics on microalgal biomass production and composition. *Chem. Eng. J.* 510:161656. doi: 10.1016/j.cej.2025.161656

Luo, J., Xu, Y., Wang, J., Zhang, L., Jiang, X., and Shen, J. (2021). Coupled biodegradation of *p*-nitrophenol and *p*-aminophenol in bioelectrochemical system: mechanism and microbial functional diversity. *J. Environ. Sci.* 108, 134–144. doi: 10.1016/j.jes.2021.02.017

Mallikarjuna, C., and Dash, R. R. (2020). A review on hydrodynamic parameters and biofilm characteristics of inverse fluidized bed bioreactors for treating industrial wastewater. *J. Environ. Chem. Eng.* 8:104233. doi: 10.1016/j.jece.2020.104233

Mei, X., Liu, J., Guo, Z., Li, P., Bi, S., Wang, Y., et al. (2019). Simultaneous *p*-nitrophenol and nitrogen removal in PNP wastewater treatment: comparison of two integrated membrane-aerated bioreactor systems. *J. Hazard. Mater.* 363, 99–108. doi: 10.1016/j.jhazmat.2018.09.072

Mu, Y., Yu, H., Zheng, J., Zhang, S., and Sheng, G. (2004). Reductive degradation of nitrobenzene in aqueous solution by zero-valent iron. *Chemosphere* 54, 789–794. doi: 10.1016/j.chemosphere.2003.10.023

Ram, S. K., Kumar, L. R., Tyagi, R. D., and Drogui, P. (2018). Techno-economic evaluation of simultaneous production of extra-cellular polymeric substance (EPS) and lipids by *Cloacibacterium normanense* NK6 using crude glycerol and sludge as substrate. *Water Sci. Technol.* 77, 2228–2241. doi: 10.2166/wst.2018.140

Ruthi, J., Blsterli, D., Pardi Comensoli, L., Brunner, I., and Frey, B. (2020). The "Plastisphere" of biodegradable plastics is characterized by specific microbial taxa of alpine and arctic soils. *Env. Sci.* 8:562263. doi: 10.3389/fenvs.2020.562263

Sponza, D. T., and Kuscu, Z. S. (2011). Relationships between acute toxicities of *Para* nitrophenol (*p*-NP) and nitrobenzene (NB) to *Daphnia magna* and *Photobacterium phosphoreum*: physicochemical properties and metabolites under anaerobic/aerobic sequentials. *J. Hazard. Mater.* 185, 1187–1197. doi: 10.1016/j.jhazmat.2010.10.030

Sun, C., Li, C., Zhang, K., Ma, X., and Zhang, Y. (2022). Six complex microbial inoculants for removing ammonia nitrogen from waters. *Water Environ. Res.* 94:e10823. doi: 10.1002/wer.10823

Sun, J., Yuan, M., Zhou, H., Chen, Z., Wang, Y., and Cheng, H. (2025). Enhanced printing and dyeing wastewater treatment using anaerobic-aerobic systems with bioaugmentation. *J. Hazard. Mater.* 486:136982. doi: 10.1016/j.jhazmat.2024.136982

Tang, P., Deng, C., Tang, X., Si, S., and Xiao, K. (2012). Degradation of *p*-nitrophenol by interior microelectrolysis of zero-valent iron/copper-coated magnetic carbon galvanic couples in the intermittent magnetic field. *Chem. Eng. J.* 210, 203–211. doi: 10.1016/j.cej.2012.08.089

Tong, J., Cui, L., Wang, D., Wang, X., and Liu, Z. (2022). Assessing the performance and microbial structure of biofilms in membrane aerated biofilm reactor for high *p*-nitrophenol concentration treatment. *J. Environ. Chem. Eng.* 10:108635. doi: 10.1016/j.jece.2022.108635

Vo, H. N. P., Ngo, H. H., Guo, W., Liu, Y., Chang, S. W., Nguyen, D. D., et al. (2020). Selective carbon sources and salinities enhance enzymes and extracellular polymeric substances extrusion of *Chlorella* sp. for potential co-metabolism. *Bioresour. Technol.* 303:122877. doi: 10.1016/j.biortech.2020.122877

Wang, H., He, X., Nakhla, G., Zhu, J., and Su, Y. (2020). Performance and bacterial community structure of a novel inverse fluidized bed bioreactor (IFBBR) treating synthetic municipal wastewater. *Sci. Total Environ.* 718:137288. doi: 10.1016/j.scitotenv.2020.137288

Wang, L., Hu, Z., Hu, M., Zhao, J., Zhou, P., Zhang, Y., et al. (2022). Cometabolic biodegradation system employed subculturing photosynthetic bacteria: a new degradation pathway of *4*-chlorophenol in hypersaline wastewater. *Bioresour. Technol.* 361:127670. doi: 10.1016/j.biortech.2022.127670

Wang, J., Wang, D., Su, Z., Song, Y., Zhang, J., and Xiahou, Y. (2024). Green synthesis of chitosan/glutamic acid/agarose/ag nanocomposite hydrogel as a new platform for colorimetric detection of cu ions and reduction of *4*-nitrophenol. *Int. J. Biol. Macromol.* 259:129394. doi: 10.1016/j.ijbiomac.2024.129394

Wang, C., Yu, G., Yang, F., and Wang, J. (2020). Formation of anaerobic granules and microbial community structure analysis in anaerobic hydrolysis denitrification reactor. *Sci. Total Environ.* 737:139734. doi: 10.1016/j.scitotenv.2020.139734

Xu, J., Wang, B., Zhang, W., Zhang, F., Deng, Y., Wang, Y., et al. (2021). Biodegradation of *p*-nitrophenol by engineered strain. *AMB Expr.* 11:124. doi: 10.1186/s13568-021-01284-8

Yan, H., Gu, Z., Zhang, Q., Wang, Y., Cui, X., Liu, Y., et al. (2024). Detoxification of copper and zinc from anaerobic digestate effluent by indigenous bacteria: mechanisms, pathways and metagenomic analysis. *J. Hazard. Mater.* 469:133993. doi: 10.1016/j.jhazmat.2024.133993

Yan, H., Lu, R., Liu, Y., Cui, X., Wang, Y., Yu, Z., et al. (2022). Development of microalgae-bacteria symbiosis system for enhanced treatment of biogas slurry. *Bioresour. Technol.* 354:127187. doi: 10.1016/j.biortech.2022.127187

Yang, X., Liao, Y., Zeng, M., and Qin, Y. (2024). Nitrite accumulation performance and microbial community of algal-bacterial symbiotic system constructed by *Chlorella* sp. and *Navicula* sp. *Bioresour. Technol.* 399:130638. doi: 10.1016/j.biortech.2024.130638

Ye, F., Ye, Y., and Li, Y. (2011). Effect of C/N ratio on extracellular polymeric substances (EPS) and physicochemical properties of activated sludge flocs. *J. Hazard. Mater.* 188, 37–43. doi: 10.1016/j.jhazmat.2011.01.043

Zhang, S., Sun, W., Xu, L., Zheng, X., Chu, X., Tian, J., et al. (2012). Identification of the *Para*-nitrophenol catabolic pathway, and characterization of three enzymes involved in the hydroquinone pathway, in *pseudomonas* sp. 1-7. *BMC Microbiol.* 12, 1471–2180. doi: 10.1186/1471-2180-12-27

Zheng, M., Bai, Y., Han, H., Zhang, Z., Xu, C., Ma, W., et al. (2021). Robust removal of phenolic compounds from coal pyrolysis wastewater using anoxic carbon-based fluidized bed reactor. *J. Clean. Prod.* 280:124451. doi: 10.1016/j.jclepro.2020.124451

Zhou, L., Deng, D., Zhang, D., Chen, Q., Kang, J., Fan, N., et al. (2016). Microbial electricity generation and isolation of exoelectrogenic bacteria based on petroleum hydrocarbon-contaminated soil. *Electroanalysis* 28, 1510–1516. doi: 10.1002/elan.201501052

Frontiers in Microbiology

Explores the habitable world and the potential of microbial life

The largest and most cited microbiology journal which advances our understanding of the role microbes play in addressing global challenges such as healthcare, food security, and climate change.

Discover the latest Research Topics

See more →

Frontiers

Avenue du Tribunal-Fédéral 34
1005 Lausanne, Switzerland
frontiersin.org

Contact us

+41 (0)21 510 17 00
frontiersin.org/about/contact